**UNIVERSIDAD NACIONAL AUTÓNOMA DE MEXICO**
PROGRAMA DE MAESTRÍA Y DOCTORADO EN GEOGRAFÍA

Elementos estadísticos y cartográficos para el análisis del riesgo de desastre por inestabilidad de laderas: retos y oportunidades

TESIS
QUE PARA OPTAR POR EL GRADO DE:
DOCTOR (A) EN GEOGRAFÍA

PRESENTA:
FRANNY GISELLE MURILLO GARCÍA

DIRECTOR(A) DE TESIS
IRASEMA ALCÁNTARA AYALA
INSTITUTO DE GEOGRAFÍA UNAM

Ciudad Universitaria, Cd. Mx, Mayo 2021

**Agradecimientos**

Esta tesis no hubiese sido posible sin la coordinación, asesoramiento y ayuda de varias personas:

**Dra. Irasema Alcántara Ayala**, asesora de la investigación.

A los sinodales de este trabajo:

Dr. Manuel Suárez Lastra
Dr. Víctor Oliva Aguilar
Dra. Silvia Guadalupe Ramos Hernández
Dra. Patricia Flores Olvera
Dr. José Juan Zamorano Orózco

A los investigadores y compañeros del Posgrado en Geografía y del Instituto de Geografía de la UNAM, en especial al Dr. Ricardo Garnica Peña y al Dr. José Lugo Hubp.

A los investigadores del CNR-IRPI de Perugia, Italia.

A los investigadores de la BOKU University de Viena, Austria, división de Ingeniería Geotécnica.

A los investigadores de la Universidad de Viena, Austria, Departamento de Geografía.

Así mismo, se agradece a tods aquellas personas que ayudaron o colaboraron en la realización de esta tesis.

# Tabla de contenido

# INTRODUCCIÓN

La tarde del 5 de octubre del año 1999, en la colonia que lleva por nombre La Aurora, en la cabecera municipal del Teziutlán, Puebla, México, ocurrió un evento conocido como derrumbe o desgajamiento que cobró la vida de por lo menos 109 personas (Fig. 1) (Capra *et al.* 2003, Alcántara-Ayala 2004). La colonia La Aurora está localizada al este del centro de Teziutlán, una ciudad construida en la parte alta y plana de una mesa conformada por material volcánico de textura arenosa conocido como depósitos de piroclastos.
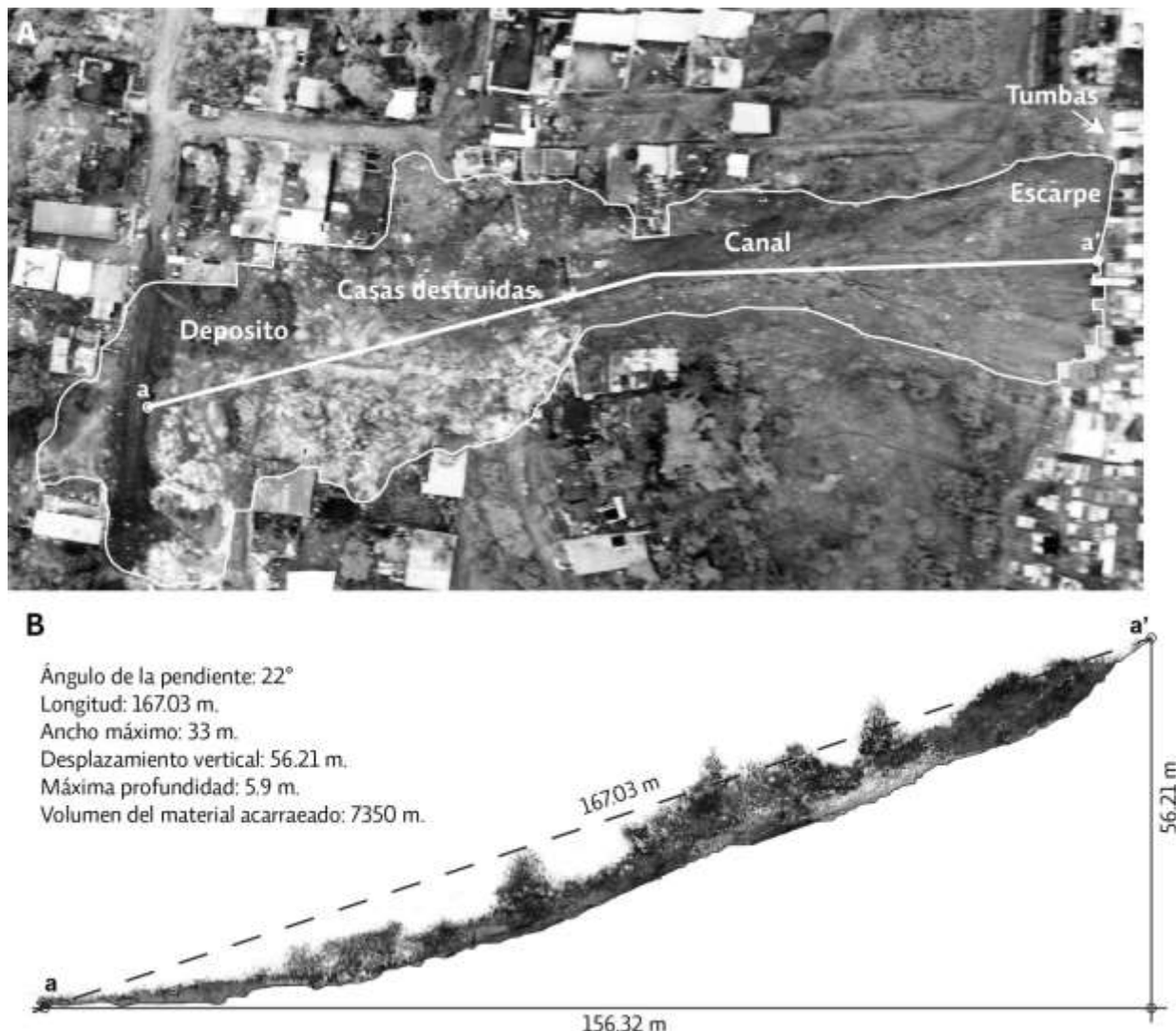


**Figura 1.** *A) Vista aérea donde se muestra el área de impacto del PRM ocurrido en la colonia La Aurora, Teziutlán el 5 de octubre de 1999 (fotografía adquirida por el CENAPRED). B) morfología de la ladera después del evento gravitacional.*

El municipio de Teziutlán tenía en el año 2000 una población de 81,156 habitantes (http://www.inafed.gob.mx), en el pasado, se había mantenido de las actividades primarias y de la minería, extracción de plata, cobre y zinc (Chavelas Lluck *et al.* 1991). En el último cuarto del siglo XX, con la apertura comercial entre México, Estados Unidos y Canadá, se instalaron en Teziutlán una serie de maquiladoras textiles: la población dedicada a la industria creció en el municipio de 1,910 trabajadores en 1988 a 12,412 trabajadores en 1998 (INEGI 2002).

La cabecera municipal se extendió y la población comenzó a asentarse en las laderas de piroclastos (flujos y caídas). Eso fue lo que ocurrió en la colonia La Aurora. Una fotografía aérea del año 1942 demuestra que en el pasado la vertiente no estaba poblada, de hecho, parece haber evidencia que de que años antes de la toma de la fotografía aérea ahí ya había ocurrido un fenómeno similar al que ocurrió en 1999 (líneas punteadas en la Fig. 2 (A)).

En octubre de 1999, la Depresión Tropical nº11 del Golfo de México ocasionó lluvias extraordinarias en la región de la Sierra Norte de Puebla (región fisiográfica montañosa en dónde está localizado Teziutlán). Durante un solo día cayeron más de 300 mm de lluvia, lo que detonó la ocurrencia del movimiento hacia abajo de los materiales que conformaban la superficie inclinada donde los habitantes de La Aurora habían construido sus casas; de hecho, el evento de La Aurora no fue el único, hubo miles de estos fenómenos naturales en la región de la Sierra Norte de Puebla (Lugo-Hubp *et al.* 2005), afortunadamente ninguno fue tan mortal como el ocurrido en La Aurora.
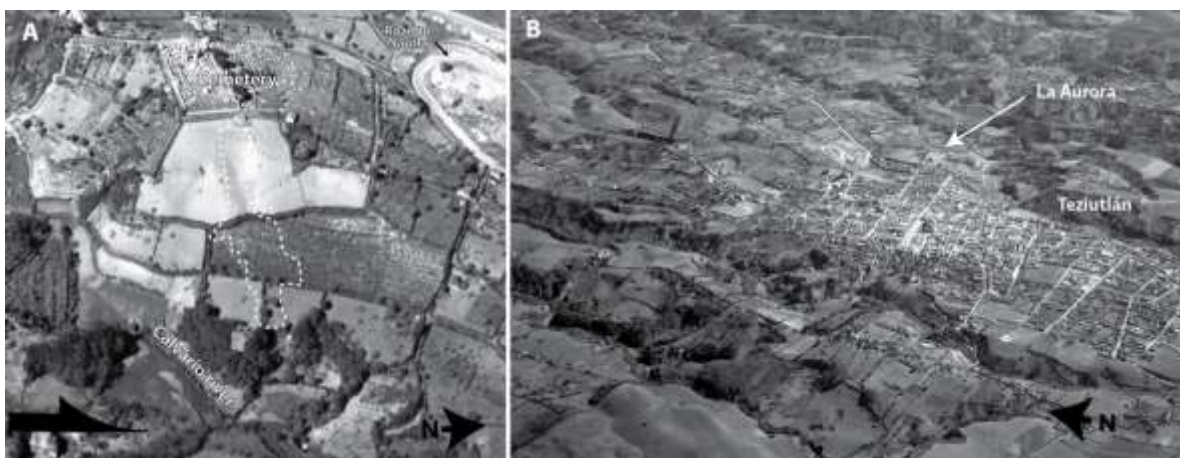


*Figura 2.* A) Evidencia morfológica de un PRM anterior a 1942, B) Localización de la Colonia La Aurora respecto al centro del poblado de Teziutlán  (fotografías  del archivo fotográfico Fundación ICA).

A partir de lo ocurrido en la Sierra Norte de Puebla comenzaron a publicarse más trabajos académicos en México acerca de este tipo de fenómenos cuya denominación correcta es el de procesos de remoción

en masa (PRM), procesos de ladera, procesos gravitacionales o movimientos de ladera (Alcántara-Ayala 2000).

Sin embargo, el desastre de 1999 no había sido el primero en su tipo en México, ya en 1959 un PRM había ocasionado la muerte de alrededor de 900 personas luego de sepultar casi por completo al poblado de Minatitlán en el estado de Colima (Padilla-Lozoya 2007). Incluso, en la región de la Sierra Norte de Puebla ya se tenían antecedentes de este tipo de eventos en los años 1944 y los de 1955 asociados al huracán Janet (Murillo-García y Alcántara-Ayala 2017).

No obstante, lo ocurrido en la Sierra Norte de Puebla había sido de tal magnitud que el gobierno en turno lo denominó como el peor desastre en México luego del Terremoto de 1985; hecho que motivó diversos trabajos de investigación, como los elaborados por Flores-Lorenzo y Alcántara-Ayala (2002), Capra *et al.* (2003), Alcántara-Ayala (2004), Lugo-Hubp *et al.* (2005), Alcántara-Ayala *et al.* (2006), Borja-Baeza *et al.* (2006) u Oliva-Aguilar *et al.* (2011). Además, tesis de licenciatura y posgrado, manuales, infografías, guías y reportes de instituciones como el Centro Nacional de Prevención de Desastres (CENAPRED), así como de las distintas instancias de Protección Civil.

Estos trabajos no solo se concentraron en la región de la Sierra Norte de Puebla y a lo ocurrido en el año 1999, también fueron de zonas en los estados de México, Baja California, Baja California Sur (Antinao y Farfán 2013, Oliva González *et al.* 2014), Michoacán (Alcántara-Ayala *et al.* 2012), Guerrero (Gaidzika *et al.* 2017) y Chiapas (Caballero *et al.* 2006, Hernández-Madrigal *et al.* 2011), entre otros. Estos esfuerzos se dedicaron a entender el fenómeno natural de los PRM como tal en sus mecanismos de ocurrencia, pero también hubo algunos que describieron y analizaron las condiciones sociales que en cada caso llevaron a situaciones que comúnmente son llamadas desastres. Más aún, desarrollos de alertas tempranas o mapas de *predicción* de PRM, también comenzaron a trabajarse en los últimos veinte años, además de propuestas metodológicas y herramientas para su estudio.

El mérito y utilidad de lo mencionado en el párrafo anterior no puede ser puesto en duda. Sin embargo, en comparación con lo realizado en otros países, y en proporción con la magnitud y cantidad de desastres ocurridos y que pueden ocurrir en México por PRM, el trabajo realizado resulta todavía insuficiente. Faltan aspectos por cubrir, desde el punto de vista académico, gubernamental y social. Respecto a cualquiera de las llamadas amenazas de origen natural (sismos, terremotos, inundaciones, tsunamis, huracanes, erupciones volcánicas, sequias o incendios forestales) y no solo de los PRM. Por ello, las investigaciones que tratan de entender los PRM y sus consecuencias, no pueden menos que ser bienvenidas.

En este trabajo se señalan diversas carencias en la falta de datos para realizar investigaciones, modelos y estimaciones de los diversos aspectos relacionados con los PRM. Esto dificulta la labor y la

innovación en este campo. Por lo anterior, el objetivo general de esta investigación es lograr la aplicación de una metodología en el estudio y análisis de la inestabilidad de laderas, cubriendo los aspectos generales básicos de la estimación del riesgo: (i) identificación del peligro (registro y cartografía de la amenaza), (ii) análisis del peligro y de la distribución espacial de los PRM y los factores relacionados a su ocurrencia, y (iii) análisis de la vulnerabilidad de la población (Fig. 3). Todo ello desde un enfoque estadístico, con el fin último de reducir la probabilidad de que la población y sus bienes se vean negativamente afectados por este tipo de fenómenos.
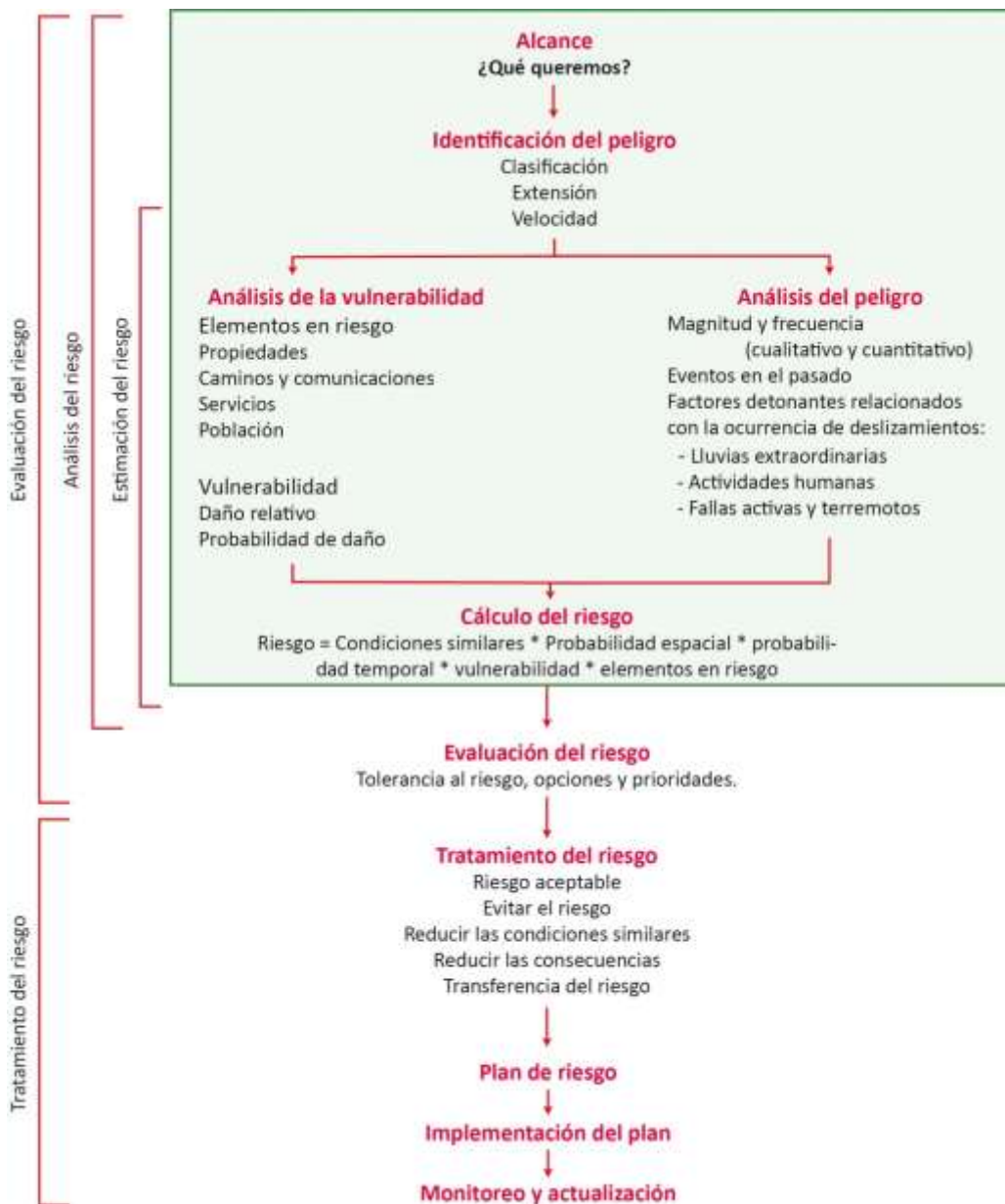


**Figura 3.** *Aspectos generales que abarca el estudio de riesgo por procesos de remoción en masa (Fuente: Crozier 2005).*

Los aspectos generales expuestos en la Fig. 3, serán explicados ampliamente en el capítulo I de esta investigación. Así mismo, este esquema concuerda con el enfoque general seguido en este trabajo, que se denomina *alternativo-estructuralista* y que también se explica de forma detallada en el capítulo I. En ese sentido, en esta investigación se trabajó de manera concreta en la aplicación, modificación, mejora y adaptación de las metodologías ya probadas para la estimación del riesgo y cada uno de sus componentes, en cada capítulo se especifica que fue lo que se consiguió, cuáles fueron las dificultades, adaptaciones, si se propuso algo nuevo o si se mejoró algún procedimiento.

Es necesario señalar que en un principio, en el proyecto inicial el objetivo general era más ambicioso: la construcción de un sistema para la evaluación del riesgo por PRM. Durante la investigación, se tomó conciencia de que no sería posible cumplir con ese objetivo en el tiempo y forma, por lo que se decidió, en conjunto con el comité tutor, el cambio de enfoque de esta tesis y el ajuste de su alcance (parte señalada en verde en la Fig. 3).

Específicamente, los objetivos particulares de este trabajo están organizados de acuerdo a cada etapa del análisis del riesgo por PRM.

De esta forma, este trabajo cuenta con casi cinco años de investigación (2013-2018) en donde se elabora un inventario de PRM como punto de partida. Este registro cuenta con expresión cartográfica y una matriz de datos. El inventario es el primer paso para el análisis de la amenaza, la vulnerabilidad y el riesgo (conceptos que serán ampliamente explicados en el primer capítulo de esta tesis). De esta forma, el primer objetivo particular consiste en aplicar una metodología y herramientas acordes para la elaboración de inventarios de PRM en las condiciones particulares de nuestro país.

El segundo objetivo es determinar la susceptibilidad (componente de la amenaza) por PRM a partir de métodos estadísticos, aprovechando el insumo de los inventarios de PRM elaborados. En este sentido hay que decir que se consiguió mejorar una serie de modelos estadísticos para la estimación de la susceptibilidad por PRM (Capítulo V).

El tercer objetivo particular consiste en explorar y aplicar una metodología útil para la estimación de la amenaza y vulnerabilidad por PRM. Esta es quizás la parte más compleja de este trabajo y en los capítulos correspondientes a esta cuestión se discuten y exponen algunas de las dificultades, subjetividades y carencias que existen en nuestro país para lograr una aceptable estimación de la vulnerabilidad.

Es necesario aclarar que la estructura de esta tesis se presenta en forma de cinco artículos publicados en revistas académicas indexadas en la Web of Science, por lo que cada capítulo corresponde no solo a un objetivo particular de este trabajo, sino a un artículo ya publicado. Lo anterior representó una gran ventaja: el que la información aquí presentada fuera sometida a un riguroso proceso de evaluación por

expertos en cada uno de los temas. Solo el capítulo I, el correspondiente al marco teórico, no fue publicado como artículo científico. En los capítulos II, III, IV, V y VI, se mantiene el idioma original en el que fueron publicados esos textos, en todos los casos nos referimos al idioma inglés.

Esta investigación se realiza en dos territorios, ambos localizados en la Sierra Norte de Puebla, en los límites entre la región fisiográfica del Eje Neo-volcánico Transversal y la Sierra Madre Oriental, en el centro de México (Fig. 4).

La primera es la zona Teziutlán-Chignautla (Fig. 5) y la segunda es la zona de Pahuatlán (Fig. 6). Aunque están localizados en la misma Región Fisiográfica, presentan características físicas y sociales distintas. En cada uno de los capítulos se describen las características particulares de cada una de estas zonas.

De esta forma, la estructura de esta investigación es la siguiente:

- En el capítulo I se revisan los fundamentos teóricos indispensables para el estudio del riesgo, la amenaza y la vulnerabilidad por amenazas de origen natural. Se comienza por establecer cuál es la base de los distintos enfoques generales que actualmente prevalecen para el estudio de los conceptos mencionados, entendiendo que la búsqueda de un nuevo enfoque está todavía en construcción teórica y práctica. Se destaca que más allá de descartar un enfoque u otro, lo que parece más oportuno es tomar en cuenta las distintas perspectivas para la construcción de un enfoque más efectivo.

  Posteriormente se mencionan las diferentes técnicas y herramientas que han sido utilizadas para el estudio de la amenaza y la vulnerabilidad, tanto de manera general como en específico de los PRM. A ese respecto se presenta un resumen del estado del arte de estos aspectos, el cuál es mucho más extenso en relación a la amenaza (en específico estudios de susceptibilidad) que a la determinación de la vulnerabilidad. A pesar de esta revisión inicial de conceptos, en la introducción de cada capítulo se retoma la revisión teórica de cada aspecto técnico a tratar en cada apartado.

- En el capítulo II se hace referencia a la percepción remota, en este caso particular las imágenes satelitales de muy alta resolución (pixel menor a 3m) y que pueden utilizarse para generar estereoscopia (ilusión de ver en 3D). Estos recursos son utilizados para identificar los distintos tipos de procesos de remoción en masa presentes en el terreno. De manera general, el compendio, organización y análisis de esos datos es lo que se conoce como un inventario de procesos de remoción en masa, insumo primordial para el reconocimiento de la amenaza e incluso de la vulnerabilidad. El artículo en el que se trata este tema fue publicado en la revista

*Landslides*©, lleva por título "*Satellite stereoscopic pair images of very high resolution to build landslide inventory in Pahuatlán, Puebla*".



***Figura 4***. *Localización de Pahuatlán y Teziutlán.*

- En el Capítulo III, cuyo artículo publicado se titula "*Landslide inventory map of the municipality of Teziutlán, Puebla, México (1942-2015)*", se aborda de manera detallada la descripción espacial de la distribución de PRM ocurridos en la zona Teziutlán-Chignautla durante el periodo 1942-2015, además de la construcción de un inventario multitemporal para esta zona (el inventario del Capítulo II corresponde a la zona de Pahuatlán y no es un inventario multitemporal completo). En el capítulo referido se explica qué es y porqué es mejor un inventario multitemporal. Aunque ambas zonas de aplicación están localizadas en el mismo sistema montañoso las condiciones físicas y sociales son distintas, por lo que la construcción de ambos inventarios de PRM conllevó distintos desafíos en cada una de estas zonas. Como parte de los Anexos de la tesis, se presenta el mapa de inventario publicado junto con el artículo en la revista *Jornal of Maps*©, al final de esta tesis (Anexo 5).

Aire Libre

San Juan Acateno

Mexcalcuautla

San Diego

Atoluca

San Sebastian

Huehueymico

3ª Sección

Primera Sección

Ayotzingo

Valle Dorado

Foviste

Las Moraledas

Tlacopan

Arboledas de San Rafael

Cipreses

Chignautla
(2.660)

Las Camelias

Chignaulingo

Coyotzingo

Taxcalá

El Calvario

Ixtlahuaca

Cuarta

La Aurora

Teziutlán

Chignautla

Linda Vista

Coahuixco

Juárez

Sosa

La Cofradía

Azteca

La Garita

Xoloco

San Juan Xiutetelco

San Francisco

15

*Figura 5. Cartografía de la zona Teziutlán-Chignautla.*

- En el capítulo IV se aborda la estimación de la susceptibilidad por PRM, aspecto fundamental de la amenaza y que busca responder a la interrogante de dónde ocurrirán los próximos eventos de PRM. Esto se realiza mediante la combinación de diversas técnicas y modelos estadísticos que tienen como base los datos del inventario descrito en el capítulo II. Es necesario señalar que el nivel de agregación de este análisis, consistió en unidades de ladera (*slope units*) determinadas de manera semi-automática tomando como referencia los parteaguas y cauces del terreno. En este caso el texto se publicó como capítulo de libro en la obra "*Recent Advances in Modeling Landslides and Debris Flows ©*", y lleva por título: *"Landslide susceptibility analysis and mapping using statistical multivariate techniques: Pahuatlán, Puebla, Mexico"*.

- En el Capítulo V se retoma nuevamente la susceptibilidad, ahora en el área de Teziutlán-Chignautla, pero utilizando una unidad de agregación diferente: pixeles. Este cambio genera toda una nueva serie de consideraciones que varían con respecto al análisis basado en unidades de ladera. En el capítulo se realiza una comparación entre delimitaciones espaciales distintas así como de resoluciones diferentes (distinto tamaño de pixel). Los resultados de este análisis no son solo los mapas de susceptibilidad sino la discusión entre cuál es el mejor resultado obtenido y qué factores hay que tomar en cuenta para mejorar este tipo de trabajos. Finalmente, este texto se publicó en la revista *Journal of Mountain Science©* en el año 2018 y tuvo como valor agregado el haber sido realizado utilizando únicamente software libre. Dicho artículo se titula: *"Landslide susceptibility: a statistically-based assessment on a depositional pyroclastic ramp"*.

- En el capítulo VI se abordan los temas de la vulnerabilidad y el riesgo, aunque este último se advierte que es solo un acercamiento inicial pues hace falta un considerable avance para una estimación más precisa. Se describen los obstáculos que se encontraron para dicha estimación y la incertidumbre y alcance de esa información. Al final del capítulo no se pretende dar una evaluación definitiva al problema, más bien se establece la dirección a continuar para poder mejorar el diseño y la aplicación de los métodos seleccionados. El texto correspondiente a este capítulo fue publicado en la revista *Journal of Mountain Science ©* y lleva por título: *"Hazard and population vulnerability analysis: a step towards landslide risk assessment"*.

- Finalmente se presentan las conclusiones, esperando que en un futuro se pueda continuar con la investigación en este campo, ampliando y mejorando los métodos y herramientas propuestos en esta tesis. Así mismo una serie de Anexos con información complementaria.

Se debe aclarar que cada capítulo, que corresponde a un artículo o apartado de libro publicado, contiene información que podría repetirse en alguna u otra de las secciones que componen esta tesis, incluyendo figuras o mapas. En sentido, se respetó en la edición de este trabajo la versión final de cada uno de los artículos, sin eliminar esta información que podría parecer redundante. Esto con el objetivo de mantener la cualidad de que cada parte pueda leerse y comprenderse de manera independiente sin forzosamente tener que revisar los otros capítulos de esta tesis. Esto último incluye las referencias bibliográficas, ubicadas al final de cada capítulo y no de manera general al final del documento de tesis.

## Referencias

Alcántara-Ayala I. (2004) Hazard assessment of rainfall induced landsliding in Mexico. Geomorphology 61, 19-40. doi:10.1016/j.geomorph.2003.11.004

Alcántara-Ayala I, Esteban-Chávez O, Parrot JF (2006) Landsliding related to land-cover change: A diachronic analysis of hillslope instability distribution in the Sierra Norte, Puebla, Mexico. CATENA 65(228): 152-165.

Alcántara-Ayala I, López-García J, Garnica RJ (2012) On the landslide event in 2010 in the monarch butterfly biosphere reserve, Angangueo, Michoacán, Mexico. Landslides.

Antinao JL, Farfán LM (2013) Occurrence of landslides during the approach of tropical cyclone Juliette (2001) to Baja California Sur, Mexico. Atmósfera 26(2): 183-208

Borja-Baeza RC, Esteban-Chávez O, Marcos-López J, Peña-Garnica RJ, Alcántara-Ayala I (2006) Slope Instability on Pyroclastic Deposits: Landslide Distribution and Risk Mapping in Zacapoaxtla, Sierra Norte de Puebla, Mexico. Journal of Mountain Science 3(1): 1~19.

Caballero L, Macias JL, García-Palomo A, Saucedo GR, Borselli L, Sarocchi D, Sánchez JM (2006) The September 8–9, 1998 Rain-Triggered Flood Events at Motozintla, Chiapas, Mexico. Natural Hazards 39, 103–126.

Capra, L., Lugo-Hubp, J., & Borselli, L. (2003). Mass movements in tropical volcanic terrains: The case of Teziutlán (Mexico). Engineering Geology, 69, 359–379. doi:10.1016/S0013-7952(03)00071-1

Chavelas Lluck F, Flores Ayala M Gómez Alvarado LA, Monroy Espinoza JL, Rosales Mejía SG (1991) Geología y Prospección Minera en el Área "Aire Libre", Municipio de Teziutlán, Puebla. Tesis Profesional, Ingeniero Geólogo, Facultad de Ingeniería, UNAM. p 91.

Crozier MJ (2005) Management frameworks for landslie hazard and risk: issues and options. In: Glade T, Anderson MG and Crozier MJ (eds.) Landslide risk assessment. John Wiley, 331-350.

Gaidzika K, Ramírez-Herrera MT, Bunnb M, Leshchinskyc BA, Olsenb M, Regmi N (2017) Landslide manual and automated inventories, and susceptibility mapping using LIDAR in the forested mountains of Guerrero, Mexico. Geomatics, natural hazards and risk 8(2): 1054–1079.

Hernández-Madrigal V, Mora-Chaparro J, Garduño-Monroy V (2011) Large block slide at San Juan Grijalva, Northwest Chiapas, Mexico. Landslides 8:109–115 DOI 10.1007/s10346-010-0212-1

INEGI (2002) Sistema de Cuentas nacionales 1997-2002. INEGI. México.

Lugo-Hubp J, Zamorano-Orozco JJ, Capra L, Inbar M, Alcántara-Ayala I (2005). Los procesos de remoción en masa en la Sierra Norte de Puebla, octubre 1999; causas y efectos. Revista Mexicana de Ciencias Geológicas, 22(2) ,212–228.

Oliva González AO, Mascareño Jiménez D, Alvarez Garcia IN, González Nicieza C, Álvarez Vigil E (2014) Hillside instability in the Tijuana metropolitan area. Analysis of landslide-provoked building collapse. Engineering Failure Analysis 46, 166-178.

Padilla-Lozoya R (2007) Huracanes en el estado de Colima 1573-1999. Memorias en extenso VI congreso internacional y XII nacional de ciencias ambientales, p. 6. https://www.scribd.com/doc/6492333/Huracanes-en-el-estado-de-Colima-1573-1999-ocurrencia-del-riesgo-por-fenomeno-hidrometeorologico#

# Capítulo I. MARCO TEÓRICO

## 1.1 El riesgo de desastre

La forma en que actualmente concebimos, asimilamos y actuamos ante los desastres de origen natural y los riesgos, mantiene una relación directa con la forma en cómo nos posicionamos en el mundo. Es decir, la identidad que asumimos, de manera individual y como sociedad, frente al hecho de la existencia.

En este apartado se realiza una exposición sucinta de los diferentes enfoques y conceptos bajo los que se han asumido los riesgos y desastres de origen natural. En un principio, las amenazas de origen natural y sus consecuencias eran consideradas como actos de un poder divino y, por lo tanto, incontrolables desde el punto de vista material, en concordancia con una identidad relacional con el medio natural. Actualmente, la civilización moderna occidental y capitalista (CMOC) ha actuado frente a los desastres de origen natural desde la visión de una identidad individual que considera que todo lo puede conocer y controlar; esto es la base de la visión *fisicalista* de los desastres (Hewitt 1983). Esta visión ha fallado en gran medida y está siendo parcialmente complementada por una postura surgida desde las críticas a la Modernidad (nos referimos a la Modernidad como el periodo iniciado después de la Edad Media). Esta postura, comúnmente llamada alternativa o estructuralista, aún está en desarrollo. Lejos de significar un retroceso o una filiación con el pasado remoto, el nuevo enfoque busca tomar en cuenta otros puntos de vista que se relacionan con lo social y con una relación responsable con el medio natural. El postulado que lo define habla por sí mismo: los desastres no son naturales.

### 1.1.1 La identidad relacional y su modo de explicar los desastres

Tomando como referencia a Childe (1986), los seres humanos comenzamos a poblar el mundo hace aproximadamente 600,000 años y tan solo hace 15,000 años se pudo establecer que había seres humanos viviendo en cada región de los cinco continentes. En ese tiempo el género humano ha experimentado eventos de tal magnitud que afectaron a la vida y al ambiente, ya sea a nivel local, regional o incluso global. En la Tabla 1 del **Anexo 1** de esta tesis se muestra un compendio de algunos de estos eventos.

¿De qué forma las sociedades anteriores al periodo que llamamos Modernidad interpretaban los eventos que hoy llamamos desastres naturales? No existen evidencias arqueológicas, datos o registros suficientes para esbozar un marco completo al respecto, pero el análisis del concepto de identidad puede dar algunas claves.

El concepto de identidad establece relaciones de comparación entre personas o cosas. Además, es un proceso (como ser o llegar a ser) que se define como el establecimiento sistemático y la significación entre individuos y entre colectividades, de relaciones de similitud o diferencia (Jenkins 1996).

No hay identidades naturales o innatas, por tanto, el concepto implica, en principio, la identificación de cada nuevo ser humano que nace con los seres humanos que le rodean (progenitores, familia, grupo social) y por consecuencia la identidad se construye de manera social o cultural (Hernando 2002). Al mismo tiempo, la identidad permite una "negociación" con la realidad y con una forma de estar y de supervivencia efectiva dentro de esta (Hernando 2002).

Hernando (2002) apunta que la identidad es el principal recurso de los seres humanos para generar la imprescindible sensación de seguridad que nos hace posible tomar decisiones ante la complejidad del mundo en que habitamos. Esto es así porque mediante este concepto se desarrollan mecanismos cognitivos que nos permiten tener la sensación de que tenemos cierto control sobre la realidad (más allá de si esa sensación sea real o no).

Por otra parte, los seres humanos tenemos dos modos fundamentales de representar la realidad: la metonimia y la metáfora (Olson 1994). En la metonimia la representación de lo real se simboliza con elementos contiguos o de causa y efecto (por ejemplo: "se vino el cerro" para referirse a un proceso de remoción en masa).

En cambio, en la metáfora la representación y el signo que se usan para representar la realidad son cosas diferentes a esta (la escritura, el discurso científico, son ejemplos de metáfora).

Para explicar las amenazas naturales cuyo mecanismo ha sido parcialmente descifrado se utiliza la metáfora y, al contrario, se utilizará la metonimia para aquellas que no han logrado ser explicadas conforme a una lógica causal independiente de los humanos. Cuando un fenómeno natural se representa a través de la metonimia generalmente inspira temor y se le atribuirá la lógica del comportamiento humano. De esta manera habrá ríos con furia, volcanes enfadados o huracanes asesinos. Las explicaciones metonímicas se construyen generalmente desde la identidad relacional.

En las sociedades donde existe la identidad relacional el grupo humano no representa amenaza alguna pues no hay competencia (se tiene un modo de organización comunitaria), de esta forma, la identidad última se deposita en el grupo, pues no existe el "yo". Esto se representa en la apariencia común de todos los miembros del grupo en una indisociable vinculación entre el cuerpo y la identidad (vestimenta, perforaciones, tatuajes, modo de llevar el cabello) (Moragón 2013; Hernando 2015). También se personifica en la forma en cómo se hacen las cosas: cómo se caza, cómo se pesca, cómo se cultiva (González Ruibal et al, 2011; Ong 1996; Havelock 1996). Se es siendo y no pensando en lo que se es (Hernando 2015). Esta postura es lo contrario al *cogito ergo sum* ("pienso luego existo").

En este tipo de identidad relacional, se tienen pocos recursos para mejorar la situación frente a las amenazas naturales salvo la oración, la corrección de la conducta moral y la asistencia mutua después de un evento de desastre (Oliver-Smith *et al.* 2016).

Es tentador asignar este tipo de identidad relacional a todos los grupos de cazadores-recolectores y a las primeras sociedades agrícolas de la historia en cualquiera de los continentes. Sin embargo, no es fácil asumir que esta identidad está todavía presente en la civilización moderna occidental y capitalista (CMOC). Oliver-Smith et al (2016) menciona que las viejas narrativas para explicar los desastres no han sido sustituidas por otras nuevas, sino que se han acumulado como parte de la narrativa en curso; por lo tanto, lo que existe es una tipología de las cusas del desastre en evolución constante.

Finalmente, más arriba se mencionó que el sentido de pertenencia a un grupo es fundamental para la confianza y para afrontar la complejidad del mundo que se habita, esto es algo que no elimina el otro tipo de identidad que se contrapone a la identidad relacional y que a continuación se describe: la identidad individual.

### 1.1.2 La identidad individual y los desastres en la Modernidad

Hay que advertir que el surgimiento y desarrollo de la identidad individual no responde a una lógica diacrónica que transita de estados de salvajismo o barbarie a estados de civilización pues la Historia no es un relato de éxito moral, sino que es un intrincado conjunto de relaciones temporales y espaciales, relaciones cambiantes y cambiables (Wolff 2000). Por lo tanto, el cambio de explicar las amenazas naturales de manera metonímica a una forma metafórica y científica, no necesariamente significó un "triunfo" y control sobre estas, tampoco se puede considerar que las sociedades anteriores y asociadas a la identidad relacional eran primitivas o atrasadas solo por eso.

La especialización del trabajo en las sociedades más complejas incrementó el control material del medio natural (Hernando 2002). Este control relativo de un fenómeno de la naturaleza permite explicar la lógica que lo gobierna (modo metafórico). De acuerdo a Amin (1989) existía en estas civilizaciones antes de la Modernidad una práctica empírica científica (modo metafórico) en la agricultura, la crianza de ganado, la navegación, la construcción y la producción artesanal; pero no un pensamiento científico todavía.

Por otra parte, la especialización de funciones dentro de una sociedad generó que cada uno de los distintos individuos ocuparan posiciones e interacciones distintas dentro de esa sociedad configurando jerarquías religiosas, sociales y políticas. Así, comienza a aparecer la sensación del "yo" interno, diferenciado no solo del resto de los individuos del grupo sino también del medio natural (Elias 1990). Esta consciencia del "yo interno" diferente al "mundo exterior" implica asumir que este último no se

comporta de manera igual al ser humano sino que tiene una lógica propia (Hernando 2002). Por ello, para explicar dichos fenómenos naturales se crearon abstracciones.

La distancia emocional que impone la identidad individual sobre el medio natural permite una sensación de poder controlar los fenómenos naturales. Tan solo, describir y explicar estos fenómenos a través de una herramienta de abstracción como lo es la escritura, implica ya un modo de distanciamiento con esa naturaleza, estableciendo así, una relación racional con esta (Hernando 2015). Esto será una sensación primordial respecto a las amenazas de origen natural durante el nacimiento y desarrollo de la CMOC, donde la abundancia de explicaciones lógicas y el control de los fenómenos naturales mediante la tecnología afianzarán esta impresión.

La Modernidad comenzó hace aproximadamente 500 años, Dussel (2006) localiza el comienzo en 1492, pero por ejemplo Toulmin (1992) lo ubica en el año 1436, el año de la imprenta de Gutemberg) y no solo significó el comienzo del capitalismo, del colonialismo y del eurocentrismo, sino que fue el comienzo de un tipo de civilización: el de la civilización occidental moderna capitalista (CMOC). Es un acontecimiento mundial-global cuya esencia es la "colonialidad", un patrón de dominación originado en el colonialismo europeo del siglo XVI (Quijano 1992; Quintero 2010; Erazo Pantoja y Erazo Pantoja 2015).

De lo único que se puede estar seguro en este mundo es de la existencia de la propia mente (solipsismo), dice Descartes (Descartes 2010). Es aquí que nace el concepto del individuo como persona (Mauss 1991, Weintraub 1993) y este sujeto pensante, racional, matemático, no ve necesaria la mediación en un sujeto que reconozca la condición de viviente y sufriente del otro (Gandarilla Salgado 2012), o de lo otro, en el caso del medio natural. En resumen, el *ego cogito* de Descartes situaría a todo lo colonizado, humano o no humano, como *entes* a disposición del hombre. Este paradigma llamado solipsista será reproducido y retomado por Spinoza, Leibniz, Hume, Kant, Hegel y hasta Sastre.

Además, la postura afianzada desde Descartes se ocupará de buscar la regularidad de las leyes que gobiernan no solo el cuerpo humano sino de toda la naturaleza (Gandarilla Salgado 2012). En el Discurso del Método, Descartes (2010), propone que para llegar a conocer el todo se debe primero conocer las cosas más simples y luego ya, en un segundo momento, establecer correlaciones y extrapolaciones para el conocimiento de lo más complicado (Descartes 2010). El resultado de este procedimiento fue el florecimiento de especialidades y disciplinas en todos los campos de conocimiento de su tiempo (Gandarilla Salgado 2012) que a su vez sería una de las bases de la llamada revolución científica de los siglos posteriores.

Con esta nueva concepción aparecen nuevas ideas como: todo en la naturaleza tiene una causa y un efecto, es el principio de causalidad por el cuál es posible entender el origen de todas las cosas (Kant

2003). Y de hecho, los constantes avances de las ciencias parecían dar razón y entusiasmo de que en realidad, todo podría ser entendido y por lo tanto, dominado.

En el marco específico de los desastres de origen natural, durante la Revolución industrial, científica y tecnológica de los siglos XVIII y XIX, comenzaron a estudiarse los fenómenos naturales, realizando mediciones, tratando de entender su mecanismo y registro detallado de todas las investigaciones (Smith 1991). Así, se empezaron a entender las causas, los periodos de recurrencia y la magnitud de algunos fenómenos naturales, aspectos fundamentales para el enfoque *fisicalista*.

Un evento clave en este desarrollo fue el terremoto (y tsunami) de Lisboa del 1 de noviembre de 1755. Este desastre no solo causó la muerte de más de treinta mil personas y desencadenó por primera vez la respuesta de un gobierno ante un desastre, en este caso del reino del Portugal; también generó una discusión teológico-filosófica entre los círculos de intelectuales de la época, sobre la naturaleza de la catástrofe. Incluso, esta discusión contempló entre las casusas del desastre las condiciones sociales de la población en Lisboa (Toscana-Aparicio 2006).

Posteriormente, a principios del siglo XX sucedieron eventos como el paso del huracán de Galvestone en 1900 (Blake 2011), la erupción del Monte Pelee en Martinica en 1901 (Sigurdsson 2015), el terremoto de San Francisco de 1906 (Siodla 2017), la gran inundación del Río Amarillo de 1931 y de 1936 (Fucheng *et al.* 1987) que generaron cambios en cuanto a la aplicación de la ciencia y la ingeniería para mitigar futuros eventos como estos (una lista más completa de eventos de desastre se muestra en la Tabla 2 del **Anexo 1** de esta tesis). Se construyeron rompeolas, diques, se crearon sistemas de alarma y se procuró que las nuevas construcciones fueran más resistentes a los peligros (Smith 1991). En algunos casos esto funcionó, pero en otros el despliegue tecnológico solo creó un falso sentido de confianza que derivó, entre otras cosas, en el poblamiento de zonas de riesgo (Oliver-Smith *et al.* 2016).

En este contexto de revolución científica y tecnológica, a finales del siglo XIX la Geografía se encontraba estancada como instrumento de dominación en las sociedades geográficas de cada país, o anclada a las universidades bajo una visión naturalista y utilitaria (Moreira 2009). Fue durante el comienzo de la Revolución Digital de la segunda mitad del siglo XX que la geografía adoptó el enfoque de la llamada *new geography*: explicar el espacio a través de patrones que expresan modelos matemáticos (Moreira 2009). De esta forma, la matemática, los modelos cuantitativos y la computadora se convirtieron en herramientas útiles para el estudio de las amenazas naturales desde la geografía y la geomorfología, adhiriéndose así al enfoque *fisicalista*.

Pero, ¿qué es el enfoque fisicalista específicamente? Hewitt (1983) apunta tres características fundamentales: (i) se asume que por medio de obras ingenieriles las amenazas naturales serán

contenidas; (ii) el monitoreo de estas y su explicación científica, permitirán modelar y predecirlas; (iii) se da prioridad a la atención de la emergencia en lugar de la prevención.

En contraste con las explicaciones técnicas y cuantitativas, las sociedades coloniales que sobrevivieron a la conquista europea y que mantenían una marcada identidad relacional con su medio natural, fueron calificadas como primitivas o atrasadas. La Modernidad, ya fuera secularista, católica o protestante, negó el valor de las religiones no cristianas, y destruyó el núcleo mismo del conocimiento y sentido de vida de las sociedades no europeas (Dussel 2003). La historia oficial omitió la colectividad social y borró las leyes de convivencia, algunas de las cuales perviven trasformadas por los cambios que se produjeron durante cinco siglos en las tradiciones, las costumbres y memorias colectivas (Gargallo 2015). El conocimiento milenario de estas sociedades se fragmentó, situación que dificultó su relación con su propio medio natural y los desastres. El paradigma *fisicalista* apuntó que la solución a tal problemática se daría con el simple traspaso de tecnología "anti-desastre" de los lugares más civilizados a los más "atrasados" (Smith 1991).

Lo anterior, fue cuestionado y criticado por una nueva visión de los desastres de origen natural a finales de los 60 y principios de los 70: el enfoque alternativo-estructuralista.

### 1.1.3 La crítica a la Modernidad y el enfoque alternativo-estructuralista

Las posturas críticas se centraron en gran medida en el sistema económico capitalista, predominante en la Modernidad, y sus consecuencias. El capitalismo es un sistema económico caracterizado por la propiedad privada, la competencia, la alta productividad (en menos tiempo producir más) y la explotación del trabajo (Isidro Luna 2015); ya en la práctica, dio lugar a injusticias sociales como las que describen Marx en "El Capital" (Marx 1980) y Engels en la "Situación de clase obrera en Inglaterra" (Engels 1978).

Contrariamente al capitalismo, Marx considera al ser humano como parte del medio natural y, más aún, considera que el ser humano y la naturaleza son inseparables (Marx 1980). Marx llama *fractura metabólica* a la separación del ser humano del medio natural, aspecto que es fundamental para el capitalismo (Sacristán 1984; Busqueta *et al.* 2017). Este punto de vista es contrario con el enfoque de la economía neoclásica capitalista, es por esta razón que estas ideas serían la base para la formulación de los enfoques ambientalistas críticos marxistas y anarquistas durante el siglo XX (Bellamy Foster 2000; Pierri 2001).

Específicamente en el marco de los desastres de origen natural, a principios del siglo XX, el geógrafo Gilbert White fue el primero que los analizó desde una perspectiva social (White 1936, 1945; Smith 1991). Sus trabajos e ideas surgieron durante el auge del paradigma *fisicalista*, por lo que el trabajo de

White inauguró un nuevo enfoque que consideraba las decisiones de los individuos y de la sociedad como parte de las causas de los desastres (Smith 1991).

El enfoque alternativo-estructuralista retomó el trabajo de White y fue llevado mucho más lejos por autores como Ian Davis (1981), Fred Cuny (1983); Hewitt (1983), Andrew Maskrey (1989), Terry Canon (1994), Keith Smith (1991) y Piers Blaikie (1994) entre otros. Estos autores afirmaron que los *desastres naturales* no son naturales sino socialmente construidos. El contexto histórico en el que desarrollaron este nuevo enfoque era el de la Revolución Cultural del 68, el del cambio hacía el neoliberalismo, pero principalmente el de un aumento, a partir de la década de 1970, de catástrofes de origen natural cuyos efectos eran dramáticos en los países de la periferia.

Advertían que era demasiada casualidad que las peores consecuencias tuvieran sede en países del entonces llamado tercer mundo (Smith 1991). Varios de estos autores habían vivido estos desastres de primera mano mientras se encontraban trabajando para diversos organismos internacionales, y por lo tanto se habían dado cuenta de cómo las condiciones sociales incrementaban la tragedia hasta situaciones indignantes (Smith 1991).

La revisión de los textos del marxismo y los estructuralistas fue inevitable en ese contexto, no así los métodos de los países del entonces bloque socialista que no eran muy diferentes a como el resto de los países trataban la problemática de los desastres.

La influencia del movimiento ambientalista reconsideraba la posición del ser humano ante el medio natural, por ejemplo, el concepto de internacionalización del capital fue retomado por la teoría marxista de la Dependencia sostenida entre otros por Ruy Mauro Marini (Mauro Marini 1991) que explicaba las desigualdades entre los países capitalistas centrales y los países de las periferias. Aunque esta teoría sería criticada por otras posturas y por los marxistas mismos, la idea sería clave para el movimiento ambientalista de 1968 y para las primeras obras del enfoque alternativo-estructuralista de los desastres en sus explicaciones de las "causas de fondo", estructurales, fundamentales o subyacentes de los mismos durante las siguientes dos décadas (Blaikie *et al.* 1994; Smith 1991).

De esta manera, nuevos autores exploraron más fondo las causas de los desastres desde un punto de vista crítico (Oliver-Smith *et al.* 2016). En esta nueva construcción de conocimiento, conceptos como el de vulnerabilidad, exposición o resiliencia, se convirtieron en fuertes variables explicativas (Smith 1991; Oliver Smith 2016). Esto llevó al análisis de las causas de fondo de los desastres (Oliver-Smith *et al.* 2017) desde perspectivas más cercanas al sistema-mundo de Wallerstein, la internacionalización del capital o el propuesto por la teoría de la Dependencia marxista.

Lo anterior implicó, tomar en cuenta el contexto donde la población vive su día a día. De esta forma, variables como la clase social, el género, el nivel de ingreso, la educación, la ocupación, la casta, la

etnicidad, la salud, la edad y el estatus de migración fueron integradas al análisis de los riesgos (Hufshmidt y Glade 2010). A su vez, significó también entender el porqué de las grandes desigualdades existentes entre los afectados o no por los desastres.

El nuevo enfoque comenzó a enseñarse en las universidades y para la década del 2000 había comenzado a permear fuertemente en los esfuerzos de los organismos internacionales encargados de la reducción de riesgos de desastre.

### 1.1.4 El modelo de liberación y presión (PAR).

Desde el enfoque alternativo-estructuralista los desastres son cambios identificables en el tiempo y el espacio en los que el sistema humano se ve afectado en su funcionamiento normal. Cuando el sistema humano no es flexible y no puede absorber dichos cambios aparece la crisis, esta acarrea daños y surge el desastre (Wilches-Chaux, 1993).

Por sistema humano se entiende a las personas que lo conforman, pero también a los aspectos tangibles: sus edificaciones públicas y privadas, vías y medios de comunicación, servicios públicos, toda la infraestructura física; pero también a los aspectos no tangibles como la forma de organización, las instituciones, la religión, el estado, las leyes, las tradiciones, el sistema económico, la ciencia, la historia y la cultura (Murillo-García 2013).

El desastre nace de la relación entre una (o más de una) amenaza natural (*natural hazard* en inglés) y un determinado número de personas cuya condición de vulnerabilidad varía dependiendo de la amenaza específica y su nivel de exposición (*exposure* en inglés) a la misma (Cuny, 1983; Blaikie *et al.* 1994; Wisner *et al.* 2003). De esta forma hay tres elementos en relación constante: riesgo ($R$) (desastre si se expresa en la realidad), vulnerabilidad ($V$) y amenaza ($A$):

$$R = A \; X \; V$$

Al hablar de desastre siempre hay un daño y un impacto implícitos. En ese sentido el daño se define como el cálculo de la pérdida de: vidas, económicas, de infraestructura y equipamiento o del medio natural. El concepto de impacto es más amplio y abarca no sólo el daño sino todo tipo de consecuencias. Es difícil pensar que un desastre puede traer consigo aspectos positivos para una sociedad, pero si es posible (Cardona, 1993). El impacto es medido por una serie de variables éticas, objetivas y verificables como la mortalidad, la morbilidad, el daño a propiedad e infraestructura, disminución de la capacidad de ahorro de la población (Wisner *et al.* 2003).

No existe un consenso universal sobre lo que el término desastre incluye. Es problemático basarse en las cifras de muertos, desaparecidos, afectados o desplazados pues existen eventos que solo ocasionan una baja cifra de muertos y heridos a nivel local pero que pueden tener efectos severos a largo plazo en la población afectada (Wisner *et al.* 2003).

Luego de que ocurre un desastre sucede la etapa de la emergencia, que es a la que ponen atención los medios de comunicación y los gobiernos en general. Al ser una etapa que rompe con la normalidad de una sociedad la rutina se interrumpe, lo cual afecta a la economía, además es en esta etapa en dónde la relación entre la sociedad y su gobierno pueden afianzarse o romperse (Macías 1993). Posteriormente, pasadas una semanas puede hablarse del periodo de retorno a la normalidad, aunque esto es subjetivo y en ocasiones no es algo que suceda ya que como menciona Wisner *et al.* (2003) en algunos lugares la recuperación nunca llega y al contrario, el daño del último desastre se suma a la condiciones de vulnerabilidad de la población para enfrentar el siguiente peligro.

Uno de los modelos surgidos a partir de la visión alternativa-estructuralista fue el modelo de liberación y presión. El modelo de liberación y presión (PAR por sus siglas en inglés) (Wisner *et al.* 2003) combina los conceptos de desastre, amenaza y vulnerabilidad (Fig. 7). Los desastres ocurren, según el modelo PAR, por la convergencia entre las llamadas causas de fondo, las condiciones inseguras de la población y un peligro (Wisner *et al.* 2003). El modelo trata el desastre como el punto de crisis cuyo resultado es el daño que existe cuando las personas son incapaces de hacer frente a la magnitud o intensidad de un fenómeno (Oliver-Smith *et al.* 2016).

Las amenazas, junto con las condiciones imperantes de exposición, vulnerabilidad y resiliencia, causan el riesgo, que si se convierte en realidad se expresará como un desastre. En la Fig. 7 se muestra el esquema propuesto por Blaikie *et al.* (1994) y actualizado por Wisner *et al.* (2003). En el esquema, la vulnerabilidad está representada por tres aspectos interconectados en el proceso que conduce a un desastre: causas de fondo, presiones dinámicas y condiciones inseguras (Wisner *et al.* 2003).

Las causas de fondo consisten en contradicciones económicas, demográficas y políticas (ideológicas por consiguiente) en conflicto dentro de las estructuras de los sistemas socio-culturales (Wisner *et al.* 2003; Oliver-Smith *et al.* 2016). Es decir, la desigual distribución de la riqueza, la pobreza y las diversas formas culturales con que los pueblos viven en el mundo. Las causas de fondo también reflejan el ejercicio y la distribución del poder en una sociedad (Wisner *et al.* 2003) y aquí se incluye no solo la pobreza sino relaciones de casta, etnia, de color de piel, de movilidad, de edad y de género. Lo anterior implica un acceso diferenciado a ingresos, derechos y recursos en una sociedad.

*Figura 7. Modelo de presión y liberación, elaborado con base en Wisner et al. 2003.*

En las causas de fondo es también donde encontramos el concepto de identidad que se ha esbozado en este capítulo. De esta forma, estas causas serían aquellos aspectos que al mismo tiempo definen a nuestra civilización. Por ello, no basta cambiar un solo campo de este conjunto como el sistema económico, aunque sin duda, la sustitución de un sistema económico que tiene como fin último la tasa de ganancia por sobre todo lo demás, incluyendo la vida y dignidad humanas, por otro que tenga a la vida en el centro, probablemente aportaría a la reducción de las causas de fondo. Lo anterior, sin embargo, implicaría ya un cambio en la identidad.

Las causas de fondo conducen a un trastorno funcional interno del sistema, equivalente a las presiones dinámicas dentro del modelo PAR (Oliver-Smith *et al.* 2016). Por ejemplo, la falta de inversión por parte del gobierno en planes y programas para prevenir desastres, epidemias, rápida urbanización y el proceso de migración rural-urbano (cinturones de pobreza de las ciudades), guerras y conflictos armados, deuda externa o pública impagable, y la degradación de los recursos naturales como el bosque, los suelos y las fuentes de agua (Wisner *et al.* 2003).

Wisner *et al.* (2003) actualizaron el modelo PAR hace ya casi dos décadas y desde entonces, en el mundo se han revelado procesos que pueden ser clasificados como Presiones Dinámicas. Por ejemplo, las crisis económicas generadas por burbujas económicas y especulación, además de la transformación de las actividades del crimen organizado. Aunque en el año 2003 la corrupción ya era un componente importante en la organización política-económica y social de varios Estados, multinacionales y sociedades en el mundo, esta destacó luego de las crisis económicas de los años 90 y la del 2007. En México, la corrupción y el narcotráfico (que derivó pronto en un crimen organizado de actividades diversificadas como el secuestro o la trata de personas), representan hoy en día presiones dinámicas.

Estas presiones dinámicas derivan en una serie de condiciones de inseguridad para la población que son formas específicas en las que la vulnerabilidad se expresa en el tiempo y el espacio (Wisner *et al.* 2003). Son síntomas o señales de alerta que determinan las condiciones del momento (Oliver-Smith *et al.* 2016) y que incluyen aspectos tangibles como las condiciones de las construcciones, la infraestructura, la agricultura y los recursos con los que cuenta una población, así como aspectos intangibles como las redes de apoyo, el conocimiento de las amenazas o la capacidad para sobreponerse a situaciones de crisis (Wisner *et al.* 2003).

Finalmente, en el extremo contrario del modelo PAR se representan los peligros y la amenaza. Las amenazas, cuando se materializan en un evento físico concreto, pueden desencadenar una escalada de condiciones inseguras, un estado de crisis o una emergencia (Oliver-Smith *et al.* 2016). Así, cuando una población vulnerable se encuentra ante un peligro, se considera que está en riesgo, si el riesgo se hace realidad, hablamos de la ocurrencia de un desastre.

El concepto de amenaza está directamente relacionado con los fenómenos naturales (y algunos aspectos sociales) y con otro término que comúnmente se utiliza como sinónimo: el peligro. Hay fenómenos naturales o aspectos sociales que por su magnitud, recurrencia o lo inesperado de su ocurrencia pueden causar daños al sistema humano, este tipo de fenómenos naturales son lo que se llama un peligro. Cuándo la ocurrencia de un peligro pasa de la mera posibilidad a una probabilidad muy concreta entonces surge el concepto de amenaza (Wilches-Chaux 1998). Entonces como el concepto de amenaza y el de peligro son distintos, la amenaza implica una probabilidad de ocurrencia y el peligro está más enfocado al fenómeno natural y sus características; así mismo, su expresión cartográfica también es distinta (Murillo-García 2013).

Hay distintos tipos de amenaza y los procesos de remoción en masa son una de ellas. En el siguiente esquema (Fig. 8) se muestra una clasificación de amenazas.

En la Figura 8 los procesos de remoción en masa están en dos sitios distintos de la clasificación, ya que pueden tener un origen completamente natural o ser la combinación entre procesos naturales y antrópicos. Esto es así porque las amenazas socio-naturales se expresan a través de fenómenos que parecen ser producto de la dinámica de la naturaleza, pero que su ocurrencia o agudización de sus efectos interviene la acción humana (Wilches-Chaux 1998; Oliver-Smith *et al.* 2016).
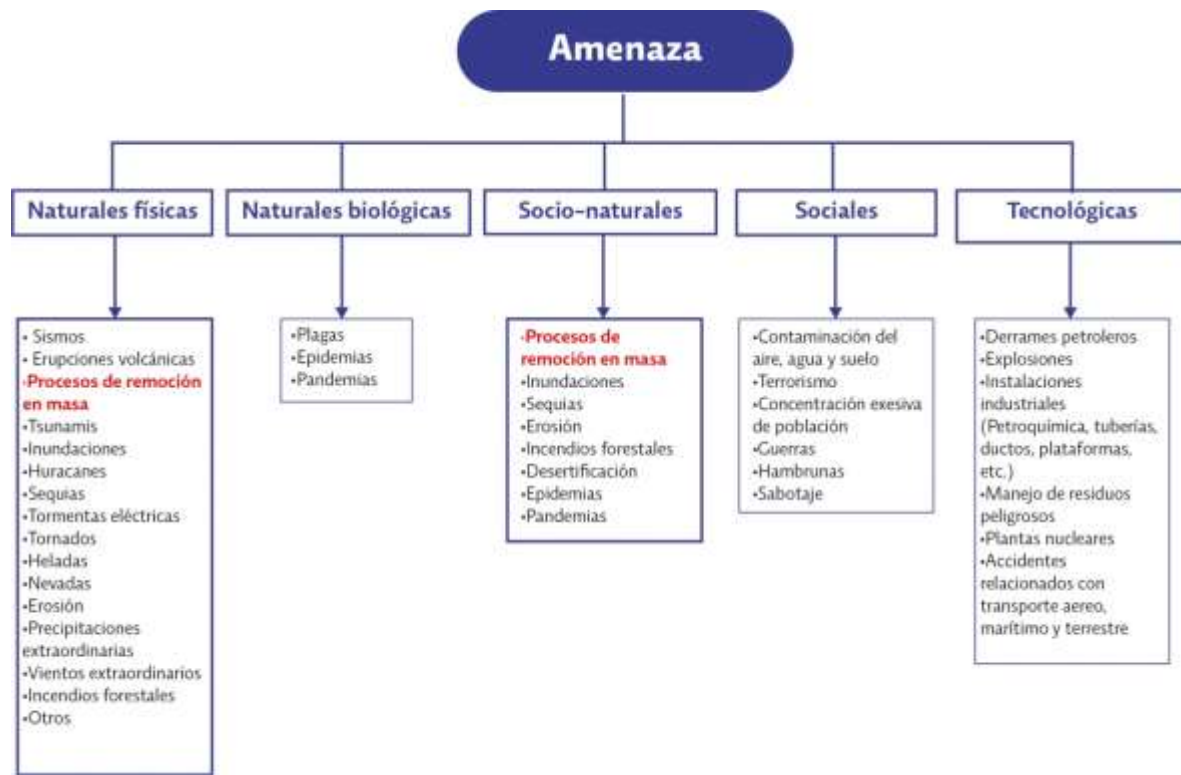
*Figura 8. Clasificación de las amenazas (Murillo-García 2013).*

### 1.1.5 La vulnerabilidad

El concepto de vulnerabilidad, principal aporte del enfoque alternativo-estructuralista, es eminentemente social y se relacionada con la susceptibilidad de sufrir daño y tener dificultad o incapacidad para recuperarse de ello (Maskrey, 1993).

La vulnerabilidad ha sido abordada desde diferentes perspectivas y no existe un consenso en la definición de la misma por lo que diferentes enfoques han trabajado sobre su propia definición (Birkmann *et al.* 2013). Varias razones explican esta heterogeneidad, en primer lugar no existe una metodología uniforme y muchos valores se dan por sentados, además, numerosos estudios se basan en observaciones empíricas. En segundo lugar, es un concepto que depende de la escala y por lo tanto es dinámico ya que cambia a lo largo del tiempo. Por esta multidimensionalidad y diferencialidad, es compleja y representarla cuantitativamente es difícil (Crozier y Glade 2004).

Básicamente, los diferentes enfoques se podrían agrupar en dos grandes conglomerados: aquellos que entienden la vulnerabilidad relacionada con la fragilidad y la capacidad de recuperación de las comunidades ante las amenazas, y aquellos enfoques que parten de la cuantificación de un posible grado de daño (Birkmann *et al.* 2013; Papathoma-Köhle *et al.* 2011). De forma más específica, el modelo PAR puede clasificarse como un modelo político-social (Birkmann *et al.* 2013).

Quizás el modelo que mejor expone las distintas caras de la vulnerabilidad es el propuesto por Wilches-Chaux (1998) donde la vulnerabilidad global está conformada por diferentes *vulnerabilidades* que no están aisladas entre sí: (i) natural, todos los seres humanos son vulnerables a sufrir daño por algún peligro y no existe en el planeta un lugar completamente seguro; (ii) física, se refiere a localización de un sistema humano en el contexto espacial en el que podría ocurrir una amenaza; (iii) económica; (iv) social, es el nivel de cohesión interna que posee una comunidad; (v) política; (vi) técnica; (vii), ideológica, incluye la cosmovisión, filosofía o creencias religiosas e identidad; (viii) cultural, aquí se considera la manera en que los medios de comunicación abordan los desastres; (ix) educativa; (x) ecológica; e (xi) institucional.

Por otra parte, el concepto de riesgo es complejo y en los medios de comunicación se confunde a veces con el de amenaza o peligro.

El riesgo es la probabilidad de consecuencias nocivas y pérdidas resultado de la interacción entre un peligro natural, socio-natural, social o tecnológico y situaciones de vulnerabilidad (ONU/ISDR, 2002). Más simple: es la probabilidad de que ocurra un desastre.

El riesgo y la vulnerabilidad pueden concebirse como un *continuum* no estático y el desastre como un momento específico o materialización de estas condiciones subyacentes (Birkmann *et al.* 2013). Una población puede ser vulnerable pero si no está expuesta a una amenaza no hay riesgo, por el otro lado una amenaza que no se cruza con una sociedad no representara un riesgo. Por lo tanto, se requiere que ambas condiciones estén presentes. Además, el riesgo estará relacionado con el comportamiento, organización, conocimiento y control material del medio, y la percepción del riesgo de una sociedad.

De esta forma, el riesgo dependerá en parte de la amenaza a la que esté relacionado, por ello, no es lo mismo estar en riesgo de desastre por procesos de remoción en masa que a inundaciones o a huracanes, pues en los tres casos se deberán tomar medidas distintas para mitigarlo y gestionarlo. Sin embargo, lo común es que una sociedad este expuesta a diferentes tipos de amenaza lo que hace más complejo estimar el riesgo.

Además, es importante conocer quién o qué está en riesgo. Los elementos expuestos al riesgo son distintos en cada sociedad y son todos aquellos atributos valorados por el ser humano y van desde la propia vida humana hasta las construcciones e infraestructura, los modos de producción y organización, los recursos naturales o los sitios o lugares con valor religioso o cultural (Crozier y Glade 2004).

Por otra parte, hablamos de *riesgo específico* como el grado de pérdidas esperadas debido a la ocurrencia de un evento en particular y como una función de la amenaza y la vulnerabilidad. Mientras que el "riesgo total" es la cuantificación acumulada del riesgo específico de cada uno de los sujetos o elementos expuestos.

Las sociedades no siempre son ignorantes de los riesgos a los que están expuestas, y parece contradictorio que en algunos casos la gente acepte vivir en lugares riesgosos aun conociendo las posibles consecuencias; esto es lo que se llama riesgo aceptable: un valor admisible de probabilidad de consecuencias sociales y económicas que la población está dispuesta a tomar debido a que los beneficios de permanecer en ese lugar son importantes o no tienen otra opción (Cardona, 1993).

De esta manera no sólo basta con cuantificar el riesgo (estimación del riesgo), se debe evaluar el riesgo (evaluación del riesgo) y de esta manera poder establecer los beneficios y consecuencias de estar expuesto a éste, determinado si el riesgo es tolerable, intolerable o aceptable. La implementación de medidas racionales apropiadas para la reducción del riesgo es el manejo o administración del riesgo (Crozier y Glade 2004). Como el riesgo no puede ser totalmente eliminado, no se puede hablar de eliminación del riesgo sino de mitigación del mismo, que son todas las medidas encaminadas a reducir el riesgo al que una comunidad está expuesta y que, desde el punto de vista del paradigma alternativo-estructuralista, estas acciones deben encaminarse a la reducción de la vulnerabilidad, sin desestimar las medidas ingenieriles o técnicas que puedan aplicarse a las amenazas.

El desarrollo teórico expuesto hasta ahora, es la base sobre la que se fundamentan gran cantidad de las investigaciones que tratan sobre el estudio de las amenazas, la vulnerabilidad y el riesgo. Es el mismo caso para esta investigación, en donde estos aspectos se mantienen siempre presentes para evitar una visión sesgada de la problemática, como por ejemplo, entender como estimación del riesgo resultados que únicamente se refieren a cuantificar ciertas características del peligro. Básicamente, el lugar de esta investigación en todo lo que se ha expuesto anteriormente, es el de continuar hacía la comprensión del riesgo y no solo de la amenaza, un paso en esa dirección.

## 1.2 Inestabilidad de laderas

### 1.2.1 Clasificación, tipos y atributos de los PRM

A continuación, se describirán brevemente algunos de los aspectos claves acerca de la amenaza que interesa a este trabajo: los procesos de remoción en masa. Por consenso se consideran los términos de proceso de remoción en masa, procesos de ladera, procesos gravitacionales y movimientos de ladera, correctos para referirse al fenómeno al que se hace referencia: la inestabilidad de laderas (Alcántara-Ayala 2000). En inglés es común encontrar el termino *landslides* para referirse de manera general a los PRM. Ya en 1894, Penck distinguía entre movimientos en masa y transporte en masa, identificando a la gravedad como el principal agente de remoción en masa (Hansen 1984). Actualmente se considera a los

procesos de remoción en masa como aquellos involucran el movimiento hacía debajo de los materiales que forman los declives montañosos bajo la influencia de la gravedad y sin la asistencia primordial de un transporte fluido (Alcántara 2000).

Los procesos de remoción en masa son un tipo de amenaza geológica pero su ocurrencia está relacionada con otras amenazas o fenómenos naturales tales como lluvias extraordinarias o los sismos. Estos fenómenos son llamados factores detonantes (*predisposing factors*) y por si mismos pueden representar una amenaza como es el caso de los huracanes. Los fenómenos detonantes de los procesos de remoción en masa pueden ser terremotos, huracanes u otros fenómenos atmosféricos relacionados con una alta pluviosidad, explosiones ocasionadas por el ser humano o la desestabilización de una ladera por la construcción de una carretera o camino. Además, la ocurrencia de los procesos de remoción en masa también está relacionada en ocasiones con actividades sociales tales como la deforestación, estos procesos se engloban en los llamados factores preliminares (Crozier y Glade 2004). La Fig. 9 muestra de manera teórica las diferentes etapas y amenazas relacionadas luego de la ocurrencia de un evento de procesos de remoción en masa.

| | Fenómeno detonante (Lluvia extraordinaria) | Inmediatamente después del PRM | En las primeras dos semanas | De dos semanas a un año |
|---|---|---|---|---|
| **Amenaza subsecuente** | PRM | Inundaciones, explosiones, incendios, derrames y fugas de sustancias peligrosas, más PRM. | Inundaciones, epidemias, hambrunas, contaminación del agua, suelo y aire, saqueos, sabotajes. | Erosión, hambruna, malnutrición. |
| **Consecuencias en el sistema humano** | Pérdida de vidas, destrucción del equipamiento e infraestructura, interrupción de los servicios y actividad económica, destrucción de los medios de subsistencia, pérdida de bienes. | Pérdida de vidas, destrucción del equipamiento e infraestructura, interrupción de los servicios y actividad económica, destrucción de bienes. Pérdida de suelo. | Emergencia sanitaria, interrupción del comercio y la actividad económica, falta de empleo, inseguridad, dependencia de la ayuda externa. | Descenso en la actividad económica, emigración, falta de empleo, falta de recursos, dependencia de la ayuda externa. Pérdida de los medios de subsistencia |
| **Escala** | Desde escala local hasta regional (se considera la ocurrencia de varios PRM) | Local | Local o regional | Local o regional |

*Figura 9. Amenazas asociadas a los procesos de remoción en masa. Tomada de Murillo-García 2013.*

Hay distintos tipos de PRM y diversas clasificaciones de los mismos. De acuerdo a su tipología la clasificación más aceptada es la de Varnes (1978) (Fig. 10) y en este trabajo se trabajará con una actualización de este sistema de clasificación: el propuesto por Hungr *et al.* (2013) (Fig. 11). Este sistema de clasificación y la actualización mencionada, distinguen distintos tipos de PRM con base en el tipo de material involucrado, la profundidad, el grado de actividad, la edad y la velocidad del movimiento. Con base en lo anterior, y a lo propuesto por Alcántara (2000) para el uso de estas tipologías en el idioma español, se determinan los tipos básicos de PRM: caídas (*falls*), vuelcos

(*topple*), deslizamientos (*landslides*), flujos (*flows*) y movimientos complejos (que involucran más de un solo tipo). Además, esta clasificación estableció los atributos geomorfológicos básicos que pueden estar presentes en un PRM (Fig. 12) y que son esenciales para la identificación de los PRM en campo o a través de técnicas de percepción remota, lo cual a su vez es la base de la elaboración de inventarios de PRM.

| Mecanismos de movimiento | Tipo de material involucrado | | |
| --- | --- | --- | --- |
| Tipología | Roca | Derrubios | Suelo |
| Caída | Caída o desprendimiento de roca | Caída o desprendimiento de derrubios | Caída o desprendimiento de suelo |
| Vuelco o desplome | Vuelco o desplome de rocas | Vuelco o desplome de derrubios | Vuelco o desplome de suelo |
| Deslizamiento rotacional simple | Individual<br>Múltiple<br>Sucesivo | Individual<br>Múltiple<br>Sucesivo | Individual<br>Múltiple<br>Sucesivo |
| Deslizamiento transnacional | Deslizamiento de roca en bloque | Deslizamiento de derrubios en bloque | Deslizamiento de roca en suelo |
| Flujos | Flujo de rocas | Flujo de derrubios | Flujo de suelo |
| Expansión lateral | Expansiones laterales en rocas | Expansiones laterales en derrubios | Expansiones laterales en suelos |
| Movimientos complejos | Ejemplo: alud de rocas | Ejemplo: flujo deslizante | Ejemplo: rotación con flujo de tierras |

*Figura 10* Clasificación de PRM (Varnes 1978).

| | Tipo de material involucrado | |
| --- | --- | --- |
| Tipología | Roca | Suelo |
| Caída | Caída de hielo/roca | Caída o desprendimiento de detritos/limo/bolos |
| Vuelco o desplome | Vuelco o desplome de rocas | Vuelco o desplome de grava/arena/limo |
| Deslizamiento | Deslizamiento rotacional<br>Deslizamiento planar<br>Deslizamiento en cuña<br>Deslizamiento compuesto<br>Deslizamiento irregular | Deslizamiento rotacional de arcilla/limo<br>Deslizamiento planar de arcilla/limo<br>Deslizamiento en cuña de grava/detritos/arena<br>Deslizamiento compuesto de arcilla/limo |
| Expansión lateral | Expansión de rocas en ladera | Licuefacción de arena/limo<br>Expansión lateral de arcilla |
| Flujos | Avalancha de rocas/hielo | Flujo seco de arena/limo/detritos<br>Flujo de arena/limo/detritos<br>Flujo de arcillas<br>Flujo de detritos<br>Flujo de lodo<br>Avalancha de detritos<br>Flujo de tierra<br>Flujo de permafrost |
| Deformación de ladera | Deformación de ladera de montaña<br>Deformación de ladera de rocas | Deformación de ladera de suelo<br>Reptación de suelo<br>Soliflucción |

*Figura 11.* *Clasificación de PRM (Varnes 1978 modificada por Hungr et al. 2014).*
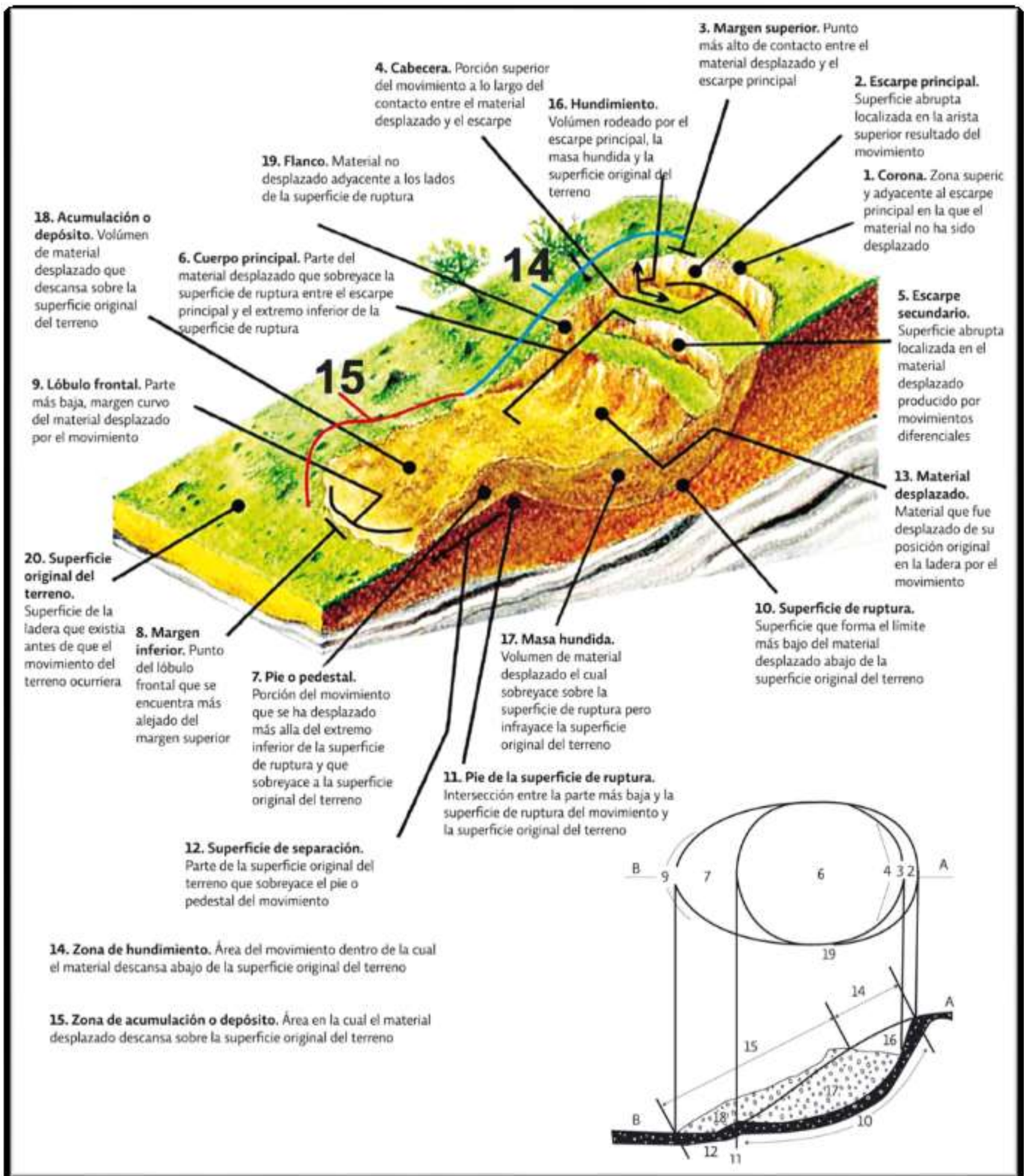
*Figura 12. Atributos geomorfológicos de los procesos de remoción en masa (Cruden y Varnes 1996).*

Como se ha mencionado, la clasificación de Varnes (1978) toma en cuenta la velocidad del movimiento (Fig. 13), este aspecto es importante cuando se analiza la amenaza de los PRM ya que los movimientos extremadamente rápidos son mucho más destructivos que los movimientos lentos o muy lentos. La razón de la última afirmación radica en que los movimientos extremadamente rápidos pocas veces permiten la evacuación de la población que se ve afectada por el movimiento.

| Velocidad | Descripción | Naturaleza del impacto |
|---|---|---|
| 3 m/s | Extremadamente rápido | Catástrofe de gran violencia por el impacto del material desplazado o por la disgregación del material desplazado. |
| 0.3 m/min | Muy rápido | Pérdida de vidas debido a la velocidad del movimiento que no permite que todas las personas escapen. |
| 1.5 m/día | Rápido | Posible escape y evacuación. Infraestructura y equipamiento destruidos por la masa desplazada. |
| 1.5 m/mes | Moderado | Estructuras poco sensibles y a una distancia considerable pueden ser mantenidas. Estructuras localizadas en la masa desplazada son dañadas en gran medida. |
| 1.5 m/año | Lento | Estructuras poco sensibles y a una distancia considerable pueden ser mantenidas con trabajo de mantenimiento si el movimiento no es de mucha duración. |
| 0.06 m/año | Muy lento | Algunas estructuras permanentes no son dañadas y si son agrietadas por el movimiento pueden ser reparadas. |
|  | Extremadamente lento | No hay daño en las estructuras construidas con precaución. |

*Figura 13.* *Velocidad de los PRM (Varnes 1978).*

Respecto al estado de actividad y edad se refieren a aspectos diferentes aunque relacionados entre sí. Básicamente un PRM es **activo** cuando registra movimiento (aquí se incluyen los PRM que ocurren por primera vez o son reactivados), y es **inactivo** cuando no registra movimiento. Dentro de la inactividad existen, de acuerdo a Cruden y Varnes (1996), algunas variantes. Al PRM que en la última temporada de lluvias se encuentran evidencias morfológicas de que no existe desplazamiento se le llama **suspendido**. Se dice que un PRM es **inactivo** cuando ha pasado más de un año del evento que lo causó y no ha presentado movimiento desde entonces. Si este último tipo de movimiento está expuesto en los siguientes años al fenómeno que lo detonó, entonces se le llama **dormido**. Si existe una corriente fluvial y esta cambia su curso debido a la acumulación de material de depósito de un PRM, tanto que el río en cuestión no erosione el pie del PRM, se llama **abandonado**. Si además de esto último se han aplicado medidas ingenieriles para evitar que el PRM se mueva o se reactive se le llama **estabilizado**.

Finalmente, cuando ha pasado la cantidad de tiempo suficiente (por lo general, más de cien años) para que sobre el PRM original ocurran otros PRM más pequeños, y las condiciones geomorfológicas o incluso climáticas hayan cambiado, el PRM original será llamado **relicto**.

El estado de actividad tiene relación directa con la edad del movimiento. Los PRM generalmente se clasifican en **recientes**, **antiguos** y **relictos**. La frontera para definir a PRM recientes varía de un estudio a otro pero por lo general se define por su morfología o el tiempo transcurrido desde su fecha de ocurrencia si es que esta se conoce (por ejemplo, aquellos que han ocurrido en el último año). Respecto a los PRM **antiguos** o **viejos**, corresponden con los estados de actividad abandonados o estabilizados. Estos PRM son todavía identificables por medio de la percepción remota o en campo cuando se analizan detalladamente las características geomorfológicas de una ladera. De esta manera, aunque los atributos morfológicos aparecen suavizados o borrados por la erosión, la vegetación u otros procesos, el área de afectación de este tipo de PRM puede ser delimitada. Por su parte, los PRM **relictos** pueden identificarse en las imágenes de satélite de alta resolución cuando se trata de PRM de magnitud considerable, es decir, PRM con un área de afectación bastante extensa. Son PRM con cientos o quizás miles de años de antigüedad.

Otra cualidad de los PRM útil para su estudio es la profundidad. La determinación de la profundidad se basa en el tipo de falla y la morfología del PRM. En una imagen de satélite o fotografía aérea, la determinación de la profundidad, depende de la apariencia de éste y de relacionar las características litológicas y estructurales de la zona, además de la fecha de adquisición de la imagen (Antonini *et al.* 2002; Fiorucci *et al.* 2011).

## 1.2.2 Inventarios y determinación de amenaza por PRM

En esta investigación se realizaron dos inventarios de PRM. Los inventarios de PRM son el registro ordenado de la localización y tipología de los PRM que han ocurrido en un área determinada (Pašek 1975; Hansen 1984, 1984a; Wieczorek 1984; Guzzetti *et al.* 2000; Guzzetti *et al.* 2012), son útiles para la comprensión de la amenaza por PRM. Hay distintos tipos de inventarios, técnicas y herramientas para elaborarlos (Fig. 14).

Existen diferentes técnicas y herramientas para la elaboración de este tipo de insumos que van desde el registro de los PRM durante el trabajo de campo, la revisión de archivos históricos y la detección por medio de sensores basados en percepción remota. En este trabajo se utilizaron todas estas técnicas, específicamente las mencionadas en la Fig. 14.
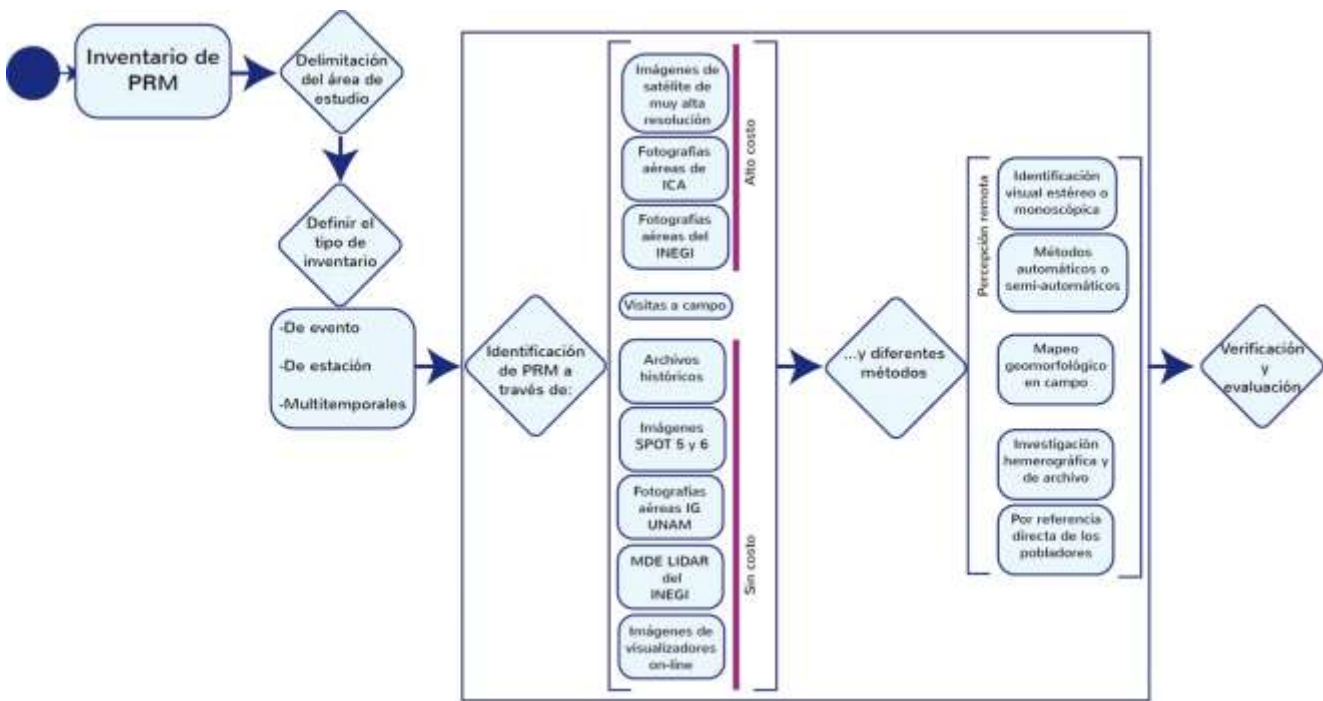
*Figura 14* *Diagrama de flujo de la elaboración de un inventario de PRM.*

La teledetección o percepción remota es la más utilizada actualmente (y en este trabajo también fue así) y es aquella técnica que permite adquirir y procesar imágenes de la superficie terrestre desde sensores instalados en plataformas espaciales (Chuvieco 2008). La figura 15 representa el ideal de un sistema de teledetección, la ilustración parece referirse solo a las imágenes tomadas desde satélites, pero habría que agregar como plataforma los aviones (fotografía aérea o imágenes LiDAR) y más recientemente a los drones. Durante mucho tiempo, y aún hoy en día, la identificación (automática, semi-automática o visual heurística) de PRM a través de técnicas de Percepción Remota se lleva a cabo sobre fotografías aéreas de distintas escalas, e imágenes de satélite de muy alta resolución (Nale 2002; Weirich y Bleisus 2007).

Los mapas de inventario de PRM documentan la extensión de un evento de PRM en un área o región. Son utilizados de forma general para investigar la distribución, tipología, patrones, recurrencia y estadísticas básicas de los PRM, todo ello con el fin de determinar la susceptibilidad, amenaza, vulnerabilidad y riesgo de una población por PRM (Guzzetti *et al.* 2012).

Los inventarios se clasifican por su escala y por su tipo. Por su tipo se dividen en de archivo o geomorfológicos. Los de archivo son aquellos en los que la información se obtiene de archivos históricos. Los geomorfológicos a su vez pueden clasificarse en inventarios de evento, estacionales y multitemporales (Guzzetti *et al.* 2012).
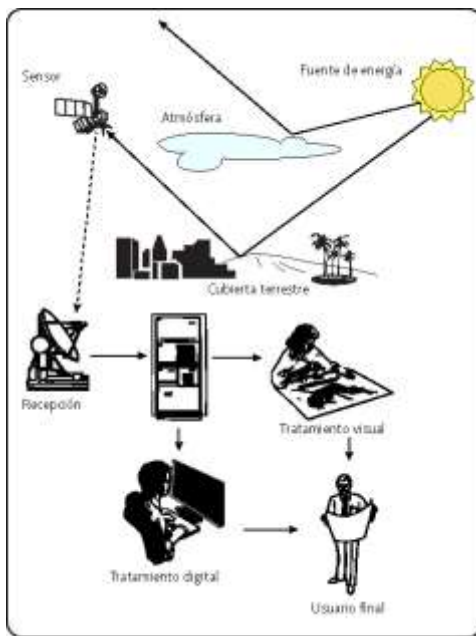
*Figura 15. Elementos de un sistema de teledetección (Chuvieco 2008).*

Los inventarios estacionales muestran los PRM ocasionados por uno o varios eventos detonantes en el periodo de una estación. Por ejemplo, un inventario que registre todos los PRM que ocurrieron durante la temporada de lluvias en un determinado año en un determinado lugar.

Los inventarios de evento son aquellos que registran los PRM ocurridos por un solo evento detonante. Por ejemplo, cuando ocurre un evento de lluvia extraordinaria o huracán. Sirven para documentar la extensión y magnitud de un evento y obtener información sobre la vulnerabilidad.

Los inventarios multitemporales son aquellos que registran PRM de distintitos años, suelen incluir PRM viejos y relictos, este tipo de inventarios son los que se realizaron en este trabajo.

Los mapas de inventario no pueden ser considerados mapas de amenaza, ya que estos últimos presentan una predicción cuantitativa de la distribución espacial de los PRM que un mapa de inventario no da. Tomando en cuenta lo anterior, la amenaza por PRM (*hazard*) puede determinarse en base a tres aspectos: (i) la susceptibilidad (*landslide susceptibility*), (ii) la frecuencia (*frequency*) y (iii) la magnitud (*magnitude*).

La susceptibilidad es el grado inherente de estabilidad de una ladera asociada a todos aquellos factores que puedan desencadenar un movimiento de ladera en la misma (Crozier y Glade 2004). Desde un punto de vista cuantitativo, la susceptibilidad es el grado de probabilidad de que una unidad de área presente o no en el futuro un PRM.

La susceptibilidad responde la pregunta: ¿dónde podemos esperar futuros PRM? (Guzzetti *et al.* 1999). Existen diferentes enfoques para determinar la susceptibilidad (Fig. 16), desde las basadas en la experiencia de quién realiza el estudio (heurísticos), pasando por los complejos y detallados estudios de las propiedades geotécnicas de los materiales (enfoque determinístico), hasta las técnicas estadísticas más simples o complejas (enfoque estadístico). En este trabajo se trabajó bajo el enfoque estadístico, utilizando las técnicas de regresión logística (*logistic regression*), análisis discriminante en su forma linear y en su variante cuadrática (*linear discriminant analysis y cuadratic discriminant analysis*), redes neuronales (*neural networks*), modelo general aditivo (*generalize additive model*, GAM) y soporte de vectores (*support vector machine*).

La evolución de las diferentes técnicas está relacionada con el avance tecnológico que ha permitido un procesamiento de información mucho más robusto y veloz (Fig. 17). En la actualidad, con computadores con gran capacidad de memoria RAM (hasta 64 o más GB) disponibles a bajo costo y al público en general, fue posible aplicar las técnicas mencionadas el párrafo anterior a nuestros datos de los inventarios, en conjunto con procedimientos de evaluación y validación basados en repeticiones y combinaciones de modelos, todo esto, con un consumo de tiempo mínimo en comparación con el tiempo que era necesario hace diez o veinte años.

De esta forma, la adopción de una u otra técnica u enfoque estará determinada por factores como la disponibilidad de datos y recursos materiales, tecnológicos, económicos y humanos, el tiempo que se tiene para la investigación y las condiciones físicas y sociales de la zona de estudio. En la Fig. 18 se presenta el esquema de flujo de trabajo general utilizado en este trabajo para la realización de una estimación de la susceptibilidad por PRM, aclarando que al final de todos los cálculos y modelos, se debe presentar una evaluación o al menos una discusión al respecto, esto es esencial para cualquier trabajo actual.

En la tabla del **Anexo 2** se muestra un resumen de la revisión bibliográfica de 436 artículos publicados y que consistió en la clasificación de estas publicaciones de acuerdo a algunos aspectos claves como su año de publicación, zona de estudio, resolución espacial y método o técnica utilizada para obtener la susceptibilidad. El resultado de esa revisión dejó ver la gran variedad de caminos y tendencias que existen para obtener una estimación de la susceptibilidad.
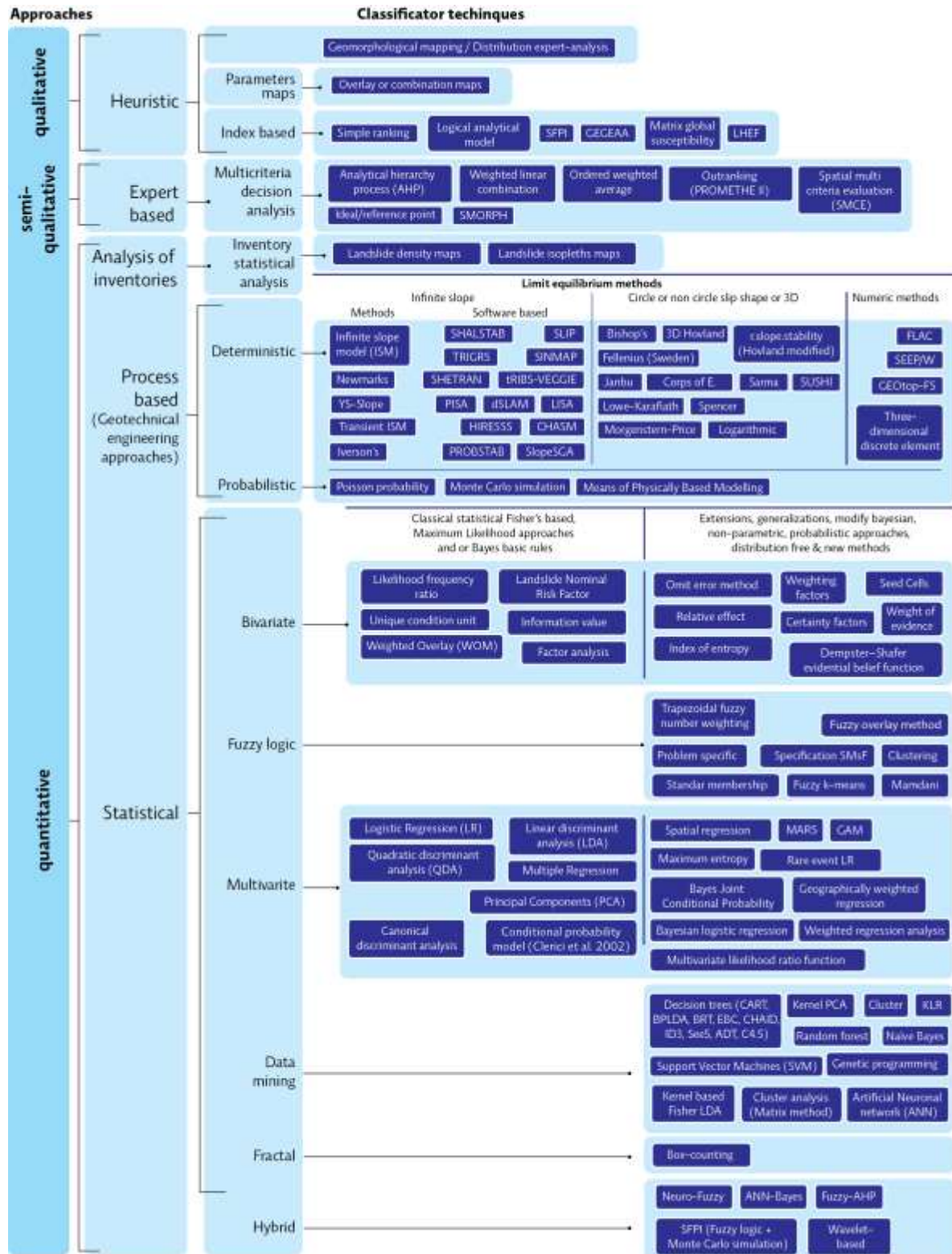
**Figura 16.** *Enfoques y técnicas para estimar la susceptibilidad.*
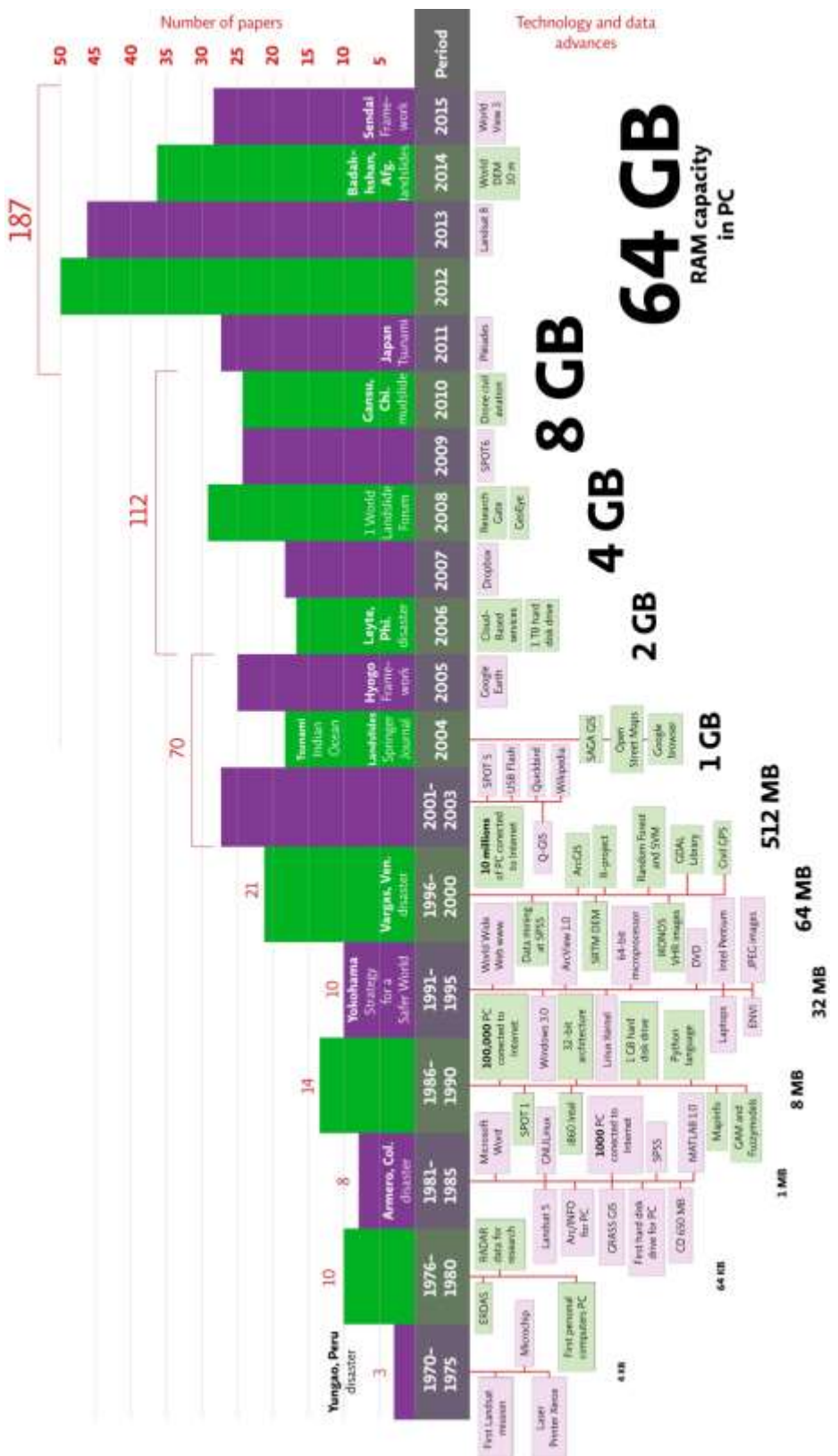
*Figura 17. Avances tecnológicos y estudios de susceptibilidad por PRM.*
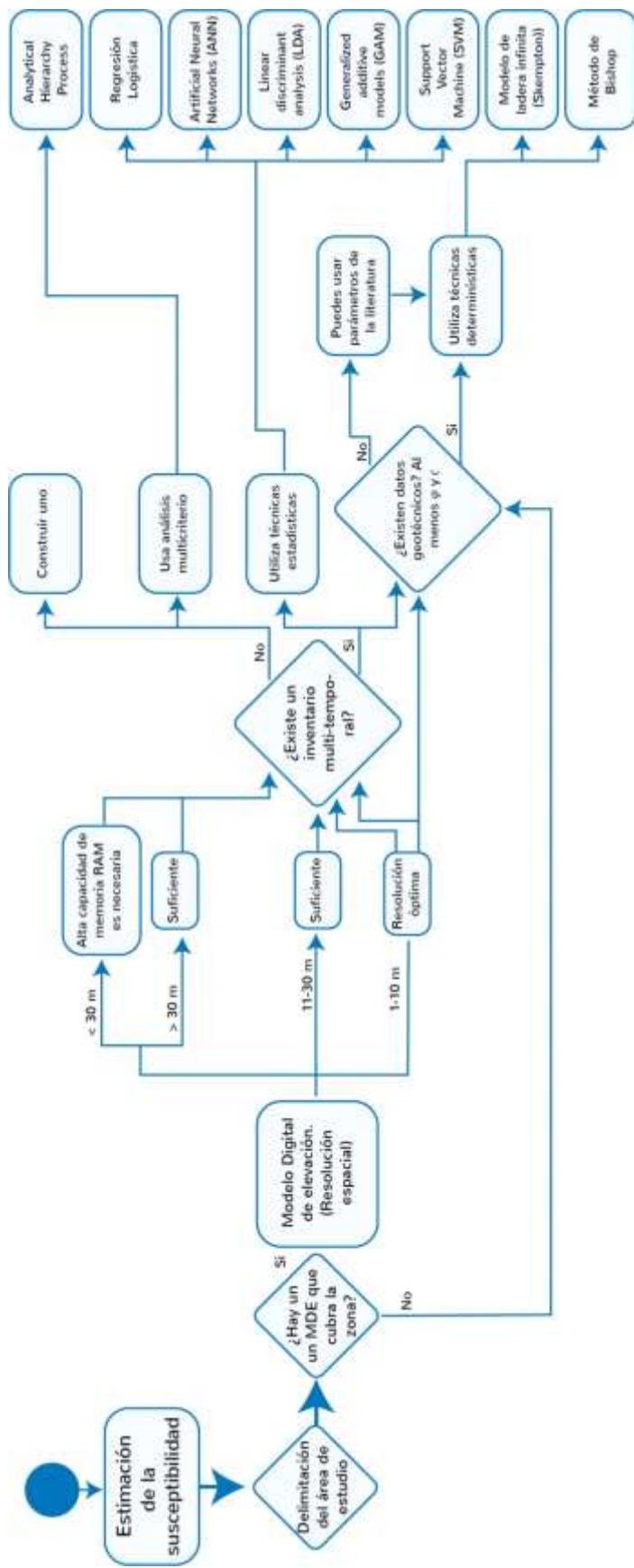
**Figura 18.** *Flujo de trabajo general para el estudio de la susceptibilidad de PRM en esta investigación.*

En ese sentido, la figura 19 muestra las resoluciones espaciales que se han utilizado en cada uno de los mapas de susceptibilidad en los artículos revisados, tomando en cuenta que con el avance de las tecnologías digitales, actualmente se pueden contar con datos del terreno a muy alta resolución (tamaños de pixel menores a 10 metros). Como se verá en el capítulo dedicado a este tema (capítulo V), no existe una resolución espacial perfecta para este tipo de estudios ni tampoco una mayor resolución espacial significa necesariamente la obtención de mejores resultados.
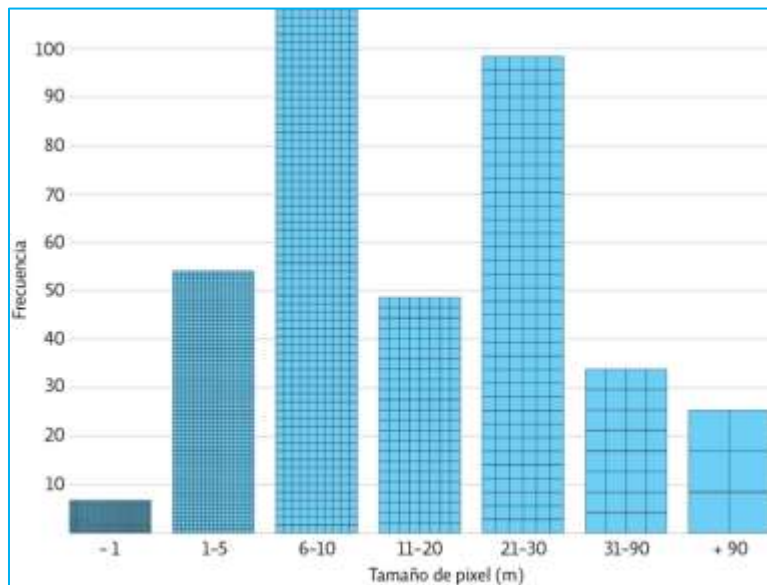


*Figura 19.* *Número de investigaciones por resolución espacial.*

La resolución espacial seleccionada en cada estudio tiene relación directa con la extensión del área de estudio, de esta forma es entendible que escalas nacionales o regionales se trabajen de manera más eficiente con tamaños de pixel mucho mayores (menor resolución espacial) en comparación con áreas de estudio integradas por unos pocos kilómetros cuadrados.

Así mismo, en la Fig. 20 se puede apreciar que la mayor parte de los estudios que generaron la literatura científica revisada tratan sobre zonas de estudio localizadas en países centrales como Estados Unidos, Japón, Italia; aunque en los últimos años han sido realizadas numerosos investigaciones y trabajos en países que han tenido un crecimiento económico importante como es el caso de China o India. También es evidente que aunque la inestabilidad de laderas es un problema persistente en México, la cantidad de trabajos académicos no es tan numerosa comparada con los países ya mencionados o incluso con países como Turquía o Irán.
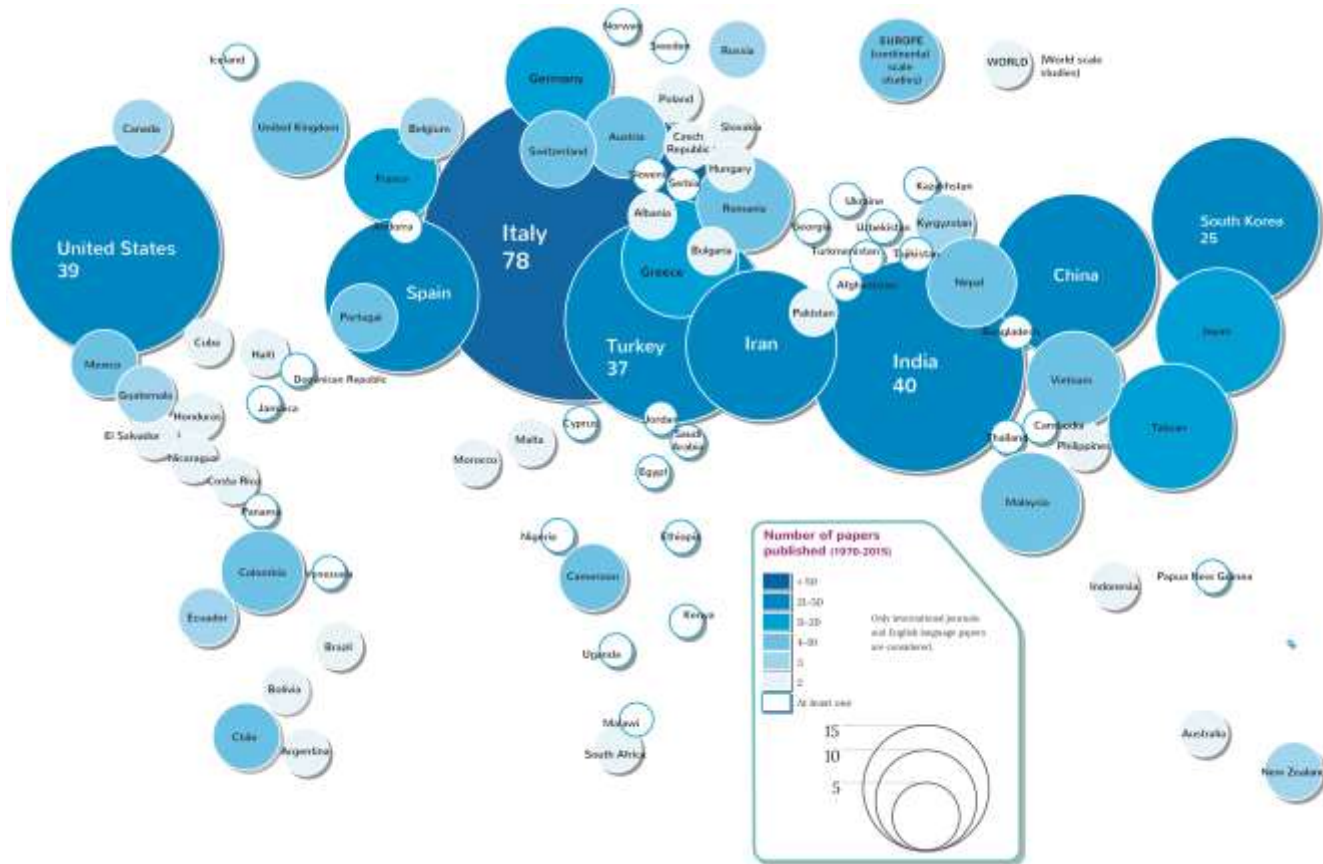
*Figura 20. Número de investigaciones por localización de la zona de estudio.*

Sin duda, uno de los enfoques más utilizados en la literatura es el que tiene como base el análisis estadístico de los PRM ocurridos en el pasado y su relación con una serie de factores conocidos como determinantes (*conditional factors*) (**Anexo 3**). Estos métodos son conocidos como estadísticos y el más popular en la literatura es la Regresión Logística y en la Fig. 21 se presenta un resumen de la revisión de la bibliografía realizada para este trabajo de acuerdo al tipo de técnica estadística utilizada, se dejan los nombres en inglés para una identificación más sencilla en la literatura especializada. Dentro de este tipo de técnicas las hay principalmente bivariadas, multivariadas y las más modernas basadas en minería de datos (*data minning*).

Por su parte la frecuencia temporal se refiere a cuándo se podrían esperar los siguientes PRM y la magnitud generalmente se refiere al área o volumen de los PRM aunque también puede combinarse con la velocidad del movimiento. Los estudios para determinar estos dos aspectos de la amenaza son menos abundantes en la literatura en comparación con lo existente referente a la susceptibilidad.

| Técnica | Primer artículo en que fue utilizada | Número de veces utilizada |
| --- | --- | --- |
| Logistic regression (LR) | Cox, 1958. | 100 |
| Artificial Neural Networks (ANN) | Lee *et al.* 2003 | 40 |
| Analytical hierarchy process (AHP) | Saaty, 1980. | 37 |
| Likelihood frequency ratio (LFR) | Van Westen, 1997. | 36 |
| Weight of evidence (WofE) | Bonham-Carter *et al.* 1988; Lee *et al.* 2002. | 31 |
| Information value (Statistical method index) (IV) | Yin and Yan, 1988; van Westen, 1997 | 26 |
| Distribution expert-analysis | Carrara and Merenda, 1976 | 20 |
| Linear discriminant analysis (LDA) | Fisher, 1936. | 19 |
| Conditional probability model (CPM) | Clerici *et al.*, 2002. | 18 |
| Decision tree (DT) | | 17 |
| Infinite Slope Model (ISS) | | 16 |
| Fuzzy standard membership (FSMs) | | 15 |
| Support Vector Machine (SVM) | Vapnik, 1995. Brenning, 2005. | 14 |
| SHALSTAB | Montgomery and Dietrich 1994 | 14 |

*Figura 21. Número de investigaciones basadas en el enfoque estadístico de acuerdo a la técnica utilizada.*

Debido a que en varias regiones del mundo la ocurrencia de los PRM ocurre en mayor número durante eventos de precipitación extraordinarios (huracanes, depresiones tropicales, temporadas de lluvia abundante), uno de los enfoques más utilizados para determinar la frecuencia temporal de PRM consiste en la estimación de periodos de retorno y el cálculo de umbrales de precipitación. Para este tipo de enfoque es requerido que existan datos meteorológicos de la precipitación en resoluciones temporales y espaciales finas. Esto último no es algo frecuente en México todavía. Si bien este tipo de enfoques pueden también realizarse con parámetros prestablecidos de la literatura, en este trabajo se ha optado por utilizar un enfoque estadístico basado en los propios datos del inventario de PRM, el cual tiene registrado, con cierta limitación, la fecha de ocurrencia de cada uno de los PRM registrados.

### 1.2.3 Vulnerabilidad y riesgo por PRM

Si los trabajos referentes a la determinación de la amenaza son escasos, los referentes a la vulnerabilidad y el riesgo lo son aún menos. Determinar estos aspectos es laborioso pues la vulnerabilidad es compleja, dinámica en el tiempo y espacio, además de multidimensional (Birkmann 2006; Fuchs *et al.* 2011; Papathoma-Köhle *et al.* 2011; Birkmann *et al.* 2013). Por si fuera poco, la estimación de la vulnerabilidad requiere una serie de datos que no siempre están disponibles en la escala requerida.

Específicamente, en la literatura relacionada con los PRM existen tres enfoques utilizados con mayor frecuencia: (i) los elaborados con base en curvas que relacionan los elementos en riesgo con la intensidad de los PRM (Galli and Guzzetti 2007; Papathoma-Kohle *et al.* 2015); los basados en

matrices de daños (Zezere *et al.* 2008); y los elaborados con base en indicadores (Mejia-Navarro *et al.* 1994; Papathoma-Köhle *et al.* 2007).

En el enfoque basado en indicadores se asocian múltiples características socio-económicas con los elementos en riesgo (Kappes *et al.* 2012) como representaciones operacionales de la vulnerabilidad en la realidad (Birkmann 2006; Kappes *et al.* 2012). Este tipo de enfoque es el que se utilizó en este trabajo y en el capítulo VI se describe a detalle la construcción de estos indicadores.

Es necesario señalar también que en gran parte de la literatura de la vulnerabilidad por PRM, el elemento en riesgo analizado suelen ser las edificaciones y no las personas. En este trabajo se exploró la estimación de la vulnerabilidad tomando en cuenta como elementos de riesgo a las personas. Para ello se utilizó el modelo propuesto por Turner *et al.* (2003). En el modelo de Turner *et al*. los elementos en riesgo se engloban en cuatro grupos:

- Las personas (su vida o su salud).
- Las actividades económicas.
- El equipamiento y la infraestructura (vivienda, equipamiento urbano, carreteras, caminos, escuelas y en general todo tipo de construcción humana).
- Los recursos naturales (elementos biofísicos relacionados con las actividades económicas: el suelo, las fuentes de agua, la vegetación, etc.).

El enfoque se basa en el supuesto de que existe una interacción entre las condiciones y procesos humanos y ambientales a distintas escalas. Considera lo que llama un Sistema Humano-Ambiental, es decir, la dinámica entre las condiciones humanas y ambientales de un lugar determinado (Fig. 22).

En la Fig. 22 se muestra que hay elementos a escala global y regional, como el sistema económico y político, las instituciones nacionales o internacionales, además de procesos culturales y tecnológicos que influyen en las condiciones ambientales y humanas de un lugar determinado (escala local), los diferentes cambios en estos elementos hacen que las condiciones humanas y ambientales cambien a escala mundial, regional y local modificando así el Sistema Humano-Ambiental. Así mismo, el sistema ambiental (atmósfera, clima, etc.) a escala global o regional influye sobre las condiciones humanas y ambientales en un lugar determinado. Cambios o variaciones en estos elementos pueden dar origen a las amenazas, que pueden ser de escala global, regional o local, por ello su posición abarcando los tres colores. Estas amenazas pueden afectar al sistema entero o sólo al Sistema Humano-Ambiental a escala local.
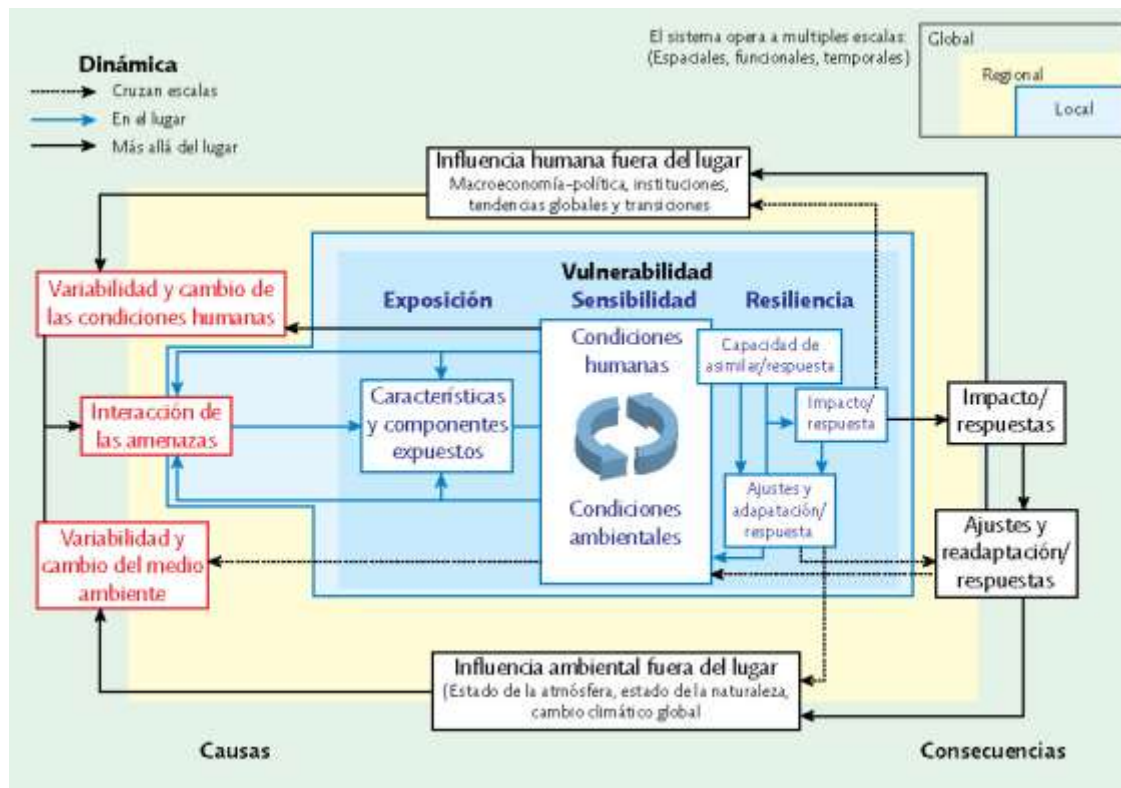
**Figura 22.** *Enfoque de la vulnerabilidad (Turner et al. 2003).*

La vulnerabilidad se localiza a escala local e implica los tres elementos: exposición, sensibilidad y resiliencia. La exposición está definida por las características de los componentes expuestos que pueden ser asentamientos humanos (incluida la población y el equipamiento e infraestructura) así como procesos (por ejemplo la economía), y entidades como el estado. En el enfoque, la exposición va más allá de la presencia de la amenaza ya que se debe considerar la manera en que el Sistema Humano-Ambiental experimenta la amenaza. Además, la exposición estará relacionada con las características de la amenaza: su frecuencia, magnitud y duración. Por su parte, las condiciones humanas y ambientales de un lugar determinan la sensibilidad a cualquier amenaza a la que estén expuestos. Dentro de estas condiciones se incluyen el capital humano y ambiental que pueden ser considerados como elementos de resistencia ante una amenaza. Por ejemplo, acceso de la población a los recursos, instrumentos legales o nivel socioeconómico de la población del lugar. Las respuestas, ya sean de carácter autónomo o propuestas por la iniciativa privada o el gobierno, a corto o largo plazo, de prevención o de atención de la emergencia, determinan la resiliencia del Sistema Humano-Ambiental (Fig. 23). Estas respuestas a veces pueden trascender a otras escalas, no solamente influir en lo local.
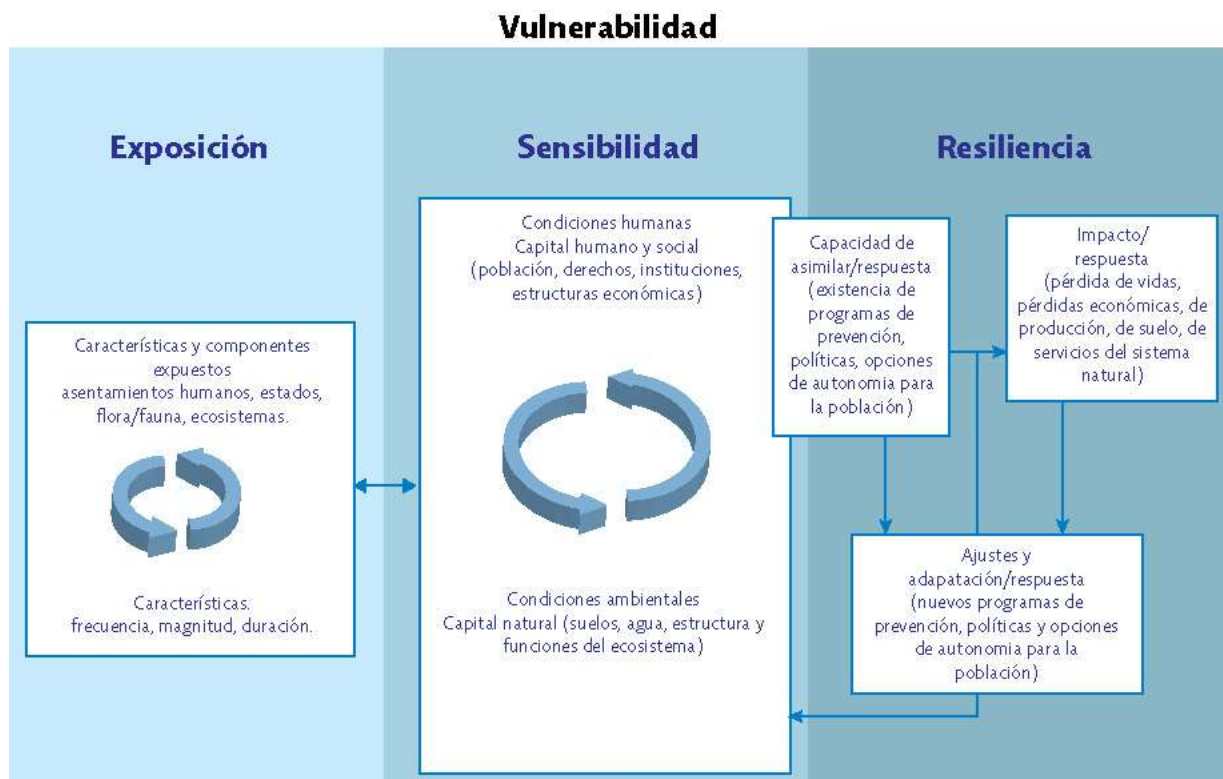
**Figura 23.** *Enfoque de la vulnerabilidad (Turner et al. 2003).*

El enfoque de Turner *et al.* (2003) es un enfoque conceptual que muestra las interacciones y relaciones entre los distintos componentes que influyen en la vulnerabilidad a diferentes escalas espacio-temporales. Esto último permite inferir que el análisis espacial puede ser aplicado para poder generar un enfoque operacional de evaluación de la vulnerabilidad.

## 1.3 Discusión y conclusiones

En este capítulo se menciona que hay dos grandes enfoques desde los que se han abordado los riesgos y desastres de origen natural, el enfoque *fisicalista* y el alternativo-estructuralista. Ambos enfoques están sustentados en una postura del lugar que ocupa el ser humano dentro de la complejidad del mundo a través de dos tipos de identidad: la relacional y la individual.

El enfoque *fisicalista* pretende poder controlar las amenazas de origen natural desde una identidad individual. Gran parte de los textos, los métodos y herramientas de esta tesis, surgen y coinciden con esa postura: medir, conocer la amenaza, cuantificarla. Podemos afirmar que eso es útil en la medida en que permite conocer los peligros y amenazas de origen natural. Incluso, falta investigar y trabajar para poder conocer lo necesario y suficiente sobre los procesos de remoción en masa.

Sin embargo, con lo que ya sabemos se puede (y se debe) empezar a buscar otros alcances, aquellos que tienen que ver con la parte de la construcción social del riesgo y que es lo que propone el enfoque alternativo-estructuralista. Un mundo más justo está más cerca de ser un mundo sin desastres, ya que ambas cosas parecen ir en conjunto, no se puede esperar un cambio social, se debe trabajar desde ya en esa dirección. Así, se han comenzado a realizar trabajos acerca de la vulnerabilidad, no solo de los bienes materiales o económicos sino de las personas en sí, a escuchar a la gente afectada, comprender cómo se llegó a la situación de desastre y entender sus causas de fondo, como lo propone el modelo de Presión y liberación (PAR) propuesto por Weisner *et al.* (2003).

Es ahí donde este trabajo pretende incursionar de la mejor manera posible. No se trata de un regreso a una identidad relacional, ni siquiera de un intento de eliminar ese tipo de identidad o de eliminar su opuesto. Para comprender mejor los desastres, son necesarias soluciones colectivas que respeten la individualidad de las personas, y creemos que tener esta perspectiva ligada a nuestro propósito –un mundo sin desastres es posible– mantiene cierta congruencia. Los indicadores seleccionados en el capítulo VI de esta tesis para tratar de estimar la vulnerabilidad, responden a ese imperativo.

De esta manera, en esta investigación se trabaja en ambas direcciones, mucho más en entender la parte física del fenómeno, pero también se incluyó el análisis de la parte social del problema.


Finalmente, de todo lo que se ha expuesto de manera general y reducida, se pueden extraer las siguientes conclusiones y que son los puntos de partida de esta investigación:

- En las sociedades anteriores al periodo de las grandes civilizaciones, las amenazas naturales eran explicadas de manera metonímica, desde una identidad relacional.

- La identidad relacional no desapareció de la sociedad ni de la explicación de los desastres, simplemente fue integrada y acumulada a las explicaciones metafóricas y científicas.

- La identidad individual supone una separación entre el ser humano y la naturaleza, de lo que se derivó una visión fisicalista o tecnocrática de los desastres. Este enfoque sigue siendo predominante en la práctica aunque se ha complementado con el enfoque alternativo-estructuralista.

- El enfoque alternativo-estructuralista surgió de las críticas a la Modernidad y su sistema económico: el capitalismo.

- Existe una tensión constante entre quienes buscan aplicar acciones para eliminar los riesgos de desastre bajo el enfoque alternativo-estructuralista y quienes tienen el papel de tomadores de

decisiones cuya labor casi siempre está condicionada por fuertes intereses económicos y por lo tanto, políticos.

- Uno de los modelos más importantes del enfoque alternativo-estructuralista es el modelo PAR (*Pressure and Release Model*), que considera la vulnerabilidad como un sistema complejo de causas de fondo que genera condiciones inseguras.

- La vulnerabilidad es un concepto complejo, multidimensional y que no tiene, aún hoy, una definición consensuada, dependiendo este siempre del enfoque desde el que se le considere

- Los PRM son el movimiento hacía debajo de los materiales que componen una ladera, esencialmente bajo la influencia de la gravedad y sin la asistencia de algún agente fluido. La clasificación más aceptada de estos fenómenos es la de Varnes (1978).

- Los inventarios son el registro de los PRM ocurridos en una zona determinada y sirven para poder estimar o calcular aspectos como la susceptibilidad y amenaza por PRM. Son la base de esta investigación.

- Existen distintos enfoques para abordar la amenaza por PRM, el enfoque heurístico, el determinístico y el estadístico. En este trabajo se opta por un enfoque estadístico.

- La vulnerabilidad por PRM será abordada mediante un enfoque basado en la construcción de indicadores con base en el modelo propuesto por Turner *et al.* (2003).

## Referencias

Alcántara-Ayala I (2000) Landslides: ¿Deslizamientos o movimientos del terreno? Definición, clasificaciones y terminología. Investigaciones geográficas. Boletín del Instituto de Geografía. UNAM. 41, 9-23.

Amin S (1989) El eurocentrismo. Crítica de una ideología. México: Siglo XXI.

Antonini G, Ardizzone F, Cardinali M, Galli M, Guzzetti F, Reichenbach P (2002) Surface deposits and landslide inventory map of the area affected by the 1997 Umbria-Marche earthquakes. Bollettino Società Geologica Italiana, 121:2 843-853.

Bellamy Foster J (2000) Marx's Ecology. Materialism and nature. Monthly Review Press. Nueva York, Estados Unidos. pp. 289.

Blake ES (2011) the deadliest, costliest, and most intense united States tropical cyclones from 1851 to 2010 (and other frequently requested hurricane facts). NOAA Technical Memorandum NWS NHC-6. pp. 49. http://www.nhc.noaa.gov/pdf/nws-nhc-6.pdf

Blaikie P, Cannon T, Davies I, Wisner B (1994) At Risk. Routledge. Londres.

Birkmann J (2006) Measuring vulnerability to promote disaster-resilient societies: conceptual frameworks and definitions. In: Birkmann J (ed.), Measuring vulnerability to natural hazards. Towards Disaster Resilient Societies. United Nations University Press. Hong Kong. pp 9-54.

Birkmann J, Cardona OD, Carreño ML, *et al.* (2013) Framing vulnerability, risk and societal responses: the MOVE framework. Natural Hazards 67: 193-211. DOI: 10.1007/s11 069-013-0558-5

Bonham-Carter GF (1994) Geographic information systems for geoscientists: modelling with GIS. Computer Methods in the Geosciences 13, Pergamon.

Brenning A (2005) Spatial prediction models for landslide hazards, review, comparison and evaluation. Natural Hazards and Earth System Sciences, 5, 853–862. DOI: SRef-ID: 1684-9981/nhess/2005-5-853

Busqueta JM, Etxezarreta M, Fernández JI, Navarro F, Presas O, Puig Sole A, Teixidor J (2017) Apuntes sobre Marx y Naturaleza. Seminarios Taifa. España. pp. 79.

Carrara A, Merenda L (1976) Landslide inventory in northern Calabria, southern Italy. Geological Society of America Bulletin 87, no. 8;1153-1162. Doi: 10.1130/0016-7606

Cardona OD (1993) Evaluación de la amenaza, la vulnerabilidad y el riesgo. Elementos para el ordenamiento y la planeación del desarrollo. En Maskrey 1993. Los Desastres no son naturales. La Red: Red de Estudios Sociales en Prevención de Desastres en América Latina. Colombia, Ed. Tercer Mundo Editores. 45-65.

Cannon T (1994) Vulnerability analysis and the explanation of 'natural'disasters. En: Varley A (ed.) Disasters, development and environment. John Wiley and Sons. Whichester, Reino Unido. pp. 13-30.

Childe G (1986) Los orígenes de la civilización. Breviarios Fondo de Cultura Económica. México. Pp. 291.

Chuvieco E (2008) Teledetección ambiental. La observación de la Tierra desde el Espacio. Ariel Ciencia. España. Pp. 594.

Clerici A, Perego S, Tellini C, Vescovi P (2002) A procedure for landslide susceptibility zonation by the conditional analysis method. Geomorphology 48, 349–364.

Cox DR (1958) The regression analysis of binary sequences (with discussion). J Roy Stat Soc B 20: 215–242.

Crozier MJ and Glade T (2004) Landslide hazard and risk: issues, concepts and approach. In: Glade T, Anderson MG and Crozier MJ (eds.) Landslide risk assessment. John Wiley, 1-40.

Cruden DM and Varnes DJ (1996) Landslide types and processes. In: Turner AK and Schuster RL (eds.) Landslides, Investigation and Mitigation, Transportation Research Board Special Report 247, Washington D.C., 36-75.

Cuny CF (1983) Disasters and Development, Oxford University Press, Inc. New York, Oxford. (Traducido al español por Gustavo Wilches-Chaux, 1985).

Davis I (1981) Arquitectura de Emergencia, Serie Tecnología y Arquitectura, Editorial Gustavo Gili, S.A., Barcelona.

Descartes René (2010) Discurso del método. FGS, Madrid, España. pp. 101.

Dowdle WR (1999) Influenza A virus recycling revisited. Bulletin of the World Health Organization 77(10): 820-828.

Dussel E (2003) Europa, modernidad y eurocentrismo. La colonialidad del saber. Eurocentrismo y ciencias sociales CLa. C.SO. pp. 48-49.

Dussel E (2006) 20 Tesis de política. Siglo XXI. México, México. pp. 167.

Elias N (1990) La sociedad de los individuos, Barcelona, Península.

Engels F (1978) [1845] La situación de la clase obrera en Inglaterra. OME, Crítica. Barcelona. 257-259.

Erazo Pantoja VJ, Erazo Pantoja LM (2015) Modernidad, desarrollo y educación: de las causas de lo civilizatorio hacia la crisis civilizatoria. Revista de la Facultad de Ciencias Económicas y Administrativas. Universidad de Nariño XVI, 1, 99-124.

Fiorucci F, Cardinali M, Carlà R, Rossi M, Mondini AC, Santurri L, Ardizzone F, Guzzetti F (2011) Seasonal landslides mapping and estimation of landslide mobilization rates using aerial and satellite images. Geomorphology 129 (1–2), 59–70.

Fisher RA (1936) The use of multiple measurements in taxonomic problems. Ann Eugen 7:179–188.

Fucheng S, Yuanjun Y, Manhua H (1987) Investigation and verification of extraordinarily large floods on the Yellow River. Journal of Hydrology 96(1–4): 69-78. https://doi.org/10.1016/0022-1694(87)90144-2

Fuchs S, Kuhlicke C, Volker M (2011) Editorial for the special issue: vulnerability to natural hazards the challenge of integration. Natural Hazards 58: 609-619. DOI: 10.1007/s11069-011-9825-5

Galli M, Guzzetti F (2007) Landslide vulnerability criteria: a case study from Umbria, Central Italy. Environment Management 40: 649-664. DOI:10.1007/s00267-006-0325-4

Gandarilla Salgado (2012) Asedios a la totalidad. Poder y política en la modernidad desde un encare de-colonial. Anthropos. Barcelona, España. pp. 368.

Gargallo F (2015) Feminismos desde abya yala. Ua. C.M. México. pp. 472.

Glade T, Anderson M, Crozier MJ (2005) Landslide hazard and risk. John Wiley and Sons. ISBN 0-471-48663-9.

González Ruibal A. Hernando A, Politis G (2011) Ontology of the self and material culture: Arrow-making among the Awá hunters-gatherers (Brazil). Journal of Anthropological Archaeology 30: 1-16.

Guzzetti F, Carrara A, Cardinali M, Reichenbach P (1999) Landslide hazard evaluation: an aid to a sustainable development. Geomorphology, 31: 181-216.

Guzzetti F, Cardinali M, Reichenbach P, Carrara A (2000) Comparing landslide maps: A case study in the upper Tiber River Basin, central Italy. Environmental Management, 25:3, 247-363.

Guzzetti F, Modini A, Cardinali M, Fiorucci F, Santangelo M, Chang KT (2012) Landslide inventory maps: New tools for an old problem. Earth-Sciences Reviews, 112, 42-66.

Hansen MJ (1984) Strategies for classification of landslides. Brunsden, D. and Prior, D.B. (eds.) Slope Instability. John Wiley and Sons, 1-25.

Hansen A (1984) Landslide hazard analysis. In: Brunsden, D. and Prior, D.B. (eds.) Slope instability, Wiley & Sons, New York, 523-602.

Harvey D (2007) Breve historia del neoliberalismo. Akal. Madrid España. pp. 2013.

Havelock EA (1996) La musa aprende a escribir, Barcelona, Paidós.

Hernando A (2002) Arqueología de la identidad. Akal. España. pp. 224.

Hernando A (2015) Identidad relacional y orden patriarcal. En: Hernando A (ed.) Mujeres, hombres, poder. Subjetividades en conflicto. Traficantes de Sueños. Madrid España. pp. 185.

Hewitt K (1983) Interpretation of Calamity. Allen and Unwin. Boston, Estados Unidos. pp. 304. DOI: 10.1002/joc.3370040211

Hungr, O., Leroueil, S., & Picarelli, L. (2014). The Varnes classification of landslide types, an update. Landslides, 11, 167–194. doi:10.1007/s10346-013-0436-y.

Isidro Luna VM (2015) From Neoliberalism to Possible Alternatives. Economía Informa 395: 35-49. DOI: https://doi.org/10.1016/j.ecin.2015.10.004

Jenkins R (1996) Social Identity. Routledge. Reino Undio. pp. 206

Kant I (2003) Crítica de la razón pura. Biblioteca Virtual Universal. Buenos Aires, Argentina. pp. 206.

Kappes MS, Papathoma-Köhle M, Keiler M (2012) Assessing physical vulnerability for multi-hazards using an indicatorbased methodology. Applied Geography 32: 577-590. DOI: 10.1016/j.apgeog.2011.07.002

Lee S, Choi J, Min K (2002) Landslide susceptibility analysis and verification using the Bayesian probability model. Environ Geol 43:120–131.

Lee S, Ryu JH, Min K, Won JS (2003) Landslide susceptibility analysis using GIS and Artificial Neural Network. Earth Surf. Process. Landforms 28, 1361–1376.

Leff E (2008) Discursos sustentables. Siglo XXI Editores. México. pp. 272.

Macías JM (1993) Perspectivas de los estudios sobre desastres en México. En: Los Desastres no son naturales. La Red: Red de Estudios Sociales en Prevención de Desastres en América Latina. Colombia, Ed. Tercer Mundo Editores.

Marx K (2008) [1867] El capital. Critica de la Economía Política. Siglo XXI Editores, México. pp. 211.

Mauss M (1991) Sobre una categoría del espíritu humano: la noción de persona y la noción del "yo". Sociología y Antropología: 307-333.

Maskrey A (1989) El Manejo Popular de los Desastres Naturales. Estudios de Vulnerabilidad y Mitigación, ITDG, Lima.

Mauro Marini M (1991) [1973] Dialéctica de la dependencia. Ediciones Era. pp. 42.

Mejia-Navarro M, Wohl LEE, Oaks SD (1994) Geological hazards, vulnerability, and risk assessment using GIS: model for Glenwood Springs, Colorado. Geomorphology 10: 331–354

Montgomery, D. R., & Dietrich, W. E. (1994). A physically based model for the topographic control of shallow land sliding. Water Resources Research , 30 (4), 1153- 1171.

Moragón L (2013) Cuerpo y sociedades orales. Una reflexión sobre la concepción del cuerpo y sus implicaciones en el estudio de la Prehistoria, Tesis doctoral, Madrid, Departamento de Prehistoria/Universidad Complutense, inédita.

Moreira R (2009) Qué es la Geografía. Centro de Investigaciones Sociales. La Paz, Bolivia.

Murillo-García FG (2013) Análisis y cartografía de riesgo de desastre por procesos de remoción en masa en el municipio de Pahuatlán, Puebla. Tesis de maestría, UNAM, México.

Nale DK (2002) Quickbird – Aerial Photography Comparision Report. EMAP International. Pp. 37.

Oliver-Smith A, Alcántara-Ayala I, Burton I, Lavell AM (2016) Investigación forense de desastres. Un marco conceptual y guía para la investigación. UNAM. México, México. pp. 103.

Oliver-Smith A, Alcántara-Ayala I, Burton I, Lavell A (2017) The social construction of disaster risk: seeking root causes, International Journal of Disaster Risk Reduction, 22, 469–474.

Olson CM (1994) Understanding and Evaluating a Meta-analysis. Academy Emergency Medicine 1(4): 392-398. DOI: 10.1111/j.1553-2712.1994.tb02653.x

Ong W (1996) Oralidad y escritura. Tecnologías de la palabra, México. Fondo de Cultura Económica.

ONU/ISDR (Estrategia Internacional para la reducción de desastres) (2002) Living with Risk: A global review of disaster reduction initiatives, Geneva: UN Publications.

Papathoma-Köhle M, Neuhäuser B, Ratzinger K, *et al.* (2007) Elements at risk as a framework for assessing the vulnerability of communities to landslides. Natural Hazards and Earth System Sciences 7: 765-779. DOI: 10.5194/nhess-7-765-2007

Papathoma-Köhle M, Kappes M, Keiler M, *et al.* (2011) Physical vulnerability assessment for alpine hazards: state of the art and future needs. Natural Hazards 58: 645-680. DOI: 10.1007/s11069-010-9632-4

Pašek J (1975) Landslide inventory. International Association Engineering Geologist Bulletin 12, 73-74.

Pérez Orozco A (2014) Subversión feminista de la economía. Aportes para un debate sobre el conflicto capital-vida. Traficantes de sueños. Madrid, España. pp. 305. DOI: https://www.traficantes.net/sites/default/files/pdfs/map40_subversion_feminista.pdf

Pierri N (2001) Historia del concepto de desarrollo sustentable. En: Pierri N y Foladori G (eds.) ¿Sustentabilidad? Desacuerdos sobre el desarrollo sustentable. Uruguay: Trabajo y Capital. pp. 27-81.

Quijano A (1992) Colonialidad y Modernidad/Racionalidad. En: Bonilla H (comp.) Los Conquistados: 1492 y la población indígena de las Américas. FLACSO / Ediciones Libri Mundi, Quito, Ecuador. pp. 437-449.

Quintero P (2010) Notas sobre la teoría de la colonialidad del poder y la estructuración de la sociedad en América Latina. Papeles de Trabajo 19: 1852-4508. Centro de Estudios Interdisciplinarios en Etnolingüística y Antropología Socio-Cultutal.

Saaty TL (1980) Analytic Hierarchy Process. Wiley Online Library.

Sacristán M (1984) Algunos atisbos político-ecológicos de Marx. Mientras tanto 21: 39-49.

Siodla J (2017) Clean slate: Land-use changes in San Francisco after the 1906 disaster. Explorations in Economic History 65: 1-16. https://doi.org/10.1016/j.eeh.2017.04.001

Sigurdsson H (2015) The History of Volcanology. En: The Encyclopedia of Volcanoes (Second Edition). Academic Press. 13-32. DOI: https://doi.org/10.1016/B978-0-12-385938-9.02002-2

Smith K (1991) Environmental Hazards. Assessing risk and reducing disaster. Routledge. Londres, Reino Unido. pp. 321.

Toscana-aparicio A (2006) Los paisajes del desastre. Tesis doctorado. Posgrado en Geografía, UNAM, pp.239.

Toulmin (1992) Cosmópolis. The University of Chicago Press. Chicago, Estados Unidos de América.

Turner IIBL, Kasperson RE, Matsone PA, *et al.* (2003) A framework for vulnerability analysis in sustainability science. PNAS 100 (14): 8074-8079. DOI: 10.1073/pnas.1231335100

van Westen CJ (1997) Statistical landslide hazard analysis. In: van Westen, C.J. (Ed.), ILWIS 2.1 for Windows Application Guide. ITC Publication, Enschede, pp. 73–84.

Vapnik V (1995) The Nature of Statistical Learning Theory. Springer Verlag.

Varnes DJ (1978) Slope movement types and processes. In, Special Report 176: R.L. Schuster and R.J. Krizek (eds.), Landslides: Analysis and Control, TRB, National Research Council, Washington, D.C. Pp. 11-33.

Weintraub K (1993) La formación de la individualidad. Autobiografía e Historia. Madrid, Megazul-Endymion.

Weirich F, Blesius L (2007) Comparison of satellite and air photo based landslide susceptibility maps. Geomorphology 87 (4), 352-364.

White GF (1936) The limit of economic justification for flood protection. Journal of Land and Public Utility Economics 12: 133–48.

White GF (1945) Human Adjustment to Floods: A Geographical Approach to the Flood Problem in the United States. Research Paper 29, Chicago, IL: Department of Geography, University of Chicago.

Wieczorek GF (1984) Preparing a detailed landslide-inventory map for hazard evaluation and reduction. Bulletin of the Association of Engineering Geologist 21 (3), 337-342.

Wisner B, Blaikie P, Cannon T, Davis I (2003) At Risk: natural hazards, people's vulnerability and disasters. Second Edition. Routledge. London, England. pp. 492. http://www.preventionweb.net/files/670_72351.pdf

Wolff E (2000) Europa y la gente sin historia. FCE. Buenos Aires, Argentina.

Yin KL, Yan TZ (1988) Statistical prediction models for slope instability of metamorphosed rocks. Landslides. In: Bonnard, C. (Ed.), Proceedings of the Fifth International Symposium on Landslides. vol. 2, pp. 1269–1272 (Balkema, Rotterdam).

Zezere JL, Garcia RAC, Oliveira SC, *et al.* (2008) Probabilistic landslide risk analysis considering direct costs in the area north of Lisbon (Portugal). Geomorphology 94: 467-495. DOI: 10.1016/j.geomorph.2006.10.040

# Capítulo II. Satellite images and landslide identification

**Satellite stereoscopic pair images of very high resolution to build landslide inventory in Pahuatlán, Puebla.**

# Satellite stereoscopic pair images of very high resolution: a step forward for the development of landslide inventories.®

Franny Giselle Murillo-García
Posgrado en Geografía UNAM

Irasema Alcántara Ayala
Instituto de Geografía UNAM

Francesca Ardizzone
Istituto di Ricerca per la Protezione Idrogeologica (CNR-IRPI)

Mauro Cardinali
Istituto di Ricerca per la Protezione Idrogeologica (CNR-IRPI)

Federica Fiorucci
Istituto di Ricerca per la Protezione Idrogeologica (CNR-IRPI)

Fausto Guzzetti
Istituto di Ricerca per la Protezione Idrogeologica (CNR-IRPI)

*Development of landslide inventories based on remote sensing techniques has become one of the main tools in assessment of hazards and risk. Among those techniques, visual and automatic and semi-automatic analysis of high- and very highresolution (VHR) satellite images, or a combination of these, has recently been considered as a promising way to identify and map landslides at local and regional scales. In this context, a landslide inventory for the municipality of Pahuatlán, Puebla, in central Mexico was prepared by combining three techniques: (1) visual analysis of stereoscopic pairs of VHR satellite images (GeoEye-1), (2) visual analysis of monoscopic VHR satellite images (SPOT 5 and Google Earth images), and (3) field surveying. In this paper, particular attention is given to landslide identification and mapping based on the GeoEye-1 stereo-pairs. Additionally, as a preliminary step in the use of VHR imagery, a general review is presented of the available VHR satellite images, software and hardware that can be useful for digital mapping of landslides.*

*The landslide inventory included a total of 577 landslides, corresponding to an average density of 10.5 landslides per km2. Of these, 385 were classified as recent, 171 as old, and 21 as very old, regardless of state of activity. The total mapped area was 54.9km$^2$; 57.7% of it had been affected by landsliding. The mean area occupied by recent landslides was of the order of 1,066m2; for old landslides, it was 82,559m$^2$ and for very old landslides 1,173,952m$^2$. Debris flows were the most frequent type of movement (217) followed by 167 translational slides, 97 complex movements, 79 rotational slides, and 17 falls and topples. The cost–benefit relationships of a number of these techniques remain debatable because of the high cost of some of the VHR images and the related software and hardware. However, the appearance of new satellite sensors is likely to generate market competence, so this type of image will probably be available at a much lower cost in the near future. Additionally, it is important to consider that the use of several stereo-high-resolution images involves no cost, as downloading high-resolution images from Google Earth, using Google Earth Pro is currently available. The relative rapidity of these techniques can be highly valuable after a regional landslide disaster has occurred, since damage to roads and infrastructure usually prevents the rapid and accurate evaluation of the impact of landsliding. Most importantly, these techniques can be of great value for hazard evaluation of potentially unstable inhabited slopes.*

## 2.1 INTRODUCTION

A landslide inventory is a detailed series of records concerning quantity, location, extent, typology, and features related to landslide events in a particular area and period of time. Landslide inventories are essential to estimate and evaluate hazard, vulnerability, and risk (Ardizzone *et al.* 2013). The technique to compile such an inventory depends on the type of inventory required, the extent of the study area, and research aims. Additionally, the scale of the base cartography, the skill of the researchers involved in the investigation, and the available resources must also be considered (Guzzetti *et al.* 2000; van Westen *et al.* 2006).

Literature on landslide inventories has increased rapidly (Bertolini *et al.* 2002; Guzzetti *et al.* 2012). Traditional techniques to construct landslide inventories include: (i) field surveying, frequently to verify data (Carrara and Merenda 1976; Wieczorek 1984; Brardinoni *et al.* 2003; Akgün and Bulut 2007; (ii) historical data compilation (Guzzetti *et al.* 1994; Glade 2001; Carrara *et al.* 2003; Guzzetti *et al.* 2003); (iii) participatory mapping involving local population (Peters-Guarin *et al.* 2012); (iv) analysis of stereopair aerial photographs (Rib and Liang 1978; Cardinali *et al.* 1990; Antonini *et al.* 1993; Harp and Jibson 1996; Quantin *et al.* 2004; Remondo *et al.* 2005; Galli *et al.* 2008); and (v) visual or automatic analysis of low–medium-resolution satellite images (Gagnon 1975; Sauchyn and Trench 1978; Stephens 1988; Scanvic and Girault 1989).

More recently, developed techniques consist of: (i) analysis of high- and very high-resolution (VHR) digital elevation models (DEM) derived from LIDAR (Schulz 2004, 2007; Chen *et al.* 2006; Ardizzone *et al.* 2007; van Den Eeckhaut *et al.* 2007; Haneberg *et al.* 2009; Baldo *et al.* 2009; Booth *et al.* 2009; Corsini *et al.* 2009; Kasai *et al.* 2009; Prokop and Panholzer 2009; Derron and Jaboyedoff 2010; Lan *et al.* 2010; Miner *et al.* 2010; Razak *et al.* 2011; Mann *et al.* (2012; Liu *et al.* 2012; Brown 2012), (ii) visual analysis of monoscopic high- and VHR satellite images (Marcelino *et al.* 2009; Gao and Maroa 2010; Fiorucci *et al.* 2011), and (iii) automatic and semi-automatic analysis of high and very high resolution satellite images (supervised classification, single and multiple change detection and object-oriented image, etc.) (Nichol and Wong 2005; Lee and Lee 2006; Borghuis and Lee 2007; Yang and Chen 2010; Martha *et al.* 2010; Mondini *et al.* 2011; Ping *et al.* 2011). Two or more techniques may be combined (Guzzetti *et al.* 2012).

In recent years, analyses of stereo-pairs of VHR have been considered as a valid alternative for landslide identification (Nale 2002; Weirich and Blesius 2007). VHR images have at least 3 m of spatial resolution; this allows visual identification of recent and old landslide scars in a 3D

60

environment. With these new tools, it is possible to produce detailed regional - and local- scale landslide inventories, and the new development of digital stereoscope systems provides further possibilities to use this type of image. Recent inventories based on stereoscopic analysis of VHR images include those developed by Nichol *et al.* (2006), Alkevli and Ercanoglu (2011), and Fiorucci *et al.* (2011).

Landslide detection in VHR stereo-pair images is based on interpretation of the geomorphological terrain, mainly by identifying the typical topographic signature of different landslide types. Guzzetti *et al.* (2000) describe the latter as an intuitive process, in which the skill and experience of the researcher are key factors. There is not a single or unique method for landslide identification through stereo-pair images; recognition of landslides through imagery may be affected by land-use cover and by height, type, and density of vegetation. Additionally, landslide boundaries could also be difficult to delineate, even in the case of recent or very small landslides (less than 10×10 m).

Visual interpretation of VHR stereo-images can be helpful in recognizing features related to landslide occurrence. These features are: (i) precise location, (ii) area, (iii) type of movement, (iv) material, (v) state of activity, (vi) age, (viii) land use and vegetation, and (ix) elements at risk.

One of the main criteria for landslide classification refers to type of movement (Cruden and Varnes 1996). Therefore, landslide typology is essential for landslide inventories. The key factor in recognizing landslide type through VHR images is the shape of the movement. Generally, slide movements are elliptical in monoscopic images.

In a 3D environment, it is possible to define landslide type—rotational or translational—by the geometry of the main scarp and the position of the displacement material. It is also useful to know the lithological conditions of the area. Rotational landslides show a concave surface of rupture whereas translational slides have a plane surface of rupture, features that can be observed in 3D. Another type of movement is the flow, frequently presenting a source area, main track or channel area, and a deposition area. In a 3D environment, the observer can differentiate the flow of a slide by the clear channel zone. Again, knowledge of the local lithological conditions can be useful.

A landslide inventory for the municipality of Pahuatlán, Puebla, Mexico has been developed. It is based on the stereoscopic interpretation of GeoEye-1 VHR images, with 0.5 resolution in panchromatic band and 1.5 m multispectral bands (near infrared band included), covering an area of 54 km$^2$. This type of landslide inventory can be regarded as an essential instrument given that it can be used as a base map to produce landslide susceptibility and hazards maps. Additionally, analysis and decision-making processes concerning land-use planning and management, disaster prevention, and risk reduction and

management also can be further enriched when adequate and accurate landslide inventories are incorporated.

The paper is organized in four main sections: (1) a general introduction to the study area; (2) a review of the properties of the VHR satellite images and 3D visualization and of the required software and hardware; (3) materials and methods, namely VHR satellite imagery; landslide mapping—pre-processing; identification of old, very old, and recent landslides; and probability density of landslide areas; and (4) results, discussion, and conclusions.

## 2.2 THE STUDY AREA

The municipality of Pahuatlán, in the state of Puebla in central Mexico, covers 80 km$^2$. Within this, the study area covers 54 km$^2$ (Fig. 24). Elevation ranges from 450 to 1,500 masl. The region is characterized by mountainous terrain with deep ravines and high summits, product of the Sierra Madre Orogenesis. The gradient varies from almost zero, along the Plain of San Marcos River, to more than 70° at the top of the mountains. There are outcrops of Mesozoic conglomerates, shales, siltstones, and limestones. The main rock units are: (i) Lower Jurassic Huayacocotla sandstone and shale sequence; (ii) Cahuas siltstone–sandstone formation; (iii) Middle Jurassic Tepéxic limestone formation; (iv) Late Jurassic Tamán clayey limestone and shale sequence; (v) Late Jurassic Pimienta black limestone–shale sequence; (vi) Low Cretaceous Tamaulipas limestone–shale sequence; (vii) Pliocene basalt, andesite, and pyroclastic deposits; and (viii) recent alluvial and colluvial deposits (Sánchez Rojas and De la Callejera Moctezuma 2004).

Each lithological group comprises diverse rocks of varying strength: Hard rocks are massive limestones, sandstones, siltstones, basalts, and andesites; rocks of low resistance include shales, pyroclastic, alluvial, and colluvial deposits. Rocks are mostly layered and have been altered by geotectonic processes and local metamorphism (Oliva Aguilar *et al.* 2011). Soil types reflect the variations of lithology. Among the most significant geological structures are the Huayacocotla anticline (a macrostructure with a NNW–SSE axis) and San Pablo syncline. The Paciotla normal fault and Xolotla inverse fault are two of the main structural discontinuities of the region (Fig. 25).

The climate is temperate, with abundant precipitation all year and mean annual rainfall of 2,500 mm. The vegetation includes rainforest and coniferous forest, but high levels of deforestation are also present. Landslides of diverse types, with varying depth and age, are abundant in the municipality, most of them triggered by intense and prolonged rainfall associated with hurricanes, tropical depressions, and a combination of various hydrometeorological conditions.
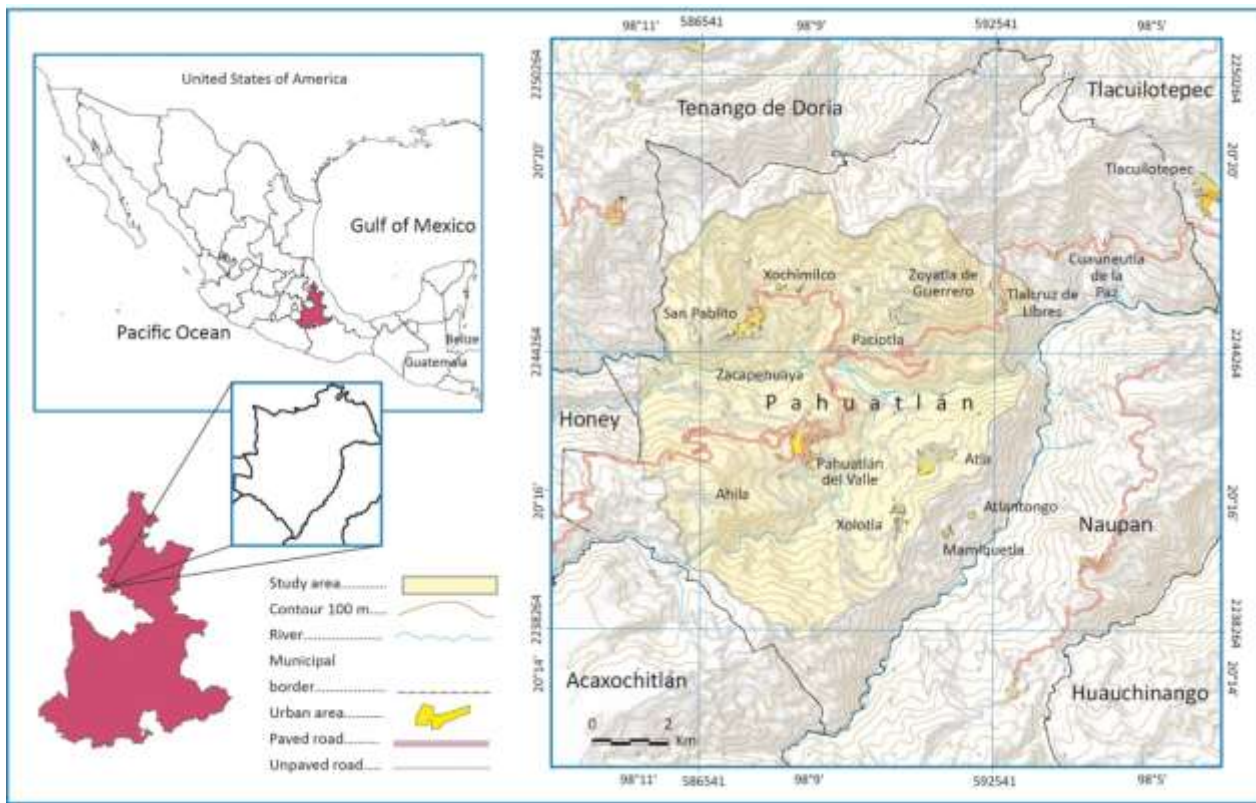
*Figure 24. Location of Pahuatlán municipality, Puebla, Mexico.*

# 2.3 VHR STEREOSCOPIC SATELLITE IMAGES AND 3D VISUALIZATION

The use of satellite images for landslide recognition dates back to the 1970s, when images originally available to the military were also made available to researchers. The first satellite platforms for acquisition of images of the Earth's surface for civil research were government Landsat and SPOT projects, but their spatial resolution (more than 30 m) only allowed the identification of very large landslides. In 1986, SPOT was the first satellite to provide 3D stereo-images of inaccessible areas (Nikolakopoulos and Lathourakis 2005). In the late 1990s, VHR satellite images were acquired by the first commercial platforms: IKONOS and OrbView. Nowadays, many platforms give access to VHR stereo-images (Fig. 26). They can be obtained by the sensors in two ways: across track and along track.
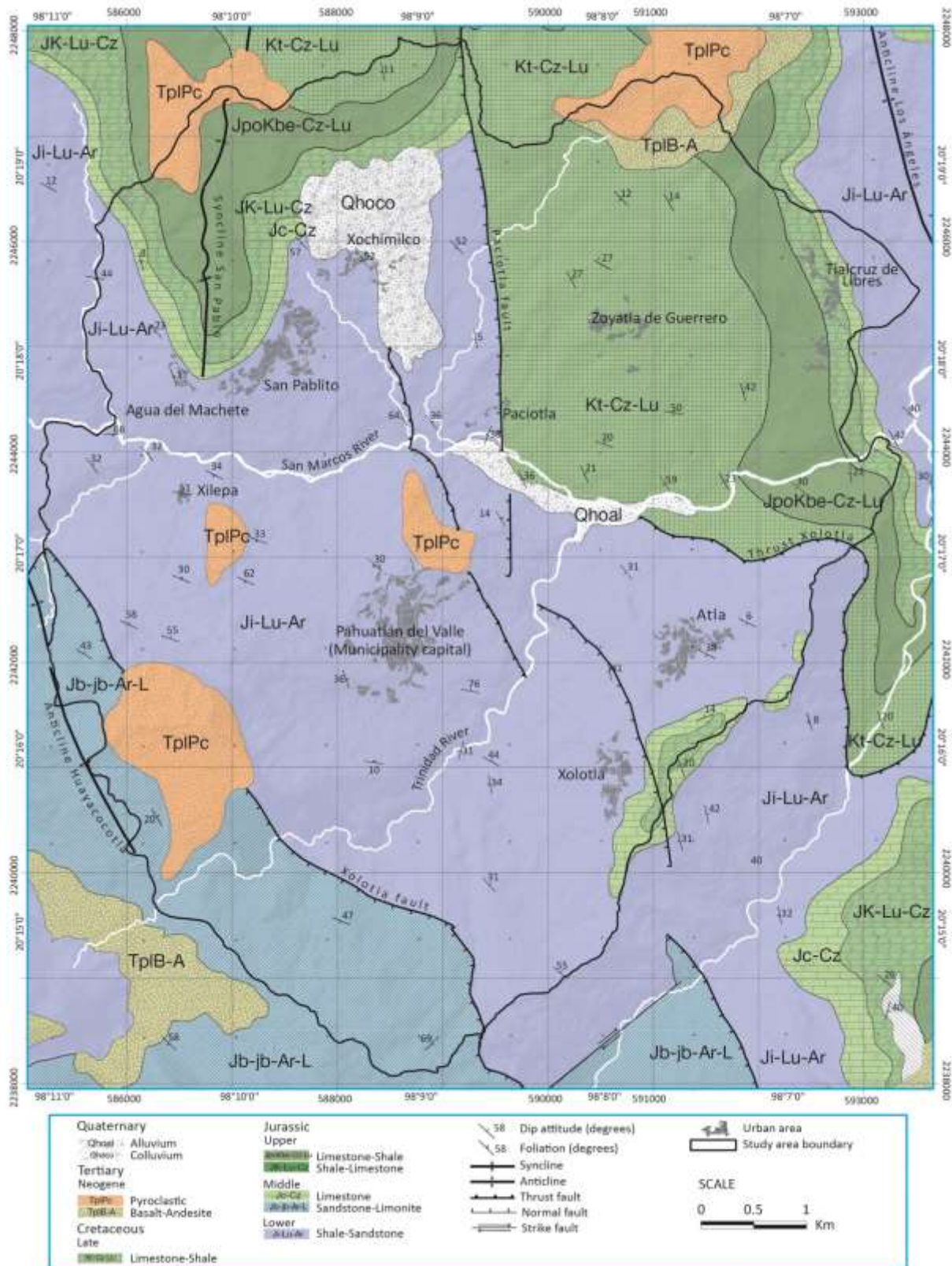
**Figure 25** *Lithology of the study zone (source: adapted from Loaeza-García and Zárate-Barradas 2005 and Sánchez-Rojas and De la Callejera-Moctezuma 2004.*

Across track, two scenes from the same area are acquired from two perspectives through different passes of the satellite within a period of hours or days. Along track, two scenes from the same area are acquired from two perspectives on the track of the satellite with only seconds of difference; this time lapse is a function of the difference between the forward and backward viewing angles (60–100 s, depending on the satellite) (Krishnaswamy and Kalyanaraman 2005).

| Platform | Country | Launch date | Radiometric resolution | Bands (µm) | Spatial resolution | Stereo mode |
|---|---|---|---|---|---|---|
| IKONOS | USA | 1999 | 11 bits | PAN 0.45-0.90, B 0.45-0.52, G 0.52-0.60, R 0.63-0.69, NIR 0.76.0.90 | 0.82 m PAN<br>4 m MS | AL |
| Quickbird | USA | 2001 | 11 bits | PAN 0.45-0.90 , B 0.45-0.52,G 0.52-0.60, R 0.63-0.69,NIR 0.76-0.90 | 0.61 m PAN<br>2.4 m MS | AL |
| WorldView-1 | USA | 2007 | 11 bits | PAN 0.45-0.90 | 0.50 m MS | AL |
| WorldView-2 | USA | 2008 | 11 bits | PAN 0.45-0.80, B 0.40-0.45, B 0.45-0.50, G 0.50-0.58, G 0.58-0.62, R 0.60-0.70, NIR 0.70-0.74, IR 0.86-1.0 | 0.46 m PAN<br>1.8 m MS | AL |
| OrbView-3 | USA | 2003 | 10 bits | PAN 0.45-0.90, B 0.45-0.52, G 0.52-0.60, R 0.63-0.69, NIR 0.76-0.90 | 1 m PAN<br>4 m MS | AL |
| GeoEye-1 | USA | 2008 | 11 bits | PAN 0.45-0.90, B 0.45-0.52 ,G 0.52-0.60, R 0.62-0.69,NIR 0.76-0.90 | 0.4 m PAN<br>1.64 m MS | AL |
| SPOT-5 | France, Belgium, Sweden | 2002 | 8 bits | PAN 0.48-0.71, G 0.50-0.59, R 0.61-0.68, NIR 0.78-0.89, MIR 1.58-1.75. | 2. 5 or 5 m PAN<br>10 m MS<br>20 m MIR | AL-AC |
| SPOT-6 | France, Belgium, Sweden. | 2012 | 8 bits | PAN 0.45-0.74, B 0.45-0.52, G 0.53-0.59, R 0.62-0.69, NIR 0.76-0.89 | 1.5 m PAN<br>8 m MS | AL |
| EROS-A | Israel | 2000 | 8 bits | PAN 0.48-0.71 | 1.9 m | AC-AL |
| EROS-B | Israel | 2006 | 8 bits | PAN 0.48-0.71 | 0.7 m | AC-AL |
| Pleidades-1A and 1B | France | 2011-2012 | 12 bits | PAN 0.48-0.83, B 0.43-0.55, G 0.49-061, R 0.60-0.72, NIR 0.75-0.95 | 0.7 m PAN<br>2.0 m MS | AL |
| Resurs-DK1 | Rusia | 2006 | 10 bits | PAN 0.58-0.80, G 0.50-0.60, R 0.60-0.70, NIR 0.70-0.80 | 0.8 m PAN<br>2.0 m MS | - |
| KOMPSAT-2 | South Korea | 2006 | 8 bits | PAN 0.50-0.90, B 0.45-0.52, G 0.52-0.60, R 0.63-0.69, NIR 0.76-0.90 | 1 m PAN<br>4 m MS | AL |
| IRS Cartosat-1 | India | 2005 | 10 bits | PAN 0.50-0.85 | 2.5 m | AL |
| IRS Cartosat-2 | India | 2007 | 8 bits | PAN 0.50-0.85 | 1 m | AL |
| IRS Cartosat-2B | India | 2010 | 8 bits | PAN 0.50-0.85 | 1 m | AL |
| Formosat | Taiwan | 2004 | 8 bits | PAN 0.45-0.90, B 0.45-0.52, G 0.52-0.60, R 0.63-0.69, NIR0.76-0.90 | 2 m PAN<br>8 m MS | AL |
| Theos | Thailand | 2007 | 12 bits | PAN 0.45-0.90, B 0.45-0.52, G 0.53-0.60, R 0.62-0.69, NIR 0.67-0.90 | 2 m PAN<br>15 m | AL |
| TopSat | UK | 2005 | 8 bits | PAN 0.50-0.70, B 0.45-0.50, G 0.50-0.60, R 0.60-0.70 | 2.5 m PAN<br>5 m MS | AL |
| ALOS | Japan | 2006 | 8 bits | B 0.4-0.5, G 0.5-0.6, R 0.61-0.69, NIR 0.76-0.89, PAN 0.52-0.77 | 2.5 m PAN<br>10 m MS | AL |
| RazakSat | Malaysia | 2007 | 8 bits | PAN 0.51-0.73, B 0.45-0.52, G 0.52-0.60, R 0.63-0.69, NIR 0.76-0.89 | 2.5 m PAN<br>5 m MS | AL |
| DubaiSat-1 | UAE | 2009 | 8 bits | PAN 0.42-0.72, B 0.420-0.510, G 0.51-0.58, R 0.600-0.720, NIR 0.76-0.89 | 2.5 m PAN<br>5 m MS | - |

*Figure 26. Characteristics of platforms for the acquisition of VHR satellite images. USA United States of America, UK United Kingdom, UAE United Arab Emirates, PAN panchromatic, MS multispectral, B blue band, G green band, R red band, NIR near infrared band, MIR medium infrared, AL along track, AC across track.*

With the along-track mode, the short time interval between the images reduces radiometric variation and increases the rate of image matching (Nikolakopoulos and Lathourakis 2005). The stereoscope satellite images can be used to prepare 3D views, depending on the available software (Nichol *et al.* 2006; Ardizzone *et al.* 2013; Guzzetti *et al.* 2012). Pleiades for instance has four images for better stereo analysis (Bernard *et al.* 2012; Poli *et al.* 2013).

Human binocular vision unifies two separate monocular views into a cyclopean view (Blake and Fox 1973). This system is imitated by stereoscopic vision in which the observer has the 3D depth perception arising from binocular disparities (Howard and Rogers 2012). Interpretation of aerial photography uses traditional mechanical stereoscopy (analog photogrammetry). More recently, digital stereoscope systems combine hardware and software to obtain stereoscopic visualization on computer monitor screens (digital photogrammetry). The new systems simplify the acquisition of information from stereoscopic images that can be stored directly in a GIS database, reducing the acquisition time and errors associated with manual digitalization in traditional analog stereoscopes (Ardizzone *et al.* 2013). Digital instruments can be simpler and more compact than analog systems (Navarrete 2003).

The most common ways to achieve an adequate interpretation from 2D-pair satellite images are: (i) use of a stereogram, which involves two different images of the same area from two different perspectives, either digital or printed, where the images can be used on a conventional stereoscope; (ii) generating a stereo-pair using a single orthoimage and a digital elevation model (e.g., ILWIS software); and (iii) draping the satellite images over a generated DEM (Nichol *et al.* 2006).

The current 3D digital stereogram viewing methods (Figure 27) can be summarized as follows (Petrie 2001; Olm and Gaffney 2010):

1. Binocular viewing

- Dual stacked projectors: twin monitors viewed with a mirror stereoscope
- Split-screen stereo: single monitor display with split-screen viewing

2. Complementary filters

- Twin monitors viewed through polarizing passive glasses (MVPG)
- Anaglyph

3. Alternating images (alternating images on the monitor screen with alternating shutters for 3D stereo-viewing)

- Passive glasses
- Active glasses (circular polarization or linear polarization)

4. Auto-stereoscopic display systems (lenticular screens obviating the use of glasses)

| Current Methods | Systems | Special monitor | Cost approximately (2012) | Examples of used on landslide identification: |
|---|---|---|---|---|
| **Dual stacked projectors (DSP)** | I2S DPW | No, but need two monitors. | Now out of the market | |
| **Split-screen stereo** | Kern DSP1 DPW, LH Systems' 600 series DPWs SOCET SET software suite, GeoSystems Delta Workstation and KLT Associates Atlas DPW | No | Now out of the market | |
| **Anaglyph** | Standard Anaglyph | No | Low cost | Nichol *et al.*, 2006; Abdallah et. al., 2010; Chen and Chen, 2012, |
| | NVIDIA 3D Vision Discover | No | Free | |
| | iZ3D driver for ATI | No | Company doesn't work anymore, closed since 2013. Drivers still on line free. | |
| | NVIDIA GPUs | No | High | |
| **MVPG** | Planar's SD StereoMirror™ technology | Yes (two) | $3700 USD | Ardizzone *et al.*, 2011. |
| | Topcon PI-1000 DPW | | Now out of the market | |
| | Galileo/Siscam's Stereodigit | | Now out of the market | |
| | Microdigit DPWs | | Now out of market | |
| **Passive 3D glasses** | Zalman 3D Monitors | Yes | $500 USD | |
| | iZ3D Monitor | Yes | Company doesn't work anymore. | |
| | Miracube 3D monitors | Yes | Discontinue | |
| | Hyunday 3D, Acer Aspire 5738DG. | | | |
| **Active 3D (shutter) glasses** | NVIDIA 3D Vision | No | $600 USD | |
| | True3Di | Yes | | |
| **Auto-stereoscopic display systems** | Philips autostereoscopic LCD monitor, Sharp PC-RD3D and LL-151D, Tridelity MV42. | Yes | $10 000 -13 000 USD | In development for Geosciences since 2009. |

*Figure 27* Hardware technologies available for digital stereoscope (source: based on Boulos and Robinson 2009. DSP dual stacked projectors a Price of stereo-images should also be added (US $3–120 km2 depending on the sensor, number of bands, and level of the images pre-processing).

67

Alternating images and auto-stereoscopic methods, common in home-theater movies and videogame systems, are still at the experimental phase in digital photo-interpretation. For landslide identification, anaglyph and, less commonly, MVPG systems are used. Anaglyph is the least expensive and easiest way to view but has limited and desaturated color fidelity; it produces a ghosting effect and retinal rivalry (Boulos and Robinson 2009; Olm and Gaffney 2010). On anaglyph stereoscopy, left and right images are color encoded by respective complementary color filters (cyan and red), to separate the images as required for a 3D effect (Beiser 1981). Each filter excludes the corresponding image in the stereo pair and creates the necessary separation of the left and right images (Ostnes *et al.* 2004). Anaglyphs are fatiguing for the observer, and the experience can be less than optimal. They cannot be used with color images, and it is not very well possible to digitize the interpretations with anaglyphs as the cursor is located above the terrain. Additionally, split screen stereo (Tempfli *et al.* 2009) is extensively used (e.g., developed by ITC, the Netherlands), and also alternating image interpretation in ERDAS is a common feature and used extensively for landslide interpretation.

GIS software, first recognized in 1962, is used for capturing, creating, structuring, managing, and presentation and visualization of geo-referenced information (Steiniger and Weibel 2010; Bektas and Coltekin 2012). Stereoscopic visualization has developed remarkably in the past decade (Fig. 28).

| Software | License | Available for: | Stereo visualization support | Method |
|---|---|---|---|---|
| ESRI ARCGIS | Commercial | Windows, Linux and Unix. | Arc scene and Stereo Analyst extension | Anaglyph, MVPG, AG and PG. |
| Quantum GIS | Free | Windows, Mac, Linux, Unix. | Globe Plugin | Anaglyph, AG and PG. |
| ERDAS Imagine | Commercial | Windows. | Stereo Analyst | Anaglyph, MVPG, AG and PG. |
| GRASS | Free | Unix, Mac, Linux, Unix. | ppmtorgb3 and rgb3toppm commands | Anaglyph |
| gvSIG | Free | Windows, Mac, Linux, Unix. | 3D y animación and StereoWebMap extensión. | Anaglyph, Split-screen stereo, PG, AG, |
| Intergraph | Commercial | Windows. | Image station Stereo for GeoMedia | AG and PG. |
| ILWIS | Free | Windows | Stereoscope window | Anaglyph and Split-screen stereo |
| Autodesk AutocadMap | Commercial | Windows and Linux. | LandXplorer ELCOVISION 10 Super/Imposition | Anaglyph and AG. |
| Bentley | Commercial | Windows | P600, Super/Imposition | Anaglyph, AG and PG. |
| Map Info | Commercial | Windows and Unix. | MapInfo Engage 3D | Anaglyph and PG |
| IGiS | Commercial | Windows | 3D modeling module | Anaglyph |
| Remote view | Commercial | Windows | | Anaglyph and MVPG |
| StereoGIS | Commercial | Windows | Viewer Module | Anaglyph, PG and AG. |
| PurVIEW | Commercial | Windows | | Anaglyph and AG |
| SOCET | Commercial | Windows and UNIX | Stereo | Split-screen |

| | | | | |
|---|---|---|---|---|
| **GXP and SOCET SET** | | | | stereo, MVPG, AG, PG, |
| **ENVI** | Commercial | Windows | | Anaglyph |
| **IDRISI** | Commercial | Windows | | Anaglyph |
| **PHOTOMOD** | Commercial (There's a limited free version) | Windows | | Anaglyph, AG and PG. |
| **MicroImages TN Tmips** | Free | Windows and Mac | Stereo Viewing | Anaglyph, AG and PG. |
| **Vr Mapping Cardinal Systems** | Commercial | Windows | Vr Two | Anaglyph, MVPG, AG and PG. |
| **DAT/EM** | Commercial | Windows | Summit Evolution | AG and MVPG |
| **DVP digital photogrammetry** | Commercial | Windows | | MVPG |
| **GeoCue** | Commercial | Windows | OthoPro | MVPG |
| **Inpho** | Commercial | Windows | Submit evolution | Anaglyph, MVPG, AG and PG, Split-screen stereo and DSP. |
| **Fledermaus** | Commercial | Windows, Mac, Linux, Unix. | | Split-screen stereo, MVPG. |
| **KLT ATLAS/DSP** | Commercial | Windows | Digital Stereoplotter | Split-screen stereo, MVPG, PG, AG. |
| **PCI Geomatica** | Commercial | Windows, Unix. | Orthoengine | Anaglyph, AG, PG. |

*Figure 28. Software available to obtain stereo-view (source: based on Bektas and Coltekin 2009).*

# 2.4 MATERIALS AND METHODS: LANDSLIDE MAPPING

### 2.4.1 Materials: VHR satellite imagery

The landslide inventory for Pahuatlán was prepared by a combination of three techniques: (i) visual analysis of stereoscopic pairs of VHR satellite images (GeoEye-1), (ii) visual analysis of monoscopic VHR satellite images (SPOT 5 and Google Earth images), and (iii) field surveying. In this paper, particular attention is given to the process involved for landslide identification based on the GeoEye-1 stereo-pairs.

GeoEye-1 stereoscopic pair images with 0.5 m spatial resolution on panchromatic band and 1.0 m spatial resolution, taken on 31 March 2010, were used to prepare a landslide inventory map (Fig. 29). GeoEye-1 was launched on 6 September 2008, and its sensor can be pointed up to 60° off nadir to generate stereo-images (Kliparchuk and Collins 2010). The images were available in panchromatic and multispectral bands. The average sun azimuth and elevation angles at the acquisition time were 124.3° and 63.6°, respectively (www.digitalglobe.com).

| Acquisition | 31 March 2010 at 17:10 GTM |
|---|---|
| Level processing | Geometric standard correction |
| Interpolation | Cubic convolution |
| Projection | Geographic |
| Datum | WGS84 |
| Units | Degrees |
| Format | Tiff |
| Overlap | 95% |

*Figure 29. Characteristics of the GeoEye-1 image acquired for the area of study*

Each image was provided with rational polynomial coefficients (RPCs), which represent the relationship of the ground to image geometry, allowing photogrammetric processing (Nichol *et al.* 2006; Ardizzone *et al.* 2013). The RCPs generate the 3D models via specialized software. Planar's SD StereoMirror™ technology improved the identification of landslides in 3D.

The system works with two monitors active matrix liquid crystal display (AMLCD) oriented with 110° of angular distance. A passive beam splitter mirror bisects the angle formed between the two monitors. One side of the glass mirror has a reflective coating, and the other side has an anti-reflective coating, thus allowing the user to see the two stereo-images of the monitors at the same time. When stereo-pair images from the two monitors are viewed through crossed polarizing glasses, the user only sees the left-eye image with one eyepiece and the right-eye image with the other eyepiece with different polarization angles (Fig. 30). The result is a single, fused stereoscopic image (Planar 2008).
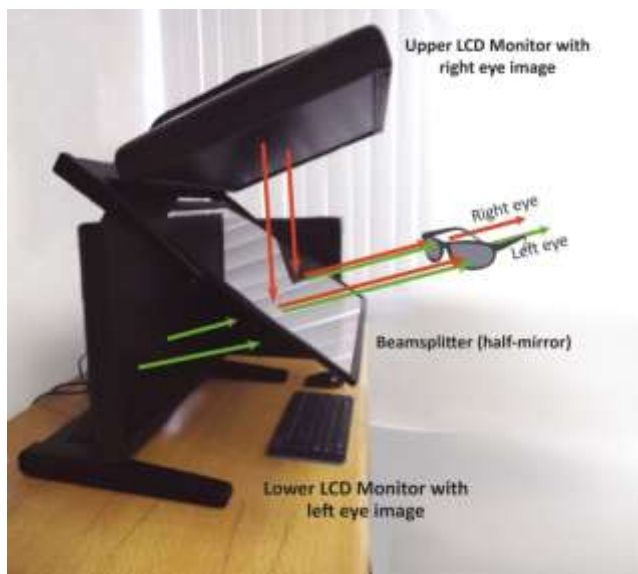


*Figure 30. Diagram of the basic components of the PLANAR StereoMirror system*

### 2.4.2 Landslide mapping: pre-processing

To test the stereoscopic landslide recognition, visual interpretation of the GeoEye-1 images was selected instead of a multispectral analysis. Nonetheless, pre-processing was necessary to optimize this visual interpretation. The pre-processing of raw satellite images includes: (i) pansharpening, (ii) orthorectification, (iii) coregistration, and (iv) radiometric correction (Guzzetti *et al.* 2012).

For this research, the Gram–Schmidt Spectral Sharpening algorithm was used for combining (pansharpening) higher-resolution panchromatic and lower-resolution multispectral information from GeoEye-1 images. Pansharpening produced a single high resolution false-color (blue–green–red bands) or near-infrared (blue–green–near-infrared bands) image. Pansharpened images increase the visual impact of landslide detection and mapping (Guzzetti *et al.* 2012). In this case, ENVI 4.8® software generated the pansharpened image, but other software can also be useful for this process (Fig. 28).

The next step consisted of generating the 3D model. RPCs, incorporated with the images, provided a representation of the ground-to-image geometry, thereby allowing the photogrammetric processing and the generation of 3D models for the stereo-pair (Ardizzone *et al.* 2013). The Leica Photogrammetry Suite (LPS) ERDAS IMAGINE® module was used to create an orientated block with the RPCs. Files of this block type are compatible with the Stereo Analyst ArcGIS® extension. A 3D view of the GeoEye-1 pansharpened images was generated on the Stereo Analyst module, and the Planar StereoMirrror® technology was used for visualization of the 3D view. The Stereo Analyst extension works with a floating cursor; here, the cursor is on the topographic surface in order to draw vectors.

Finally, in the 3D view environment, it was possible to identify shallow and deep-seated slides and flows and also a few rock falls and old and very old landslides. Source, travel, and deposit areas were all drawn in 3D and directly stored in a GIS database, reducing the time and errors associated with manual digitalization (Galli *et al.* 2008; Ardizzone *et al.* 2013). Differentiation between scarps and bodies was also made.

### 2.4.3 Identification of old and very old landslides

The criteria for landslide identification in stereo-pair VHR images followed those of the interpretation of stereoscopic aerial photographs. Features related to the signatures of the mass movement were shape, size, tone, color, mottling, texture, pattern, and topography (Ray 1960; Allum 1966; Rib and Liang 1978; van Zuidam 1985; Ardizzone *et al.* 2013; Guzzetti *et al.* 2012), in addition to climate, geology, soil, and land use as the main physical conditions. The relative age of the mass movements was inferred from the local morphological characteristics, the appearance of the landslide on the

71

GeoEye-1 stereo-images, the lithological and structural setting, and in a few cases only, by historical records provided by the inhabitants of Pahuatlán.

Old landslides were considered to be those that occurred more than 20 years ago. However, the range does not cover a specific period of time since it has not yet been possible to date its occurrence. These landslides may be dozens, hundreds, or even thousands of years old, and the state of activity of some of them can be regarded as dormant or stabilized (Cruden and Varnes 1996). In this type of landslide, recolonization by vegetation is present in addition to the dissection of the new topography by drainage (Cruden and Varnes 1996). Moreover, the occurrence of more recent landslides within the main body of an old and large landslide was also used as a criterion to define the category of very old landslides (Cruden and Varnes 1996).

Both old and very old landslides were recognized on the VHR stereo-pairs, regardless of the state of activity. It was possible to identify the scarps or crowns and the area of deposit (Fig. 31). It is important to point out that the occurrence of small movements cannot be excluded, as maximum resolution of images is 0.5 m. Furthermore, assessing the state of activity or the level of hazard of an "old landslide" will depend on the particular geomorphological attributes and conditions of the vegetation cover, so that landslide recognition will vary from one landslide to another. Therefore, in this area, identification of old and very old landslides, state of activity, and small movements needs to be further and carefully assessed, given that the principal towns in the municipality of Pahuatlán (Pahuatlán de Valle, Xolotla, Atla, and San Pablito) are located on very old landslides.

### 2.4.4 Identification of recent landslides

Recent landslides are those that have occurred no more than 20 years ago. They can be easily recognized by identifying the scarp and deposit zone in addition to changes of vegetation patterns. Under such circumstances, soil exposure shows a color, tone, and texture (depending on the soil type and humidity level) that differ from those of the surrounding area. Another key element is size; the 0.5-m spatial resolution of the GeoEye-1 images allowed the identification of very small landslides (25 m$^2$ or less). Additionally, the zoom software function of the GeoEye-1 could modify the stereo-images and improve them from a total image view (scale 1:50,000) to a very detailed view (1:5,000). This capability allowed the identification of many landslides with a range of sizes. In contrast to the old landslides, recent landslides frequently have small areas, and their signatures are smoothed or totally removed by natural and anthropic processes in less time. In the study zone, shrubby vegetation can develop very rapidly; thus, if landslides are no longer active, 2 or 3 months are enough for vegetation recovery, and this may affect the identification process.
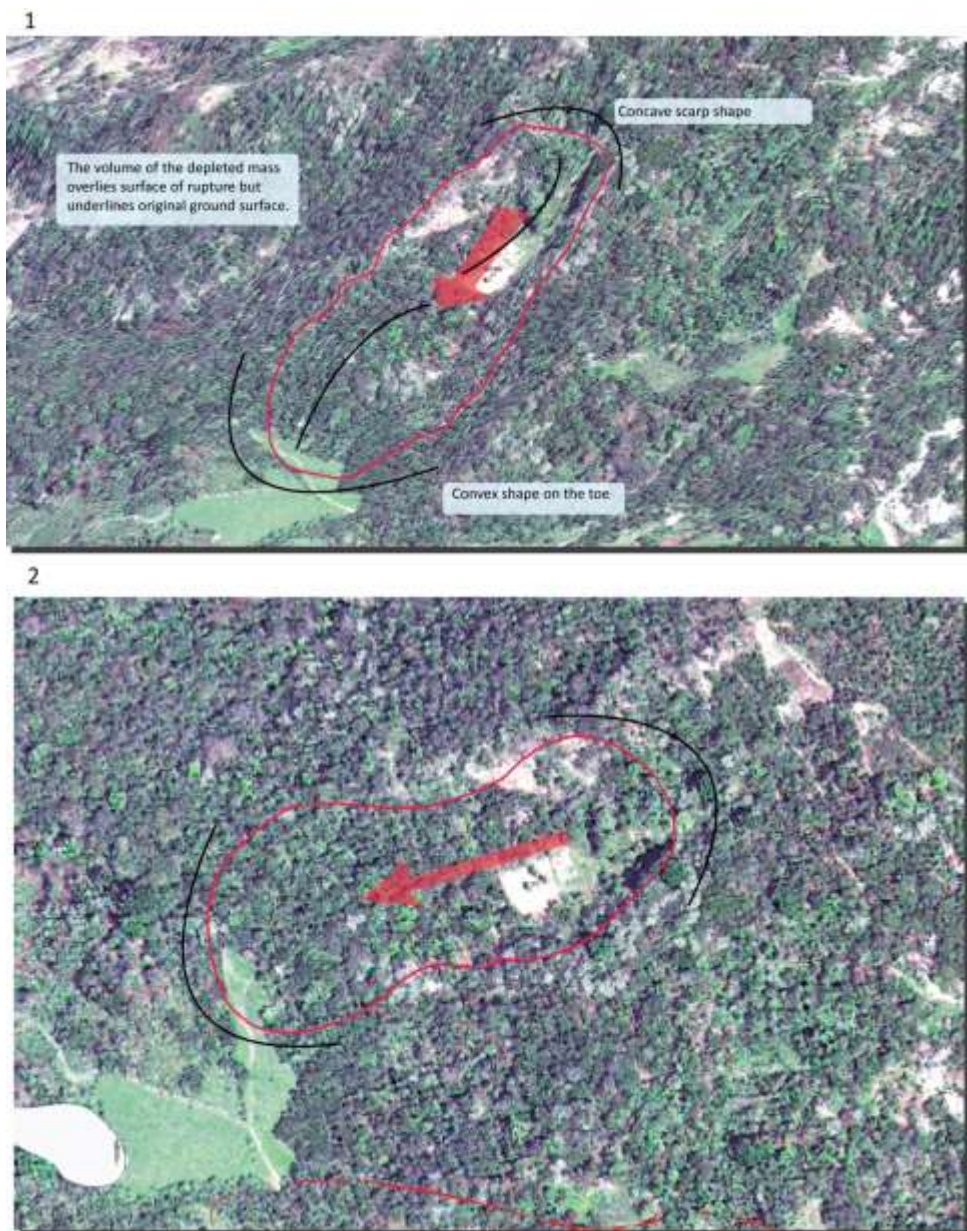
*Figure 31. 3D view (1) and 2D view (2) of an old rotational landslide near Xolotla town, in Pahuatlán. Lack of the third dimension hinders the interpretation of geomorphological evidence.*

One of the major difficulties of this work involved the identification of landslides in urban environments and involving roads because landslide deposits are quickly cleared to restore vehicular transit; in the village of Pahuatlán, a landslide along the main street, 5 de mayo, is a clear example of this (Fig. 32). Here, mitigation works including small dams or blockades and nets were implemented, and therefore, the appearance of the landslide was modified; this made the accurate delimitation of the affected area more difficult.
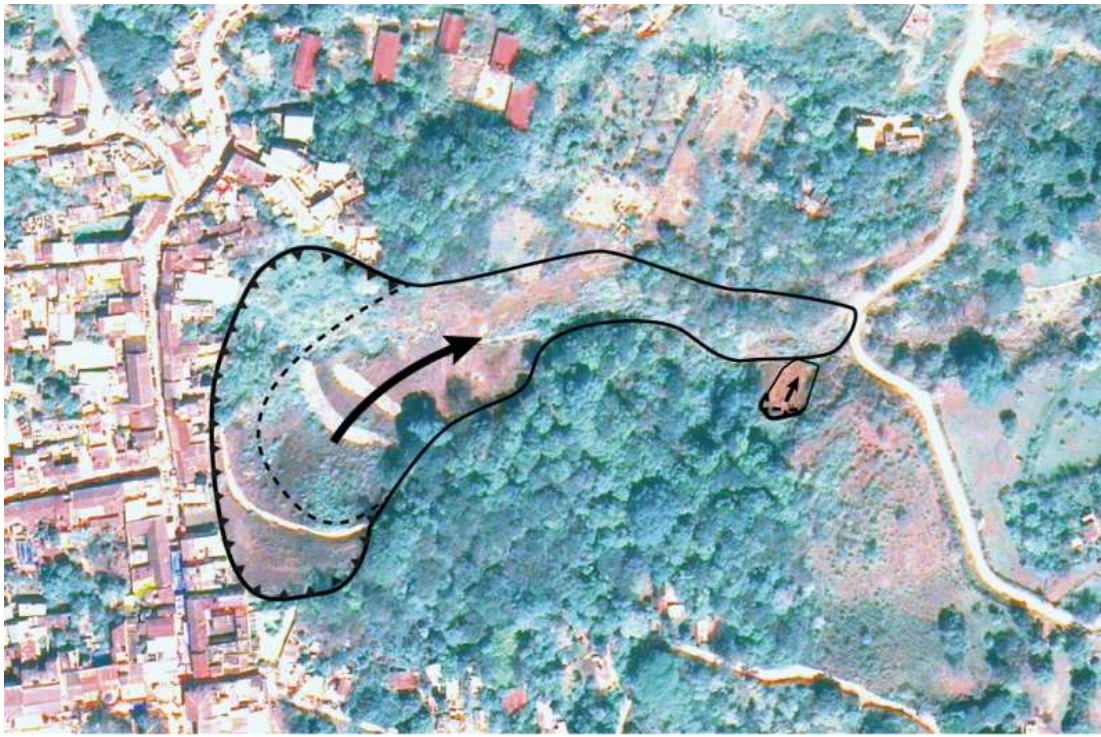
**Figure 32.** *Landslide along 5 de mayo Street, Pahuatlán village. Mitigation works were performed in order to stabilize the slope.*

### 2.4.5 Probability density of landslide areas

Finally, as the areas of individual recent landslides in the inventory were established, the probability density function of landslide areas was ascertained through power law models. Three models were applied: double Pareto distribution (Rossi *et al.* 2012), inverse Gamma distribution (Rossi *et al.* 2012), and double Pareto simplified distribution using parametric and non-parametric approaches (Al-Athari 2011). The non-parametric approaches included: (a) histogram density estimation (HDE), (b) Kernel density estimation (KDE), and (c) maximum likelihood estimation (MLE).

## 2.5 RESULTS

The landslide inventory developed for the municipality of Pahuatlán comprised a total of 577 landslides, corresponding to an average density of 10.5 landslides per km$^2$ (Fig. 33 and 34). Of those 577 movements, 385 were classified as recent, 171 as old, and 21 as very old. The total mapped area was 54.9 km$^2$; 57.7 % of it had been affected by landsliding, but only 1 % was affected by recent landslides. This difference can be explained since very old landslides were generally very large; the area of individual landslides varied from 11.9 to 20,229 m$^2$ for the recent landslides, whereas for the

old and very old landslides it ranged from 1,764 to 4,142,569 m$^2$. The mean extension occupied by recent landslides was of the order of 1,066 m2, 82,559 m$^2$ for old landslides, and 1,173,952 m$^2$ for the very old landslides. Of the 577 landslides, 390 (67.5 %) were detected directly on the GeoEye-1 stereo-pairs, and the rest (32.5 %) were recorded by field surveys, observations made by the inhabitants or other remote sensing materials (1:20,000 orthophotograph from 1994, a SPOT5 2.5-m spatial resolution pansharpened monoscopic image, Google Earth® air photographs from 2004, VHR images from the Google Earth® 2009 and 2011). Old and very old landslides were entirely detected in the GeoEye-1 stereo-pairs; this meant the identification of 198 recent landslides in these images.

| | Very old landslides | Old landslides | Recent landslides | Total |
|---|---|---|---|---|
| Total area (km$^2$) | n/a | n/a | n/a | 54.9 |
| Total number of landslides | 21 | 171 | 385 | 577 |
| | | | | |
| Landslide % | 3.6 | 29.6 | 66.8 | 100 |
| Total surface affected by landslides (km$^2$) | 27.9 | 15.1 | 0.50 | 43.5 |
| Total area affected by landslides (%) | 50.8 | 40.9 | 0.94 | 57.7 |
| Landslide density (landslides/km$^2$) | 0.4 | 3.1 | 7.0 | 10.5 |
| Area of the smallest landslide (m$^2$) | 249,132 | 1,764 | 11.9 | 11.9 |
| Area of the largest landslide (km$^2$) | 4.1 | 0.4 | 0.02 | 4.1 |
| Mean landslide area (km$^2$) | 1.1 | 0.08 | 0.001 | 0.07 |

*Figure 33. Landslide data for Pahuatlán, Puebla, Mexico derived from the inventory.*

Of the movements mapped, 217 were flows, 167 translational slides, 97 complex movements, 79 rotational slides, and 17 were falls and topples. Debris flows were the most frequent type of movement. Complex movements have an intricate geometry in the depletion and accumulation zone; although this kind of movement was recognizable on stereo-view, it was also necessary to do field surveys to validate the type and to understand the particular features in relation to the other types of movements. Rock falls and topples were more complicated to detect on 3D, since they occur on vertical or almost-vertical slopes, and the extent of the deposits was difficult to identify because they frequently occurred along the roads.

The type of movement is closely related to the material involved, and the key feature for defining the type of material by stereo-interpretation is texture. In this work, different materials—rocks, soil, and debris—were surveyed in the field before the stereo-view interpretation was made; this was of great help in defining the type of material for each movement recorded. Figure 35 shows an example of a debris flow detected by stereointerpretation.
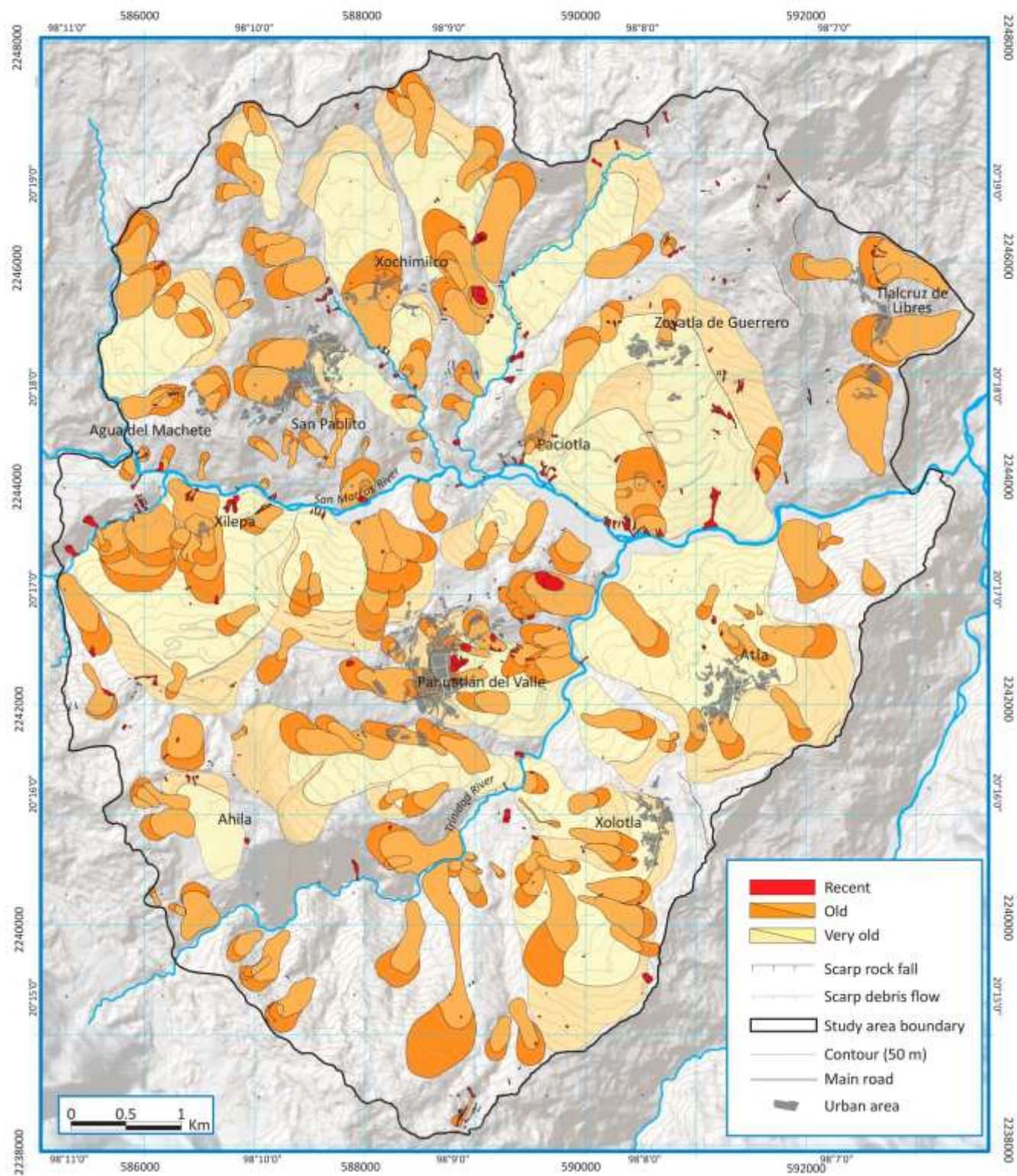
***Figure 34*** *Landslide inventory map for Pahuatlán municipality developed by visual interpretation of the GeoEye-1 stereoscopic images acquired on 31 March 2010.*

As can be seen in Fig. 25, the most extensive unit in the study zone is shales–sandstones from the Lower Jurassic; on it, 212 recent movements, 103 prevailing debris flows, and 57 translational slides were identified. Debris flows were also frequent over pyroclastic deposits. Slides were mainly over shales, mostly intercalated with hard rocks that had been altered by local metamorphism. Falls were most frequently on limestones. Additionally to typology, landslides were also classified as deep-seated or shallow; only 25 out of 385 recent landslides were classified as deep-seated. The range of persistence, in other words where recent landslides occurred over old landslides, was 36 %.

Results of the application of the power law models (Fig. 36 and 37) included the estimation of $r$ value, the parameter α (which controls the slope of the high-value tail distribution), β and η (which do the same for low values), and t and λ (which indicate the position of the maximum of the distribution functions and the maximum and minimum areas (m and c)) (Rossi *et al.* 2012). Furthermore, estimations of value, standard errors, and the estimated error variance (t value) were also obtained for each landslide size distribution model. The $r$ value refers to the rollover value and presents a variation on each applied method with a range between 75 and 339. KDE showed higher values for $r$ (more than 300), whereas HDE and MLE showed $r$ values less than 100. Nevertheless, KDE showed less standard error. The KDE $r$ values showed that the most frequent landslide area in the study zone is close to 340 m$^2$ (Fig. 36 and 37).
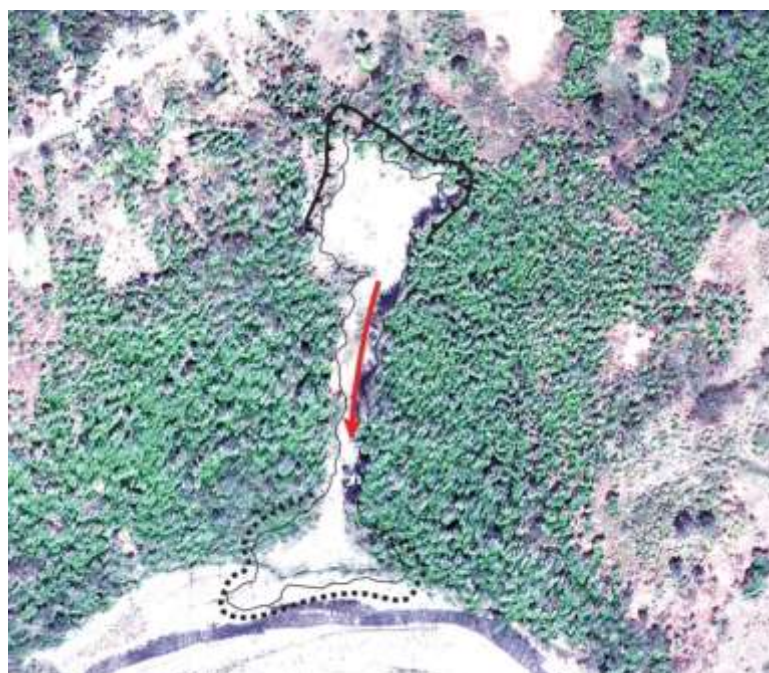


***Figure 35.*** *A debris flow in a 3D view based on a very high-resolution digital elevation model derived from GeoEye-1 stereo-pairs. The source area, channel, and deposit area (partially removed by the river) are visible.*

| Estimation method | | Histogram density estimation | | | Kernel density estimation | | | Maximum likelihood estimation | | |
|---|---|---|---|---|---|---|---|---|---|---|
| | | value | Standar error | t value | value | Standar error | t value | value | Standar error | t value |
| **Double Pareto simplified** | α | 1.13 | 0.07 | 15.63 | 1.15 | 0.01 | 176.21 | 1.22 | 0.1 | 12.02 |
| | β | 1.88 | 0.2 | 9.19 | 1.73 | 0.02 | 96.56 | 1.41 | 0.22 | 6.36 |
| | t | 191.88 | 54.29 | 3.53 | 227.15 | 5.76 | 39.46 | 340.72 | 97.42 | 3.5 |
| | r | 88 | NA | NA | 338 | NA | NA | 85 | NA | NA |
| **Double Pareto** | α | 1.13 | 0.07 | 15.71 | 1.15 | 0.01 | 178.07 | 1.19 | 0.12 | 10.16 |
| | β | 1.88 | 0.2 | 9.2 | 1.73 | 0.02 | 97.22 | 1.35 | 0.26 | 5.24 |
| | t | 192.86 | 54.45 | 3.54 | 227.83 | 5.73 | 39.77 | 347.78 | 119.33 | 2.91 |
| | c | 4.73 | NA | NA | 4.73 | NA | NA | 4.73 | NA | NA |
| | m | 30736.49 | NA | NA | 30736.49 | NA | NA | 30736.49 | NA | NA |
| | r | 88 | NA | NA | 339 | NA | NA | 75 | NA | NA |
| **Inverse Gamma** | α | 1.08 | 0.11 | 9.72 | 1.11 | 0.01 | 119.75 | 1.14 | 0.11 | 10.41 |
| | η | 6.51 | 1.01 | 6.45 | 7.73 | 0.1 | 72.91 | 7.88 | 0.91 | 8.65 |
| | λ | 16.64 | 1.97 | 8.46 | 17.77 | 0.18 | 99.89 | 19.01 | 1.67 | 11.39 |
| | r | 91 | NA | NA | 347 | NA | NA | 107 | NA | NA |

**Figure 36.** *Probability density of landslide areas for Pahuatlán.*
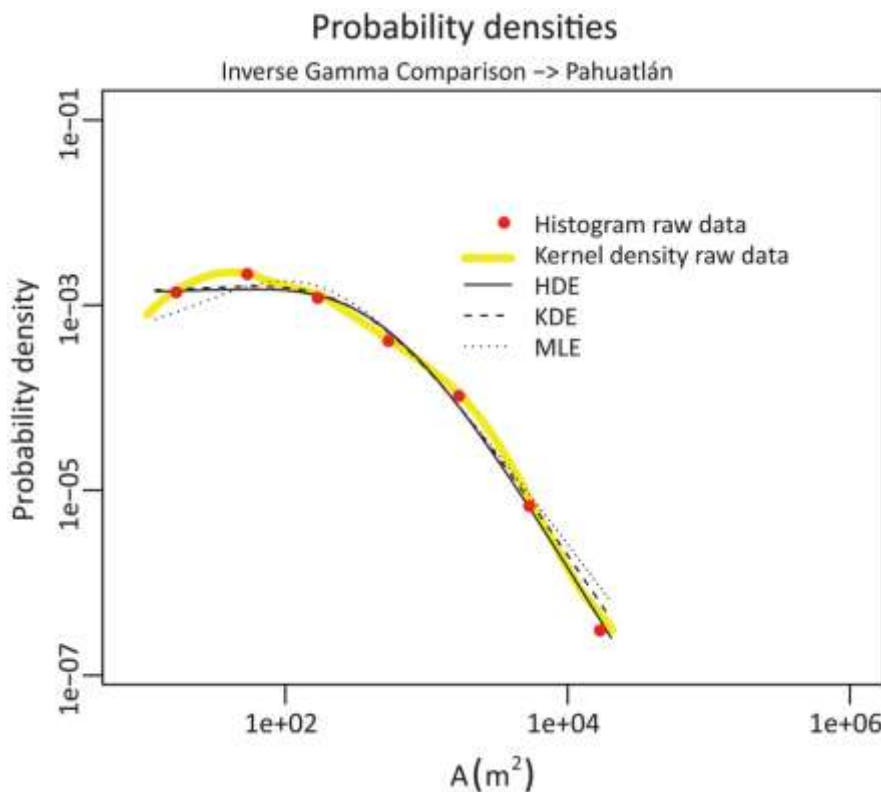


**Figure 37** *Probability density of landslide area, p(AL), for Pahuatlán. Circles represent frequency values calculated by means of histogram estimation of logarithm data.*

## 2.6 Discussion and conclusions

This paper has presented a general review of the available VHR satellite images, software and hardware that can be useful for digital landslide mapping. GeoEye-1 satellite images (0.5 spatial resolution) combined with PLANAR StereoMirror system hardware and Stereo Analyst extension for ArcGIS software were applied to 3D visual identification of landslides within 54 $km^2$ in Pahuatlán, Puebla, central Mexico. The information was directly entered in a digital data base to compile a landslide inventory; the data included the relative age, size, and typology of each landslide. This inventory can provide information needed for landslide hazard assessment.

These results reinforce reports in the literature that the use of VHR images can reduce the time required for landslide recognition and mapping and can improve the accuracy of landslide identification. The spatial resolution of the GeoEye images was good enough for identifying very small landslides (20×20 m), but also for recognizing very old and very large landslides. Furthermore, it was possible to define landslide typology through the 3D landslide identification process. Consequently, it can be said that, by using the tools considered in this research, photo-interpretation can achieve a quality comparable with that achieved by traditional aerial photographs and analog stereoscopes. Moreover, digital tools have the advantage of eliminating manual digitalization errors and reducing the time needed to prepare the landslide inventory.

The cost–benefit relationships of a number of these techniques remain debatable because of the high cost of some of the VHR images and the related software and hardware. However, the appearance of new satellite sensors is likely to generate market competence, so this type of image will probably be available at a much lower cost in the near future. Additionally, it is important to consider that the use of several stereo-high-resolution images involves no cost, as downloading high-resolution images from Google Earth using Google Earth Pro is currently available. A stereo-pair can then be prepared with the free software ILWIS, which also allows split screen interpretation using a screen stereoscope. Perhaps the most important issue regardless of cost is that this rapidity of analysis can be highly valuable after a regional landslide disaster has taken place, since damage to roads and infrastructure usually prevents the rapid and accurate evaluation of the impact of landsliding. Most importantly, these techniques can be of great value for hazard evaluation of potentially unstable inhabited slopes.

# References

Abdallah C, Baghdadi N, Boukheir R (2010) Exploratory GIS & remote sensing analysis for the development of statistical correlations between environmental parameters and mass movements' occurrence. Geophysical Research Abstracts Vol. 12, EGU2010. http://meetingorganizer.copernicus.org/EGU2010/EGU2010-8778.pdf. Accessed 18 Jan 2014

Akgün A, Bulut F (2007) GIS-based landslide susceptibility for Arsin-Yomra (Trabzon, North Turkey) region. Environ Geol 51:1377–1387. doi:10.1007/s00254-006-0435-6

Alkevli T, Ercanoglu M (2011) Assessment of ASTER satellite images in landslide inventory mapping: Yenice-Gökçedbey (Western Black Sea Region, Turkey). Bull Eng Geol Environ 70:607–617. doi:10.1007/s10064-011-0353-z

Allum JAE (1966) Photogeology and regional mapping. Pergamon Press, Oxford

Al-Athari FM (2011) Parameter estimation for the double Pareto distribution. J Math Stat 7:289–294

Antonini G, Cardinali M, Guzzetti F, Reichenbach P, Sorrentino A (1993) Carta Inventario dei Fenomeni Franosi della Regione Marche ed aree limitrofe. CNR Gruppo per la Difesa dalle Catastrofi Idrogeologiche Publication 580, 2 sheets, scale 1:100,000 (in Italian)

Ardizzone F, Cardinalli M, Guzzetti F, Reichenbach P (2007) Identification and mapping of recent rainfall induced landslides using elevation data collected by airborne LIDAR. Nat Hazards Earth Syst Sci 7:637–650

Ardizzone F, Fiorucci F, Santangelo M, Cardinali M, Mondini A, Rossi M, Reichenbach P, Guzzetti F (2013) Very-high resolution stereoscopic satellite images for landslide mapping. Proc Second World Landslide Forum 3–7

Baldo M, Bicocchi C, Chiocchini U, Giordan D, Lollino G (2009) LiDAR monitoring of mass wasting processes: the Radicofani landslide, Province of Siena, Central Italia. Geomorphology 105:193–201

Beiser L (1981) Anaglyph stereoscopy. Google patents. http://www.google.com.mx/patents/US4290675. Accessed 19 Jan 2014

Bektas K, Coltekin A (2009) A survey of stereoscopic visualization support in mainstream geographic information systems. In: Proceedings, True 3D in cartography, 1st international conference on 3D maps, 24–28 August 2009, Dresden, Germany, pp 24–28

Bektas K, Coltekin A (2012) Area of interest based interaction and Geovisualization with WebGL. In: Proceedings of the graphical web conference 2012, Zurich, Switzerland

Bernard M, Decluseau D, Gabet L, Nonin P (2012) 3D capabilities of Pleiades satellite. International archives of the photogrammetry. Remote Sens Spat Inf Sci 39:553–557

Bertolini G, Canuti P, Casagli N, de Nardo MT, Egidi D, Mainetti M, Pignoner, Pizziolo M (2002) Carta della Pericolosità Relativa da Frana della Regione Emilia-Romagna. SystemCart, Rome, Italy (also in English).http://ambiente.regione.emilia romagna.it/geologia-en/divulgazione/pubblicazioni/cartografia-geo-tematica/carta-dellapericolosita-relativa-da-frana-ai-fini-di-protezione-civile. Accessed 19 Jan 2014

Booth AM, Roering JJ, Perron JT (2009) Automated landslide mapping using spectral analysis and high-resolution topographic data: Puget Sound lowlands, Washington, and Portland Hills, Oregon. Geomorphology 109:132–147

Borghuis AM, Lee HY (2007) Comparison between automated and manual mapping of typhoon-triggered landslides from SPOT-5 imagery. Int J Remote Sens 28:1843–1856. doi:10.1080/01431160600935638

Boulos M, Robinson L (2009) Web GIS in practice VII: stereoscopic 3-D solutions for online maps and virtual globes. Int J Health Geogr 8:59. doi:10.1186/1476-072X-8-59

Blake B, Fox R (1973) The psychophysical inquiry into binocular summation. Percept Psychophys 14:161–185. doi:10.3758/BF03198631

Brardinoni F, Slaymaker O, Hassan MA (2003) Landslide inventory in a rugged forested watershed: a comparison between air-photo and field survey data. Geomorphology 54:179–196

Brown K (2012) Landslide detection and susceptibility mapping using LiDAR and artificial neural network modeling: a case study in glacially dominated Cuyahoga River valley, Ohio. Thesis Master Science, Bowling Green State University

Cardinali M, Guzzetti F, Brabb EE (1990) Preliminary map showing landslide deposits and related features in New Mexico. U.S. Geological Survey Open File Report 90/293, 4 sheets, scale 1:500000

Carrara A, Merenda L (1976) Landslide inventory in northern Calabria, southern Italy. Geol Soc Am Bull 87:1153–1162

Carrara A, Crosta G, Frattini P (2003) Geomorphological and historical data in assessing landslide hazard. Earth Surf Process Landf 28:1125–1142

Chen H-C, Chen WW (2012) High resolution 3D images of natural terrains and landslides. In: Proceedings of the 2012 International Symposium on Computer, Consumer and Control. IEEE Computer Society, Washington, pp 598–601. doi:10.1109/IS3C.2012.156

Chen RF, Chang KJ, Angelier J, Chan YC, Deffontaines B, Lee CT, Lin ML (2006) Topographical changes revealed by high-resolution airborne LIDAR data: the 1999 Tsaoling landslide induced by the Chi-Chi earthquake. Eng Geol 88:160–172

Corsini A, Cervi F, Daehne A, Ronchetti F (2009) Coupling geomorphic field observation and LiDAR derivatives to map complex landslide. In: Malet JP, Remaître A, Bogaard T (eds) Landslides processes—from geomorphologic mapping to dynamic modelling: proceedings of the landslide processes conference. Strasbourg, pp 15–18

Cruden DM, Varnes DJ (1996) Landslide types and processes. In: Turner AK, Schuster RL (eds) Landslides, investigation and mitigation, Transportation Research Board special report, vol 247., pp 36–75

Derron MH, Jaboyedoff M (2010) Preface to the special issue: LiDAR and DEM techniques for landslides monitoring and characterization. Nat Hazards Earth Syst Sci 10:1877–1879

Fiorucci F, Cardinali M, Carlà R, Rossi M, Mondini AC, Santurri L, Ardizzone F, Guzzetti F (2011) Seasonal landslides mapping and estimation of landslide mobilization rates using aerial and satellite images. Geomorphology 129:59–70. doi:10.1016/j.geomorph.2011.01.013

Gagnon H (1975) Remote sensing of landslides hazards on quick clays of eastern Canada. In: Proceeding 10th International Symposium Remote Sensing of Environment.Environmental Research Institute of Michigan, Ann Arbor, pp 803–810

Galli M, Ardizzone F, Cardinali M, Guzzetti F, Reichenbach P (2008) Comparing landslide inventory maps. Geomorphology 94:268–289. doi:10.1016/j.geomorph.2006.09.023

Gao J, Maroa J (2010) Topographic controls evolution of shallow landslides in pastoral Wairarapa, New Zealand, 1979–2003. Geomorphology 114:373–381. doi:10.1016/j.geomorph.2009.08.002

Glade T (2001) Landslide hazard assessment and historical landslide data—an inseparable couple? Adv Nat Technol Hazards Res 17:153–168. doi:10.1007/978-94-017-3490-5_12

Guzzetti F, Cardinali M, Reichenbach P (1994) The AVI project: a bibliographical and archive inventory of landslides and floods in Italy. Environ Manag 18:623–633

Guzzetti F, Cardinali M, Reichenbach P, Carrara A (2000) Comparing landslide maps: a case study in the upper Tiber River Basin, central Italy. Environ Manag 25(3):247–363

Guzzetti F, Reichenbach P, Cardinali M, Ardizzone F, Galli G (2003) The impact of landslides in the Umbria region, central Italy. Nat Hazards Earth Syst Sci 3:469–486

Guzzetti F, Modini A, Cardinali M, Fiorucci F, Santangelo M, Chang KT (2012) Landslide inventory maps: new tools for an old problem. Earth Sci Rev 112:42–66

Haneberg WC, Cole WF, Kasali G (2009) High-resolution LiDAR-based landslide hazard mapping and modeling, UCSF Parnassus Campus; San Francisco, USA. Bull Eng Geol Environ 68:263–276. doi:10.1007/s10064-009-0204-3

Harp EL, Jibson RL (1996) Landslides triggered by the 1994 Northridge, California earthquake. Seismol Soc Am Bull 86:319–S332

Howard I, Rogers B (2012) Perceiving in depth. Stereoscopic vision. Volume II. Oxford University Press, New York

Liu JK, Hsiao KH, Shih PTY (2012) A geomorphological model for landslide detection using airborne LIDAR data. J Mar Sci Technol 20:629–638. doi:10.6119/JMST-012-0412-1

Kasai M, Ikeda M, Asahina T, Fujisawa K (2009) LíDAR-derived DEM evaluation of deepseated landslides in a steep and rocky region of Japan. Geomorphology 113:57–69. doi:10.1016/j.geomorph.2009.06.004

Kliparchuk K, Collins D (2010) Evaluation of stereoscopic GeoEye-1 satellite imagery to assess landscape and stand level characteristics. In: Proceedings of the ISPRS Canadian Geomatics Conference and Symposium of Commission I, Calgary, AB, Canada, pp 15–18

Krishnaswamy M, Kalyanaraman S (2005) Indian remote sensing satellite Cartosat-1: technical features and data products. http://www.gisdevelopment.net/technology/rs/techrs023.htm. Accessed 19 Jan 2014

Lee S, Lee M (2006) Detecting landslide location using KOMPSAT 1 and its application to landslide-susceptibility mapping at the Gangneung area, Korea. Adv Space Res 38:2261–2271. doi:10.1016/j.asr.2006.03.036

Lan H, Martin CD, Zhou C, Lim CH (2010) Rockfall hazard analysis using LiDAR and spatial modeling. Geomorphology 118:213–223. doi:10.1016/j.geomorph.2010.01.002

LoaezaGarcía JP, ZárateBarradas RG (2005) Carta Geológico-Minera Huauchinango F14-D83. Servicio Geológico Mexicano, scale 1:50000. (In Spanish)

Mann U, Pradhan B, Prechtel N, Buchroithner M (2012) An automated approach for detection of shallow landslides from LiDAR derived DEM using geomorphological indicators in a tropical forest. In: Terrigenous mass movements. Springer, Berlin, pp 1–22

Marcelino EV, Formaggio AR, Maeda EE (2009) Landslide inventory using image fusion techniques in Brazil. Int J Applied Earth Obs Geoinformation 11:181–191. doi:10.1016/ j.jag.2009.01.003

Martha TR, Kerle N, Jetten V, van Westen C, Vinod Kumar K (2010) Characterizing spectral, spatial and morphometric properties of landslides for semi-automatic detection using object-oriented methods. Geomorphology 116:24–36

Miner AS, Flentje P, Mazengarb C, Windle DJ (2010) Landslide recognition using LiDAR derived digital elevation models, lessons learnt from selected Australian examples. In: Williams AL, Pinches GM, Chin CY, McMorran TJ, Massey CI (eds) Geologically active: proceedings of the 11th IAEG congress of the International Association of Engineering Geology and the Environment. Auckland, New Zealand, pp 1–9

Mondini AC, Guzzetti F, Reichenbach P, Rossi M, Cardinalli M, Ardizzone F (2011) Semiautomatic recognition and mapping of rainfall induced shallow landslides using satellite optical images. Remote Sens Environ 115:1743–1757

Nale DK (2002) Quickbird—aerial photography comparison report. EMAP International, Reddick

Navarrete Pacheco JA (2003) Digital stereo image interpretation of natural hazard assessment. Dissertation, ITC

Nichol J, Wong MS (2005) Satellite remote sensing for detailed landslide inventories using change detection and image fusion. Int J Remote Sens 26:1913–1926. doi:10.1080/01431160512331314047

Nichol EJ, Shaker A, Wong MS (2006) Application of high-resolution stereo satellite images to detailed landslides hazard assessment. Geomorphology 76:68–75. doi:10.1109/URS.2009.5137737

Nikolakopoulos KG, Lathourakis G (2005) Along the track vs across the track satellite stereo-pair for DTM creation. In: Geoscience and Remote Sensing Symposium, 2005. IGARSS'05. Proceedings. 2005 IEEE International 8:5324–5327, 25–29

Oliva Aguilar VR, Garza Merodio GG, Alcántara Ayala I (2011) Configuration and temporal dimension of vulnerability: spaces and disasters in the Sierra Norte de Puebla. Investigaciones Geográficas, Boletín del Instituto de Geografía, UNAM 75:61–74

Olm J, Gaffney B (2010) 3D stereo digital intermediate workflow. In: Okun J, Zwerman S (eds) The VES handbook of visual effects: industry standard VFX practices and procedures. Focal Press, Oxford, pp 434–447

Ostnes R, Abbott V, Lavender S (2004) Visualization techniques: an overview—part 2. Hydrogr J 114:3–9

Peters-Guarin G, McCall MK, van Westen CJ (2012) Coping strategies and risk manageability: using participatory geographical information systems to represent local knowledge. Disasters: J disaster Stud Policy Manag 36:1–27

Petrie G (2001) 3D stereo-viewing of digital imagery: is auto-stereoscopy the future for 3D. GeoInformatics 4:24–29

Ping L, Stumpf A, Kerle N, Casagli N (2011) Object-oriented change detection for landslide rapid mapping. Geosci Remote Sens Lett IEEE 8:701–705. doi:10.1109/LGRS.2010.2101045

Planar (2008) SD2620W stereoscopic monitor user's guide. Planar Systems, Beaverton

Poli D, Remondino F, Angiuli E, Agugiaro G (2013) Evaluation of Pleiades-1a triplet on Trento testfield. International Archives of the Photogrammetry, Remote Sens Spat Inf Sci 40:287–292

Prokop A, Panholzer H (2009) Assessing the capability of terrestrial laser scanning for monitoring slow moving landslides. Nat Hazards Earth Syst Sci 9:1921–1928

Quantin C, Allemand P, Delacourt C (2004) Morphology and geometry of Valles Marineris landslides. Planetary Space Sci 52:1011–1022. doi:10.1016/j.pss.2004.07.016

Ray RG (1960) Aerial photographs in geological interpretation and mapping. Geological survey professional paper, Washington, USA. http://pubs.usgs.gov/pp/0373/report.pdf. Accessed 18 Jan 2014

Razak KA, Straatsma MW, van Westen CJ, Malet JP, de Jong SM (2011) Airborne laser scanning of forested landslides characterization: terrain model quality and visualization. Geomorphology 126:186–200

Remondo J, Bonachea J, Cendrero A (2005) A statistical approach to landslide risk modeling at basin scale: from landslide susceptibility to quantitative risk assessment. Landslides 2:321–328. doi:10.1007/s10346-005-0016-x

Rib HT, Liang T (1978) Recognition and identification. In: Schuster RL, Krizek RJ (eds) Landslide analysis and control, National Academy of Sciences, Transportation Research Board special report 176, pp 34–80

Rossi M, Ardizzone F, Cardinalli M, Fiorucci F, Marchesini I, Mondini A, Santangelo M, Gosh S, Riguer DEL, Lahousse T, Chang KT, Guzzetti F (2012) A tool for the estimation of the distribution of landslide area in R. Geophysical Research Abstracts, 14, EGU2012-9438-1

Sánchez Rojas LE, De la Callejera Moctezuma AE (2004) Carta Geológico-Minera Pahuatlán F14-D73. Servicio Geológico Mexicano, scale 1:50 000. (On Spanish)

Sauchyn DJ, Trench NR (1978) Landsat applied to landslide mapping. Photogramm Eng Remote Sens 44:735–741

Scanvic JY, Girault F (1989) Imagerie SPOT-1 etinventaire des mouvements de terrain: l'exemple de La Paz (Bolivie). Photo Interpretation 89:1–20 (In French)

Schulz WH (2004) Landslides mapped using LIDAR imagery, Seattle, Washington, US. Geological Survey open-file report 2004-1396. http://pubs.usgs.gov/of/2004/1396/OF2004-1396_508.pdf. Accessed 18 Jan 2014

Schulz WH (2007) Landslide susceptibility revealed by LIDAR imagery and historical records, Seattle, Washington. Eng Geol 89:67–87. doi:10.1016/j.enggeo.2006.09.019

Steiniger S, Weibel R (2010) GIS software. In: Warf B (ed) Encyclopedia of geography. SAGE, Thousand Oaks, pp 1319–1322. doi:10.4135/9781412939591.n518

Stephens PR (1988) Use of satellite data to map landslides. In: Proceedings 9th Asian Conference on Remote Sensing, Bangkok, Thailand, 11, pp 1–7

Tempfli K, Huurneman GC, Bakker WH, Janssen LLF, Bakker WH, Feringa WF, Gieske ASM, Grabmaier KA, Hecker CA, Horn JA, Huurneman GC, Kerle N, van der Meer FD, Parodi GN, Pohl C, Reeves CV, van Ruitenbeek FJA, Schetselaar EM, Weir MJC, Westinga E, Woldai T (2009) Principles of remote sensing: an introductory textbook. ITC, the Netherlands

van Den Eeckhaut M, Poesen J, Verstraeten G, Vanacker V, Moeyersons J, Nyssen J, van Beek LPH, Vandekerckhove L (2007) Use of LiDAR-derived images for mapping old landslides under forest. Earth Surf Process Landf 32:754–769. doi:10.1002/esp.1417

Weirich F, Blesius L (2007) Comparison of satellite and air photo based landslide susceptibility maps. Geomorphology 87:352–364. doi:10.1016/j.geomorph.2006.10.003

van Westen CJ, van Asch TWJ, Soeters R (2006) Landslide hazard and risk zonation—why is it still so difficult? Bull Eng Geol Environment 65:167–184. doi:10.1007/s10064-005-0023-0

Van Zuidam RA (1985) Aerial photo-interpretation in terrain analysis and geomorphological mapping. International Institute for Aerospace Survey and Earth Sciences (ITC). Smiths, the Hague

Wieczorek GF (1984) Preparing a detailed landslide-inventory map for hazard evaluation and reduction. Bull Assoc Eng Geol 21:337–342

Yang X, Chen L (2010) Using multi-temporal remote sensor imagery to detect earthquake- triggered landslides. Int J Appl Earth Obs Geoinformation, Geospatial Technologies Disaster Manag 12:487–495. doi:10.1016/j.jag.2010.05.006

# Capítulo III. Landslide multi-temporal maps

**Landslide inventory map of the municipality of Teziutlán, Puebla, México (1942-2015).**

# Landslide inventory map of the municipality of Teziutlán, Puebla, México (1942-2015) ®

Franny Giselle Murillo-García
Posgrado en Geografía UNAM


Irasema Alcántara Ayala
Instituto de Geografía UNAM

*This article describes the spatial distribution of landslides in Teziutlán, Puebla, Mexico, which has been historically affected by mass movement processes. The most significant disaster associated with landslides in October 1999. Rainfall-triggered landslides and floods caused more than 100 deaths in Teziutlán and economic losses of US$233 million in Sierra Norte de Puebla. A multi-temporal landslide inventory map (1:25,000) for the period 1942–2015 was constructed by means of field observation and the analysis and interpretation of aerial photographs and satellite images. The inventory map includes 662 landslides and covers 163 km². The total landslide area is in the order of 0.71 km². Taking into account the scarp, channel and depositional area, the mean surface of the landslides is 1075 m². The largest documented area was 17,512 m². The smallest landslide area mapped was 24 m². Most movements can be considered as having been small.*

# 3.1 INTRODUCTION

Unconsolidated deposits that cover volcanic edifices and surrounding terrains have a great potential for landsliding induced by precipitation or earthquakes (Nocentini, Tofani, Gigli, Fidolini, & Casagli, 2015; Pareschi *et al.*, 2000). In areas where vulnerable people are exposed to such hazards, disasters can occur. This propensity for landsliding can persist for centuries or millennia after a volcanic eruption (Miyabuchi, Maeno, & Nakada, 2015). Heavy rainfall and seismicity can remobilize the volcaniclastic layer and generate slides and debris flows (Nocentini *et al.*, 2015; Smith & Lowe, 1991). There have been a series of disasters associated with the occurrence of landslides in volcanic terrains. One of the oldest documented events took place on San Miguel Island, Portugal, in 1522, when rainfall-induced landslides on pyroclastic deposits involved 5000 fatalities (Gomes, Gaspar, Goulart, & Queiroz, 2005; Marques & Amaral, 2004). In 1999, in Teziutlán, Puebla, Mexico, hundreds of rainfall-induced landslides affected the Sierra Norte de Puebla; more than 200 fatalities were registered and Teziutlán was the most affected municipality of the region. In just a single event in the La Aurora neighborhood, 109 people died as they were swept away by a complex landslide. There is a clear need to produce an inventory map of landslides of the area to understand their temporal and spatial distribution.

In this study, we present a description of the spatial distribution of landslides that have occurred in Teziutlán during the period 1942–2015. This study involved the construction of a multi-temporal landslide inventory map based on field recognition and identification and the analysis and interpretation of aerial photographs and satellite images.

# 3.2 STUDY AREA

### 3.2.1 Physiographical setting

Teziutlán municipality lies in the Sierra Norte de Puebla mountain system, within the transition of the Sierra Madre Oriental and the Trans-Mexican Volcanic Belt physiographic provinces (Fig. 38). Its capital town is also called Teziutlán, and this is situated on a plateau formed by lava flows and pyroclastic materials from Los Humeros caldera. The altitude of the study area ranges from 1221 m.a.s.l. in the northeast to 2660 m.a.s.l. in the south and west. The climate is warm temperate: temperature varies from 12° to 22°C (mean 15.5°C) and rainfall occurs all year long and is in the order of 1100–3600 mm (mean precipitation 1658 mm) (INEGI, 2009). The main drainage system has an N–

S and NE–SW orientation and is probably controlled by tectonic lineaments (Capra, Lugo-Hubp, & Borselli, 2003). Because of their volcanic origin, soils are predominantly andosols (INEGI, 2009). The north is still covered by pine/oak woodlands but in the rest of the area the original vegetation has been changed to grassland, arable land and urban areas. The extent of the study area is 163 km$^2$. Maps of elevation, slope gradient and stream power index of the study area were added as complementary materials.

### 3.2.2 Antecedents of instability and the disaster of October 1999

Heavy rainfall events have occurred in historical time. Inhabitants of Teziutlán recall precipitation events of 1999, 1944 and 1955, in that order of importance, and according to the impact of landslides on the population. Records show that those events involved a high accumulation of rain in a short period of time and at least one day with more than 300 mm of rain.
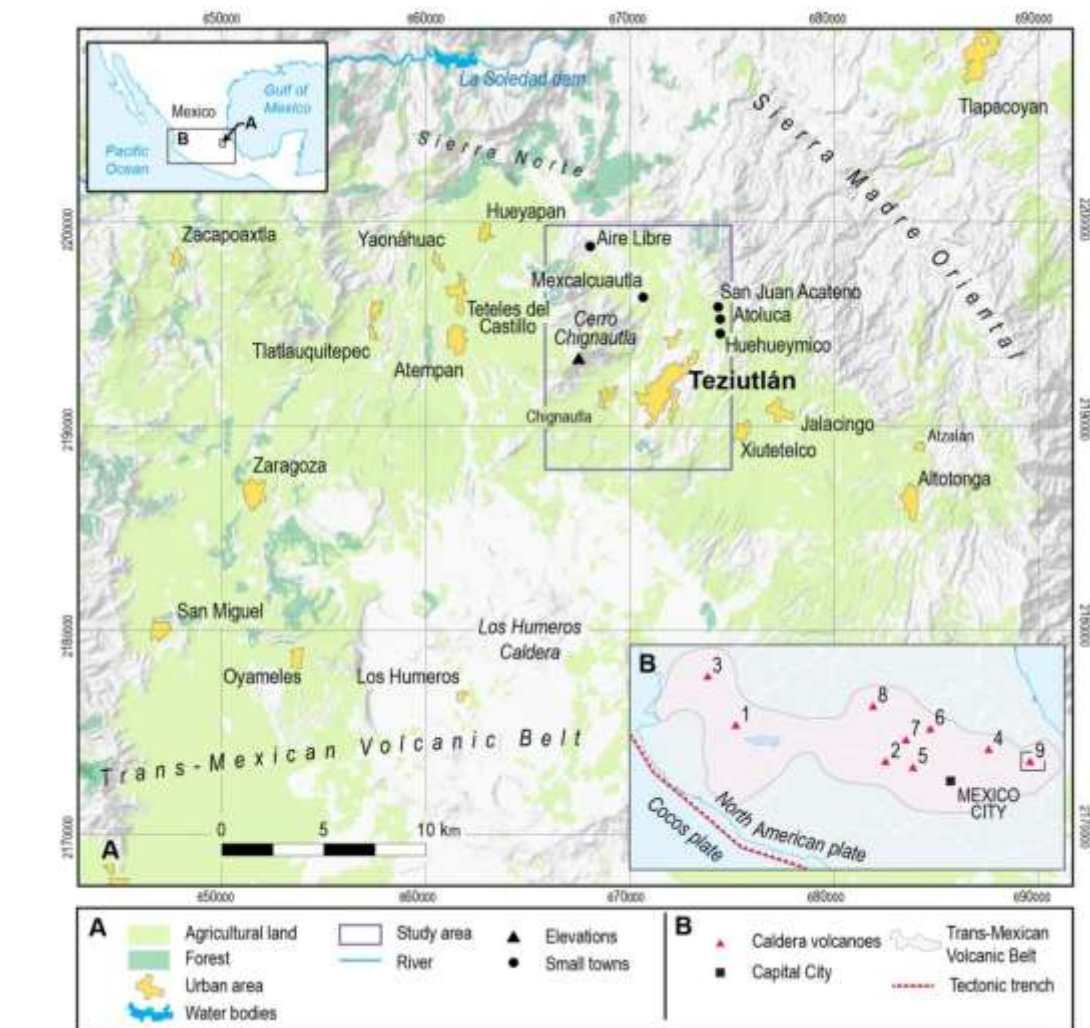


*Figure 38.* *Location of Teziutlán, Mexico. Caldera volcanoes: (1) La Primavera; (2) Los Azufres; (3) Ceboruco; (4) Acoculco; (5) Mazahua; (6) Huichapan; (7) Amealco; (8) Palo Huérfano; (9) Los Humeros.*

On 5 October 1999, 109 people died in a landslide in the La Aurora neighborhood of Teziutlán city (Alcántara-Ayala, 2004). This was triggered by extraordinarily heavy rains associated with Tropical Depression N°11 in the Gulf of Mexico. This mass movement was not unique; thousands of landslides affected an area of approximately 4000 km$^2$ (Lugo-Hubp, Zamorano-Orozco, Capra, Inbar, & Alcántara-Ayala, 2005).

### 3.2.3 Geological context

The Trans-Mexican Volcanic Belt is characterized by extensive basaltic volcanism and late Tertiary and Quaternary strato-volcanoes, cinder cones, calderas, domes and maars (Alcántara-Ayala, 2004; Alva-Valdivia *et al.*, 2000). It is an E−W oriented volcanic arc produced by the subduction of the Cocos tectonic plate beneath the North American tectonic plate (Alaniz-Alvarez, Nieto- Samaniego, & Ferrari, 1998; Concha-Dimas, Cerca, Rodríguez, & Watters, 2005; Pardo & Suarez, 1995). Its caldera volcanoes include, in its eastern sector, Los Humeros (Fig. 38), which rises in central Mexico, 180 km east of Mexico City, and is considered to be one of the Pleistocene silica centers (Dávila-Harris & Carrasco- Núñez, 2014). The geology of Teziutlán (Fig. 39) is directly linked to Los Humeros.

Eruptive products derived from Los Humeros range from basalt to the high-silica rhyolite that covers a Mesozoic section with a thickness of up to 3000 m (Ferriz & Mahood, 1984). Evolution of the volcano center began 1.6 Ma ago. Paleozoic crystalline rocks, folded Mesozoic sedimentary rocks, and Tertiary intrusions and andesites can be found on the surface (Ferriz & Mahood, 1984). This basement of sedimentary rocks was extensively affected by the Laramide Orogeny, with a NE–SW compression, faulting and folding (Dávila-Harris & Carrasco-Núñez, 2014).

The oldest layer that outcrops in the study area is the schist of the Chililis formation (280 Ma.), this is composed of chloritemuscovite and andesite metalava (Salinas-Rodríguez & Castillo-Reynoso, 2011). The Chililis schist is overlaid by the siltstone and polymictic conglomerate of the Cahuasas Formation (170 Ma.), limestone-shale Tepexic, Santiago, Tamán and Pimienta formations (166–140 Ma.) (Salinas-Rodríguez & Castillo-Reynoso, 2011). Likewise, the Teziutlán Massif (Viniegra, 1965) outcrops in the western sector; it is formed by a Paleozoic metamorphic and granite intrusive complex (Ferriz & Mahood, 1984) (Fig. 39).
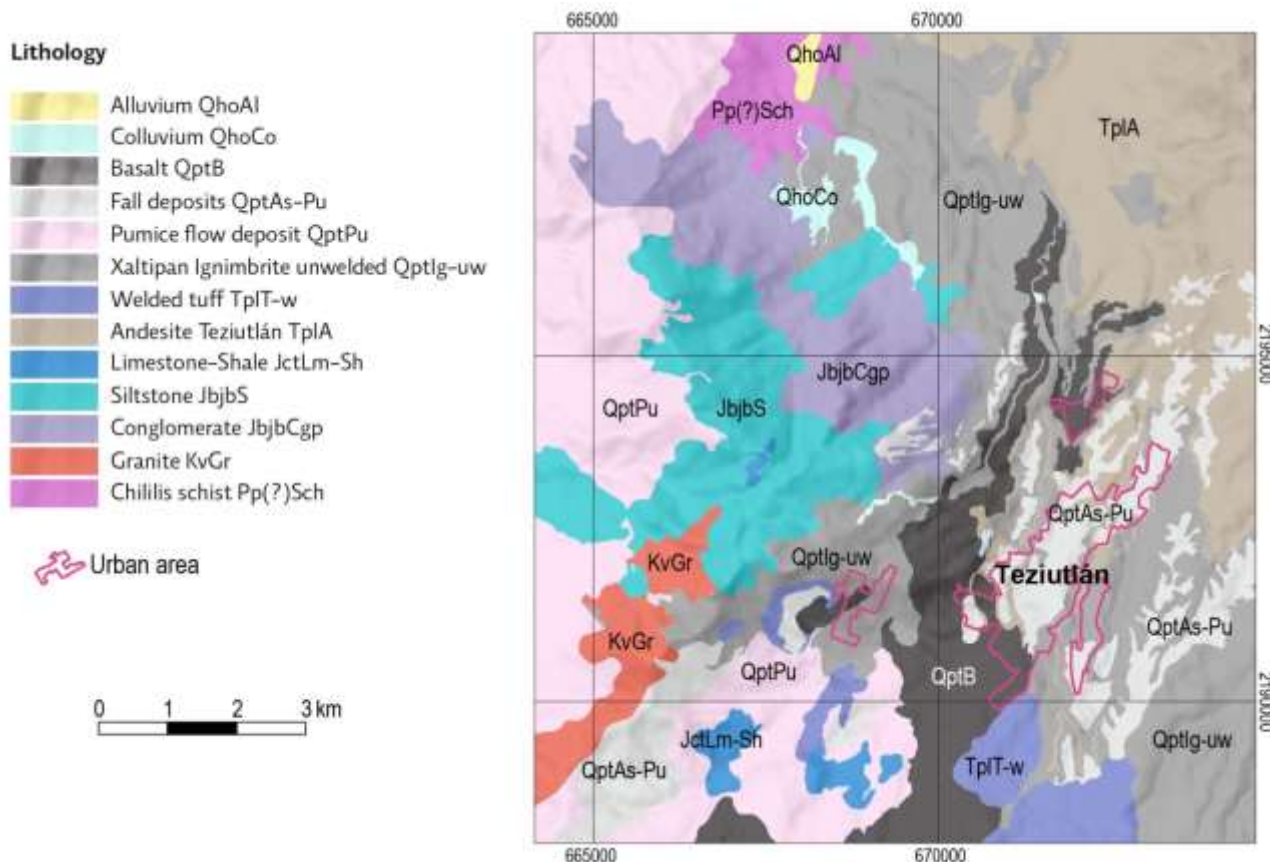
*Figure 39. Lithology of the studied area.*

The oldest igneous rocks that can be observed are porphyritic two-pyroxene andesite lavas and breccias, and ferro-basaltic lavas of the Teziutlán Formation (1.55 Ma) (Ferriz & Mahood, 1984), which could be considered as pre-caldera events (Dávila-Harris & Carrasco- Núñez, 2014). The following stage (0.47 Ma), was the accumulation of a 115 km$^3$ magma eruption of the Xaltipan ignimbrite (Ferriz & Mahood, 1984), a type 7 eruption according to the Volcanic Explosivity Index (VEI). The Xaltipan ignimbrite resulted from the final activity of the first active phase and subsidence of Los Humeros caldera (Dávila-Harris & Carrasco-Núñez, 2014). Most of the ignimbrite deposits found in the study area are non-welded and composed of aphyric high-silica rhyolite material that can be recognized specifically as ash-pumice flow deposits. The pyroclastic flows filled low areas of the rugged preexisting landscape covering 3500 km$^2$ (Ferriz & Mahood, 1984).

After another long period of inactivity that allowed further erosive and pedogenetic processes, an eruptive episode gave rise to the Zaragoza ignimbrite (0.06–0.1 Ma.). The Zaragoza ignimbrite is a non-welded ignimbrite covered by a lithic-rich fall deposit (Zaragoza tuff) and can be regarded as a pumice flow.

Numerous deposits of pumice and lapilli falls covered the Zaragoza ignimbrite, including the Xoxoctic member pumice fall, the Tilca lithic-rich layer and finally the pumice fall layer Cuicuiltic member from the Holocene (Dávila-Harris & Carrasco-Núñez, 2014). The final stage of the Los Humeros caldera, ~20,000 years ago (Ferriz & Mahood, 1984), was the eruption of the San Antonio volcano, consisting of rhyodacitic and andesite lava flows, and eruptions of olivine basalt. This has diverse vents and covers the south-center of the study area. General data on the mechanical properties of the deposits of Teziutlán can be found in Alcántara-Ayala (2004).

## 3.3 METHODS

### 3.3.1 Aerial photographs

The photographs of 1956 are the best available source to identify the landslides that occurred in the 1955 event. The 1942 oblique photographs were also useful for comparative purposes. Four vertical photographs dated from 1942 were found in the archives of the Geography Institute of UNAM. These photographs were taken on December 13rd, from a height of 9300 m (30,000 ft) (1:20,000 approximate scale) using the trimetrogon system that consisted of three cameras assembled at different angles to take one vertical and two oblique photographs simultaneously. Figure 40 summarizes the aerial photograph material used.

| Number of photographs | Archive | Date | Scale | Format | Angle | Smallest recognized landslide (m$^2$) |
|---|---|---|---|---|---|---|
| 4 | ICA foundation | 1942 | | Digital 1200 dpi | Oblique | 282 |
| 4 | Geography Institute | Dec.1942 | 1:20,000 | Paper | Vertical | 133 |
| 4 | ICA foundation | 1956 | 1:50,000 | Digital 1200 dpi | Vertical | 59 |
| 3 | INEGI | Nov. 1974 | 1:50,000 | Digital 1200 dpi | Vertical | 225 |
| 5 | INEGI | Mar. 1978 | 1:50,000 | Digital 1200 dpi | Vertical | 157 |
| 4 | INEGI | Nov. 1980 | 1:80,000 | Digital 1200 dpi | Vertical | - |
| 6 | INEGI | Ago. 1991 | 1:30,000 | Digital 1200 dpi | Vertical | 96 |
| 30 | INEGI | Jul. 2007 | 1:20,000 | Digital 1200 dpi | Vertical | 30 |
| 45 | CENAPRED | October 1999 | 1:1,800 | Paper | Vertical | 24 |

*Figure 40. Air photograph material used to generate the landslide inventory.*

### 2.2 Satellite images

IKONOS, SPOT 5 and 6, and QuickBird images were used (see Fig. 41). The principal input set of images for this work was a series of IKONOS images at 1 m resolution in the panchromatic band and 4 m in the multispectral bands. The images were available in mosaic true color and near-infrared

composition. Multispectral bands were resampled via a pan-sharpened process to obtain the true color and near-infrared composite images with the resolution of the panchromatic band. The date of the images was December 2000, only one year after the disaster event of 1999; a number of landslides were identified by analyzing this image mosaic. These images and all the satellite images used in this research were only available in the monoscopic display (Fig. 41).

Besides the use of satellite images, images in Google Earth, Bing Maps and SAS Planet were also used. Specifications for Google Earth images were not available, although some of them can be very high resolution (VHR) or aerial photographs. These tools are free, and landslides can be drawn directly onto the software and exported as a .kmz file extension to then be converted into a shape file. These images were useful as a complement for landslide identification as they provided information for each year, from 2003 to 2015. The SAS Planet program allows geo-referenced images (or maps) to be downloaded from other systems (e.g. Google Earth, Bing Maps, ESRI, etc.), but it does not provide detailed information about the type or date of the images. In spite of this, it was possible to use a Bing Map image probably dated in 2015 and also images from ESRI. Analysis of buildings recently constructed in Teziutlán determined that the ESRI images were taken after 2011.

| Image | Date | Mode | Resolution (m) | Smallest recognized landslide (m$^2$) |
|---|---|---|---|---|
| IKONOS | Dec. 2000 | True composite colour | 1 | 33 |
| SPOT 5 | 27-Dec-2003 | Panchromatic | 2.5 | 879 |
| From Google Earth | 17-Mar-2003 | True composite colour | Unknown | 682 |
| From Google Earth | 19-Oct-2004 | True composite colour | Unknown | 84 |
| SPOT 5 | 12-Nov-2005 | Panchromatic | 2.5 | - |
| SPOT 5 | 28-Nov-2006 | Panchromatic | 2.5 | - |
| From Google Earth | 17-Apr-2006 | True composite colour | Unknown | - |
| SPOT 5 | 19-Feb-2007 | Panchromatic | 2.5 | - |
| SPOT 5 | 26-Oct-2007 | Panchromatic | 2.5 | - |
| SPOT 5 | 22-Dic-2007 | Panchromatic | 2.5 | - |
| QuickBird | 15-Feb-2008 | True composite colour | 0.6 | 24 |
| SPOT 5 | 26-Dec-2008 | Panchromatic | 2.5 | - |
| SPOT 5 | 20-Jan-2010 | Panchromatic | 2.5 | - |
| SPOT 5 | 13-Mar-2010 | Panchromatic | 2.5 | 1752 |
| SPOT 5 | 08-Jan-2011 | Panchromatic | 2.5 | - |
| SPOT 5 | 10-Aug-2011 | Panchromatic | 2.5 | - |
| SPOT 5 | 21-Oct-2011 | Panchromatic | 2.5 | - |
| From Google Earth | 10-Aug-2011 | True composite colour | Unknown | - |
| From Google Earth | 14-Nov-2011 | True composite colour | Unknown | - |
| From Google Earth | 04-Jun-2012 | True composite colour | Unknown | - |
| SPOT 5 | 03-Oct-2013 | Panchromatic | 2.5 | - |
| From Google Earth | 07-Feb-2013 | True composite colour | Unknown | 56 |
| SPOT 6 | 24-Feb-2014 | Panchromatic | 2.5 | - |
| From Google Earth | 26-Feb-2015 | True composite colour | Unknown | 379 |
| From Bing Maps | 2015 | True composite colour | Unknown | - |
| From ESRI | 2015 | True composite colour | Unknown | 966 |

*Figure 41. Satellite imagery used to generate the landslide inventory map.*

### 3.3.2 Field Surveys

Several field surveys were carried out from 2011 to 2015 to identify landslides, and to validate the interpretation of aerial photographs and the satellite images, in addition to obtaining relevant information about the relation between geology and landslide distribution (Fig. 42).
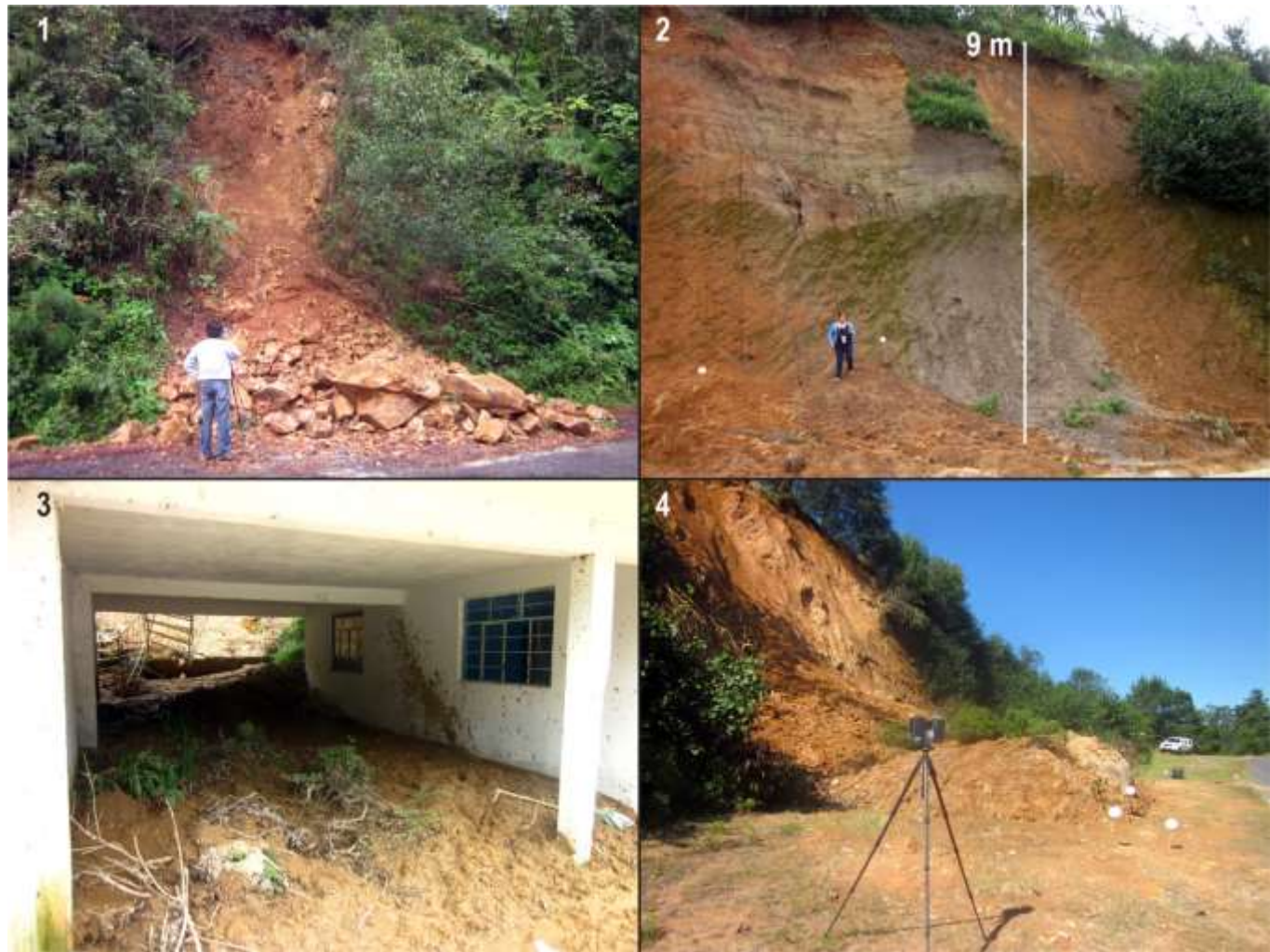


*Figure 42. Examples of landslides identified by field surveys: (1) Small rock and soil fall along the road near the Aire Libre neighborhood; (2) Translational slide that was transformed into a silt flowslide in a road cut near Teziutlán city; (3) Damage caused by a complex landslide that was initiated as a rotational slide and then transformed into a silt flowslide in the Aire Libre neighborhood; (4) Soil fall at the highway that connects Teziutlán with central sector of Mexico.*

Field surveys allowed the identification of recent landslides. If a landslide is inactive, the vegetation will have completely covered the area in less than a month. Even if the landslide is active, vegetation will have begun to grow soon after the mass movement. Hence, the only landslides that could be recognized by reference to vegetation were those that had occurred in recent time. In addition to direct observation in the field, landslides can also be identified by interviews with the local people, especially for old landslides. Some of the landslides that occurred in 1999 were identified thanks to the

information provided by the local inhabitants who pointed out specific locations on which landslide scars were subsequently traced. It also included the case of nine movements in 1955 that were unclear in analyses of the 1956 aerial photographs. This information on landslides associated with the 1955 and 1999 rainfall events was supplied by people from Aire Libre, San Juan Acateno and, in particular, from La Aurora neighborhoods. The Civil Protection office of Puebla State (Protección Civil de Puebla) provided landslide reports registered between 2010 and 2015. All the information obtained from field surveys was compared with that derived from the aerial photographs and satellite images. The landslides identified were afterwards digitized. The ortho-mosaic generated from the 2007 aerial photographs of INEGI was taken as the cartographic base.

### 3.3.3 Software

In order to use the aerial photographs, at least six points of control were identified by using LPS ERDAS software. The *x* and *y* coordinates were collected using the topographic maps, the Google Earth system and field surveys. The *z* coordinates were obtained from a 15 m spatial resolution digital elevation model (DEM) developed from aerial LiDAR data acquired from INEGI. An ortho-mosaic was generated using the 2007 photographs from INEGI and was used as a base to geo-reference the rest of the photographs. Then the photographs were used to generate stereo-models using the software mentioned above. Tie points were generated automatically and a block file (.blk) was generated for each stereo model and exported into the Stereo Analyst ArcGis extension from ERDAS. This application combined with the adequate hardware, in this case a digital stereo-mirror PLANAR system, created a 3D stereoscopic environment within which the landslides could be identified and mapped directly in a digital display. More details of this procedure can be found in Murillo-García *et al.* (2015). Some of the landslides were identified on the VHR images by visual interpretation using Quantum GIS software (QGIS Development Team, 2012). They were recognized by the scarp and deposit zone in addition to changes in vegetation patterns (Fig. 43) (Murillo-García *et al.*, 2015). In general, soil exposure produces a color, tone and texture that differ from those of the surrounding area, and this is clear in the type of landslides registered in the study area; this corresponded to silt or debris flowslides. The final landslide inventory map (Main map) was edited using QGIS software.

***Figure 43.*** *Landslide identification using VHR satellite images. The original image was a nearinfrared color composite. The landslide occurred in 1999 in a mine in the Aire Libre neighborhood.*

## 3.4 RESULTS

### 3.4.1 Statistical data

The inventory is composed of 662 landslides (Fig. 44). The total landslide area is 0.71 km$^2$ (0.43% of the study area). Taking into account the scarp, channel and deposit area, the mean area of the landslides is 1075 m$^2$. The largest documented area (17,512 m$^2$) for the 1999 event corresponds to one deep-seated slide transformed into mud flow that partially destroyed the building of the Technological University of Teziutlán near the Aire Libre neighborhood (Figure 3.4 and capital letter A in Figure 3.5 and Main Map). The smallest area of a landslide in 1999 mapped was 24 m$^2$ (Fig. 45).

It was not feasible to determine the chronological distribution of all landslides since the exact date of some of them was not available. However, they were classified by taking into account the date of the photographs, satellite image and/or field surveys (Figure 46). From the aerial photographs for 1942, 65 landslides were mapped, of which 32 were very likely to have occurred before that year since they do not appear to have been active at the moment the photograph was taken (in the main inventory map these landslides are identified as 'Old landslides'). For the 1999 disaster event, 298 landslides were identified; four times the number of those that were mapped for the disaster event of 1955.
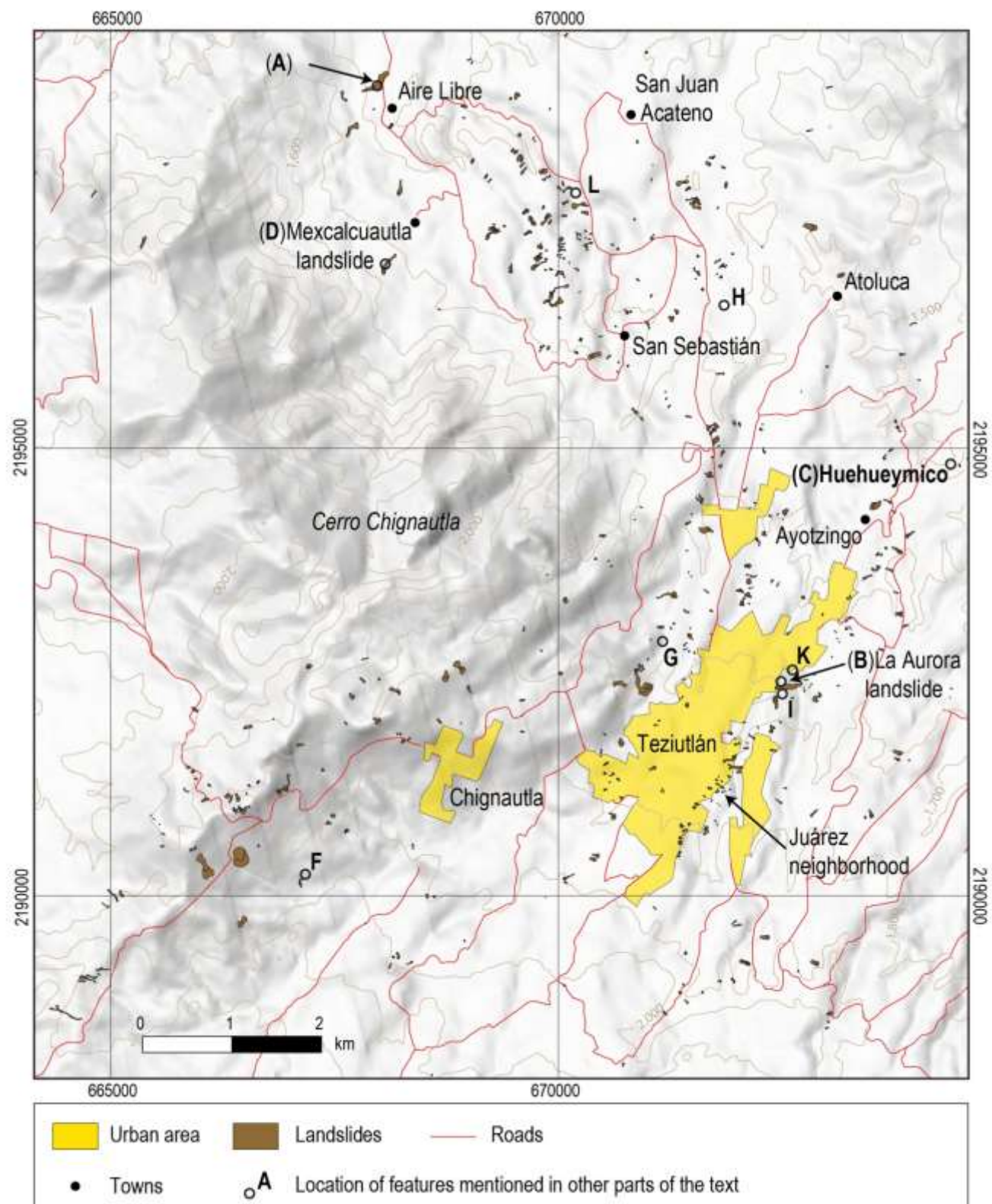
*Figure 44. Landslide inventory of Teziutlán.*

| | General | 1955 event | 1999 event | Seasonal landslides | Relict landslides (before 1942) |
|---|---|---|---|---|---|
| Study area | | | 163 km$^2$ | | |
| Total number of landslides | 662 | 61 | 292 | 277 | 32 |
| Mean area landslides | 1,075 m$^2$ | 969 m$^2$ | 849 m$^2$ | 844 m$^2$ | 5,198 m$^2$ |
| Total area landslides | 0.71 km$^2$ | 0.08 km$^2$ | 0.24 km$^2$ | 0.23 km$^2$ | 0.16 km$^2$ |
| Maximum landslide area | 29,586 m$^2$ | 6,357 m$^2$ | 18,627 m$^2$ | 11,910 m$^2$ | 29,586 m$^2$ |
| Minimum landslide area | 24 m$^2$ | 58 m$^2$ | 24 m$^2$ | 25 m$^2$ | 163 m$^2$ |

*Figure 45. Basic landslide inventory statistics. Relict landslides were identified by persistent geomorphological evidence, in the Main Map these are indicated as 'Old landslides'.*

Visual interpretation of the landslides identified in the aerial images and field surveys indicated that 78 (11.7%) were harmful to people and caused damage to infrastructure, including arable land and roads; 118 fatalities were registered and 29 buildings were affected. Three significant landslides occurred in 1999: La Aurora landslide (B), Huehueymico landslide (C) and Mexcalcuautla silt flowslide (D) (Figure 3.5 and Main Map); these were associated with the greatest damage. According to the official information provided to Alcántara-Ayala (2004), 109 people died in La Aurora, although neighbors claimed that not all the bodies were recovered after the tragedy. Flores-Lorenzo and Alcántara-Ayala (2002) reported 24 deaths in the Huehueymico landslide, and at least three persons died and six were reported as missing after the Mexcalcuautla silt flowslide.

| Year | Number of landslides | % |
|---|---|---|
| Before 1942 | 32 | 4 |
| 1942 | 65 | 9.8 |
| 1956 | 61 | 10.2 |
| 1974 | 17 | 2.5 |
| 1978 | 21 | 3.1 |
| 1980 | 1 | 0 |
| 1991 | 31 | 4.6 |
| 1999 | 292 | 45 |
| 2003 | 9 | 1.3 |
| 2004 | 22 | 3.3 |
| 2006 | 2 | 0 |
| 2007 | 110 | 16.6 |
| 2010 | 2 | 0 |
| 2013 | 11 | 1.6 |
| 2015 | 5 | 0.7 |

*Figure 46. Number of landslides by year according to visual or field identification classified according to the date of the photographs, satellite image and/or field surveys*

At the present time, 29 of the documented landslides can be considered as areas of high risk given that they are inhabited. These include the La Aurora landslide, where the area has recently been re-settled even though the people affected by the 1999 disaster were moved elsewhere.

### 3.4.2 Landslide type and lithology

Type of movement is strongly related with the lithology and soil material. Geology was used as one of the variables to interpret slope instability. Several rock types outcropping in the research area and previously described were identified in the field (Capra *et al.*, 2003; Ferriz & Mahood, 1984).

According to Alcántara-Ayala (2004), Xaltipan ignimbrite 'induced the infiltration and development of perched water table that caused slope instability'. Capra *et al.* (2003) also identified this process and classified the mass movements on this ignimbrite as 'shallow landslides with vertical [lateral] walls'. This type of shallow silt slide occurred in 1999 in one of the slopes of the Juárez neighborhood, in the west sector, near the old road from Teziutlán to Chignautla. Landslides of the same type have also occurred, to a great extent, in the north of the research area where the San Juan Acateno and San Sebastián neighborhoods are situated.

When the ignimbrite is underlaid by layers of other material, the type of landslide is different. Chililis schist outcrops at the NW part of the studied area; it can be found as a gray or very dark gray schist rock of high resistance, although when exposed to weathering or situated near a spring the schist is highly crumbly and shows a red-orange color and a high content of quartz. Soil cover thickness is in the order of 1–5 m and appears to have a clay-rich content (field survey observation). In this area, the schist is overlaid by the Xaltipan ignimbrite, and the contact is quite visible. Landslides are of rotational or planar types, and six of those landslides were transformed into clay flowslides.

Near the Mexcalcuautla neighborhood, in the foothills of Chignautla Mountain, the Xaltipan ignimbrite overlays a siltstone layer (Jbjb-S) showing a contact with the Chililis schist. In this place, a silt flowslide occurred in 1999 involving at least three fatalities (D in Figure 44 and Main Map); the movement initiated at the geological contact and flowed down into the ignimbrite zone (down slope) where more material was added. The runoff of the movement was 275 m.

In the central sector of the study area, the ignimbrite is covered by a succession of interlaid ash-pumice, lapilli fall deposits and paleosols or highly weathered materials (QptAs-Pu in the Main Map). The thickness of the set of volcanic fall deposits and paleosols sequence unit varies from 2 to 7 m and in some areas the QptAs-Pu deposits are not present. The soil (50– 100 cm thick) is developed from the pumice; it can be classified as Andosol (silt saturated). Landslides in the QptAs-Pu are commonly silt flowslides which began as silt falls or planar or rotational slides on surfaces with moderate slope

angles, but also soil falls occur along road cuts or steep slopes. Quite often, rotational or translational landslides are transformed into flows. The La Aurora landslide of 1999 can be regarded as a silt flow slide that began as a rotational slide according to the classification of Hungr, Leroueil, and Picarelli (2014) (Figure 47).

| | Class | Number of landslides. | % | Total landslide area (m$^2$) | Mean landslide area (m$^2$) |
|---|---|---|---|---|---|
| **Typology** | Silt flowslides | 160 | 24.1 | 66,790 | 417 |
| | Debris flowslides | 140 | 21.1 | 49,992 | 357 |
| | Silt planar slides | 119 | 17.9 | 58,302 | 490 |
| | Slides (planar or rotational) or silt falls to flow slides* | 95 | 14.3 | 112,445 | 1,183 |
| | Silt Rotational slides | 76 | 11.4 | 66,854 | 879 |
| | Soil silt falls | 65 | 9.8 | 10,524 | 162 |
| | Rock falls | 6 | 0.9 | 1,539 | 307 |
| | Rock avalanche | 1 | 0.1 | 34 | 34 |
| **Land cover** | Grasslands | 219 | 33.0 | 96,165 | 441 |
| | Secondary vegetation (arable land or grasslands abandoned) | 109 | 16.4 | 84.770 | 777 |
| | Arable land | 89 | 13.4 | 87,749 | 986 |
| | Urban areas | 62 | 9.3 | 16.991 | 278 |
| | Road Cuts | 89 | 13.4 | 36,970 | 415 |
| | Forest | 57 | 8.6 | 32,027 | 579 |
| | Material banks | 18 | 2.7 | 4,713 | 618 |
| | Without vegetation | 15 | 2.2 | 3,233 | 215 |
| | Industrial areas | 3 | 0.4 | 1935 | 645 |
| **Lithology** | Basalt | 47 | 7.0 | 33,582 | 730 |
| | Fall deposits QptAs-Pu | 41 | 6.2 | 79,399 | 2,205 |
| | Pumice flow deposit QptPu | 14 | 2.1 | 15,910 | 1,136 |
| | Xaltipan Ignimbrite unwelded QptIg-uw | 369 | 55.7 | 385,859 | 1,034 |
| | Welded tuff TplT-w | 15 | 2.3 | 7,924 | 528 |
| | Andesite Teziutlán TplA | 125 | 18.9 | 118,786 | 928 |
| | Sedimentary rocks | 18 | 2.7 | 16,958 | 997 |
| | Granite KvGr | 25 | 3.8 | 24,046 | 961 |
| | Chililis schist Pp(?)Sch | 8 | 1.2 | 30,733 | 3,841 |

*Figure 47. Landslides in the study area according to typology (Hungr et al. 2014), lithology and land cover.*

# 3.5 DISCUSSION

The inventory map presented here can be used as a main input to produce a susceptibility map, and to analyze time-frequency and landslide magnitude. However, there is a lack of data concerning the landslide event of 1944. This historical information is very difficult to obtain as no accurate images were available and local inhabitants do not recall properly the location of the movements that occurred at that time. A more detailed analysis derived from the LiDAR DEM may help to identify large landslides, but information concerning medium-scale or small landslides (those less than 65 m$^2$) is practically impossible to acquire at this point.

Furthermore, the scale and/or quality of some of the remote sensing inputs used for this work were not ideal. For instance, aerial photographs from 1980 (1:80,000 scale) lost quality when scanned. Identification of small landslides in those images was not possible. However, the present results demonstrate that remote sensing inputs available from a range of sources can help to overcome the limitations imposed by time and budget constraints.

Additionally, analysis of the past 15 years indicates that in this area landslides have occurred not only during extreme rainfall events such as in 1999, but also on a yearly basis during the rainy season. It is necessary to analyze the temporal development of this relationship to factors in addition to extreme events, and to determine which are the major controls of instability, including human interference as a possible prime agency. Although there are more and better data regarding landslide occurrence available for the period 2000–2015 than for the preceding years, it has not been possible to identify an increase in the number of landslide events in the past 15 years. However, according to the analysis produced for the historical timeframe established for this research, the frequency of landslide events recorded from 1942 to 2015 shows that since 1999 high-magnitude rainfall events like those of 1944 and 1955 have not occurred. One possibility may be to shorten the period of time of data used to prepare the inventory and focus on the years between 1999 and the present time, on which more information and references are available. Nonetheless, a lower number of landslides could be expected because of this lack of extreme rainfall events since 1999. In any case, updating and improving the historical documentation to increase landslide records remains a huge challenge especially in countries such as Mexico and other nations of Latin America where, in contrast to other regions, the number of researchers and projects focused on landslide inventories is rather low.

## 3.6 CONCLUSIONS

In Latin America, landslides occur frequently in volcanic deposits but investigations regarding landslide inventories, characterization of materials and specific mechanisms are still scarce. There are also few studies on the understanding of landslide disasters on volcanic terrains. In this paper, we described the distribution of the landslides in Teziutlán, Puebla, Mexico. The results suggested that the most frequent landslide types are flows and complex movements that generally are initiated as slides and soon after are transformed into silt and debris flowslides. Even though the 1999 disaster identified Teziutlán as an area prone to landslides, this research is the first attempt to generate a multi-temporal landslide inventory for the municipality. Large landslide events are associated with the occurrence of extraordinary rainfall episodes with at least one day with more than 300 mm of rain preceded by a

period of cumulative precipitation. Likewise, small and medium-size events take place during the rainy season. Such occurrences need to be further explored not only in terms of precipitation, but also considering the potential and actual impact of human activities on the slopes. Events like those of 1944, 1955 and 1999 are likely to occur again in the Sierra Norte de Puebla region. This inventory map will be useful in future research on landslide susceptibility and hazard mapping, along with risk assessments at municipal and local scales.

References

Alaniz-Alvarez, S. A., Nieto-Samaniego, A. F., & Ferrari, L. (1998). Effect of strain rate in the distribution of monogenetic and polygenetic volcanism in the Transmexican Volcanic Belt. Geology, 26(7), 591–594. doi:10.1130/00917613(1998)026<0591:EOSRIT>2.3.CO;2

Alcántara-Ayala, I. (2004). Hazard assessment of rainfallinduced landsliding in Mexico. Geomorphology, 61, 19– 40. doi:10.1016/j.geomorph.2003.11.004

Alva-Valdivia, L. M., Urrutia-Fucugauchi, J., Zamorano-Orozco, J. J., Goguitchaichvili, A., Ferrari, L., & Rosas-Elguera, J. (2000). Paleomagnetic data from the Trans- Mexican Volcanic Belt: Implications for tectonics and volcanic stratigraphy. Earth, Planets and Space, 52, 467–478. doi:10.1186/BF03351651

Capra, L., Lugo-Hubp, J., & Borselli, L. (2003). Mass movements in tropical volcanic terrains: The case of Teziutlán (Mexico). Engineering Geology, 69, 359–379. doi:10.1016/S0013-7952(03)00071-1

Concha-Dimas, A., Cerca, M., Rodríguez, S.-R., & Watters, R. J. (2005). Geomorphological evidence of the influence of pre-volcanic basement structure on emplacement and deformation of volcanic edifices at the Cofre de Perote – Pico de Orizaba chain and implications for avalanche generation. Geomorphology, 72, 19–39. doi:10.1016/j.geomorph.2005.05.004

Dávila-Harris, P., & Carrasco-Núñez, G. (2014). An unusual syn-eruptive bimodal eruption: The Holocene Cuicuiltic member at Los Humeros caldera, Mexico. Journal of Volcanology and Geothermal Research, 271, 24–42. doi:10.1016/j.jvolgeores.2013.11.020

Ferriz, H., & Mahood, G. (1984). Eruption rates and compositional trends at Los Humeros volcanic center, Puebla, Mexico. Journal of Geophysical Research, 89, 8511–8524. doi:10.1029/JB089iB10p08511

Flores-Lorenzo, P., & Alcántara-Ayala, I. (2002). Cartografía morfogenética e indetificación de procesos de ladera en Teziutlán, Puebla. Investigaciones geográficas, Boletín del Instituto de Geografía, UNAM.

Gomes, A., Gaspar, J. L., Goulart, C., & Queiroz, G. (2005). Evaluation of landslide susceptibility of Sete Cidades Volcano (S. Miguel Island, Azores). Natural Hazards and Earth System Science, 5, 251–257. doi:10.5194/nhess-5-251-2005

Hungr, O., Leroueil, S., & Picarelli, L. (2014). The Varnes classification of landslide types, an update. Landslides, 11, 167–194. doi:10.1007/s10346-013-0436-y.

INEGI. (2009). Prontuario de información geográfica municipal de los Estados Unidos Mexicanos (9). Teziutlán: InstitutoNacional de Geografía y Estadística.

Lugo-Hubp, J., Zamorano-Orozco, J. J., Capra, L., Inbar, M., & Alcántara-Ayala, I. (2005). Los procesos de remoción en masa en la Sierra Norte de Puebla, octubre 1999; causas y efectos. Revista Mexicana de Ciencias Geológicas, 22(2), 212–228.

Marques, R., & Amaral, P. (2004). Avaliacao do Risco geológico associado a ummovimento de Vertentena freguesia dos. Mosteiros (ilha de S.Miguel), Relatório Técnico-Científico DTC44/CVARG/03, Centro de Vulcanologia e Avaliacao de Riscos Geológicos, 8.

Miyabuchi, Y., Maeno, F., & Nakada, S. (2015). The October 16, 2013 rainfall-induced landslides and associated lahars at Izu Oshima volcano, Japan. Journal of Volcanology and Geothermal Research, 302, 242–256. doi:10.1016/j.jvolgeores.2015.07.012

Murillo-García, F. G., Alcántara-Ayala, I., Ardizzone, F., Cardinali, M., Fiourucci, F., & Guzzetti, F. (2015). Satellite stereoscopic pair images of very high resolution: A step forward for the development of landslide inventories. Landslides, 12(2), 277–291. doi:10.1007/s10346-014-0473-1

Nocentini, M., Tofani, V., Gigli, G., Fidolini, F., & Casagli, N. (2015). Modeling debris flows in volcanic terrains for hazard mapping: The case study of Ischia Island (Italy). Landslides, 12, 831–846. doi:10.1007/s10346-014-0524-7

Pardo, M., & Suarez, G. (1995). Shape of the subducted Rivera and Cocos plates in southern Mexico: Seismic and tectonic implications. Journal of Geophysical Research: Solid Earth, 100, 12357–12373. doi:10.1029/95JB00919

Pareschi, M. T., Favalli, M., Giannini, F., Sulpizio, R., Zanchetta, G., & Santacroce, R. (2000). May 5, 1998 debris flows in circum-Vesuvian areas (southern Italy): Insights for hazard assessment. Geology, 28, 639–642. doi:10.1130/0091-7613(2000)28<639:MDFICA>2.0.CO;2

QGIS Development Team. (2012). QGIS Geographic Information System. Open source Geospatial Foundation. Retrieved from http://qgis.osgeo.org

Salinas-Rodríguez, J. M., & Castillo-Reynoso, J. E. (2011). Carta Geologica Minera. Teziutlán E14B15 Puebla. Servicio Geológico Mexicano.

Smith, G. A., & Lowe, D. L. (1991). Lahars: Volcano-hydrologic events and deposition in the debris flow-hyperconcentrated flow continuum. In R. V. Fisher & G. A. Smith (Eds.), Sedimentation in volcanic settings (vol 45, pp. 123–137). SEPM Special Publication.

Varnes, D. J. (1978). Slope movements: Types and processes. In R. L. Schuster, & R. J. Krizek (Eds.), Landslide analysis and control National Academy of Sciences, Special Report 176. (pp. 11–33). Washington, D.C.: Transportation Research Board.

Viniegra, F. (1965). Geología del macizo de Teziutlán y la cuenca Cenozoica de Veracruz. Bol. Asc. Mex. Geol. Pet., 17, 101–163.

# Capítulo IV. Landslide susceptibility using slope units

**Landslide susceptibility analysis and mapping using statistical multivariate techniques: Pahuatlán, Puebla, Mexico.**

# Landslide susceptibility analysis and mapping using statistical multivariate techniques: Pahuatlán, Puebla, Mexico ©

Franny Giselle Murillo-García
Posgrado en Geografía UNAM

Irasema Alcántara Ayala
Instituto de Geografía UNAM

*Susceptibility analyses are frequently based on the idea that landslides occur in the same areas where they have taken place previously, and also in areas under similar conditions. Based on that assumption, four different statistical techniques—Linear Discriminant Analysis (LDA), Quadratic Discriminant Analysis (QDA), Logistic Regression (LRA), and Neural Networks (NN) —have been applied for the municipality of Pahuatlán, Puebla, México. The base for the analysis was a geomorphological landslide inventory derived from the stereo-interpretation of Very High Resolution (VHR) satellite images. The quality of each model was controlled by using ROC curves and Cohen's Kappa coefficient. Also, a temporal validation with a data set of landslides occurred on 2012 was carried out for each model. The resulting analysis showed that the aspect, the slope angle and the lithological unit were the variables with the highest weight associated with the occurrence of landslides in the study area.*

# 4.1 INTRODUCTION

Landslides affect human society on a variety of spatial and temporal scales (Glade and Crozier 2005). Its occurrence depends on many factors and geo-environmental conditions. Landslide susceptibility refers to the landslide spatial dimension, as one of the elements comprised within landslide hazard assessments. Landslide susceptibility is very much interconnected to the question where landslides may occur? (Guzzetti 2006) Susceptibility to landsliding is also related to a set of geo-environmental conditions that influences hillslope stability (Guzzetti 2006, Rossi *et al.* 2010). Susceptibility analyses are frequently based on the idea that the "past is the key to the future"; meaning that it is more likely that landslides occur in the same areas where they have taken place previously, and also in areas under similar conditions. Based on this, it is possible to predict where landslides can occur.

Landslide susceptibility is the probability of spatial occurrence of landslides (Guzzetti 2006, Chung and Fabri 1999). It can be estimated for large areas, even at national scale, or only for a single slope. However, the variety of spatial behaviour requires specifically adapted research methods (Glade and Crozier 2005). Since the seventies, the number of digital based methods has increased considerably and became more popular as the development of new computer technologies progressed (Glade and Crozier 2005). Pioneering works on landslide susceptibility maps included Brabb *et al.* (1978) and Carrara (1978, 1983), but there is not yet a universal methodology (Guzzetti 2006).

Models for landslide susceptibility estimation can be classified into quantitative (numerical estimates) or qualitative (heuristically, descriptive and subjective estimates) (Glade and Crozier 2005, Guzzetti 2006). The heuristic approaches are based on a priori knowledge and depend on the skill and experience of the professional judgment. Approaches using quantitative methods are more objective and repeatable (Glade and Crozier 2005).

Five main categories of these methods have been identified by Glade and Crozier 2005: (1) direct geomorphological mapping; (2) analysis of landslides inventories; (3) heuristic or index based methods; (4) statistical methods and (5) process based conceptual models. Geomorphological mapping relies on the ability of the researcher to recognize the potential slope failures. Analysis of landslide inventories consists of landslide density maps. Process based models are deterministic or based on physically controlling slope instability principles (Guzzetti 2006).

The statistical methods use functional relationships between instability factors and the past distribution of landslides (landslide inventory) (Guzzetti 2006, van Westen et al 2008). Most of these methods are based on the relation between the landslide spatial distribution and a set of thematic layers. Such techniques are: (a) Classical statistic techniques include bivariate analysis, factor analysis, discriminant

analysis (Rossi *et al.* 2010, Guzzetti *et al.* 2006, He *et al.* 2012), logistic and regression analysis (Rossi *et al.* 2010, (Yesilnacar *et al.* 2005, van Den Eeckhaut *et al.* 2006, Nefeslioglu *et al.* 2008, Yilmaz 2009, Bai *et al.* 2010, Das *et al.* 2010, Nandi and Shakoor 2010, Yalcin *et al.* 2011, Choi *et al.* 2012, Schicker and Moon 2012, Xu *et al.* 2012, Wang *et al.* 2012); (b) Modern statistical methods comprise generalized additive models (GAM), weight of evidence methods, weight factors, information value, and modified Bayesian estimation; (c) Fuzzy logic systems; (d) Neuronal networks (Rossi *et al.* 2010, Yesilnacar *et al.* 2005, Nefeslioglu *et al.* 2008, Yilmaz 2009, Choi *et al.* 2012, Xu *et al.* 2012, and support vector machines (Kanungo *et al.* 2006, Melchiorre *et al.* 2008, Melchiorre *et al.* 2011, Kawabata and Bandibas 2009, Pradhan and Lee 2010, Vahidnia *et al.* 2010, Oh and Pradhan 2011, Tien Bui *et al.* 2012, Pradhan 2013); and (e) Expert based systems. Many authors have compared and/or combined different statistical methods.

Landslide susceptibility estimations involve several requirements (Fell *et al.* 2008), among them, development of landslide inventories, integration of data and maps on a GIS platforms, and data treatment/analysis to establish quantitative ratings and obtaining susceptibility classes. Model or techniques selection depends on tree criteria (Frattini *et al.* 2010): (1) the mathematical and conceptual adequacy in describing the system behavior, (2) its robustness to small changes on the input data, and (3) its accuracy in predicting the observed data.

In this research a combination model of statistic techniques has been applied in terms of four different statistical techniques that are frequently used in landslide susceptibility analysis: Linear Discriminant Analysis (LDA), Quadratic Discriminant Analysis (QDA), Logistic Regression (LRA), and Neural Networks (NN). The study area (54 km$^2$) was divided into slope units. In the combination model a probability value (0 to 1) is assigned to each slope unit. The base for the analysis was a geomorphological landslide inventory derived from the stereo-interpretation of Very High Resolution (VHR) satellite images, the review of historical data and field surveys. Temporal validations were applied and compared.

## 4.2 STUDY AREA

The Pahuatlán municipality covers 89 km$^2$ and is situated in the mountainous region of Sierra Norte of Puebla at the Cazones River basin. The study area was concentrated on the central portion of the municipality: 54 km$^2$ and includes the most populated tows of the region: Pahutlán del Valle, Xolotla, Atla, San Pablito, Paciotla and Xochimilco towns (Fig. 48). Lithological rock units are as follows: (i) Low Jurassic Huayacocotla sandstone and shale sequence; (ii) Cahuas siltstone-sandstone formation; (iii) Middle Jurassic Tepéxic limestone formation; (iv) Late Jurassic Tamán clayey limestone and shale

sequence; (v) Late Jurassic Pimienta black limestone-shale sequence; (vi) Low Cretaceous Tamaulipas limestone-shale sequence; (vi) Pliocene basalt, andesite and pyroclastic deposits and recent; (vii) alluvial; and (viii) colluvium deposits (Sánchez-Rojas and De la Callejera-Moctezuma 2004). Slopes range from almost zero, along the plain of San Marcos River (alluvial quaternary deposits), to more than 70° at the top of the mountains (Middle Jurassic Tepéxic limestone formation). Most of natural vegetation is rainforest (mesophyll woods) (Oliva Aguilar *et al.* 2011), although there is also coniferous forest (pine and oak woods) in the upper mountains of Aila region. This area is highly deforested due to agricultural activity; most of the land use is agricultural land and cattle. Original vegetation can be found on very steep slopes and deep and stretch ravines. Climate is temperate and mean annual rainfall as high as 2500 mm/year. The orientation of Cazones River and the strong variation on altitude are additional factors that contribute to the saturation of the soils most of the year in Pahuatlán (Oliva Aguilar *et al.* 2011).
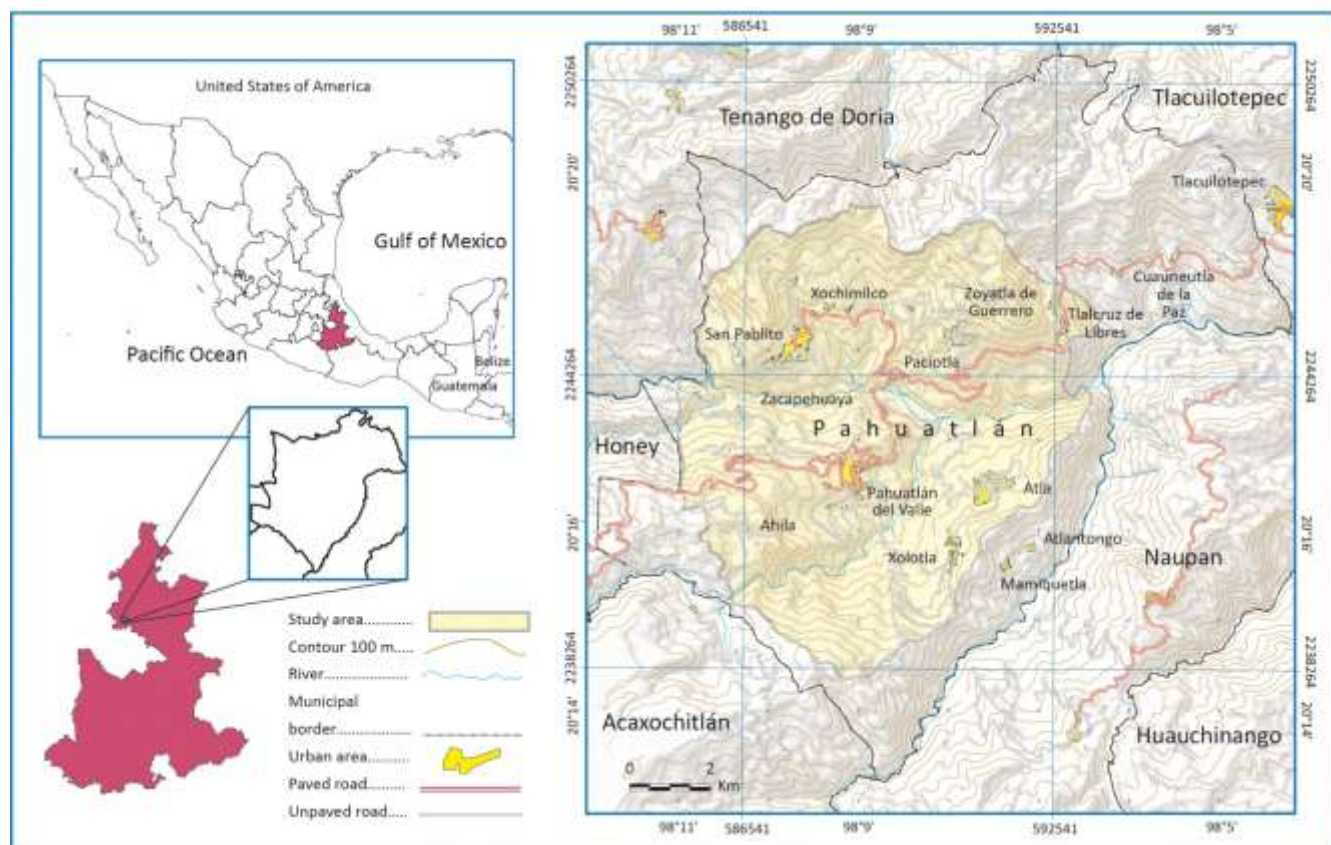


***Figure 48.*** *Location of Pahuatlán municipality, Puebla, Mexico.*

Landslides in this area are mainly triggered by heavy rainfall. They have occurred particularly in wet years such as 1955, 1999, 2005 and 2007. These extraordinary rainfall events are usually related to hurricanes and tropical depressions from the Gulf of Mexico. Main types of landslides include flows, slides, rock falls and complex movements (Alcántara-Ayala 2004). Velocity of the very big large landslides is rather slow; this has allowed evacuation of population. In 2007, a landslide (the 5 de mayo Street landslide) affected the central part of Pahuatlán; a small hospital and other houses were destroyed.

## 4.3 MATERIALS AND METHODS

### 4.3.1 Materials: Data Source and Preparation

Any landslide hazard analysis requires an inventory as complete and accurate – in space and time – as possible (van Westen *et al.* 2008, Ibsen and Brunsden 1996, Lang *et al.* 1999, Glade 2001). In the study area we have compiled a landslide inventory map (LIM) by both visual interpretation of a Very High Resolution (VHR) stereo-pairs satellite images and field surveys carried out in the period 2011-2012. The LIM comprises 385 landslides that occurred in the period 1994-2012 (Fig. 49).

A 10 meters high resolution Digital Elevation Model (DEM) was generated on the LPS Automatic Terrain Extraction module from ERDAS IMAGINE© software using a stereo-pair of VHR satellite images GeoEye1 (0.5 m of spatial resolution on panchromatic band). The DEM was used to divide the study area into slope units (SU) and to generate the relief variables for the statistical models.

The SU were generated using a tool developed on GRASS GIS by Marchesini *et al.* (2012). The tool allowed i) to identify 259 slope units and ii) to compute average value of different morphometric parameters such as slope angle, slope aspect and slope profile. The most extend SU was 1.1 km$^2$ and the smallest 17,344 m$^2$.

Additionally, the compilation of variables associated with geo-environmental conditions –relief, lithology, faults and discontinuities, land use and vegetation, and old mass movements- related to landslide occurrence was done using different sources. The selection of geo-environmental conditions depends on the availability and data quality, and is based on the following assumptions: (1) Landslides take place very likely on areas where there is a landsliding history, (2) where the topography dictates that landsliding may occur, (3) where geological and geomorphological conditions are such that landslides are possible, (4) where man-made modifications on slopes enhance failure (Fell *et al.* 2008). These environmental factors are expected to have an effect or influence on the occurrence of landslides

and the assumption is that these same factors can be used on the prediction of future landslides (van Westen *et al.* 2008).
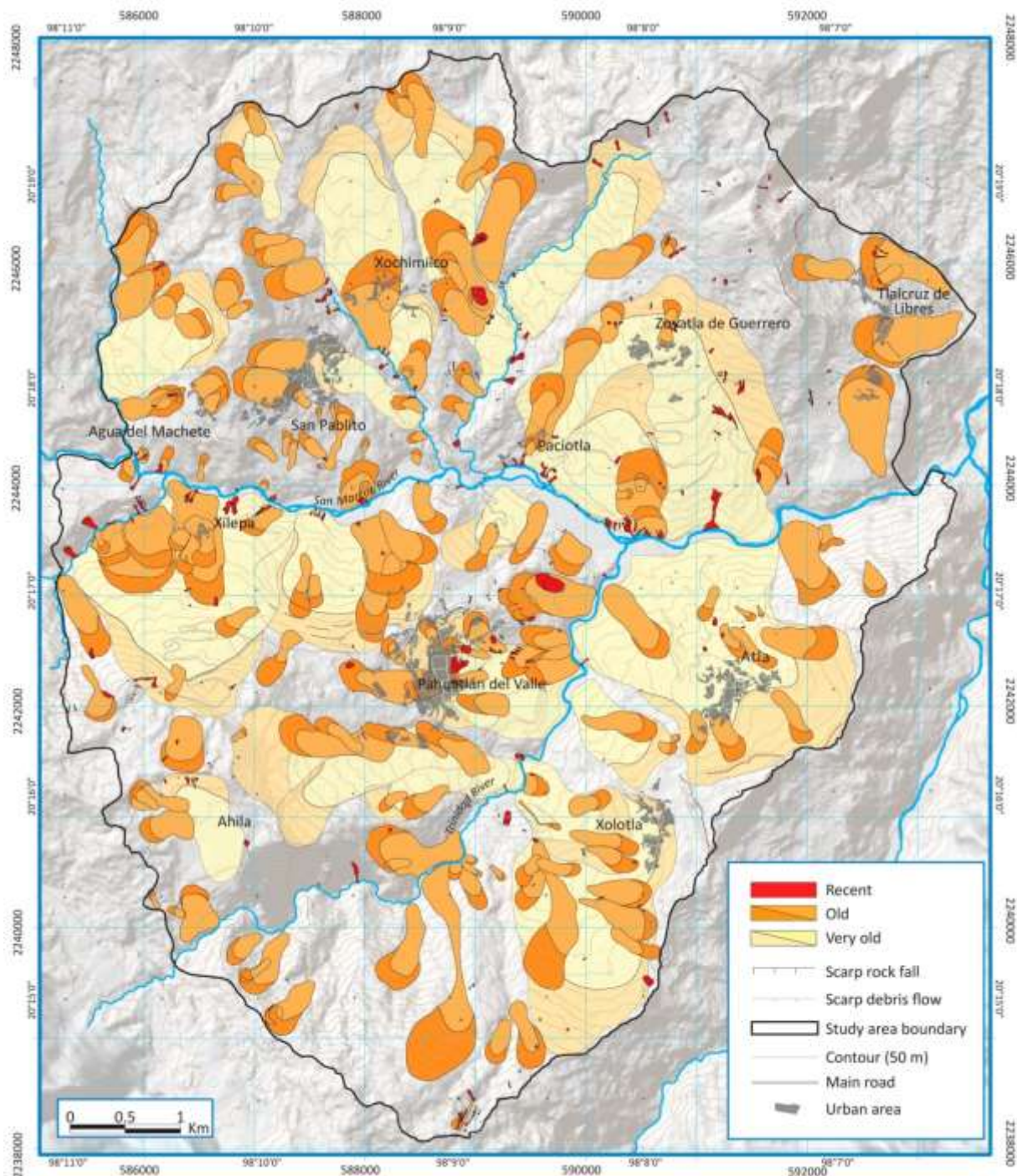


***Figure 49.*** *Landslide inventory map of Pahuatlán. It includes 557 mass movements classified as recent landslides (1994-2012) (385), old failures (171) and very old movements (21).*

Aspect, curvature, range and slope angle were the components derived from the relief considered as model variables. For the lithology and discontinuities the 1:50 000 scale geology maps (1814_F14D73 and 1814_F14D83) from the study area generated by the Servicio Geológico Mexicano (Sánchez-Rojas and De la Callejera-Moctezuma 2004) were used. The boarders of the lithological units were identified more in detail by using the VHR satellite images stereo-pairs; it allowed the identification of a new fault. Major geological structures are the Huayacocotla anticline, a macrostructure with NNW-SSE axis, and San Pablo synclinal; structural discontinuities are the Paciotla normal fault and Xolotla inverse fault. A buffer of 150 m was generated around these lines on a GIS environment.

For land use and vegetation, a supervised classification process was done using the ERDAS 2011© software and the GeoEye1 images. Land use units were classified as: forest, grassland, agriculture, urban area, roads, water and no vegetated areas. Figure 50 shows the variables used for the model data set. Lack of information on other geoenvironmental conditions for the study zone did not allow its incorporation in the susceptibility models. Information of recent landslides from the inventory was used as response variable, whereas information of the Geo-environmental conditions was considered as explanatory variables.

| Variable | Source |
|---|---|
| Week lithology | Geology maps at 1:50 000 scale |
| Hard lithology | Geology maps at 1:50 000 scale |
| Aspect | DEM |
| Slope angle | DEM |
| Old and very old landslides area | Geomorphological inventory |
| Mean elevation | DEM |
| Falls and fractures | Geology maps at 1:50,000 scale |
| Standard deviation of slope angle | DEM |
| Slope curvature | DEM |
| Urban and roads land use | VHR satellite images |
| Agricultural land use | VHR satellite images |
| Areas without vegetation land use | VHR satellite images |
| Forest land use | VHR satellite images |

*Figure 50* Variables used as explanatory variables on the statistical models.

### 4.3.2 Methods

Four statistical multivariate models were selected because of its very extensive used on landslide susceptibility. The models selected were: (1) Linear Discriminant Analysis (LDA), (2) Quadratic Discriminant Analysis (CDA), (3) Logistic Regression (LR), and (4) Neuronal Networks (NN). Percentage of landslide area in each SU was used to classify each as stable or unstable (grouping variable). Slope units with a landslide area larger than 1% were classified as unstable. The models work with a probability range, a degree of certainty value, where zero is a null probability that a landslide occurs, and 1 is the certainly of a landslide occurs. Each SU was assigned with a susceptibility value on each multivariate method. The susceptibility values obtained from the different models were combined by a logistic regression to obtain the combined landslide susceptibility zoning. All the calculations were done on the free statistical software R-Project (R Core Team 2013). Each model was run 200 times, except Neuronal Network which was run 20 times, each time varying the selected slope units.

Landslides are a complex phenomenon and as such, their natural variability results in uncertainties (Ardizzone *et al.* 2002, Petschko *et al.* 2012). Therefore, it is important to evaluate the quality of landslide susceptibility maps. Very common very little or no attention is given to the evaluation of model results; thus, the analysis of the observed data and the presence/absence of landslide on the reality is quite significant (Frattini *et al.* 2010). Cross validation, represented by contingency tables based methods is frequently use for validation (Petschko *et al.* 2012). Receiver Operator Characteristics' curves (ROC) have been adopted for model evaluation on the landslide literature (Rossi *et al.* 2010, Yesilnacar *et al.* 2005, Nefeslioglu *et al.* 2008, Frattini *et al.* 2010, Gorsevski *et al.* 2006). For this research, the ROC plot, the Heidke's skill score (Cohen's Kappa coefficient) and contingency tables are presented as confidence parameters of each model. Furthermore, for validating the results the temporal validation of a dataset field survey inventory developed at the end of 2012 was used.

Figure 51 shows the individual results for each model. It includes the frequency histogram with the values divided into five classes: (0-0.2) very low susceptibility; (0.2- 0.45) low; (0.45-0.55) medium; (0.55-0.8) high; and (0.8-1) very high. Additionally, the maps portray the five susceptibility categories. Also included are the count of slope units in unequally spaced susceptibility classes, the four-fold plots summarizing the number of true positives true negatives, false positives and false negatives, the Cohen's Kappa Value, the model probability variability (bootstrap) graphic and the receiver operating characteristic curves.
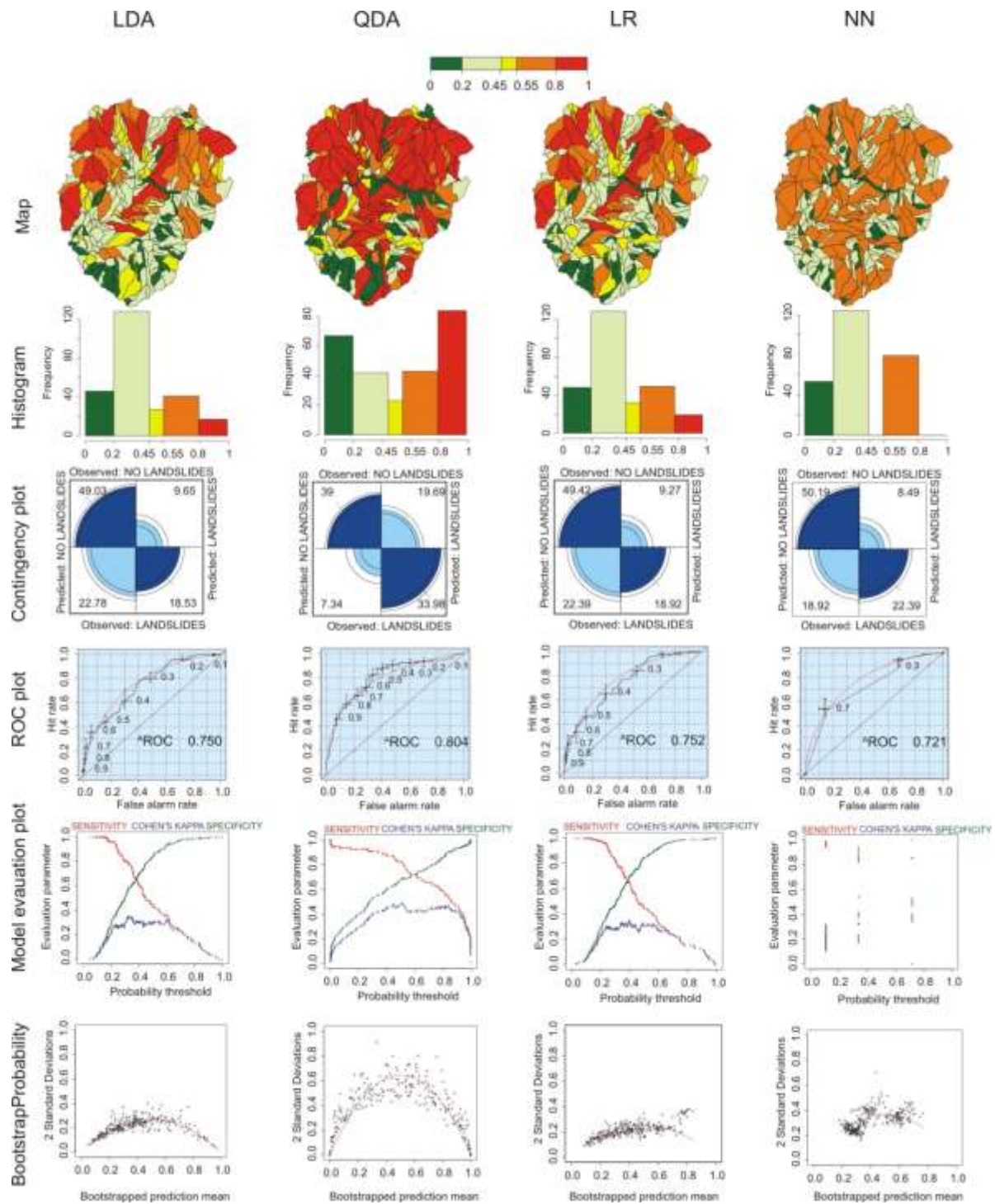
***Figure 51.*** *Model results: 1) maps portraying the four susceptibility zones; 2) count of slope units in unequally spaced susceptibility classes; 3) four-fold plots summarizing the number of true positives true negatives, false positives and false negatives; 4) receiver operating characteristic (ROC) curves; 5) Cohen's-Kappa coefficient graphic and 6) bootstrap prediction variability plot*

The ROC curve describes the capability of the statistical model to discriminate among two classes of objects (Frattini *et al.* 2010). The area under the ROC curve is used as metric to assess the quality of the model (Frattini *et al.* 2010, Hanley and McNeil 1982). A larger area under the curve implies a better model performance. The points on the ROC curve represent the pairs derived from different contingency tables for different cut-offs. Closer points to the upperright corner correspond to lower cut-off values. In short, a ROC curve is better than another if it is close to the upper left corner and the ROC value is closer to 1 (Frattini *et al.* 2010). On the Cohen's Kappa coefficient the technique measures the fraction of correct classifications after eliminating those classifications which would be correct purely due to random chance (Frattini *et al.* 2010).

The plots that show the measures of the model error ($\phi$) vs. mean probability ($\mu$) for each slope unit, provide the results of the application of the "bootstrapping" resampling technique obtained from the ensembles of model runs (200 times for LDA, QDA and LR, and 20 for NN) (Rossi *et al.* 2010). The points that are closer to the extreme x-axis and to the lower part of the graphic (low standard deviation) show a good performance of the model. Points on the center and with a high standard deviation mean that cases are classified as very high or very low susceptibility indistinctly when the models are running.

The results of the four models have differences. The maps of figure 3 show that an LR, LDA and QDA result are similar but differ from the NN results. NN is the method that shows low dichotomy results (histograms of figure 51). QDA is the model that demonstrates a better capability to divide the SU into two classes, but also shows the highest standard deviation on the bootstrapping graphic. The contingency tables illustrate that the LR and the LDA have an effectiveness of 60%. The AROC value for these models is acceptable (0.75). QDA shows an effectiveness of 73% with the highest AROC value: 0.804. The QDA presents the best performance. NN show low values.

Figure 51 shows that LR and LDA present very similar results and the linear correlation of the two techniques is shown in the dispersion plot (Figure 52). A Pearson correlation value was computed for different couples of models and LRA and LDA show a strong collinearity (Figure 53). For these reason, the combination model was run in three different ways: (i) with all the models, (ii) without the LR, and (iii) without LDA.
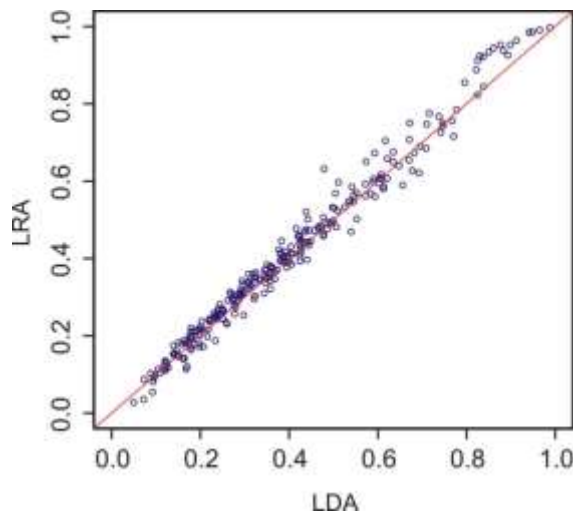
**Figure 52.** *Dispersion plot for the LDA and the LRA models that shows the linear correlation between the two models.*

| Combination | Pearson correlation (r value) |
|---|---|
| *LR-LDA* | 0.990 |
| *LR-QDA* | 0.694 |
| *LR-NN* | 0.580 |
| *LDA-QDA* | 0.686 |
| *LDA-NN* | 0.578 |
| *QDA-NN* | 0.586 |

**Figure 53.** *Pearson correlation values among the four individual models.*

## 4.4 RESULTS

For the LR Combination Model, the dependent variable was the presence or absence of recent landslides, while results of the individual models (LR, LDA, QDA and NN) were considered as "explanatory variables". In order to choose the best model performance, the Akaike Information Criterion (AIC) was used in combination with the ROC plot area and the effectiveness for training and validation data set (Figure 54).

| Model | AIC | Effectiveness | ROC | Validation data set effectiveness | ROC validation data set |
|-------|-----|---------------|-----|-----------------------------------|-------------------------|
| *The four together* | 260.45 | 74.51 | 0.821 | 67.57 | 0.706 |
| *Without LR* | 279.11 | 73.36 | 0.808 | 63.71 | 0.679 |
| *Without LDA* | 272.60 | 74.13 | 0.819 | 63.32 | 0.780 |

*Table 4.3* *Evaluation of the three models run for the analysis.*

The AIC measures the goodness-of-fit, and at the same time penalizes the model complexity to identify the simpler, but most parsimonious model (Petschko *et al.* 2012, Akaike 1994). The model that includes the four models presents the best AIC value, however, the model lacking of LDA shows better performance on the validation ROC value. In order to eliminate the collinearity problem, the model without LDA was use. Results are shown in Figure 4.5.

The grouping separation for the final model is acceptable (histogram Figure 55) with few SU on the medium range value. The model has effectiveness of 74.13%. The ROC value is 0.819. On the validation data set a 75.2% of effectiveness was obtained. The ROC value is not the best (0.708). From the individual models the best performance was QDA, whereas the worst, NN. A possible explanation might be that the data base inventory does not include landslides before 1994. The research Rossi *et al.* (2010) reports a similar problem when running the NN model only with a recent landslides data set (1997-2005). In that case, the NN model gives poor results in comparison to those resulting from a large temporal data set (1946-1996). The prediction skill for the others models (LR, QDA and LDA) does not seem to be affected by this issue. Unfortunately, the data set available for this work is not so large—in temporal scale—to be able to produce more comparisons.

The resulting variable analysis showed that the aspect, the slope angle and the lithological unit were the variables with the highest weight associated with the occurrence of landslides in the area of interest. Moreover, the presence of original and dense vegetation and the slope geometry were the variables related to the nonoccurrence landslide.
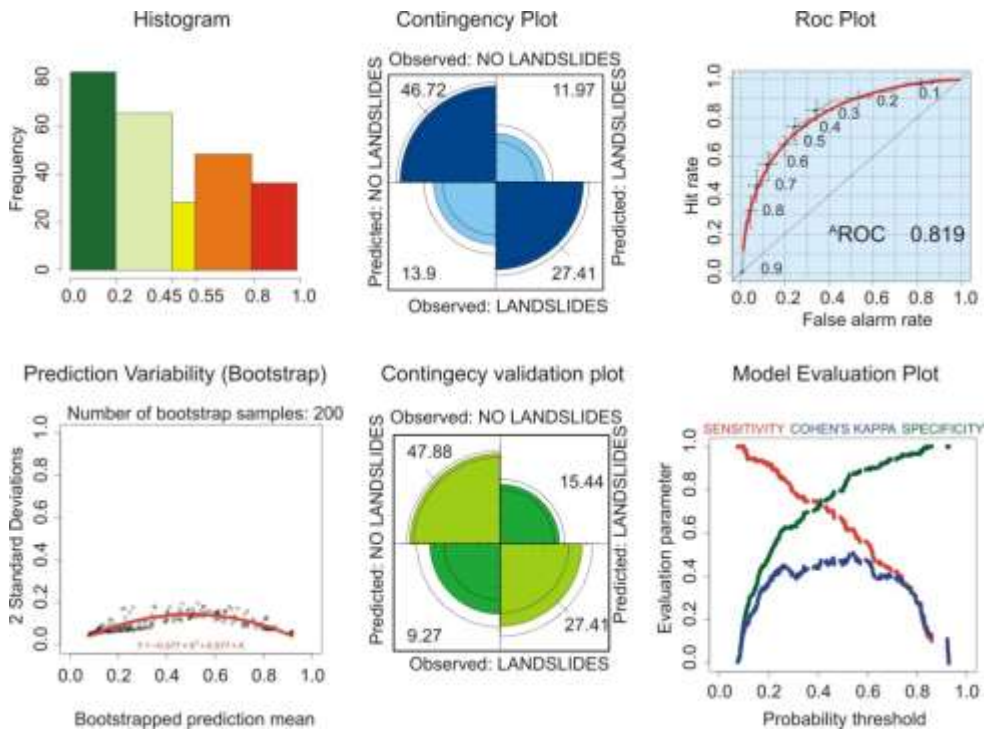
***Figure 55.*** *Results of the Combination model obtained without taking into account LDA.*

By comparing these results with those obtained by Rossi *et al.* (2010) the performance of the application of these models for the present research is not optimal. A possible explanation can be related to the need of a more complete data set used. Also, it is important to consider that results could depend on factors, such as: (i) the geomorphological setting, (ii) the type, quality and abundance of landslide information, (iii) the selection of classification methods, (iv) the ability and the experience of the researcher, and (v) the different methods that implemented the R statistical software on its different versions. Nonetheless, quite clearly, the combination process derived on a reduced number of classification errors (Rossi *et al.* 2020). Figure 56 shows that towns like Pahuatlán del Valle, Atla, San Pablito, Zoyatla, Xochimilco and Tlalcruz de Libres are located on SU with high and very high susceptibility classes. This undoubtedly represents a major issue for land use decision-making in Pahuatlán in the near future.

## 4.5 CONCLUSIONS

Four multivariate analysis statistical techniques (Logistic Regression, Linear Discriminant Analysis, Neuronal Network and Quadratic Discriminant Analysis) were used to run a Logistic Regression

Combination Model developed by Rossi *et al.* (2010). The model was applied for a 54 km$^2$ study area in the municipality of Pahuatlán, central Mexico, by using the data derived from a geomorphological landslide inventory. Training data set includes the landslides occurred from 1994 to 2010. In order to carry out a temporal validation, a data set derived from a landslide inventory field survey developed in 2012 was used. The information of recent landslide events was used as dependent variable, along with a set of geo-environmental factors used as explanatory variables. The study zone was divided into 259 slope units.

The quality of each model was controlled by using traditional contingency tables, ROC curves and Cohen's Kappa coefficient. Also, a temporal validation with a data set of landslides occurred on 2012 was carried out for each model. Three different combination models were run using: (i) the four simple forecasts, (ii) three forecasts without LRA, and (iii) three forecasts without LDA. Individually, the QDA model was the best performance model, with a 0.804 of AROC value. A collinearity problem was detected on the results of the LDA and LR; a Person Correlation Test was run to measure the level of correlation of the models.

Three models were run: one include all the models, one without the LR model, and another one without LDA. The combination of the four models produced the best Akaike Information Criteria, but the model without LDA showed the best performance for the validation. The susceptibility zonation obtained by the combination Model without LDA classifies correctly 74% of the slope units (ROC 0.819). Some of the urban zones of the area, including the capital, Pahuatlán, are located on SU with high and very high degree of landslide susceptibility. The quality of the models can be considered as acceptable, but evidently the inventory data set is not as complete as desirable due to the lack of sufficient remote sensing tools and historical information. For these reason the temporal extent of the data set is rather short and the information regarding old and very old landslides was not of any use as exact date of occurrence was unknown. However, it is important to point out that the Combination Model allows the reduction of errors for landslide susceptibility estimation. The application of multiple forecasts could be useful to obtain a better approach to landslide susceptibility.
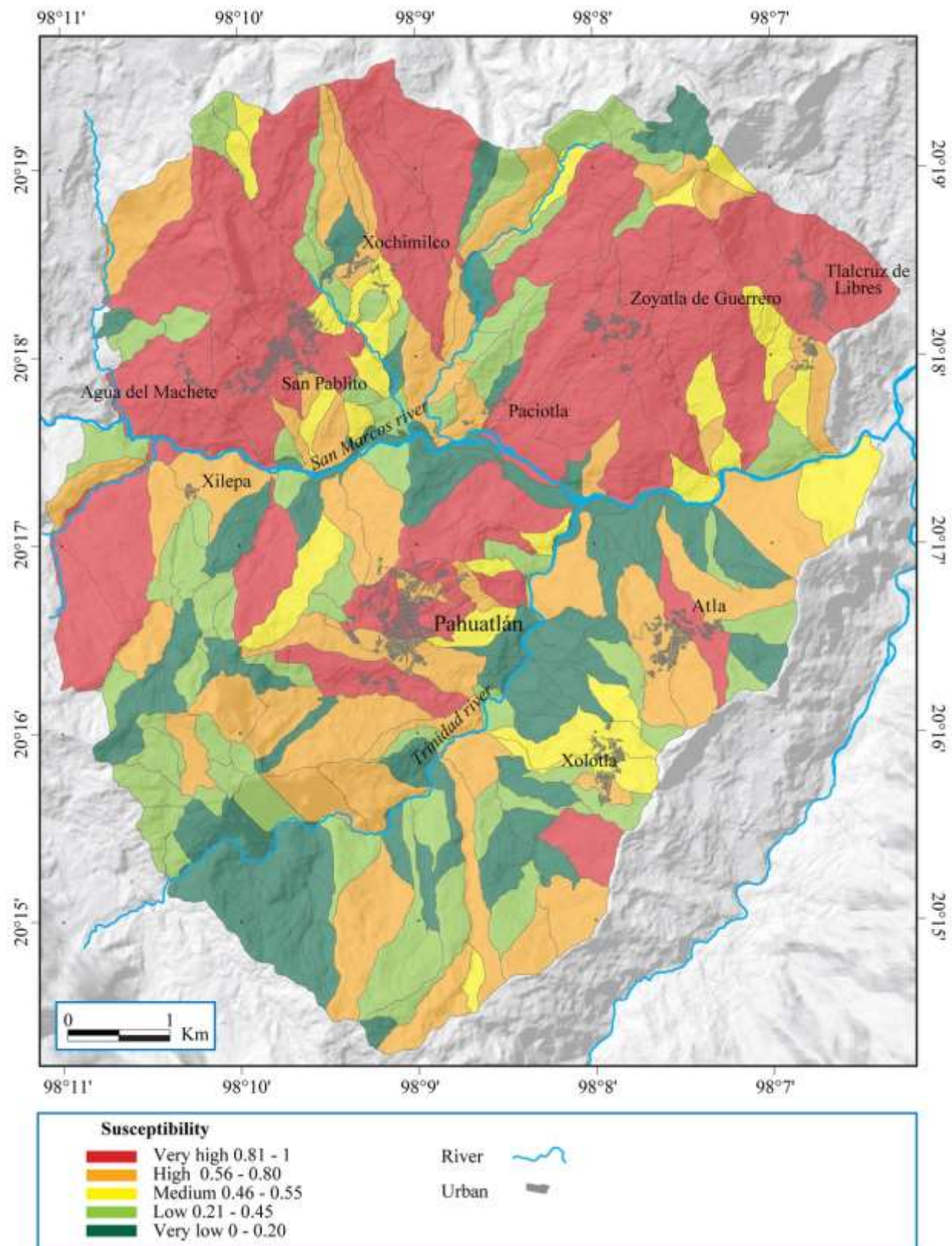
**Figure 56.** *Susceptibility map for the study area showing the distribution of the slope units where landslide susceptibility is higher. Many of these slope units coincide with the urban area of Pahuatlán.*

# References

Akaike H (1974) A new look at the statistical model identification. IEEE Transactions on Automatic Control 19(6), 716–723

Alcántara-Ayala I (2004) Hazard assessment of rainfall induced landsliding in Mexico. Geomorphology 61, 19–40

Ardizzone F, Cardinali M, Carrara A, Guzzetti F, Reichenbach P (2002) Uncertainty and errors in landslide mapping and landslide hazard assessment. Natural Hazards and Earth System Sciences 2(1-2), 3–14

Bai SB, Wang J, Lü GN, Zhou PG, Hou SS, Xu SN (2010) GIS-based logistic regression for landslide susceptibility mapping of the Zhongxian segment in the Three Gorges area, China. Geomorphology 115(1-2), 23–31

Brabb EE, Pampeyan EH, Bonilla MG (1978) Landslide susceptibility in San Mateo County, California. U.S. Geological Survey Miscellaneous Field Studies Map, MF-360, Scale 1, 62,500

Carrara A (1978) Considerazioni sulla cartografia applicata alla stabilità dei versanti. Seminario Sottoprogetto Fenomeni Franosi, Bari, 11 p. (in Italian)

Carrara A (1983) A multivariate model for landslide hazard evaluation. Mathematical Geology 15, 403–426

Choi J, Oh HJ, Lee HJ, Lee C, Lee S (2012) Combining landslide susceptibility maps obtained from frequency ratio, logistic regression, and artificial neural network models using ASTER images and GIS. Engineering Geology 4, 12–23

Chung CJF, Fabbri AG (1999) Probabilistic prediction models for landslide hazard mapping. Photogrammetric Engineering & Remote Sensing 65(12), 1389–1399

Das I, Sahoo S, van Westen C, Stein A, Hack R (2010) Landslide susceptibility assessment using logistic regression and its comparison with a rock mass classification system, along a road section in the northern Himalayas (India). Geomorphology 114(4), 627–637

Fell R, Corominas J, Bonnard C, Cascini L, Leroi E, Savage W (2008) Guidelines for landslide susceptibility, hazard and risk zoning for land use planning. Engineering Geology 102, 85–98

Frattini P, Crosta G, Carrara A (2010) Techniques for evaluating the performance of landslide susceptibility models. Engineering Geology 111, 62–72

Glade T (2001) Landslide hazard assessment and historical landslide data - an inseparable couple? In: Glade, T., Frances, F., Albini, P. (eds.) The Use of Historical Data in Natural Hazard Assessments. Advances in Natural and Technological Hazards Research, vol. 17, pp. 153–168. Springer, Berlin

Glade T, Crozier MJ (2005) A review of scale dependency in landslide hazard and risk analysis.
In: Glade T, Anderson MG, Crozier MJ (eds.) Landslide Hazard and Risk, pp. 75–138. Wiley, Chichester

Gorsevski P, Gessler P, Boll J, Elliot W, Foltz R (2006) Spatially and temporally distributed modeling of landslide susceptibility. Geomorphology 80, 178–198

Guzzetti F (2006) Landslide Hazard and Risk Assessment. Ph.D. Thesis, Mathematisch-Naturwissenschaftlichen Fakultät der Rheinischen Friedrich-Wilhelms-Universität, University of Bonn, Germany, 389 p.
http://hss.ulb.unibonn.de/diss_online/math_nat_fak/2006/guzzetti_fausto/, http://geomorphology.irpi.cnr.it/Members/fausto/PhD-dissertation

Guzzetti F, Reichenbach P, Ardizzone F, Cardinali M, Galli M (2006) Estimating the quality of landslide susceptibility models. Geomorphology 81, 166–184

Hanley JA, McNeil BJ (1982) The meaning and use of the area under a receiver operating characteristic (ROC) curve. Radiology 143(1), 29–36

He S, Pan P, Dai L, Wang H, Liu J (2012) Application of kernel-based Fisher discriminant analysis to map landslide susceptibility in the Qinggan River delta, Three Gorges, China. Geomorphology 171-172, 30–41

Ibsen ML, Brunsden D (1996) The nature, use and problems of historical archives for the temporal occurrence of landslides, with specific reference to the south coast of Britain, Ventnor, Isle of Wight. Geomorphology 15, 241–258

Kawabata D, Bandibas J (2009) Landslide susceptibility mapping using geological data, a DEM from ASTER images and an Artificial Neural Network (ANN). Geomorphology 113, 97–109

Kanungo DP, Arora MK, Sarkar S, Gupta RP (2006) A comparative study of conventional, ANN black box, fuzzy and combined neural and fuzzy weighting procedures for landslide susceptibility zonation in Darjeeling Himalayas. Engineering Geology 85, 347–366

Lang A, Moya J, Corominas J, Schrott L, Dikau R (1999) Classic and new dating methods for assessing the temporal occurrence of mass movements. Geomorphology 30(1-2), 33–52

Loaeza García JP, Zárate Barradas RG (2005) Carta Geológico-Minera Huauchinango F14- D83. Servicio Geológico Mexicano, Escala 1, 50 000

Marchesini I, Rossi M, Alvioli M, Santangelo M, Cardinali M, Reichenbach P, Ardizzone F, Fiorucci F, Balducci V, Mondini A, Guzzetti F (2012) WPS tools to support geological and geomorphological mapping. In: HEIG-VD: Open Conference Systems, OGRS 2012

Melchiorre C, Matteucci M, Azzoni A, Zanchi A (2008) Artificial neural networks and cluster analysis in landslide susceptibility zonation. Geomorphology 94, 379–400

Melchiorre C, Castellanos-Abella EA, van Westen CJ, Matteucci M (2011) Evaluation of prediction capability, robustness, and sensitivity in non-linear landslide susceptibility models, Guantánamo, Cuba. Computers & Geosciences 37, 410–425

Nandi A, Shakoor A (2010) A GIS-based landslide susceptibility evaluation using bivariate and multivariate statistical analyses. Engineering Geology 110(10), 11–20

Nefeslioglu HA, Gokceoglu C, Sonmez H (2008) An assessment on the use of logistic regression and artificial neural networks with different sampling strategies for the preparation of landslide susceptibility maps. Engineering Geology 97, 171–191

Oh HJ, Pradhan B (2011) Application of a neuro-fuzzy model to landslide-susceptibility mapping for shallow landslides in a tropical hilly area. Computers & Geosciences 37, 1264–1276

Oliva Aguilar VR, Garza Merodio GG, Alcántara-Ayala I (2011) Configuration and temporal dimension of vulnerability: spaces and disasters in the Sierra Norte de Puebla. Investigaciones Geográficas, boletín del Instituto de Geografía. UNAM 75, 61–74

Petschko H, Bell R, Glade T, Brenning A (2012) Landslide susceptibility modeling with generalized additive models – facing the heterogeneity of large regions. In: Eberhardt E, Froese C, Turner AK, Leroueil S (eds.) Landslides and Engineered Slopes: Protecting Society through Improved Understanding, pp. 769–775. Taylor & Francis, Banff

Pradhan B, Lee S (2010) Landslide susceptibility assessment and factor effect analysis: back propagation artificial neural networks and their comparison with frequency ratio and bivariate logistic regression modelling. Environmental Modelling & Software 25, 747–759

Pradhan B (2013) A comparative study on the predictive ability of the decision tree, support vector machine and neuro-fuzzy models in landslide susceptibility mapping using GIS. Computers & Geosciences 51, 350–365

R Core Team (2013) R: A Language and Environment for Statistical Computing. R Foundation for Statistical Computing, Vienna, http://www.R-project.org

Rossi M, Guzzetti F, Reichenbach P, Mondini A, Peruccacci S (2010) Optimal landslide susceptibility zonation based on multiple forecasts. Geomorphology 114, 129–142

Sánchez-Rojas LE, De la Callejera-Moctezuma AE (2004) Carta Geológico-Minera Pahuatlán F14-D73. Servicio Geológico Mexicano, Escala 1, 50 000 (in Spanish)

Schicker R, Moon V (2012) Comparison of bivariate and multivariate statistical approaches in landslide susceptibility mapping at a regional scale. Geomorphology 161-162, 40–57

Tien Bui D, Pradhan B, Lofman O, Revhaug I. Dick O (2012) Landslide susceptibility assessment in the Hoa Binh province of Vietnam: A comparison of the Levenberg–Marquardt and Bayesian regularized neural networks. Geomorphology 171-172, 12–29

Vahidnia M, Alesheikh A, Alimohammadi A, Hosseinali F (2010) A GIS-based neuro-fuzzy procedure for integrating knowledge and data in landslide susceptibility mapping. Computers & Geosciences 36, 1101–1114

van Den Eeckhaut M, Vanwalleghem T, Poesen J, Govers G, Verstraeten G, Vandekerckhove L (2006) Prediction of landslide susceptibility using rare events logistic regression: A case-study in the Flemish Ardennes (Belgium). Geomorphology 76, 392–410

van Westen CJ, Castellanos E, Kuriakose S  (2008) Spatial data for landslide susceptibility, hazard, and vulnerability assessment: An overview. Engineering Geology 102, 112–131

Wang LJ, Sawada K, Moriguchi S (2013) Landslide susceptibility analysis with logistic regression model based on FCM sampling strategy. Computers & Geosciences 57, 81–92

Xu C, Xu X, Dai F, Saraf A (2012) Comparison of different models for susceptibility mapping of earthquake triggered landslides related with the 2008 Wenchuan earthquake in China. Computers & Geosciences 46, 317–329

Yalcin A, Reis S, Aydinoglu AC, Yomralioglu T  (2011) A GIS-based comparative study of frequency ratio, analytical hierarchy process, bivariate statistics and logistics regression methods for landslide susceptibility mapping in Trabzon, NE Turkey. CATENA 85, 274–287

Yesilnacar E, Topal T (2005) Landslide susceptibility mapping: A comparison of logistic regression and neural networks methods in a medium scale study, Hendek region (Turkey). Engineering Geology 79, 251–266

Yilmaz I (2009) Landslide susceptibility mapping using frequency ratio, logistic regression, artificial neural networks and their comparison: A case study from Kat landslides (Tokat—Turkey). Computers & Geosciences 35, 1125–1138

# Capítulo V. Landslide susceptibility using pixel grid units.

**Landslide susceptibility: a statistically-based assessment on a depositional pyroclastic ramp.**

# Landslide susceptibility: a statistically-based assessment on a depositional pyroclastic ramp ©

Franny Giselle Murillo-García
Posgrado en Geografía UNAM

Stefan Steger
Institute for Earth Observation, Eurac Research.

Irasema Alcántara Ayala
Instituto de Geografía UNAM

*This study aimed to produce a high-quality landslide susceptibility map for Teziutlán municipality, a landslide-prone region in Mexico, which is characterised by a depositional pyroclastic ramp. The heterogeneous quality of available topographic information (i.e. higher resolution digital elevation model only for a sub-region) encouraged to confront modelling results based on two different study area delineations and two raster resolutions. Input data was based on the larger modelling region L15 (163 km²) and smaller S (70 km²; located inside L15) with an associated raster cell size of 15 m (region L15 and S15) and 5 m (region S5). The resulting three data sets (L15, S15 and S5) were included into three differently flexible modelling techniques (Generalized Linear Model - GLM, General Additive Model - GAM, Support Vector Machine -SVM) to produce nine landslide susceptibility models. Preceding variable selection was performed heuristically and supported by an exploratory data analysis. The final models were based on the explanatory variables slope angle, slope aspect, lithology, relative slope position, elevation, convergence index, distance to streams, distance to springs and topographic wetness index. The ability of the models to classify independent test data was. elaborated using a k-fold cross validation procedure and the AUROC (Area Under the Receiver Operating Characteristic) metric. In general, all produced landslide susceptibility maps depicted the hillslopes of the ravines, which cut the pyroclastic ramp, as prone to landsliding. The modelling results showed that predictive performances (i.e. AUROC values) slightly increased with an increasing flexibility of the applied modelling technique. Thus, SVM performed best, while the GAM outperformed the GLM. This tendency was most distinctive when modelling with the largest landslide sample size (i.e. data set L15; n = 662 landslides). Non-linear classifiers (GAMs, SVMs) performed slightly better when trained on the basis of lower raster resolution (data set S15) compared to the 5 m counterparts (data set S5). Highest predictive performance was obtained for the model based on data set L15 and the SVM classifier (median AUROC: 0.82). However, SVMs also indicated the highest degree of model overfitting. This study indicates that the decision to delineate a study area, the selection of a raster resolution as well as the chosen classification technique can affect varying aspects of subsequent modelling results. The results do not support the assumption that a higher raster resolution (i.e. a more detailed digital representation of the terrain) inevitably leads to better performing or geomorphically more plausible landslide susceptibility maps.*

# 5.1 INTRODUCTION

Landslide susceptibility can be defined as the spatial likelihood of landsliding due to a particular set of static environmental conditions (Guzzetti 2005). Susceptibility maps provide a spatial evaluation concerning the location of potential future slope instabilities and areas where landslides are not to be expected (Cardinali *et al.* 2002; Guzzetti *et al.* 1999, 2005). In general, landslide susceptibility can be elaborated using qualitative, semi-quantitative or quantitative approaches (Reichenbach *et al.* 2018). Qualitative approaches, where a domain expert determines the most susceptible zones, are considered subjective as the results are mainly founded on experience and knowledge of a person (van Westen *et al.* 1999; Chen *et al.* 2009; Chauhan *et al.* 2010). Quantitative analyses are either based on physical laws (e.g. infinite slope models) or on empirical rules (i.e. statistically-based classifiers) that allow the combination of available spatial environmental information (Fell *et al.* 2008). Despite the large number of published research in the field of quantitative landslide susceptibility modelling, there is still no encompassing agreement on which modelling approach to choose under which circumstances (Brabb 1984; van Westen *et al.* 1997; Guzzetti *et al.* 1999; Glade and Crozier 2005; Reichenbach *et al.* 2018).

In summary, statistically-based approaches built an empirical association between past landslide occurrences (and non-occurrences) and static environmental factors to elaborate typical landslide conditions. Resultant landslide susceptibility maps spatially depict the resultant classification rule in the form of a relative estimate on the propensity of spatial units to be affected by landslide susceptibility. The subsequent quantitative model validation primarily focuses on comparing the predicted susceptibility score with test data that was not applied to train the model (Chung and Fabbri 2003; Steger *et al.* 2016a).

Statistically-oriented classification techniques are especially valuable for larger areas, also because of their lower reliance on challenging to derive geotechnical information (Fell *et al.* 2008; Cascini 2008). During the last decade, a vast number of publications confronted modeling results obtained by different statistical classification techniques (Brenning 2005; Rossi *et al.* 2010; Goetz *et al.* 2011; Vorpahl *et al.* 2012; Pradhan 2013; Kavzoglu *et al.* 2014; Pourghasemi and Rahmati 2018). Other research focused on the effects of data properties on the reliability of subsequent landslide susceptibility maps concluding that the input data quality codetermines the final modelling results (Guzzetti *et al.* 2006; Cascini 2008; van Westen *et al.* 2008; Petschko *et al.* 2016; Steger *et al.* 2017; Zêzere *et al.* 2017).

According to literature, terrain derivatives extracted from Digital Elevation Models (DEMs) are regularly used in combination with thematic information as potential explanatory variables (Conforti *et*

*al.* 2014). Commonly used terrain attributes include slope, aspect, elevation, slope curvature and diverse proxies for hydrological influences (Reichenbach *et al.* 2018).

Several publications emphasize that the quality and spatial resolution (i.e. pixel size) of the underlying topographic information (i.e. DEM) codetermines the final modelling results (Lee *et al.* 2004; Akgün and Bulut, 2007; Catani *et al.* 2013; Fressard *et al.* 2014; Palamakumbure *et al.* 2015; Schlögel *et al.* 2018). Catani *et al.* (2013) emphasized that the optimal input data configuration changes with the pre-selected spatial scale in a notable manner, while Legorreta-Paulín *et al.* (2010) and Trigila *et al.* (2015) highlighted that model performance generally improved with increasing resolution of input data. Palamakumbure *et al.* (2015) concluded that a 10m DEM resolution was the optimal choice for modelling landslide prone terrain within their study site. Yet, in some areas, particularly in less developed countries, high quality topographic information, as derived by Light Detection and Ranging (LiDAR), is rarely available (Deb *et al.* 2009; Althuwaynee *et al.* 2014; Romer and Ferentinou 2016).

The aim of this study was to produce a high-quality landslide susceptibility map for Teziutlán. For this purpose, statistical-based landslide susceptibility modelling was performed. The objective was to confront modelling results based on different study area delineations (region L vs. S), different raster resolutions (5 m vs. 15 m) and differently flexible modelling algorithms in order to develop a suitable model for the study site with availability of heterogeneous data qualities. Thus, the presented research not only allowed insights into the effect of differently flexible classifiers on the modelling results, but also into the interplay between classification algorithms, study area delineation and modelling resolution. The produced nine models were evaluated quantitatively (e.g. k-fold cross validation) and qualitatively (e.g. prediction pattern).

## 5.2 STUDY AREA

Teziutlán municipality is located in the Sierra Norte of Puebla mountainous system, within the transition of the Sierra Madre Oriental and the Trans-Mexican Volcanic Belt physiographic provinces (Fig. 57). The capital town of the municipality is also called Teziutlán and it is located on the top of a plateau formed by lava flows and pyroclastic materials from Los Humeros caldera volcano (LHVC), which is situated approximately 20 km to the South of Teziutlán town.

The climate can be described as warm temperate (range 12°C-22°C) and rainfall takes place all year long (precipitation ranges per year: 1100-3600 mm) (INEGI 2009). The main drainage of the area is oriented N-S and NE-SW and influenced by tectonic lineaments (Capra *et al.* 2003). The soils of the area are of volcanic origin and can predominantly assigned to the group of andosols (INEGI 2009). Human impact led to the tendency that the original vegetation (mountainous cloud forest) has been

removed or replaced by grasslands, arable land and urban areas. Only at the north of the study area pine-oak woodlands are still present. The geology of Teziutlán (Fig. 58) is linked directly to the activity of LHVC, one of the Pleistocene silica centres (Dávila-Harris and Carrasco-Núñez 2014). Among the eruptive products derived from LHVC that range from basalt to high-silica rhyolite, the Xaltipan ignimbrite is the most significant deposit. Most of these deposits are non-welded material easily recognized as ash-pumice flow deposits. These pyroclastic flows filled low areas of the rugged preexisting terrain covering a surface of circa 3500 km$^2$ (Ferriz and Mahood 1984) and formed ramps. Further details on the geological context of the area can be found in Murillo-García and Alcántara-Ayala (2017).
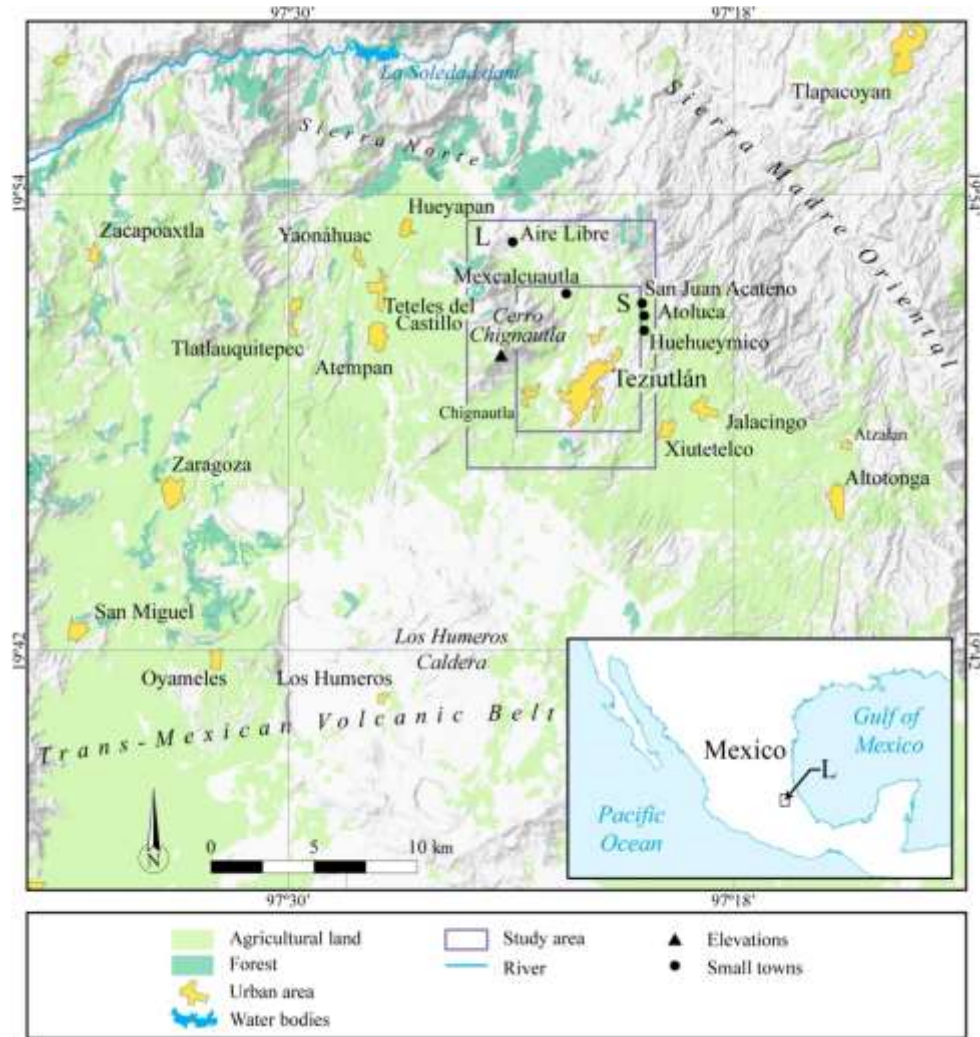


*Figure 57.* Location map. The analyses were based on two different study area delineations, L15 and S5. DEM resolution was 15 m for the data set L15, 5 m for S5 and 15 m for S15.
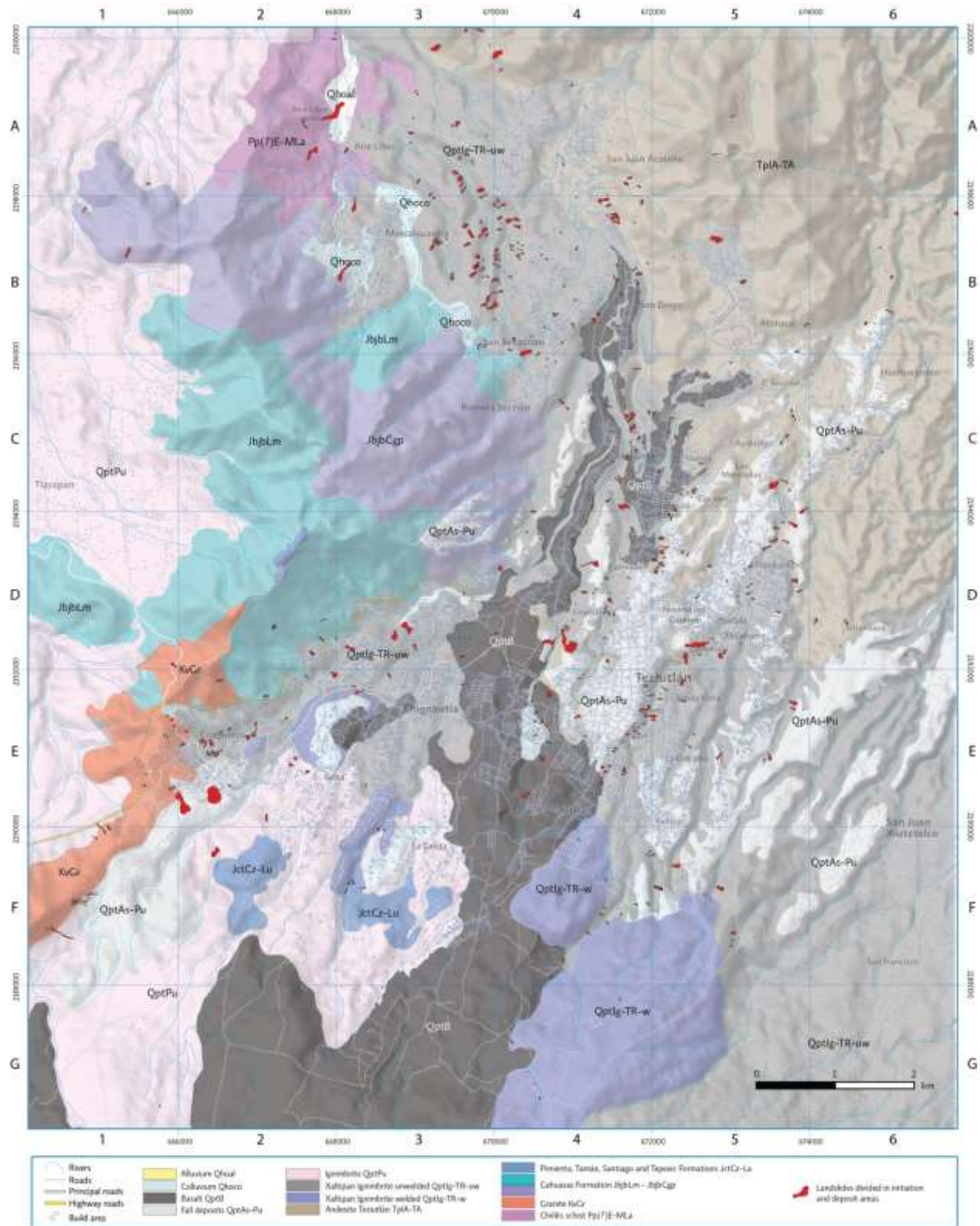
*Figure 58. Lithology map with the rock units (modified from Salinas-Rodríguez and Castillo-Reynoso 2011) Sedimentary rocks were joined on a single class. The same applied for the Andesite Teziutlán and granite layers.*

127

# 5.3 MATERIALS AND METHODS

### 5.3.1 Landslide inventory and landslide absences

The landslide inventory used within this study consists of 662 landslides of the slide-type movement (Varnes and IAEG 1984). Four different archives of aerial photographs served as the basis for the visual identification of geomorphic landslide features: (i) the archive of the National Institute of Statistics and Geography (INEGI), (ii) the archive of ICA Foundation (private entity), (iii) the library of the Geography Institute of the National University of Mexico (UNAM), and the archive of the National Centre for Disaster Prevention (CENAPRED). In summary, stereopairs of aerial photographs for the years 1942, 1956, 1974, 1978, 1980, 1991, 1999 and 2007 as well as very high resolution satellite images from the period 1999 to 2015 were adopted. Additional field surveys were carried out to cross-check the previously mapped landslides. More details on the landslide inventory can be found in Murillo-García and Alcántara-Ayala (2017).

For modelling, landslide occurrences were represented by one point per mapped landslide initiation zone as recommended by several previous investigations to avoid a weighting for landslide magnitude and to reduce the impact of spatial autocorrelation (Atkinson and Massari 1998; van den Eeckhaut *et al.* 2006; Qi *et al.* 2010; Gorum *et al.* 2011; Petschko *et al.* 2014; Goetz *et al.* 2015). Landslide absence locations related to a random sample of points outside digitized landslide bodies. The final binary response variables consisted of an identical number of landslide presence and absence observations (1:1 sampling) (Heckmann *et al.* 2014; Regmi *et al.* 2014; Goetz *et al.* 2015; Steger *et al.* 2016a). Hussin *et al.* (2016) analysed the effects of different sampling strategies for a grid-based susceptibility modelling and concluded that in some cases, even a minor proportion of 1:1 could be sufficient to obtain meaningful landslide susceptibility models.

### 5.3.2 Study area definition and environmental variables

The topographic variables of this study relate to two DEMs of varying quality. The coarser scaled DEM (i.e. 15 m) was constructed by using photogrammetric techniques (INEGI 2013a) whereas the higher resolved DEM (i.e. 5 m) was based on an aerial LiDAR campaign (flight on January 20, 2010) (INEGI 2013b). Two different study area delineations (Larger L and smaller S) were defined because only the 15 m DEM covers the entire study area (Figure 1). In detail, the entire study area extends over 163 km² (region L15) while the sub-region covers 70.3 km² (region S5).

Summarizing, region L is larger and region S represent a sub-region of L (Fig. 57). Data set L15 relates to the 163 km² large region, 662 mapped landslides and a DEM resolution of 15 m. The data set S5

relates to the mentioned sub-region (70.3 km²), 449 landslides and the 5 m DEM (Fig. 59). The third data set, namely S15, covers the same extension as region S5 (70.3 km²), but is based on a coarser DEM resolution (i.e. 15 m).

| Data set | Extent (km²) | Pixel size (m) | Landslides |
|----------|--------------|----------------|------------|
| L15 | 163 | 15 | 662 |
| S5 | 70.3 | 5 | 449 |
| S15 | 70.3 | 15 | 449 |

*Figure 59. Study area extent, pixel size and number of landslides (see also Figure 5.1).*

Comparisons of the models based on the data set L15 and S15 allowed to scrutinize the effect of study area delineation by keeping the modeling resolution constant (i.e. 15 m) (Gordo *et al.* 2017; Steger and Glade 2017). The influence of raster resolution was elaborated by confronting modeling results based on the identical study area delineation, but on different modelling resolutions (S5: 5 m vs. S15: 15 m). Within this study, candidates of frequently used explanatory variables were analysed prior to select or dismiss them for further analyses (Figure 60). The two different DEMs served as a basis to derive slope angle, slope aspect, general curvature, plan curvature, profile curvature, Topographic Wetness Index (TWI) (Beven and Kirkby 1979), Stream Power index (SPI) (Moore *et al.* 1991), Convergence Index (CI) (Olaya 2004), relative slope position (RSP) and catchment area within the SAGA GIS software (Conrad 2006). Furthermore, a reclassified lithology layer as well as the variables vertical distance to streams (VDTCHN), distance to streams, and distance to springs were produced.

| Potential explanatory variables | | Type | Producer |
|---|---|---|---|
| Topographic | Slope | Numerical (degrees) | SAGA GIS |
| | Elevation | Numerical (meters above sea level) | INEGI |
| | Aspect | Categorical: North, East, South and West. | SAGA GIS |
| | General Curvature | Numerical (dimensionless) | SAGA GIS |
| | Plan Curvature | | |
| | Profile Curvature | | |
| | Relative slope position | Numerical (0-1) | SAGA GIS |
| | Convergence index | Numerical (percent) | SAGA GIS |
| Hydrological | Vertical distance to streams | Numerical (meters) | SAGA GIS |
| | Catchment area | Numerical (square meters) | SAGA GIS |
| | Topographic Wetness Index | Numerical (dimensionless) | SAGA GIS |
| | Stream Power Index | Numerical (dimensionless) | SAGA GIS |
| | Distance to springs | Numerical (meters) | SAGA GIS and field surveys. |
| | Distance to streams | Numerical (meters) | SAGA GIS |
| Geological | Lithology units | Categorical (rock type)<br>(1) Basalt-andesite<br>(2) Sedimentary hard rock (conglomerate, limestone, Limonite)<br>(3) Tertiary igneous hard rock (andesite-basalt from Teziutlán formation, and granite)<br>(4) Falls deposits (ash-pumice-lapilli), colluviums and alluvium<br>(5) Pumice flow unwelded (QptPu)<br>(6) Pumice flow unwelded (QptlgTr-uw)<br>(7) Pumice flow welded (QptlgTr-w)<br>(8) Schist* | SGM and field surveys. |

*Figure 60. Data summary by scale, type and producer Notes: *Schist rock unit is not present at 5 m extension area and consequently not included in the S5 and S15 models. INEGI is the acronym for National Institute of Geography and Statistics of Mexico, and SGM is National Geological Service of Mexico.*

Slope angle is the most frequently used predictor in statistical landslide susceptibility modelling and commonly considered as the main static explanatory variable of landslide occurrence (Costanzo *et al.* 2012; Reichenbach *et al.* 2018).

Information on the altitude of an area, as directly represented by the DEM, can be seen as a proxy for altitude-dependent variation in weathering conditions (Costanzo *et al.* 2012). The general morphometric form of an area may be linked to the variability in overland water flow and soil moisture conditions that in turn may influence soil properties. Proxys for hydrological influences are frequently represented by second order DEM derivatives, such as curvature, CI (Ayalew *et al.* 2004; Olaya 2004; San 2014) or by variables such as the TWI or the catchment area (Dahal *et al.* 2008; Costanzo *et al.* 2012; Catani *et al.* 2013).

Slope aspect refers to the orientation of a hillslope and may represent effects related to the varying intensities of insolation (Catani *et al.* 2013; Guzzetti *et al.* 1999). The Euclidean distance to streams and the vertical distance to channels describe the proximity or remoteness to potential landslide influencing linear features. The streams of the study area have incised deep steep valleys and ravines into the pyroclastic ramp deposits. SPI represents an approximation of the erosive power and may be associated with potential slope undercutting. Field observations suggest that landslides are frequently at the top of these depth ravines. Hence, RSP can be a suitable explanatory variable as it indicates the relative position of each cell at a hillslope (e.g. ridge, middle slope, valley). Field surveys suggested an increasing landslide occurrence in closer proximity to springs. Besides higher water availability, locations closer to springs could also be indicative of the existence of faults covered by pyroclastic deposits. Thus, the proximity variable distance to springs was included as a potential variable candidate.

Lithology is a frequent proxy for the parent material. Within this study, some lithology classes were merged into a unique class in case of similar geotechnical properties (Fig. 60). The lithology layer is based on a 1:50,000 geologic map published by the National Geological Service of Mexico (Servicio Geológico Mexicano, SGM) (Salinas-Rodríguez and Castillo-Reynoso 2011).

Petschko *et al.* (2014) pointed out that land cover may often not be considered as static in time and therefore not suitable to link with historical landslide data (i.e. unknown temporal occurrence). In some cases, specific land cover units can even be linked to a systematic under- or overrepresentation of mapped landslide information (e.g. incomplete mapping in forested areas). An inclusion of land cover as a variable may therefore lead to biased statistical relationships (Steger *et al.* 2017). Since both arguments may be valid for the present study, the conducted analysis did not consider currently observable land cover conditions.

### 5.3.3 Exploratory data analysis and variable selection

The selection of explanatory variables is an important step in landslide susceptibility modeling (Costanzo *et al.* 2012). Within this study, variable selection was performed heuristically, supported by an exploratory data analysis.

An initial evaluation of the Individual Classification Power (ICP) revealed the ability of each variable to discriminate observations of the binary response. The ICP relates to model predictions (score between 0-1) which are based on classifiers trained separately for each single variable (i.e. one model per predictor). The Area Under the Receiver Operating Characteristic (AUROC) curve (Hosmer and Lemeshow 2000) was used as a metric to evaluate the ICP (Zweig and Campbell 1993; Goetz *et al.* 2015). In summary, the AUROC curve plots all positive true rates (sensitivity) against associated false positive rates (1 − specificity) for each possible probability threshold. The presented AUROC scores are based on the R package "ROCR" (Sing *et al.* 2009). An AUROC of 1 depicts that the respective single variable model enabled a perfect separation of landslide presences and absences while a value of 0.5 points to a random classification. In the case two or more variables represented a similar landslide influencing factor (i.e. curvature and convergence index), we opted to include only one in order to decrease redundancies and ensure a parsimonious and interpretable model. In this context, also the ICP was taken into account for variable selection/rejection (i.e. the respective variable had a lower mean ICP than a variable that stands for a similar landslide explanatory variable).

|  | L15 (15m) | | | | S15 (15m) | | | | S5 (5m) | | | |
|---|---|---|---|---|---|---|---|---|---|---|---|---|
|  | GLM | GAM | SVM | Trend | GLM | GAM | SVM | Trend | GLM | GAM | SVM | Trend |
| Slope | 0.538 | 0.579 | 0.607 | + | 0.504 | 0.578 | 0.621 | + | 0.643 | 0.643 | 0.658 | + |
| Lithology | 0.717 | 0.717 | 0.659 |  | 0.710 | 0.710 | 0.744 |  | 0.694 | 0.694 | 0.661 |  |
| Aspect | 0.556 | 0.556 | 0.552 |  | 0.557 | 0.555 | 0.590 |  | 0.547 | 0.547 | 0.540 |  |
| Catchment area | 0.484 | 0.514 | 0.543 | + | 0.506 | 0.560 | 0.515 | - | 0.501 | 0.513 | 0.495 | + |
| CI | 0.542 | 0.542 | 0.583 | - | 0.550 | 0.550 | 0.629 | - | 0.595 | 0.597 | 0.609 | - |
| Curvature | 0.499 | 0.522 | 0.537 | - | 0.490 | 0.509 | 0.55 | + | 0.526 | 0.546 | 0.59 | - |
| Elevation | 0.620 | 0.633 | 0.675 | - | 0.672 | 0.672 | 0.694 | - | 0.672 | 0.672 | 0.703 | - |
| Plan curvature | 0.490 | 0.537 | 0.564 | + | 0.517 | 0.517 | 0.571 | - | 0.554 | 0.554 | 0.567 | + |
| Profile curvature | 0.504 | 0.544 | 0.428 | + | 0.501 | 0.531 | 0.581 | - | 0.497 | 0.612 | 0.619 | + |
| Distance to streams | 0.595 | 0.595 | 0.625 | + | 0.64 | 0.64 | 0.671 | - | 0.579 | 0.580 | 0.620 | + |
| RSP | 0.593 | 0.612 | 0.611 | - | 0.633 | 0.633 | 0.646 | - | 0.601 | 0.628 | 0.625 | - |
| SPI | 0.506 | 0.515 | 0.525 | - | 0.518 | 0.534 | 0.542 | + | 0.414 | 0.596 | 0.581 | - |
| Distance to spring | 0.521 | 0.607 | 0.62 | - | 0.540 | 0.564 | 0.644 | + | 0.549 | 0.595 | 0.593 | + |
| TWI | 0.525 | 0.548 | 0.595 | + | 0.507 | 0.545 | 0.594 | - | 0.564 | 0.57 | 0.571 | + |
| VDTCHN | 0.580 | 0.580 | 0.589 | - | 0.646 | 0.646 | 0.658 | - | 0.533 | 0.558 | 0.553 | + |

***Figure 61.*** *Data summary Results of individual classification power (AUROC values). +/-, trend of association based on regression coefficients. GLM, logistic regression; GAM, general additive model regression; SVM, support vector machine; RSP, relative slope position index; SPI, stream power index; TWI, topographic wetness index; VDTCHN, vertical distance to channel.*

GLM regression coefficients provided insights into the direction of modelled associations between landslide occurrence and single continuously scaled predictor variables from a single-predictor perspective. Positive trends (i.e. "+" in Figure 61) indicated that the modelled likelihood of landslide occurrence increases with an increasing predictor value (e.g. increasing slope angles) while negative trend (i.e. "-" in Figure 61) depicts the opposite tendency. Variables that showed a geomorphically unreasonable association to landslide occurrence were rejected from subsequent modelling.

### 5.3.4 Classification and model validation

Three different binary soft classification techniques were used to model landslide susceptibility for the three data sets (L15, S5 and S15) leading to nine models in total. For this purpose, we opted for three differently flexible classifiers in order to find out if a more flexible algorithm would favour more reliable spatial predictions for the study site. Thus, we confronted classifiers based on a linear structure (i.e. Generalized Linear Model; GLM) with a moderately flexible semi-parametric algorithm (i.e. Generalized Additive Model; GAM) and a comparably flexible machine learning technique (i.e. Support Vector Machine; SVM).

GLM are based on a linear model structure and allow tackling two-class classification problems using a combination of scalar and categorical predictors. A GLM with a logistic link function (also referred to as binary logistic regression) is the most frequently used approach to model landslide susceptibility (Brenning 2005; Goetz *et al.* 2015; Reichenbach *et al.* 2018). The presented GLMs are based the R package "stats" (R Core Team 2016).

GAMs are semi-parametric extensions of GLMs (Hastie and Tibshirani 1986). GAMs are more flexible than GLMs and allow to account for non-linear relationships between the binary response and scalar predictor variables by applying empirically fitted smoothing functions (Hastie and Tibshirani 1990; Wood 2006). Several studies highlight that GAMs are suitable for mapping landslide-prone terrain (Park and Chi 2008; Brenning 2008; Goetz *et al.* 2011; Vorpahl *et al.* 2012; Petschko *et al.* 2013; Goetz *et al.* 2015; Youssef *et al.* 2015; Steger *et al.* 2016a). The GAMs were fitted using the "gam" R package (Hastie 2009).

Machine learning algorithms are usually more flexible than parametric or semi-parametric approaches and frequently applied for pattern recognition and classification. SVMs are popular to delineate landslide susceptibility while producing coherent spatial prediction patterns (Goetz *et al.* 2015; Steger *et al.* 2016a). A SVM is a maximum margin classifier that enables non-linear discrimination between classes (e.g. landslide presence and absence) by transforming explanatory variables (i.e. the features) into a higher-dimensional feature space (Vapnik 1998; Hong *et al.* 2015). Within this higher

dimensional feature space, data points can be separated linearly using a hyperplane whose position maximizes the "margin" between the observations (Kotsiantis 2007). SVM hyperparameter tuning (C and sigma) was conducted via internal cross validation using a systematic grid search. SVMs were based on the R package "kernlab" (Karatzoglou *et al.* 2004) while parameter tuning was based on "mlr" (Bischl *et al.* 2016).

Modelling results obtained by GLMs, GAMs and SVMs were transferred to each pixel of the study area to spatially predict landslide-prone areas. The final maps were then visualized by classifying the obtained susceptibility scores into quintiles in Quantum GIS (QGIS Development Team 2009) to ensure a systematic visual comparability (Hussin *et al.* 2016). The classes were grouped into very low (saturated green colour), low (clear green colour), medium (yellow colour), high (orange colour), and very high (red) likelihood of landslide occurrence.

The capability of a landslide susceptibility model to "foresee" landsliding can be estimated by confronting predicted susceptibility scores with model independent test data (i.e. predictive capability) (Chung *et al.* 1995). Modelling results were evaluated by confronting the obtained classification rule (i.e. spatially predicted susceptibility scores) with previously sampled landslide presence/absence data via the AUROC.

The elaboration of the predictive capability requires a splitting of the available data into training and test data. Performance estimates that are based on multiple partitions of training and test sets are less dependent on (random) variability associated with specific data partitions and enable to estimate the robustness of calculated metrics (e.g. via the interquartile range). For this study, data partitioning was based on a k-fold cross validation procedure implemented in the R package "sperrorest" (Brenning 2012). Each of the nine models has been evaluated by repeatedly splitting the initial data into multiple training and test sets. More precisely, the presented performance estimates (i.e. AUROCs) are based on 50 repetitions and 10 folds per repetition leading to 500 AUROCs for each of the nine models. More details on k-fold cross validation in the context of landslide susceptibility modelling can be found in Steger *et al.* (2016b). The inter-quartile range (IQR) of obtained AUROCs provided insights into predictive performance variabilities (i.e. ~ uncertainties). Lower IQR indicates robust model performances and vice versa (Goetz *et al.* 2015).

Additionally, an estimate on the degree of model overfitting was obtained by confronting fitting and predictive performances (i.e. median training set AUROC minus median test set AUROC).

# 5.4 RESULTS

### 5.4.1 Variable selection

The results of the initial exploratory data analysis (Fig. 61) eased to select a common set of explanatory variables for subsequent statistical modelling. The results depict that the widely used predictor slope angle showed a positive relationship (trend) to landslide occurrence within all single-predictor GLMs and an ICP of > 0.64 for all classifiers at a resolution of 5 m. At 15 m resolution, the ICP for the predictor slope angle was < 0.63 for the SVM classifier and < 0.6 for the parametric and semiparametric models (GLM, GAM). GLMs pointed to negative trend between landslide occurrence and the elevation of the area with ICPs between 0.62 (GLM, data set L15) and 0.70 (SVM, data set S5). The topographic variables aspect and TWI showed maximum ICPs of 0.59 (SVM, data set S15) and 0.595 (SVM, data set L15) respectively. The ICP associated with the RSP was > 0.59 and < 0.65 while the associated relationship was constantly estimated to be negative (lower slope positions are more likely affected by landsliding). Comparing identical data set and classifier combinations (e.g. SVM, data set L15), RSP constantly showed higher ICPs than the other variable which relates to the relative hillslope position (Vdtchn). Thus, RSP was favoured over VDTCHN for subsequent modelling. The proximity variables, distance to streams and distance to spring were associated with ICPs > 0.57 and > 0.52, respectively. We opted to dismiss the SPI variable due to its conceptual similarity with the distance to stream layer and low ICP values.

The curvature variables (general, plan and profile curvature), depicted contradictory trends in the estimated direction of association from one 15 m data set (L15) to the other (S15). Only the CI variable constantly depicted concave shaped areas as more likely affected by landslide occurrence among all data sets. Also due to its comparably high ICP values (compared with the curvature variables), CI was favoured for successive modelling. The parametric and semi-parametric models (GLM, GAM) trained with the categorical variable lithology revealed particularly high ICPs of > 0.71 for low raster resolutions (i.e. 15 m) and > 0.69 for the 5 m models. The holistic interpretation of the previously described explanatory variables, in combination with experiences made during extensive field trips, led to the selection of the following predictor combination: slope angle, aspect, lithology, RSP, elevation, CI, distance to streams, distance to springs and TWI (Figure 62).

**Figure 62 (Maps A-H).** *Visual impression of selected explanatory variables (lithology is shown in Figure 5.2) (-To be continued-).*
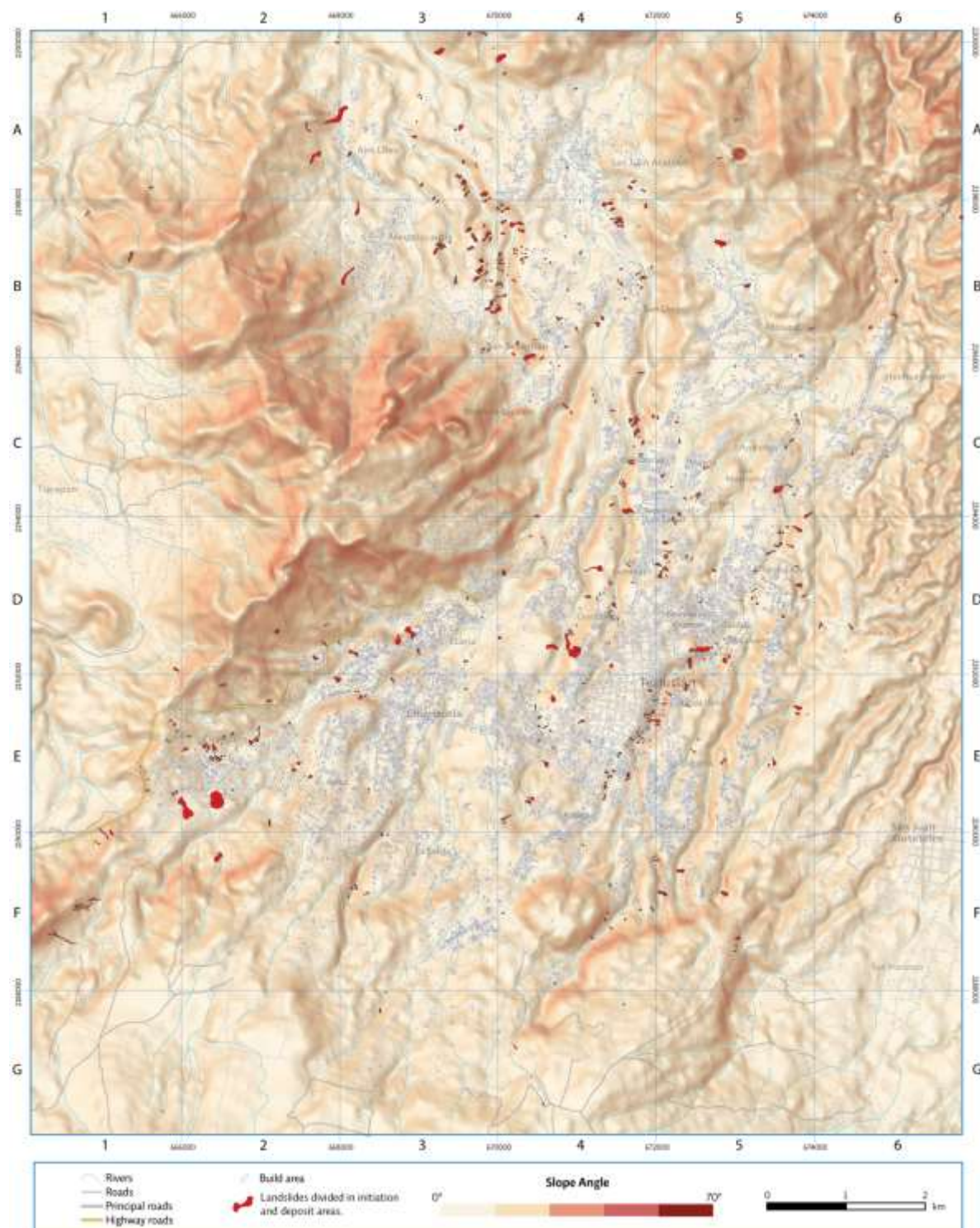


*62 A. Slope angle*
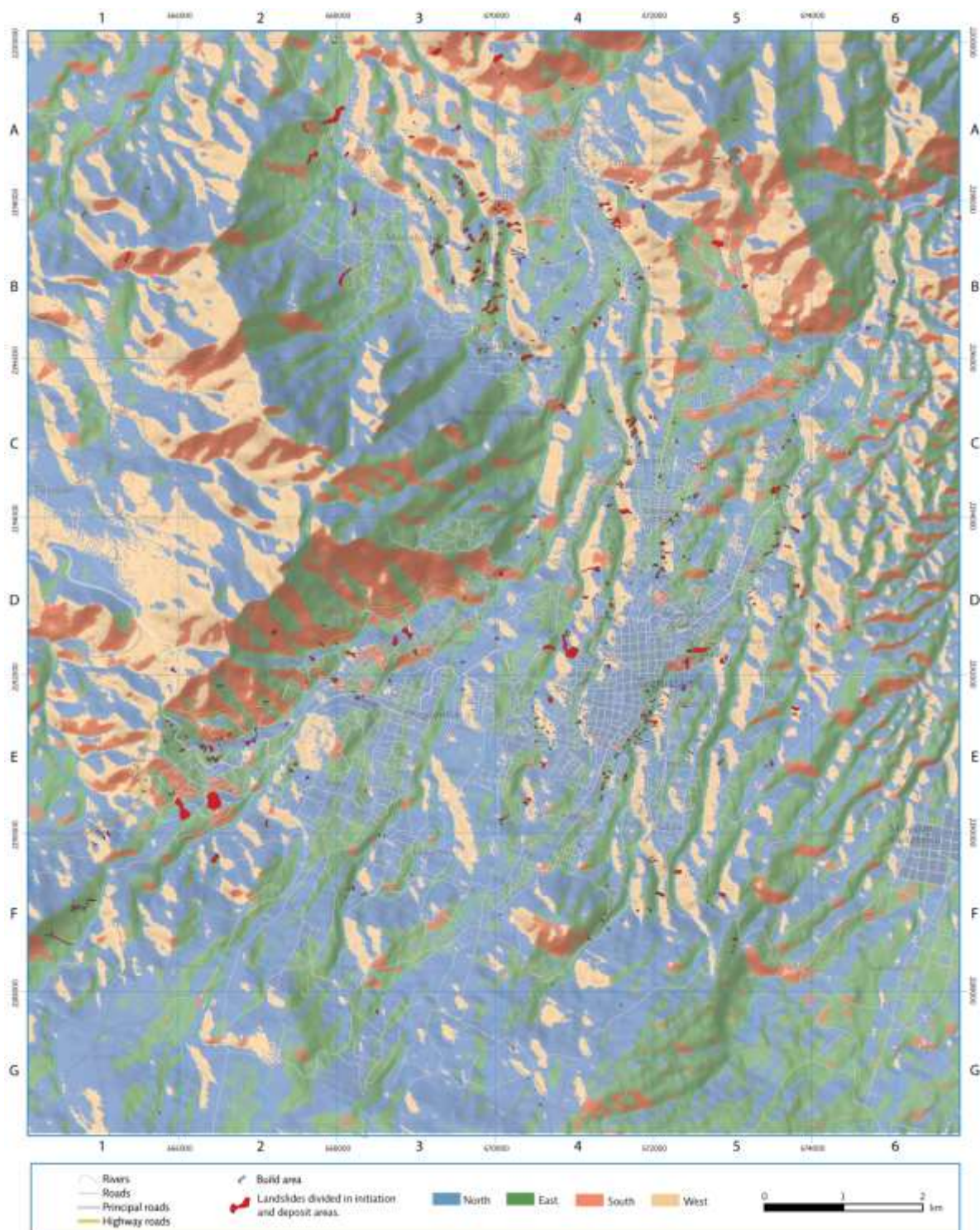
*62 B.* Aspect
*(-To be continued-)*

*62 C. Relative Slope Position (RSP)*
  *(-To be continued-)*
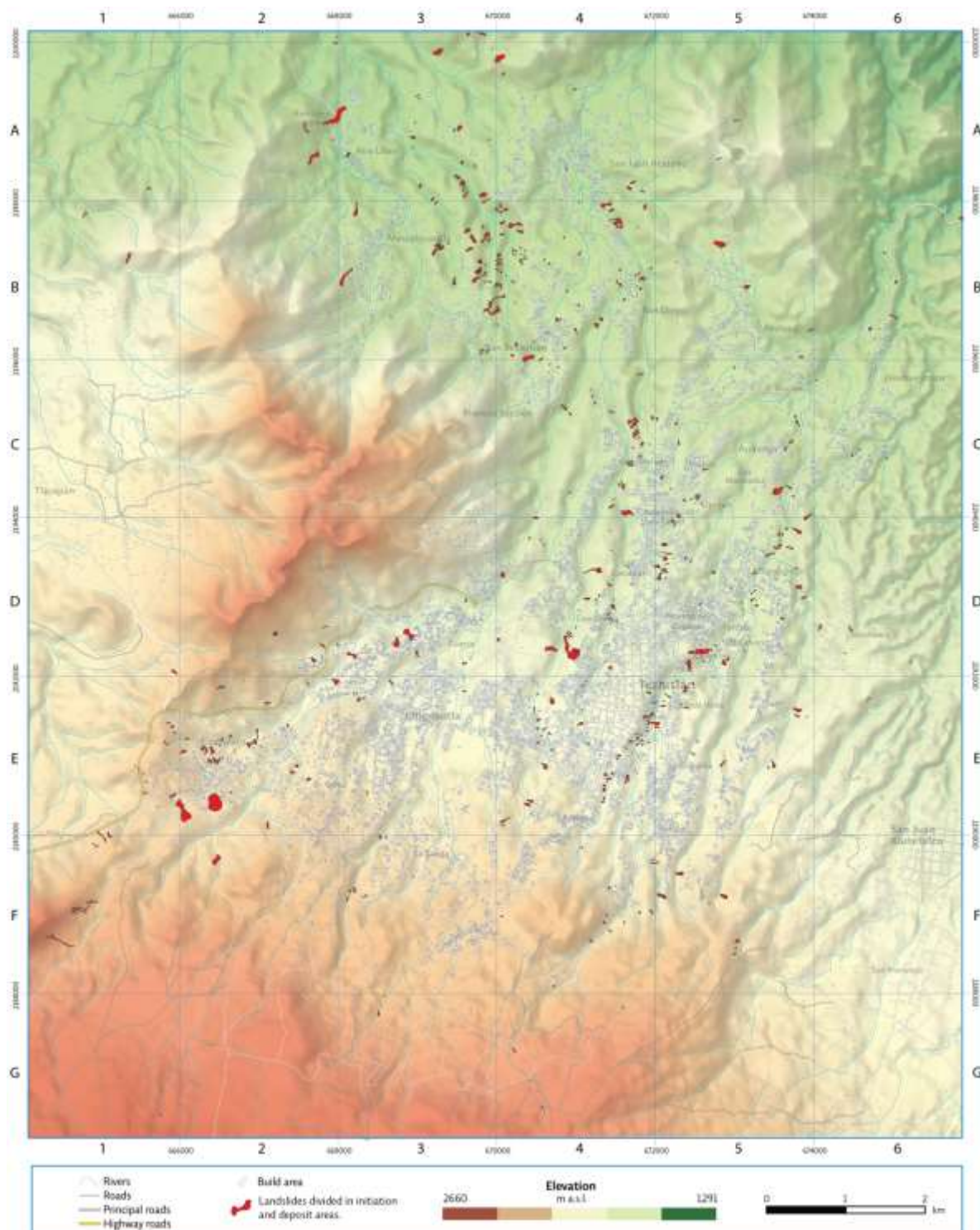
**62 D.** *Elevation*
  *(-To be continued-)*
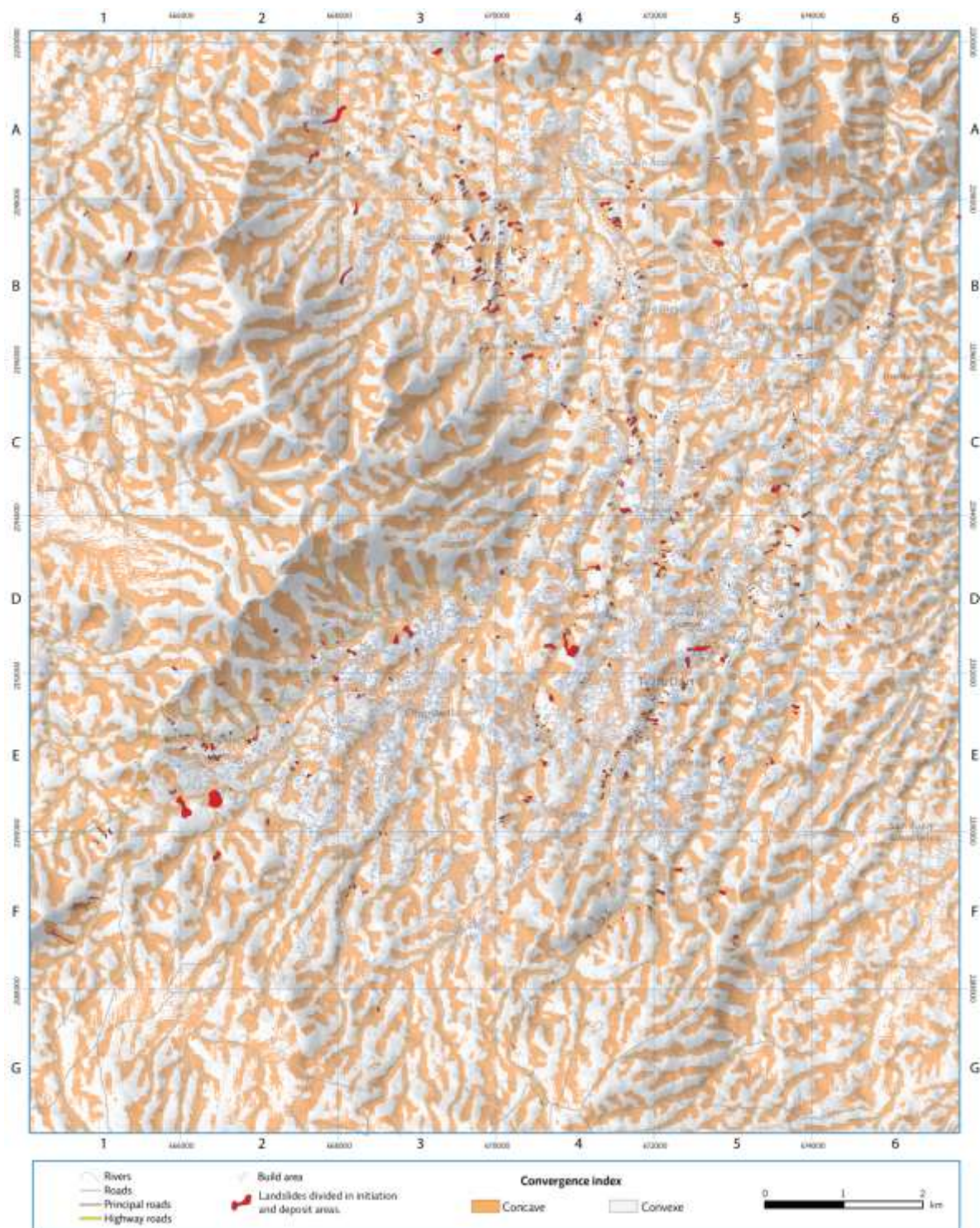
**62 E.** *Convergence Index. This variable (here visualized according two classes) was included as continuously scale variable.*

*(-To be continued-)*

139
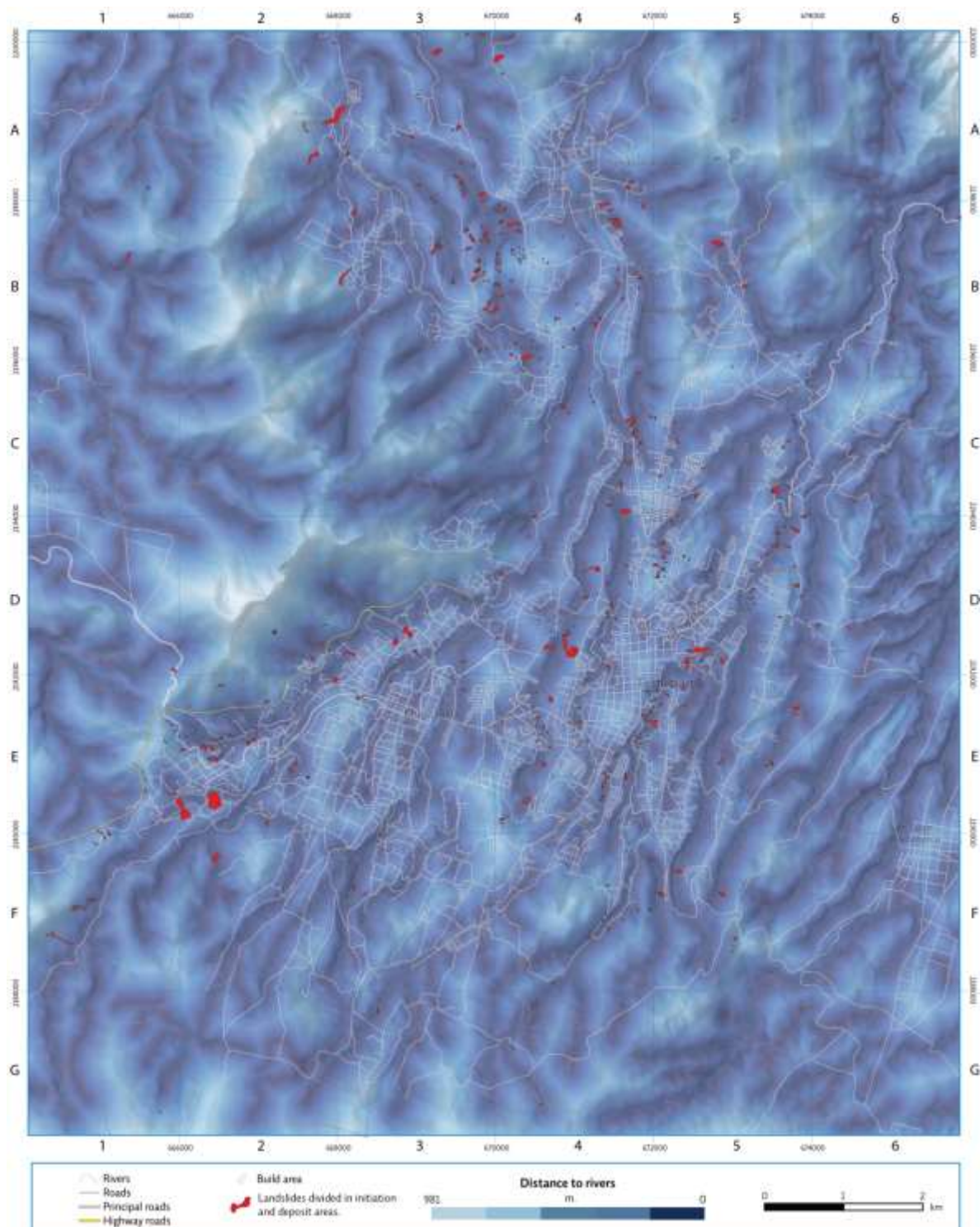
**62 F.** *Distance to streams (rivers)*
   *(-To be continued-)*
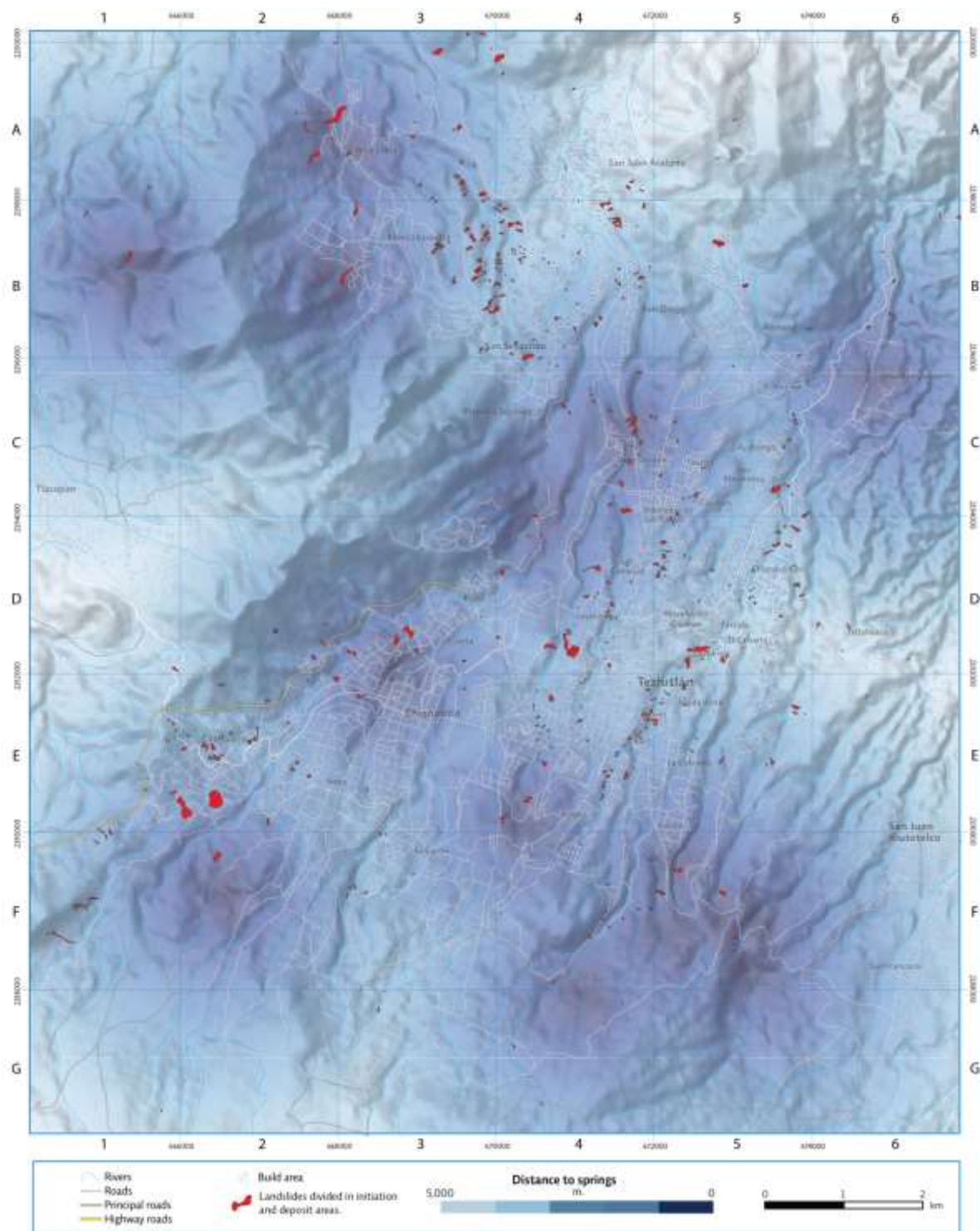
**62 G.** *Distance to springs*
  *(-To be continued-)*
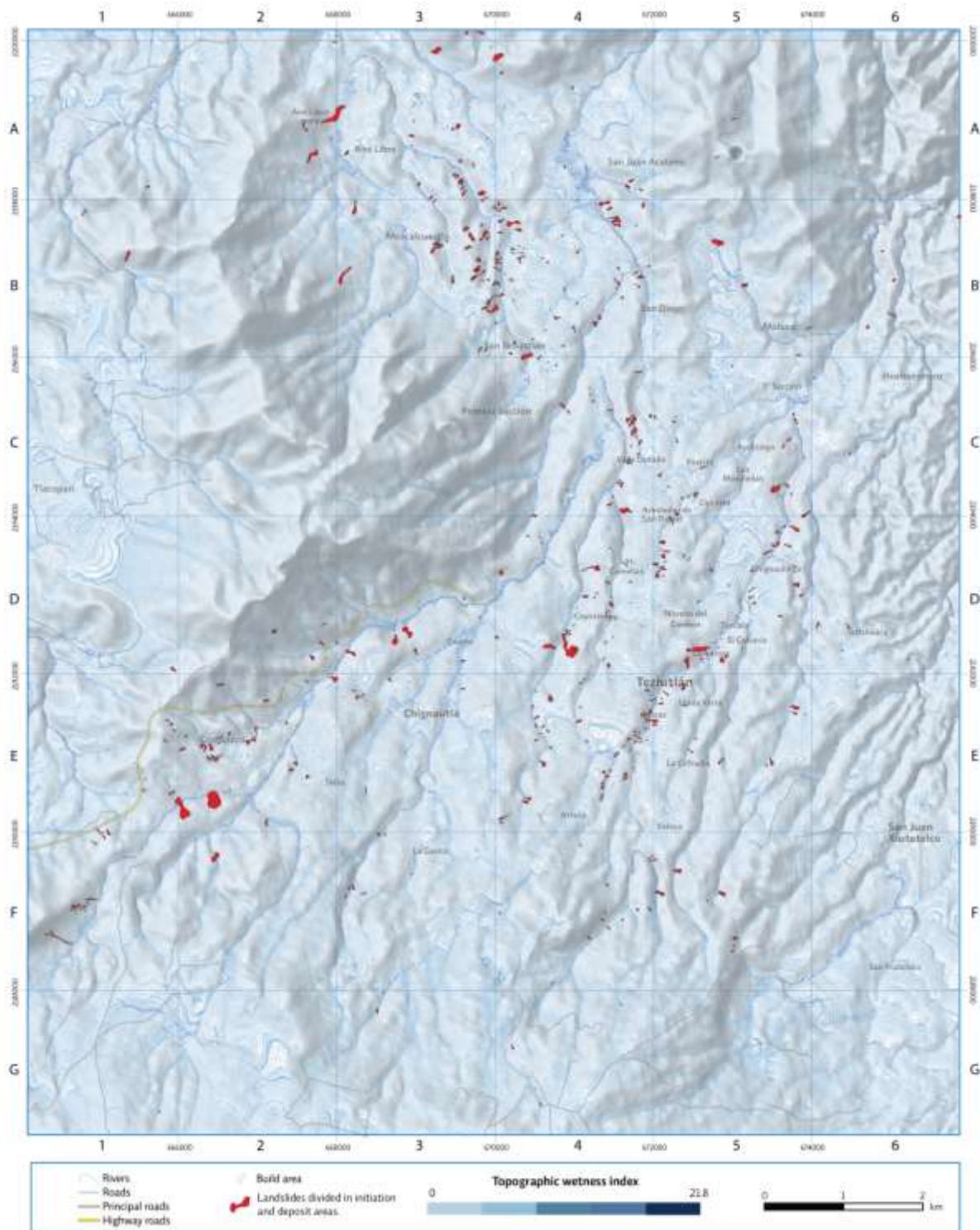
**62 H.** *Topographic Wetness Index (TWI)*

### 5.4.2 Model evaluation

Median AUROC scores (Figure 63) calculated on the basis of k-fold cross validation for all multiple variable models revealed an acceptable to excellent discrimination of model independent test cases (i.e. predictive performance) according the general rules of Hosmer and Lemeshow (2000). Predictive performance scores were > 0.76 and < 0.81. A confrontation of classification techniques highlights that SVMs persistently outperformed the GLMs and GAMs produced with identical input data sets. In this context, GAMs performed second best while GLMs performed worst from a predictive performance point of view. Surprisingly, no substantial systematic difference in model performance was observed when confronting models generated on the basis of different data sets (L15 vs. S5 vs. S15; colours in Figure 4). Median AUROCs associated with the GLMs were slightly higher for the data set S15 (0.782) in comparison to L15 (0.759) and S5 (0.781). All GAMs performed equally well with median test set AUROCs > 0.779 and < 0.791. SVMs performed better for L15 (0.817) than for S15 (0.791) and worst for the higher resolution data set S5 (0.794).
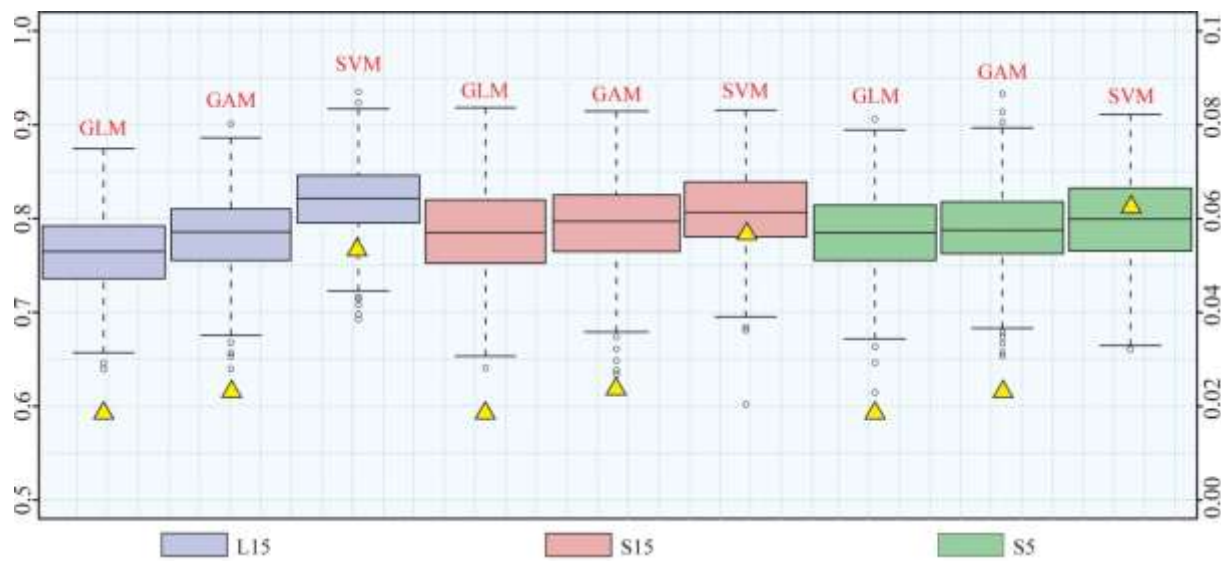


**Figure 63.** *Box plots of k-fold cross validation based AUROC scores for all nine models. Left y axis shows AUROC scores, right y axis and yellow triangles indicates the degree of model overfitting (difference between median test set AUROC and training set AUROC).*

The box plot sizes (i.e. the vertical distance between the 1st and the 3rd quartile in Figure 63) can be interpreted as an indicator of prediction performance variability, i.e. uncertainty. In this context, all nine models showed rather similar variability in predictive performance uncertainty with IQRs ranging from 0.0506 (SVM, L15) to < 0.0670 (SVM, S5).

The confrontation of obtained fitting performance scores (training data) and predictive performances (test data) allowed to gain insights into the degree of model overfitting (yellow triangles and right y

axis in Figure 63). This analysis revealed that the most flexible and quantitatively best performing (i.e. predictive performance) classifier, namely SVM, exhibited the highest degree of model overfitting. The less flexible models, GLM and GAM, depicted a considerably lower tendency to "overlearn" the training data. In numbers, the discrepancy between median training and test AUROCs for the SVMs were 0.053 (L15), 0.060 (S15) and 0.063 (S5) while GLMs and the GAMs were associated with values from 0.019 to 0.026.

### 5.4.2 Susceptibility maps

The spatial prediction patterns associated with all landslide susceptibility maps are exemplarily depicted within Figure 64 for a landslide prone area. The superimposed landslide initiation zones and buildings outlines allow a visual confrontation with estimated susceptibility scores and provide a first impression of the relative exposedness of building infrastructure to landslide occurrence. The examples also highlight that the produced maps show a general spatial agreement of larger predicted susceptibility patterns. However, a more detailed evaluation also reveals some differences between the maps because of different raster resolutions, classification algorithms and study area delineations.

The more detailed representation of topographic detail within all models based on the data set S5 is also reflected by a locally more differentiated pattern of predicted susceptibility scores. However, even if the respective maps may give rise to the impression of more detailed modelling results, associated predictive performances (Fig. 63) did not provide quantitative evidence for a higher ability of the models to "foresee" future landsliding. The comparably high influence of lithological differences on the models based on GLM and GAM was reflected by abrupt changes in predicted landslide susceptibility within the southwest portion of the area, where sedimentary rocks are located next to the ignimbrite unit. The area characterized by sedimentary rocks (Chignautla hill) was estimated to be relatively unsusceptible to landsliding. In contrast, the maps based on SVM seemed to be less influenced by this categorical variable, but more reliant on topographical predictors (Fig. 65). The observed higher portion of areas where very high and very low susceptibility values were situated in close proximity to each other went frequently hand in hand with abrupt changes in the topographical data, which is also influenced by the applied modelling resolution (i.e. smoother topography in case of lower resolution).
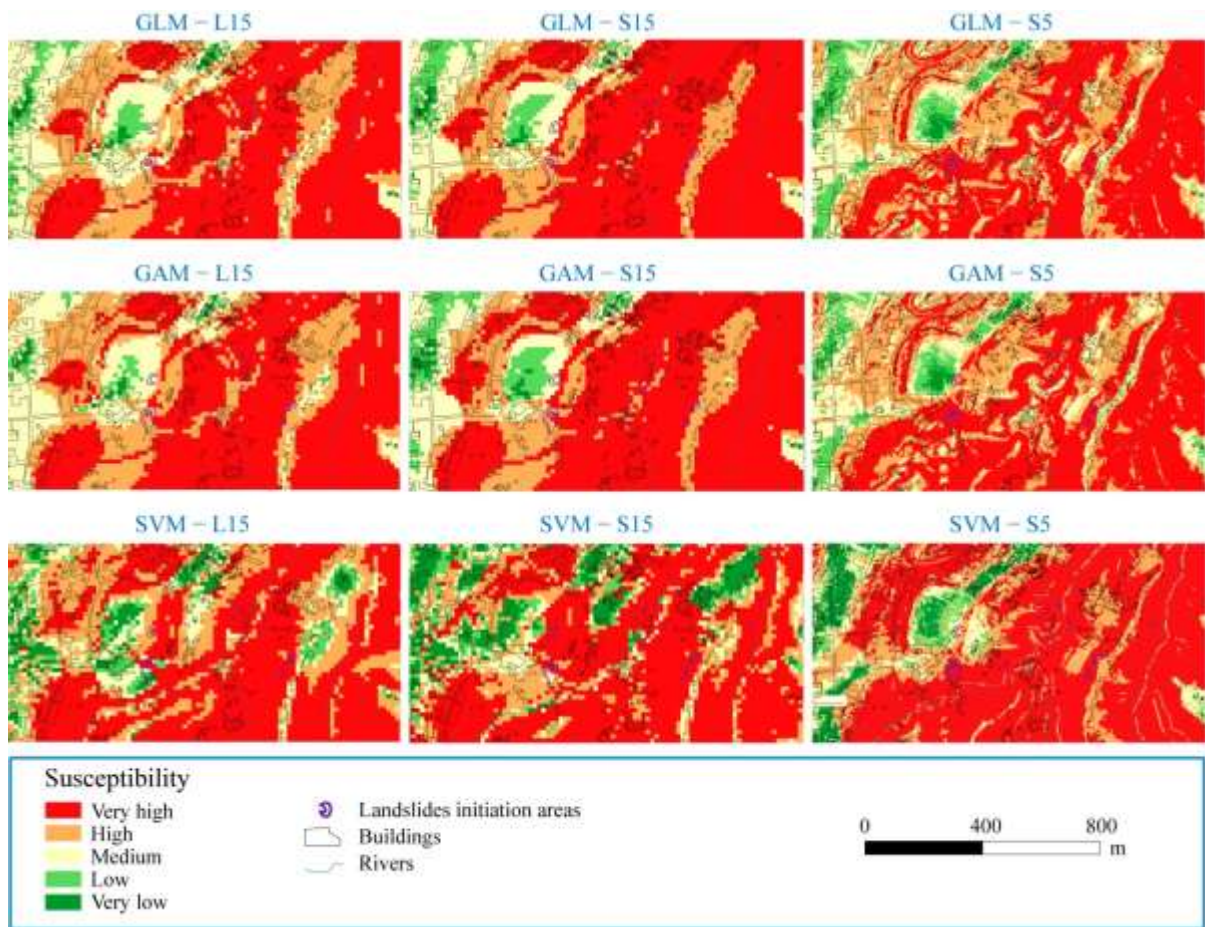
**Figure 64.** *Classified (quintiles) landslide susceptibility maps at La Aurora neighborhood.*
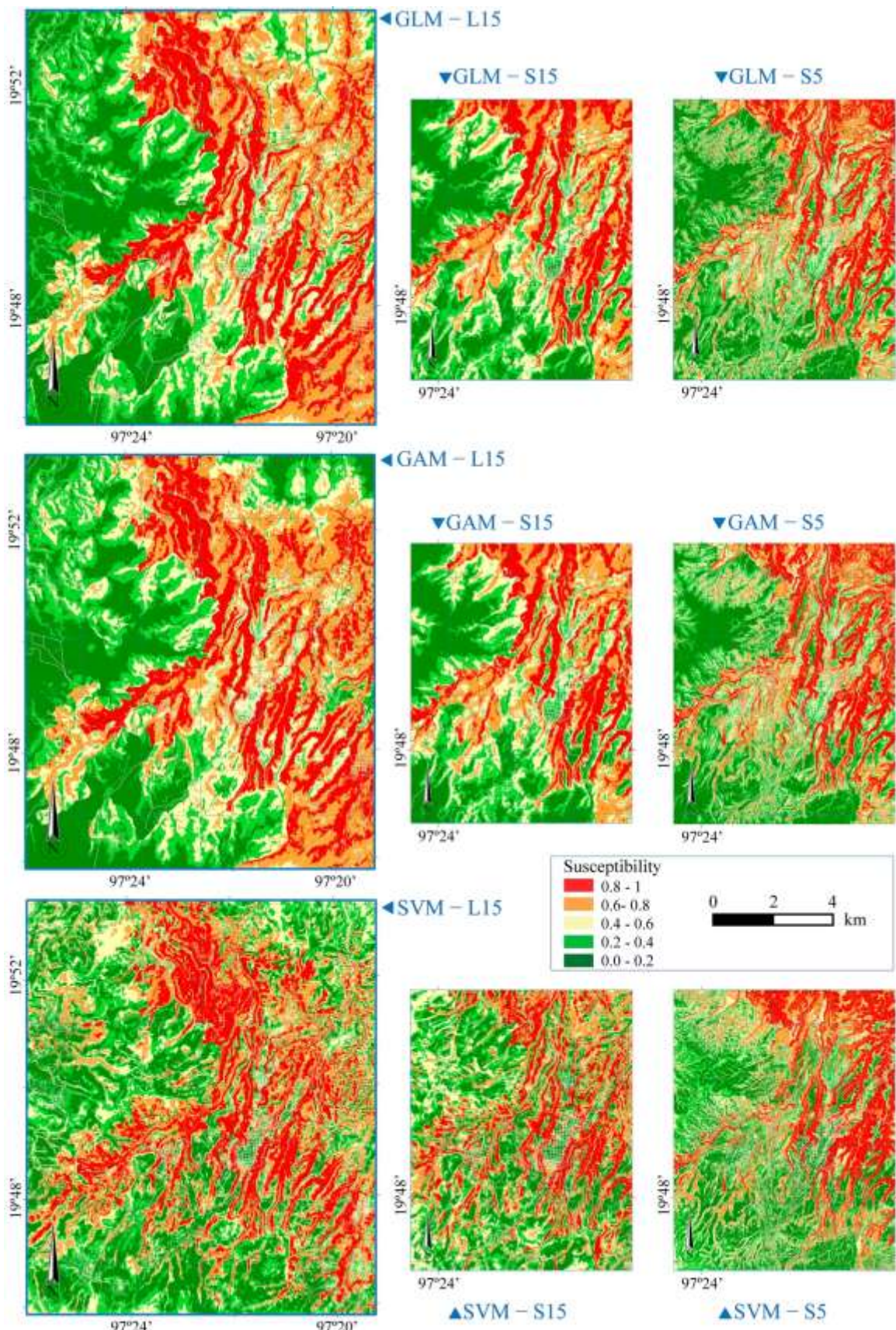
**Figure 65.** *Comparison of predictive surface of landslide susceptibility maps.*

# 5.5 DISCUSSION

One aim of this study was to make effective use of available data on landslide occurrence and environmental data sets and to explore state-of the- art modelling procedures in order to achieve a meaningful assessment of landslide-prone terrain. However, also within this study, the utilized data sets cannot be considered perfect. The complexity of the phenomenon under study, the spatially varying persistence of geomorphic landslide features and the limitations inherent in the adopted landslide mapping procedure (see section 5.3.4) inevitably influenced the spatial representativeness and accuracy of applied landslide information (Guzzetti *et al.* 1999; Glade and Crozier 2005; van Westen *et al.* 2008; Che *et al.* 2012).

It is supposed that the resulting limitations of landslide inventory data also affected the presented landslide susceptibility assessment (Ardizzone *et al.* 2002; Fressard *et al.* 2014). The influence of minor to medium positional errors of landslide data is expected to decrease with a coarser modeling resolution (Steger *et al.* 2016b). This is another argument why the utilization of larger cell sizes (in our case 15 m instead of 5 m) might not necessarily favor less meaningful analysis results. In fact, also obtained predictive performances did not reflect a superior ability of the 5 m models to predict out-of-model landslide observations. The present study highlighted that finding an optimal pixel resolution for landslide susceptibility modelling is not a trivial task. It contributes to previous research, which showed that higher DEM resolutions do not necessarily improve subsequent modelling results (Lee *et al.* 2004; Catani *et al.* 2013; Legorreta- Paulín *et al.* 2010; Palamakumbure *et al.* 2015; Trigila *et al.* 2015). A geomorphology oriented interpretation of the results indicated that emphasis should be placed to find a balance between topographic detail (i.e. DEM) and coarser scaled thematic information (e.g. Lithology) (Petschko *et al.* 2014; Steger *et al.* 2016a).It is assumed that the produced models based on a lower spatial resolution (15 m pixel size) are likely to relate more accurately to the topographic circumstances before slope failure (pre-failure morphology) and thus are more suitable to describe susceptible terrain which was not yet affected by slope instability. In contrast, modeling with higher resolutions bears the danger of training the models towards a too detailed description of past landslide morphology (i.e. performing landslide detection instead of spatial prediction) (van Den Eeckhaut *et al.* 2006; van Westen *et al.* 2008; Petschko *et al.* 2014; Steger *et al.* 2016b).

Recent landslide susceptibility studies highlighted that a change in the study area delineation can result in rather dissimilar prediction patterns within the identical sub-region and divergent model performance estimates (Gordo *et al.* 2017; Steger and Glade 2017). The conducted visual confrontation of landslide

susceptibility patterns that were based on different study area extents (but identical raster resolution and classifiers) only partly confirmed these previous observations. Compared to these previous studies, differences were not as evident, also because the enlargement of the areal extent (i.e. from data set S15 to L15) was not associated with an inclusion of a high portion of unsusceptible (e.g. flat) and easy to classify terrain. In fact, observed similar predictive performance estimates among the models associated with the data sets L15 and S15 provided quantitative evidence that the classification task (i.e. discriminating landslide presences from absences) has not been facilitated substantially by simply changing the study area extent.

Another point worth further consideration relates to the selection of a suitable set of explanatory variables. Land cover was a-priori excluded from modeling procedure to avoid a direct propagation of an expected land-cover related landslide mapping bias (cf. section 2.2) into the final modeling results (Steger *et al.* 2017).

Within this study, environmental factors were chosen heuristically (Kavzoglu *et al.* 2015) in order to take advantage of extensive field experiences (Murillo-García and Alcántara-Ayala 2017) and to reduce the danger of obtaining systematically distorted modelling results (Steger *et al.* 2016a).

Despite a careful evaluation of input data, lack of detailed information on soil properties poses a major drawback of this study, given that the importance of near surface underground conditions observed during field surveys. It is expected that the included lithology layer can just partly be seen as a useful proxy for subsurface conditions, even though this variable contributed substantially to "predict" test set data (i.e. the AUROC increased from 0.684-0.766 to 0.759- 0.817 by including lithology).

Other selected thematic variables, such as the distance to spring or the distance to streams, are as well known to not fully represent the influence of linear and punctual water supply. However, field surveys as well as a positive influence of the present spatial data sets on predictive performance estimates supported their inclusion within the models.

K-fold cross validation indicated that the models performed "acceptably well" to "excellent" (Hosmer and Lemeshow 2000) to spatially discriminate independent test data, with higher performances scores for more flexible modeling algorithms. However, it is also known that predictive performance estimates "solely" depict the degree of match between the predicted probability scores and independent test data (Chung and Fabbri 2003; Guzzetti *et al.* 2006). The sole evaluation of predictive performances of models associated with identical input data suggests that GLMs were outperformed by the GAMs while SVMs constantly perform best.

However, the inspection of the calculated model overfitting scores also highlights that an increasing flexibility of the modelling algorithm was accompanied by an increasing degree of model overfitting.

"Overlearning" might be a particular problem in the context of omnipresent error-prone data sets, due to the higher potential to model not only geomorphic plausible relationships, but also input data flaws (Steger *et al.* 2016b; Steger *et al.* 2017). The holistic evaluation of the modeling results revealed that the selection of the "best" model for an area is a challenging task and should not be driven by the interpretation of a single performance metric (Rossi *et al.* 2010; Reichenbach et al 2018). Future analyses based on a spatial cross validation framework are expected to allow deeper insights into both, model uncertainties and the relevance of predictor variables within a multiple variable modeling context (Schratz *et al.* 2018).

In synthesis, the map produced with SVM for the data set L15 (Fig. 66) was selected to be most suitable for the purpose of this study. This choice was strongly influenced by obtained predictive performance estimates, the covered areal extent (i.e. the map covers the entire study site) while simultaneously providing a slightly higher spatial differentiation of predicted susceptibility scores (i.e. in comparison to GLM and GAM). The major drawback of this selection can be associated to the comparably high degree of model overfitting. Given that past landslide locations of the area are likely to be reactivated in the future, the detected model overfitting was not judged to be a major drawback in the context of this study.

For the study area, elevation can be associated with lithology: highest elevations are in the Southwest (where the LHCV is located) and in Chignautla hill. In the Southwest portion, characterised by the presence of basalt lava flows and consolidated ignimbrite, number of landslide occurrence is low. Additionally, in Chignautla hill (composed mainly by sedimentary hard rocks) landslide occurrence is not that high either. In all the produced maps is clear that low and very low susceptibility values are predominate at the South and West areas. In contrast, in the North and Southeast sectors of the study area (with minor elevation values), where the ramp of unconsolidated pyroclastic deposits is situated (see Murillo-García and Alcántara-Ayala 2017), landslide occurrence is higher. Besides, the high capacity of water retention of the unconsolidated volcanic materials and soils of the pyroclastic ramp suggest that these materials are prone to landslides occurrence. Although the top of the pyroclastic ramp cannot be considered as a plain surface, in all maps the top of the pyroclastic ramp shows low and very low susceptibility values. In the other hand, landslides occur mainly at the slopes of ravines of the pyroclastic ramp. In all the nine susceptibility maps these slopes exhibit high and very high values. An issue to take into account, is that the urban growth of Teziutlán town (intensified in the second half of the 20thcentury) made that the slopes of the pyroclastic ramp where occupied to build new households (this is similar for Chignautla town).
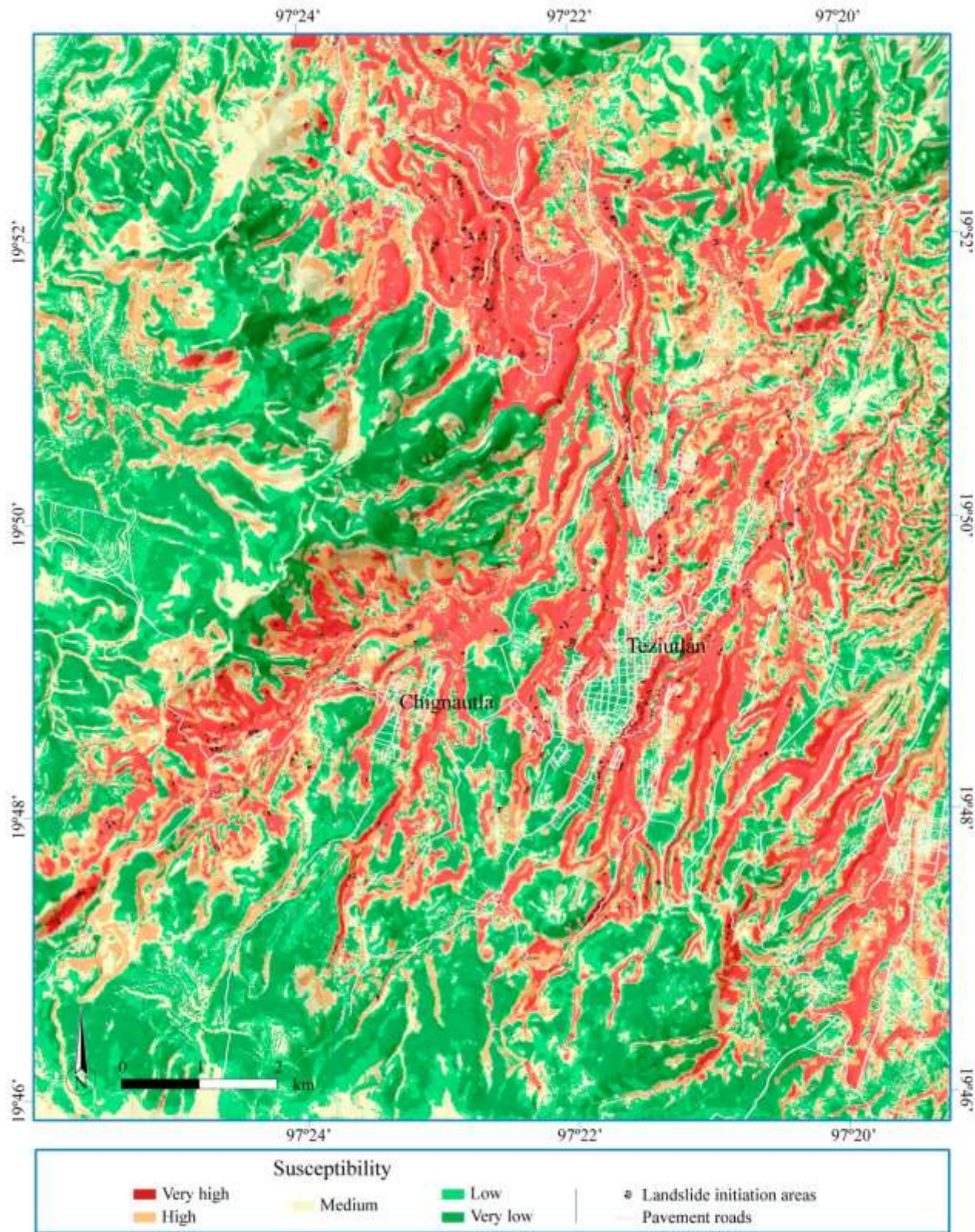
***Figure 66.*** *Landslide susceptibility map for data set L15 based on the SVM classifier and underlain by a shaded relief image.*

# 5.6 CONCLUSIONS

A data-driven landslide susceptibility analysis was carried out for an area where sedimentary rocks are overlaid by a ramp formed by unconsolidated pyroclastic and fall volcanic deposits. Besides two different study area extents (L vs. S), two different DEMs with pixel sizes of 5 m (only available for the smaller S region) and 15 m were tested in order to produce three different modelling data sets (L15 15 m, S5 5 m, S15 15 m). Furthermore, three differently flexible binary soft classification algorithms were tested using logistic regression (GLM), general additive modeling (GAM) and support vector machine (SVM). The conducted expert-based selection of explanatory variables took also into account the results of an exploratory data analysis, such as the evaluation of a variables individual classification power. The selected explanatory variables were slope angle, aspect, lithology, relative slope position, elevation, convergence index, distance to streams, distance to springs and topographic wetness index. Each model has been evaluated by repeatedly splitting the initial data into multiple training and test sets within a k-fold cross validation framework.

The final model selection was guided by the AUROC scores (i.e. highest median AUROC: 0.82), the covered areal extent (i.e. largest areal coverage) and the spatial pattern of the predicted landslide susceptibility scores. The results revealed that a higher modelling resolution does not necessarily favour better performing models. It was highlighted that differences in the modeling results (e.g. prediction patterns) were determined by an interplay of selected classification algorithm, study area delineation and pixel resolution. The most suitable model for the purpose of this study was produced with the comparably flexible SVM classifier. Finally, it is suggested that the selection of best models should not be based only on an interpretation of obtained model prediction skills, since many non-quantifiable aspects co-determine the explanatory power and usability of modeling results.

**References**

Akgün A, Bulut F (2007) GIS-based landslide susceptibility for Arsin-Yomra (Trabzon, North Turkey) region. Environmental
Geology 51:1377-1387. https://doi.org/10.1007/s00254-006-0435-6

Althuwaynee OF, Pradhan B, Park HJ, Lee JH (2014) A novel ensemble bivariate statistical evidential belief function with knowledge-based analytical hierarchy process and multivariate statistical logistic regression for landslide susceptibility mapping. Catena 114: 21-36.
https://doi.org/10.1016/j.catena.2013.10.011

Ardizzone F, Cardinali M, Carrara A, *et al.* (2002) Impact of mapping errors on the reliability of landslide hazard maps. Natural Hazards and Earth System Science 2: 3-14. https://doi.org/10.5194/nhess-2-3-2002.

Atkinson PM, Massari R (1998) Generalised linear modelling of susceptibility to landsliding in the central Apennines, Italy. Computers & Geosciences 24(4): 373-385. https://doi.org/10.1016/S0098-3004(97)00117-9

Ayalew L, Yamagishi H, Ugawa N (2004) Landslide susceptibility mapping using GIS-based weighted linear combination, the case in Tsugawa area of Agano River, Niigata Prefecture, Japan. Landslides 1: 73-81. https://doi.org/10.1007/s10346-003-0006-9

Beven KJ, Kirkby MJ (1979) A physically based, variable contributing area model of basin hydrology. Hydrology Science Bulletin 24: 43-69.

Bischl B, Lang M, Kotthoff L, *et al.* (2016) mlr: Machine Learning in R. R package version 2.9. https://CRAN.R-project.org/package=mlr

Brabb EE (1984) Innovative approaches to landslide hazard mapping. Proceedings 4th International Symposium on Landslides, Toronto 1: 307-324.

Brenning A (2005) Spatial prediction models for landslide hazards: review, comparison and evaluation. Natural Hazards and Earth System Science 5: 853-862. https://doi.org/10.5194/nhess-5-853-2005

Brenning A (2008) Statistical geocomputing combining R and SAGA: the example of landslide susceptibility analysis with generalized additive models. In: Böhner J, Blaschke T, Montanarella L (eds.), SAGA — Seconds Out (= Hamburger Beiträge zur Physischen Geographie und Landschaftsökologie, 19). pp 23-32.

Brenning A (2012) Spatial cross-validation and bootstrap for the assessment of prediction rules in remote sensing: the R package 'sperrorest'. IEEE International Symposium on Geoscience and Remote Sensing IGARSS. https://ieeexplore.ieee.org/document/6352393

Capra L, Lugo-Hubp J, Borselli L (2003) Mass movements in tropical volcanic terrains: the case of Teziutlán (Mexico). Engineering Geology 69: 359-379. https://doi.org/10.1016/S0013-7952(03)00071-1

Cardinali M, Reichenbach P, Guzzetti F, *et al.* (2002) A geomorphological approach to estimate landslide hazard and risk in urban and rural areas in Umbria, central Italy. Natural Hazards and Earth System Science 2 (1-2): 57-72. https://www.nat-hazards-earth-systsci. net/2/57/2002/nhess-2-57-2002.pdf

Cascini L (2008) Applicability of landslide susceptibility and hazard zoning at different scales. Engineering Geology 102: 164-177. https://doi.org/10.1016/j.enggeo.2008.03.016

Catani F, Lagomarsino D, Segoni S, Tofani V (2013) Landslide susceptibility estimation by random forests technique:sensitivity and scaling issues. Natural Hazards and Earth System Science 13: 2815-2831. https://doi.org/10.5194/nhess-13-2815-2013

Chauhan S, Sharma M, Arora MK (2010) Landslide susceptibility zonation of the Chamoli region, Garhwal Himalayas, using logistic regression model. Landslides 7:411- 423. https://doi.org/10.1007/s10346-010-0202-3

Che VB, Kervyn M, Suh CE, *et al.* (2012) Landslide susceptibility assessment in Limbe (SW Cameroon): A field calibrated seed cell and information value method. Catena 92: 83-98. https://doi.org/10.1016/j.catena.2011.11.014

Chen CH, Ke CC, Huang CL (2009) A back-propagation network for the assessment of susceptibility to rock slope failure in the eastern portion of the Southern Cross-Island Highway in Taiwan. Environmental Geology 57: 723-733. https://doi.org/10.1007/s00254-008-1350-9

Chung CJF, Fabbri AG (2003) Validation of spatial prediction models for landslide hazard mapping. Natural Hazards 30(3): 451-472. https://doi.org/10.1023/B:NHAZ.0000007172.62651.2b

Chung CF, Fabbri A, Van Westen CJ (1995) Multivariate regression analysis for landslide hazard zonation. In: Carrara A, Guzzetti F (eds.), Geographical Information Systems in Assessing Natural Hazards 107-133.
Conforti M, Pascale S, Robustelli G, Sdao F (2014) Evaluation of prediction capability of the artificial neural networks for mapping landslide susceptibility in the Turbolo River catchment (northern Calabria, Italy). Catena 113: 236-250. https://doi.org/10.1016/j.catena.2013.08.006

Conrad O (2006) SAGA - Program structure and current state implementation. In: Böhner J, McCloy KR, Strobl J (eds.), SAGA — Analysis and Modelling Applications, vol.115.Göttinger Geographische Abhandlungen. pp 39-52.

Costanzo D, Rotigliano E, Irigaray C, *et al.* (2012) Factors selection in landslide susceptibility modelling on large scale following the gis matrix method: application to the river Beiro basin (Spain). Natural Hazards and Earth System Science 12: 327-340. https://doi.org/10.5194/nhess-12-327-2012

Dahal RK, Hasegawa S, Nonomura A, *et al.* (2008) GIS-based weights-of evidence modelling of rainfall-induced landslides in small catchments for landslide susceptibility mapping. Environmental Geology 54(2):314-324. https://doi.org/10.1007/s00254-007-0818-3

Dávila-Harris P, Carrasco-Núñez G (2014) An unusual syneruptive bimodal eruption: The Holocene Cuicuiltic Member at Los Humeros caldera, Mexico. Journal of Volcanology and Geothermal Research 271: 24-42. https://doi.org/10.1016/j.jvolgeores.2013.11.020

Deb SK, El-Kadi AI (2009) Susceptibility assessment of shallow landslides on Oahu, Hawaii, under extreme-rainfall events. Geomorphology 108: 219-233. https://doi.org/10.1016/j.geomorph.2009.01.009

Fell R, Corominas J, Bonnard C, *et al.* (2008) Guidelines for landslide susceptibility, hazard and risk zoning for land-use planning. Engineering Geology 102(3-4): 85-98. https://doi.org/10.1016/j.enggeo.2008.03.022

Ferriz H, Mahood G (1984) Eruption rates and compositional trends at Los Humeros volcanic center, Puebla, Mexico. Journal Geophysics Research Earth 89: 8511-8524.

Fressard M, Thiery Y, Maquaire O (2014) Which data for quantitative landslide susceptibility mapping at operational scale? Case study of the Pays d'Auge plateau hillslopes (Normandy, France). Natural Hazards and Earth System Science 14(3): 569-588.
https://doi.org/10.5194/nhess-14-569-2014

Glade T, Crozier M (2005) A review of scale dependency in landslide hazard and risk analysis. In: Glade T, Anderson M, Crozier M (eds) Landslide hazard and risk. John Wiley and Sons. England. pp 75-138.

Goetz JN, Guthrie RH, Brenning A (2011) Integrating physical and empirical landslide susceptibility models using generalized additive models. Geomorphology 129(3): 376-386. https://doi.org/10.1016/j.geomorph.2011.03.001

Goetz JN, Brenning A, Petschko H, Leopold P (2015) Evaluating machine learning and statistical prediction techniques for landslide susceptibility modeling. Computers & Geosciences 81: 1-11. https://doi.org/10.1016/j.cageo.2015.04.007

Gordo C, Zêzere JL, Marques R (2017) Effects of study area delineation on landslide susceptibility assessment results using statistical methods. 8º Congresso Nacional de Geomorfologia 95-98.

Gorum T, Fan X, van Westen CJ, *et al.* (2011) Distribution pattern of earthquake-induced landslides triggered by the 12 May 2008 Wenchuan earthquake. Geomorphology 133 (3-4): 152-167. https://doi.org/10.1016/j.geomorph.2010.12.030

Guzzetti F (2005). Landslide Hazzard and Risk Assessment. PhD thesis, Bonn University, Bonn, Germany.

Guzzetti F, Carrara A, Cardinali M, Reichenbach P (1999) Landslide hazard evaluation: a review of current techniques and their application in a multi-scale study, Central Italy. Geomorphology 31: 181-216. https://doi.org/10.1016/S0169-555X(99)00078-1

Guzzetti F, Reichenbach P, Cardinali M, *et al.* (2005) Probabilistic landslide hazard assessment at the basin scale. Geomorphology 72: 272-299. https://doi.org/10.1016/j.geomorph.2005.06.002

Guzzetti F, Reichenbach P, Ardizzone F, *et al.* (2006) Estimating the quality of landslide susceptibility models, Geomorphology 81(1-2): 166-184. https://doi.org/10.1016/j.geomorph.2006.04.007

Hastie T (2009) GAM: Generalized Additive Models R package version 1.08. https://CRAN.R-project.org/package=gam

Hastie T, Tibshirani R (1986) Generalized Additive Models, Statistical Science 1(3): 297-318.

Hastie TJ, Tibshirani RJ (1990) Generalized Additive Models, 1st ed., Monographs on statistics and applied probability 43. Chapman and Hall/CRC, London; New York.

Heckmann T, Gregg K, Gregg A, Becht M (2014) Sample size matters: investigating the effect of sample size on a logistic regression susceptibility model for debris flows. Natural Hazards and Earth System Science 14: 259-278. https://doi.org/10.5194/nhess-14-259-2014

Hosmer DW, Lemeshow S (2000) Applied logistic regression, 2nd edn. Wiley, New York. pp 373.

Hong H, Pradhan B, Xua C, Tien Bui D (2015) Spatial prediction of landslide hazard at the Yihuang area (China) using two class kernel logistic regression, alternating decision tree and support vector machines. Catena 133: 266-281. https://doi.org/10.1016/j.catena.2015.05.019

Hussin H, Zumpano V, Reichenbach P, *et al.* (2016) Different landslide sampling strategies in a grid-based bi-variate statistical susceptibility model. Geomorphology 253: 508-523. https://doi.org/10.1016/j.geomorph.2015.10.030

INEGI (2009) Prontuario de información geográfica municipal de los Estados Unidos Mexicanos. Teziutlán, Puebla. Instituto
Nacional de Geografía y Estadística. p 9. (In Spanish).

INEGI (2013a) Continuo de Elevaciones Mexicano 3.0 (CEM 3.0) - descarga Antecedentes. Available online at: http://www.inegi.org.mx/geo/contenidos/datosrelieve/continental/continuoelevaciones.aspx (Accessed on 08 August 2018) (In Spanish).

INEGI (2013b) Modelo digital de elevación de alta resolución LiDAR, Tipo terreno con resolución de 5 m. Available online at: http://www.inegi.org.mx/est/contenidos/proyectos/Preview.aspx (Accessed on 08 August 2018) (In Spanish).

Karatzoglou A, Smola A, Hornik K, Zeileis A (2004) Kernlab - An S4 Package for Kernel methods in R. Journal of Statistical
Software 11(9): 1-20. http://www.jstatsoft.org/v11/i09/

Kavzoglu T, Sahin EK, Colkesen I (2014) Landslide susceptibility mapping using GIS-based multicriteria decision analysis, support vector machines, and logistic regression. Landslides 11: 425-439. https://doi.org/10.1007/s10346-013-0391-7

Kavzoglu T, Sahin EK, Colkesen I (2015) Selecting optimal conditioning factors in shallow translational landslide susceptibility mapping using genetic algorithm. Engineering Geology 192: 101-112. https://doi.org/10.1016/j.enggeo.2015.04.004

Kotsiantis SB (2007) Supervised Machine Learning: A Review of Classification Techniques. Informatica 31, 249-268.

Lee S, Choi J, Woo I (2004) The effect of spatial resolution on the accuracy of landslide susceptibility mapping: a case study in Boun, Korea. Geoscience Journal 8: 51-60. https://doi.org/10.1007/BF02910278

Legorreta-Paulín, Bursik M, Lugo-Hubp J, Zamorano-Orozco JJ (2010) Effect of pixel size on cartographic representation of shallow and deep-seated landslide, and its collateral effects on the forecasting of landslides by SINMAP and Multiple LogisticRegression landslide models. Physics and Chemistry of the Earth 35: 137-148. https://doi.org/10.1016/j.pce.2010.04.008

Moore ID, Grayson RB, Ladson AR (1991) Digital terrain modeling: a review of hydrological, geomorphological, and biological applications. Hydrological Process 5: 3-30. https://doi.org/10.1002/hyp.3360050103

Murillo-García FG, Alcántara-Ayala I (2017) Landslide inventory, Teziutlán municipality, Puebla, México (1942- 2015). Journal of maps 13(2): 767-776. https://doi.org/10.1080/17445647.2017.1381194

Olaya V (2004) A Gentle Introduction to SAGA GIS. ftp://priede.bf.lu.lv/pub/GIS/datu_analiize/SAGA/SagaManual.pdf

Palamakumbure D, Flentje P, Stirling D (2015) Consideration of optimal pixel resolution in deriving landslide susceptibility zoning within the Sydney Basin, New South Wales, Australia. Computers & Geosciences 82: 13-22. https://doi.org/10.1016/j.cageo.2015.05.002

Park NW, Chi KH (2008) Quantitative assessment of landslide susceptibility using high-resolution remote sensing data and a generalized additive model. International Journal of Remote Sensing 29: 247-264. https://doi.org/10.1080/01431160701227661

Petschko H, Bell R, Leopold P, *et al.* (2013) Landslide inventories for reliable susceptibility maps. In: Margottini C, Canuti P, Sassa K (Eds.), Landslide Science and Practice, vol. 1: Landslide Inventory and Susceptibility and Hazard Zoning. Springer.

Petschko H, Brenning A, Bell R, *et al.* (2014) Assessing the quality of landslide susceptibility maps - case study Lower Austria Natural Hazards and Earth System Science 14: 95-118. http:// doi.org/10.5194/nhess-14-95-2014

Petschko H, Bell R, Glade T (2016) Effectiveness of visually analyzing LiDAR DTM derivatives for earth and debris slide inventory mapping for statistical susceptibility modelling. Landslides 13 (5): 857-872. https://doi.org/10.1007/s10346-015-0622-1

Pourghasemi HR, Rahmati O (2018) Prediction of the landslide susceptibility: Which algorithm, which precision? Catena 162: 177-192. https://doi.org/10.1016/j.catena.2017.11.022

Pradhan S (2013) A comparative study on the predictive ability of the decision tree, support vector machine and neuro-fuzzy models in landslide susceptibility mapping using GIS. Computers & Geosciences 51:350-365. https://doi.org/10.1016/j.cageo.2012.08.023

Qi S, Xu Q, Lan H, *et al.* (2010) Spatial distribution analysis of landslides triggered by 2008.5.12 Wenchuan Earthquake, China Engineering Geology 116 (1-2): 95-108. http://doi.org/10.1016/j.enggeo.2010.07.011

QGIS Development Team (2009) QGIS Geographic Information System. Open Source Geospatial Foundation. http://qgis.osgeo.org

R Core Team (2016) R: A language and environment for statistical computing. R Foundation for Statistical Computing, Vienna, Austria. https://www.R-project.org/

Regmi NR, Giardino JR, McDonald E, Vitek JD (2014) A comparison of logistic regression based models of susceptibility to landslides in western Colorado, USA. Landslides 11: 247-262. https://doi.org/10.1007/s10346-012-0380-2

Reichenbach P, Rossi M, Malamud BD, *et al.* (2018) A review of statistically-based landslide susceptibility models. Earth-Science Reviews 180: 60-91. https://doi.org/10.1016/j.earscirev.2018.03.001

Romer C, Ferentinou M (2016) Shallow landslide susceptibility assessment in a semiarid environment —A Quaternary catchment of Kwa Zulu-Natal, South Africa. Engineering Geology 201: 29-44. https://doi.org/10.1016/j.enggeo.2015.12.013

Rossi M, Guzzetti F, Reichenbach P, *et al.* (2010) Optimal landslide susceptibility zonation based on multiple forecasts. Geomorphology 114: 129-142. https://doi.org/10.1016/j.geomorph.2009.06.020

Salinas-Rodríguez JM, Castillo-Reynoso JE (2011) Carta Geologica Minera. Teziutlán E14B15 Puebla. Servicio Geológico Mexicano.

San BT (2014) An evaluation of SVM using polygon-based random sampling in landslide susceptibility mapping: The Candir catchment area (western Antalya, Turkey). International Journal of Applied Earth Observation and Geoinformation 26: 399-412.

Schlögel R, Marchesini I, Alvioli M, *et al.* (2018) Optimizing landslide susceptibility zonation: Effects of DEM spatial resolution and slope unit delineation on logistic regression models. Geomorphology 301: 10-20. https://doi.org/10.1016/j.geomorph.2017.10.018

Schratz P, Muenchow J, Iturritxa E, *et al.* (2018) Performance evaluation and hyperparameter tuning of statistical and machine-learning models using spatial data. Journal of LATEX Templates. https://arxiv.org/abs/1803.11266

Sing T, Sander O, Beerenwinkel N, Lengauer T (2009) ROCR: Visualizing the Performance of Scoring Classifiers. R package version 1.0-4. http://cran.r-pro ject.org/package¼ROCR

Steger S, Glade T (2017) The Challenge of "Trivial Areas" in Statistical Landslide Susceptibility Modelling. In: Matjaž M et
al. (eds.) Advancing Culture of Living with Landslides WLF 2017, Springer, Cham. 2: 803-808. https://doi.org/10.1007/978-3-319-53498-5_92

Steger S, Brenning A, Bell R, *et al.* (2016a) Exploring discrepancies between quantitative validation results and the geomorphic plausibility of statistical landslide susceptibility maps, Geomorphology 262: 8-23. https://doi.org/10.1016/j.geomorph.2016.03.015

Steger S, Brenning A, Bell R, Glade T (2016b) The propagation of inventory-based positional errors into statistical landslide susceptibility models. Natural Hazards and Earth System Science 16(12): 2729-2745. https://doi.org/10.5194/nhess-2016-301

Steger S, Brenning A, Bell R, Glade T (2017) The influence of systematically incomplete shallow landslide inventories on statistical susceptibility models and suggestions for improvements. Landslides 14:1767-1781. https://doi.org/10.1007/s10346-017-0820-0

Trigila A, Iadanza C, Esposito C, Scarascia-Mugnozza G (2015) Comparison of Logistic Regression and Random Forests techniques for shallow landslide susceptibility assessment in Giampilieri (NE Sicily, Italy). Geomorphology 249: 119-136. https://doi.org/10.1016/j.geomorph.2015.06.001

Van Den Eeckhaut M, Vanwalleghem T, Poesen J, *et al.* (2006) Prediction of landslide susceptibility using rare events logistic regression: A case-study in the Flemish Ardennes (Belgium). Geomorphology 76(3-4): 392-410. https://doi.org/10.1016/j.geomorph.2005.12.003

van Westen CJ, Rengers N, Terlien MTJ, Soeters R (1997) Prediction of the occurrence of slope instability phenomenal through GIS-based hazard zonation. Geologische Rundschau 86: 404-414.

van Westen CJ, Seijmonsbergen AC, Mantovani F (1999) Comparing landslide hazard maps. Natural Hazards 20: 137-158.

van Westen CJ, Castellanos E, Kuriakose SL (2008) Spatial data for landslide susceptibility, hazard, and vulnerability assessment: An overview. Engineering Geology 102(3-4): 112-131. https://doi.org/10.1016/j.enggeo.2008.03.010

Vapnik V (1998) Statistical Learning Theory. John Wiley & Sons Inc., New York. p 736.

Varnes DJ, IAEG Commission on Landslides and other Mass- Movements (1984) Landslide hazard zonation: a review of principles and practice. The UNESCO Press, Paris. p 63.

Vorpahl P, Elsenbeer H, Märker M, Schröder, B (2012) How can statistical models help to determine driving factors of landslides? Ecol. Model 239: 27-39. https://doi.org/10.1016/j.ecolmodel.2011.12.007

Wood SN (2006) Generalized additive models: an introduction with R. Chapman & Hall/CRC, Boca Raton, FL.

Youssef AM, Pradhan B, Pourghasemi HR, Abdullahi S (2015) Landslide susceptibility assessment at Wadi Jawrah Basin, Jizan region, Saudi Arabia using two bivariate models in GIS. Geosciences Journal 19(3): 449-469. https://doi.org/10.1007/s12303-014-0065-z

Zêzere JL, Pereira S, Melo R, *et al.* (2017) Mapping landslide susceptibility using data-driven methods. Science of the Total Environment 589: 250-267. https://doi.org/10.1016/j.scitotenv.2017.02.188

Zweig MH, Campbell G (1993) Receiver-operating characteristic (ROC) plots. Clinical Chemistry 39: 561-577.

# Capítulo VI. Hazard and vulnerability

**Hazard and population vulnerability analysis: a step towards landslide risk assessment.**

# Hazard and population vulnerability analysis: a step towards landslide risk assessment ©

Franny Giselle Murillo-García
Posgrado en Geografía UNAM

Mauro Rossi
Istituto di Ricerca per la Protezione Idrogeologica (CNR-IRPI)

Francesca Ardizzone
Istituto di Ricerca per la Protezione Idrogeologica (CNR-IRPI)

Federica Fiorucci
Istituto di Ricerca per la Protezione Idrogeologica (CNR-IRPI)

Irasema Alcántara Ayala
Instituto de Geografía UNAM

*In this paper, an attempt to analyse landslide hazard and vulnerability in the municipality of Pahuatlán, Puebla, Mexico, is presented. In order to estimate landslide hazard, the susceptibility, magnitude (area-velocity ratio) and landslide frequency of the area of interest were produced based on information derived from a geomorphological landslide inventory; the latter was generated by using very high resolution satellite stereo pairs along with information derived from other sources (Google Earth, aerial photographs and historical information). Estimations of landslide susceptibility were determined by combining four statistical techniques: (i) logistic regression, (ii) quadratic discriminant analysis, (iii) linear discriminant analysis, and (iv) neuronal networks. A Digital Elevation Model (DEM) of 10 m spatial resolution was used to extract the slope angle, aspect, curvature, elevation and relief. These factors, in addition to land cover, lithology and distance to faults, were used as explanatory variables for the susceptibility models. Additionally, a Poisson model was used to estimate landslide temporal frequency, at the same time as landslide magnitude was obtained by using the relationship between landslide area and the velocity of movements. Then, due to the complexity of evaluating it, vulnerability of population was analysed by applying the Spatial Approach to Vulnerability Assessment (SAVE) model which considered levels of exposure, sensitivity and lack of resilience. Results were expressed on maps on which different spatial patterns of levels of landslide hazard and vulnerability were found for the inhabited areas. It is noteworthy that the lack of optimal methodologies to estimate and quantify vulnerability is more notorious than that of hazard assessments. Consequently, levels of uncertainty linked to landslide risk assessment remain a challenge to be addressed.*

# 6.1 INTRODUCTION

Landslides affect society on a variety of spatial and temporal scales (Glade and Crozier 2005). The consequences of these effects are, in general, negative and give rise to different levels of damage, particularly in developing countries (Alcántara-Ayala 2002; Parkash 2013). To assess the consequences of landslide impact on human activity, it is necessary to consider a framework that analyzes landslide hazard, type and magnitude of damage, the elements at risk, and social aspects. However, an all-embracing perspective of the notion of risk is not an easy task to undertake since it requires data availability at different scales and a multidisciplinary point of view. Nonetheless, this type of approach is one of the most beneficial.

Risk is the probability that a hazard can cause damage to a vulnerable human-environmental system (UN/ISDR 2004). Landslide hazard is the conditional probability of landslide magnitude, time occurrence and spatial occurrence given the local environment settings for any given area (Guzzetti *et al.* 2005). Landslide hazard implies the spatial and temporal probability of landslides occurrence, being generally its magnitude regarded as the first step into landslide risk estimation. There are many approaches to assess landslide spatial probability (landslide susceptibility), based on heuristic (Van Den Eeckhaut *et al.* 2010; Ghosh *et al.* 2011), semi-quantitative (Komac 2006; Wu and Chen 2009) and quantitative perspectives (Kanungo *et al.* 2006; Rossi *et al.* 2010; Xu *et al.* 2012). For quantitative approaches, geotechnical ground data (deterministic methodologies) or a complete record of landslide occurrence expressed through landslide inventories (statistical and new data-mining approaches) are necessary. Studies that imply the temporal distribution and the magnitude of landslides are scarce (Guzzetti 2005; Corominas and Moya 2008; Peng *et al.* 2015) and commonly require historic rainfall data and landslide information, including area, volume and velocity rate.

In contrast, vulnerability is the probability that the human-environmental system, or any one of its components, suffers damage as a result of exposure, sensitivity, and adaptive capacity (resilience) (Turner *et al.* 2003; Birkmann 2006). Vulnerability is a complex, dynamic, and multidimensional concept, hazard- and scale-dependent (Birkmann 2006; Fuchs *et al.* 2011; Papathoma-Köhle *et al.* 2011; Birkmann *et al.* 2013). For example, Wilches- Chaux (1998) suggested some of the dimensions of vulnerability, such as natural, physical, economic, social, political, cultural, educative, ecological and institutional, and that estimating these quantitatively is very complicated. Vulnerability has been analysed by using a series of frameworks due to the complex nature of its evaluation. Birkmann (2006)

presented a detailed summary of the vulnerability frameworks used in the literature, including the Pressure and Release Model (Blaikie *et al.* 1994); the Double Structure Vulnerability Model (Bohle 2001), the Sustainable Livelihood Framework (Chambers and Conway 1992), the vision of the United Nations Office for Disaster Risk Reduction (UN/ISDR 2004), the onion framework of the Institute for Environmental and Human Security of the United Nations University (Birkmann 2006), and the Global Environment Change Community framework (Turner *et al.* 2003).

For the work presented here, the Global Environment Change Community framework developed by Turner *et al.* (2003) was used to underpin the estimation of vulnerability. This assessment has a social-ecological perspective with an emphasis on the coupling of human and environmental systems (Birkmann *et al.* 2013). The framework distinguishes three basic components of vulnerability: (i) exposure, (ii) sensitivity, and (iii) lack of resilience. The exposure is the relationship between the elements at risk and the hazard (Fuchs *et al.* 2011). It depends on the features of elements at risk: people, infrastructure, economy, the social and political structures and all the elements valued by societies. Sensitivity is the predisposition of the elements at risk to damage (Birkmann *et al.* 2013) and is related to the response of the system to the impact of the hazard. Resilience refers to the ability of a system or a person to deal with disturbances and the effects of a hazard impact and its recovery (Birkmann *et al.* 2013).

Approaches to measure vulnerability can be classified based on methodology: (i) curves-based approaches that link specific features of elements at risk with the intensity of hazards (Liu and Lei 2003; Galli and Guzzetti 2007; Fuchs *et al.* 2007; Kaynia *et al.* 2008; Uzielli *et al.* 2008; Akbas *et al.* 2009; Tsao *et al.* 2010; Li *et al.* 2010; Mavrouli and Corominas 2010; Negulescu and Foerster 2010; Quan Luna *et al.* 2011; Totschnig *et al.* 2011; Papathoma-Köhle *et al.* 2011; Papathoma-Köhle *et al.* 2012; Eidsvig *et al.* 2014a; Lu *et al.* 2014; Papathoma-Kohle *et al.* 2015); (ii) damage matrices based approaches (Fell 1994; Leone *et al.* 1996; Ragozin 1996; Finlay and Fell 1997; Cardinali *et al.* 2002; Michael-Leiba *et al.* 2000; Alexander 2005; Sterlacchini *et al.* 2007; Zezere *et al.* 2008); and (iii) vulnerability indicator-based approaches (Mejia-Navarro *et al.* 1994; Cutter 1996; Michael- Leiba *et al.* 2003; Maquaire *et al.* 2004; Bell and Glade 2004; Shrestha 2005; Corominas *et al.* 2005; Papathoma-Köhle *et al.* 2007; Sterlacchini *et al.* 2007; Kappes *et al.* 2012; Duan *et al.* 2011; Mousavi *et al.* 2011; Thanapackiam *et al.* 2012; Sajinkumar *et al.* 2014; Eidsvig *et al.* 2014b). Vulnerability indicators take into account the multiple socio-economic and environmental characteristics of the elements at risk (Kappes *et al.* 2012).Vulnerability indicators are variables that can be considered as operational representations of the characteristics or the quality of a system, providing information regarding the components of its vulnerability (Birkmann 2006; Kappes *et al.* 2012). Therefore, could be said that

defining landslide vulnerability indicators is a complex task due to the lack or variability in the availability of accurate data and the elements at risk, the site specific nature of the occurrence of landslides, the merging of landslide damage with triggering phenomena (e.g., hurricanes, earthquakes) (Alcántara-Ayala 2008) and the difficulty in obtaining damage data from private property (Highland 2003; Petrucci and Gullà 2010).

The elements at risk are another significant factor when carrying out landslide vulnerability assessments. Most of the available studies are focused on the damage to buildings (e.g., Papathoma-Köhle *et al.* 2007) and/or life lines (Mejia-Navarro *et al.* 1994). According to Papathoma-Köhle *et al.* (2011), only Leone *et al.* (1996), Liu and Lei (2003) and Sterlacchini *et al.* (2007) include a multi-dimensional point of view of the vulnerability focused on the population. Duan *et al.* (2011) also included vulnerability for the population of three towns in Hubei province in China. They used a cluster analysis to obtain the vulnerability value and constructed a database through applied surveys of the inhabitants. Mousavi *et al.* (2011), calculated the vulnerability of the population (and buildings) of the Emamzadeh Ali region in Iran taking into account only the spatial location of the people (open areas, buildings and automobiles). Sajinkumar *et al.* (2014) took the same exposition method as Mousavi *et al.* (2011), but they also included socioeconomic indicators. Eidsvig *et al.* (2014b) used an indicator approach to estimate the vulnerability of six different study areas around Europe. To assign weight to indicators they used a heuristic method and applied an additive model to obtain the vulnerability value.

This paper aims to generate a preliminary landslide risk assessment by means of analyzing hazard and vulnerability of population. Firstly, the application of statistical techniques to estimate landslide hazard using information provided by a landslide inventory is presented. In addition, the Spatial Approach to Vulnerability Assessment (SAVE) model, based on the framework developed by Turner *et al.* (2003), was used to estimate the landslide vulnerability of the population of the municipality of Pahuatlán, Puebla, Mexico. In the final section, a preliminary risk map of the analysis carried out is presented, as well as the corresponding results, along with the discussion and concluding remarks.


## 6.2 THE STUDY AREA

In order to undertake the proposed landslide hazard and vulnerability analysis, a 54 km$^2$ study area was delimitated by using hydrologic criteria (dividing lines and river channels) (Fig. 67). Pahuatlán, a Municipality of Puebla state, is located in the Sierra Norte de Puebla, in the central area of México

(Fig. 67), where the mountain system of Sierra Madre Oriental joins the Trans- Mexican Volcanic Belt. The original vegetation of the region is pine oak in the highest zones and mesophyll forest; the latter is severely altered by deforestation. The annual range of precipitation is 1900-2100 mm, and the climate is classified as humid temperate (16°C mean annual temperature) (INEGI 2009). Extreme rainfall events associated with tropical depressions and hurricanes may take place. From 4-6 October 1999, a tropical depression generated 750 mm of precipitation in the region, triggering hundreds of mass movement processes that caused severe damage to the population of the Sierra Norte de Puebla region; 263 people died and more than a million inhabitants were affected not only by landslides, but also by flooding (Alcántara-Ayala 2004).

From a geological perspective, Pahuatlán is composed of the following lithological units: (i) Low Jurassic Huayacocotla sandstone, siltstone and lutite shale sequence, which is the oldest outcrop in the region (210 Ma.); (ii) Cahuasas siltstone-sandstone formation (176.5 Ma.); (iii) Middle Jurassic Tepéxic limestone formation (166 Ma.); (iv) Late Jurassic Tamán clay limestone and lutite shale sequence (154 Ma.); (v) Late Jurassic Pimienta black limestone-lutite shale sequence (145 Ma.); (vi) Low Cretaceous Tamaulipas limestone-lutite shale sequence (135 Ma.); (vi) Pliocene basalt, andesite and pyroclastic deposits (pumice tuff with 1.5-5.1 Ma.); in addition to (vii) alluvial, and (viii) colluvium deposits (Sánchez- Rojas and De la Callejera-Moctezuma 2004). The study area is mountainous with deep ravines and high summits, a product of the Sierra Madre orogenesis. The elevation ranges from 450 to 1500 m above sea level (Murillo-García and Alcántara-Ayala 2015). The gradient varies from almost zero, along the plain of the San Marcos River, to more than 70° at the top of the mountains. Landslides of diverse types, depths and ages are abundant in the municipality, most of them triggered by intense and prolonged rainfall caused by hurricanes, tropical depressions, and a combination of various hydrometeorological conditions (Murillo-García and Alcántara-Ayala 2015).

From a social perspective, Pahuatlán municipality has 19,559 inhabitants, distributed in 34 towns (INEGI 2011). Almost 50% of them are indigenous people. This population can be considered as marginalized, with many people living in conditions of poverty, social exclusion and discrimination. The economy of the region depends, to a large extent, on agriculture and livestock activities, however, in recent years, tourism and commercial activities have considerably increased. The mountainous terrain has meant that, where human settlements have grown, they have tended to extend towards unstable slopes, thus increasing the population's exposure to landslides.
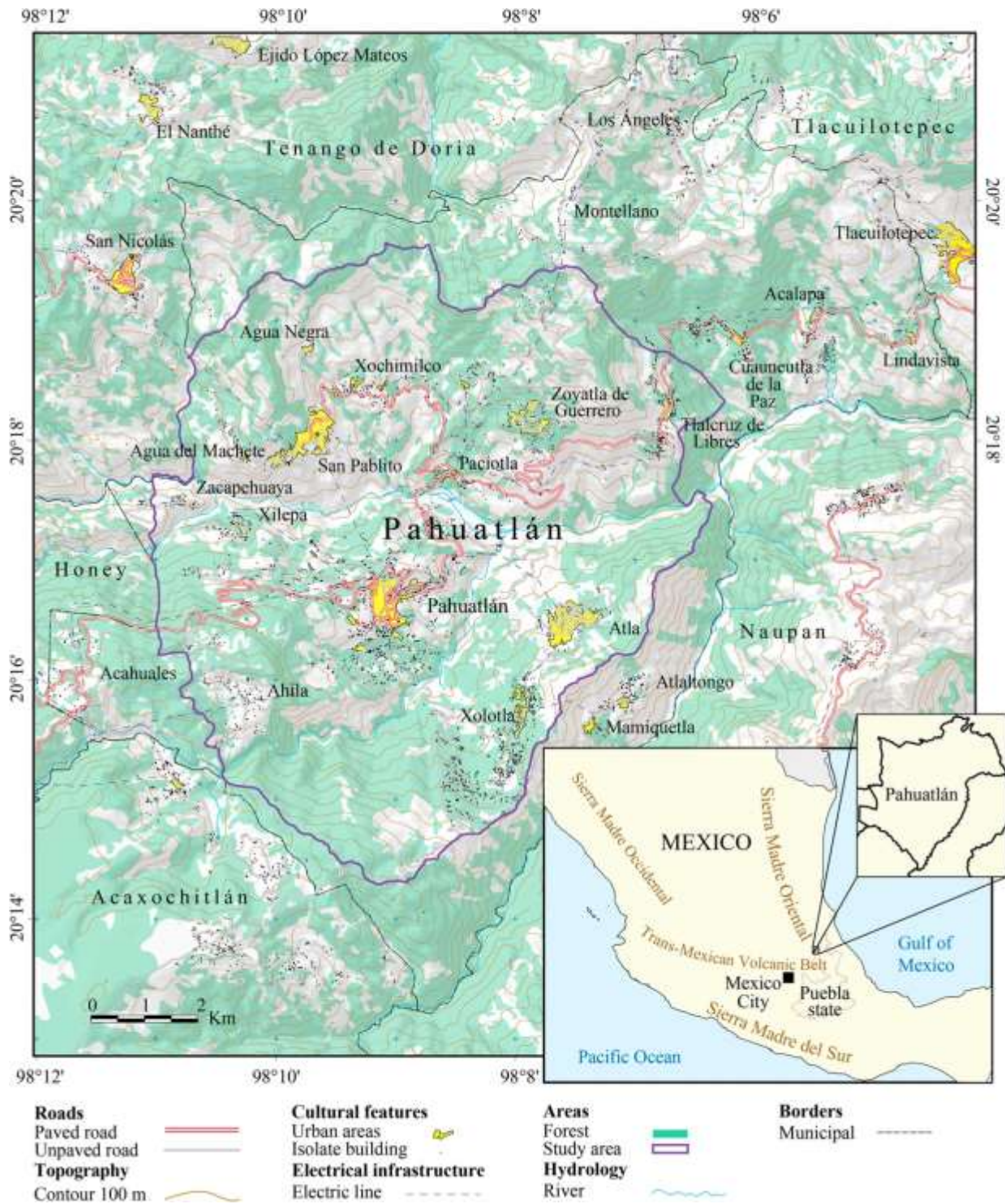
***Figure 67.*** *Location of the Pahuatlán municipality and delimitation of the polygon study area.*

# 6.3 DATA AND METHODS

### 6.3.1 Landslide inventory

A landslide inventory map, in digital format, was used (Fig. 68). The inventory was prepared by analysing pan-sharpened stereoscopic pairs of very high resolution (VHR) satellite images GeoEye-1 (0.5 m spatial resolution) dated 31 March 2010 at 17:10 GTM. Additionally, multitemporal images from Google Earth (2004, 2009 and 2011), SPOT5 monoscopical panchromatic images (2 m spatial resolution, 15 December 2008), air orthophotographs from 1994 (scale 1:20,000) (Fig. 69), a detailed review of historical newspaper records, and field surveys (Murillo-García *et al.* 2015) were utilized. A total of 577 landslides were mapped as delineated polygons (distinguishing scarp and deposit area); 66.8% were classified as recent (1994-2012), and the remaining landslides were classified, based on geomorphological features, as old and very old. The total surface affected by recent landslides was 500,000 m$^2$, (0.94% of the study area) with a density of 6.8 landslides per km$^2$. The largest recent landslide had an area of 20,000 m$^2$ and the smallest one 12 m$^2$. Among these, 217 were classified as flows, 167 as translational slides, 97 as complex movements, 79 as rotational slides, and 17 as falls and topples. The inventory database was used to carry out the susceptibility of the study area, and to estimate the magnitude and temporal probability of the hazard evaluation.

Debris flows are frequent in the study area and occur primarily on the steep slopes of the San Marcos river valley. Figure 70A shows three recent debris flows that occurred near the town of Xilepa in the western part of the study area. A mud and rock flow covered and seriously affected the town centre of Pahuatlán in 1955, and there are some photographs of the damage. According to the inhabitants, this flow was extremely rapid, but there is confusion about whether there were fatalities; some inhabitants stated that there was at least one whereas others do not remember. In the same year, several slides affected the highlands where the towns of Aila, Xolotla and Atla are located; the inhabitants identified the 1955 landslide event, caused by the extreme rainfall of Hurricane Janet (28 September 1955), as the worst event before the 1999 disaster.
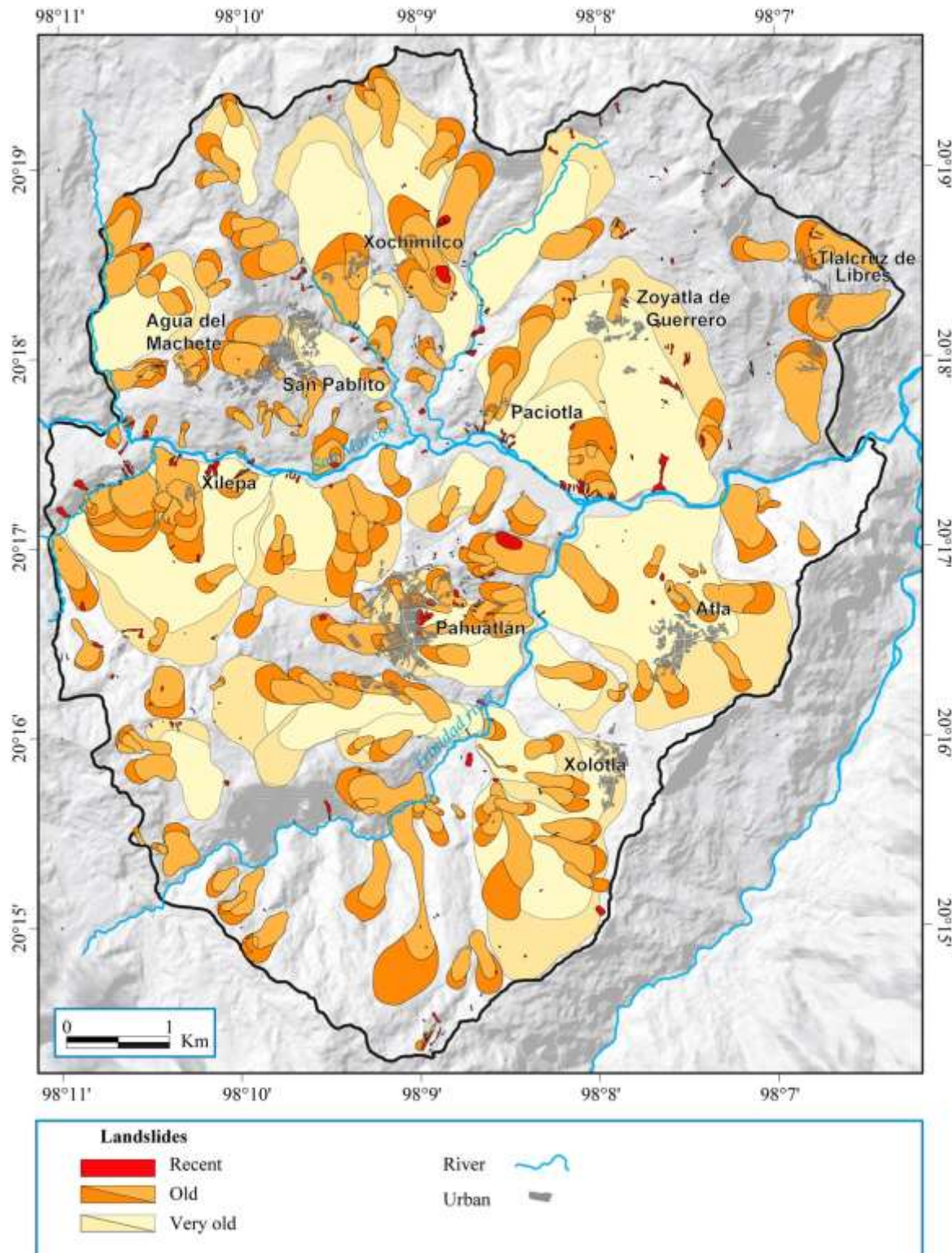
***Figure 68.*** *Landslide inventory map of the study area. Old and very old landslides are divided into initiation and deposit zones.*

In 1999, 2005 and 2007 landslides again affected the town centre of Pahuatlán; the buildings of the elementary school and two public health clinics were damaged by slides. In 2005 one of the public health clinic buildings was destroyed by a rotational landslide in the eastern part of the town (the

movement is known by the inhabitants and the press as the 'Calle 5 de mayo' landslide); this landslide was a reactivation of a movement that occurred in 1947 (Fig. 70B). In none of these three cases were there fatalities since the movements were moderate (in the case of the 'Calle 5 de mayo' landslide) or small (in the other two cases). Further landslides (Figures 70C and 70D) occurred in Pahuatlán during the 2011 rainy season and were identified by field surveys.

| Image | Spatial resolution /scale | Acquisition date | Stereoscopy | Spectral resolution |
|---|---|---|---|---|
| GeoEye1. | 0.5 m | 31/03/2010 | Yes | True color pansharpening image. |
| Google Earth. | 1 m (approximate) | 30/03/2009 09/10/2011 | No | True color image |
| SPOT 5 | 2 m | 15/12/2008 | No | True color pansharpening image. |
| Google Earth | 1m (approximate) | 25/11/2004 | No | True color image |
| Antares INEGI orthophotographs | 1:20 000 | 01/12/ 1994 | No | Panchromatic |

*Figure 69. Remote sensing imagery used to produce the landslide inventory.*

## 6.3.2 Digital elevation model

A Digital Elevation Model (DEM) with a 10 m spatial resolution was generated from the VHR stereoscopic satellite images (GeoEye1, 0.5 meters resolution). The DEM was used to subdivide the study area into slope units and to calculate the topographic factors needed for the evaluation of susceptibility.

### 6.3.3 Geology Map

The lithological units and information regarding structural lineaments such as faults were obtained from existing government cartography (scale 1:50,000) published by the Mexican Geological Service (Sánchez-Rojas and De la Callejera-Moctezuma 2004). Lithology has been widely recognised as a key factor for landslide hazard analysis given that landslide susceptibility is determined by different lithological units (Xu *et al.* 2014). To simplify the model and to reduce the possibility of bias in the statistical susceptibility analysis, the lithological units were organized into two groups: weak rock and hard rock (Cardinali *et al.* 2002; García-Rodriguez *et al.* 2008; Havenith *et al.* 2015). The lutite shale and colluvium units were classified as weak rock, while the primarily limestone, sandstone, limonite, basalt and pyroclastic rocks were classified as hard rock. The pyroclastic units were classified as hard rock due to the high degree of compaction. Xu *et al.* (2014) pointed out that hard rocks show a steeper topography than weak rocks, however, in the study area this is not the case: lutite shale outcrops are characterized by high slope inclination angles similarly to those areas of rocks classified as hard. Using

166

the VHR stereo satellite images, faults and discontinuities were added and a buffer of 150 m was obtained for use as an explanatory landslide susceptibility variable.
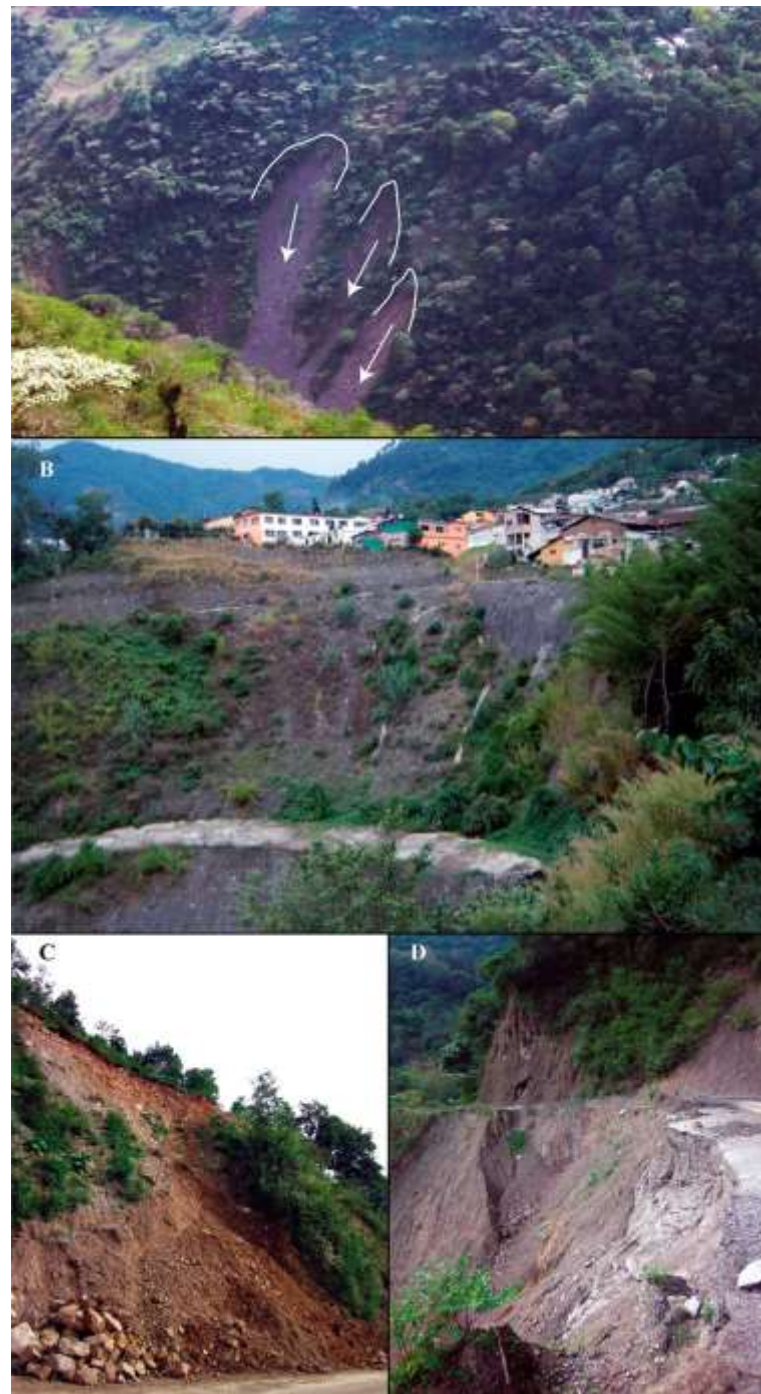


*Figure 70. Examples of landslides in the study area. A) Debris flows near Xilepa town. B) 5 May Street landslide and the control measures (nets and dams) the government put in place after the landslide. C) Translational landslide occurring in the road to Paciotla town, this type of movement is frequent on the roads of all municipalities. D) Complex landslide (slide to flow) which destroyed the road to Cuauneutla de la Paz town.*

### 6.3.4 Land cover

The original vegetation cover in the study area is pine oak and mesophyll forest however, much of it has been deforested and converted into grassland and arable lands. This change of land use took place especially in the second half of the 20th century. For this research, the land cover was obtained through a semi-automatic classification of the GeoEye1 satellite images from 2010. Six classes were considered : (i) forest (mesophyll and pine oak), (ii) altered vegetation, (iii) arable land, (iv) grassland, (v) urban, and (vi) zones without vegetation. The land cover was used as an explanatory variable for the landslide susceptibility analysis.

### 6.3.5 Elements at risk

The information used to generate the vulnerability components was derived from the 2010 national census. This includes statistics about the population. Field surveying, interviews with the inhabitants, and information produced by the VHR satellite images were also used to obtain data regarding the 1955 and 1999 disaster events, roads and infrastructure, and other social aspects. In some cases, satellite images were used to recalculate the population for some spatial units (spatial partitioning of the study area) when the national census data was too general. The average number of inhabitants per house for each town was used as criteria; each house was identified by using the satellite images so that an estimate of the total population of these areas could be obtained.

The spatial unit from the census social information is the so-called "manzana", or "block". The block units are defined by urban features (streets and built-up areas), and/or rural features (rivers, cultivated areas, boundaries of plots of land). Thus the area of these units varies significantly - from a few square metres to a few square kilometers.

### 6.3.6 Landslide susceptibility evaluation and hazard characterization

Landslide susceptibility is the spatial probability that slope failures occur in similar geoenvironmental conditions to which they occurred before (Guzzetti *et al.* 1999, 2006; Chung and Fabbri 1999; Guzzetti 2005). The 54 km$^2$ study area was divided into 259 slope units (SU) using the "WPS tools to support geological and geomorphological mapping" for GRASS 6.4.2 GIS software, developed by Marchesini *et al.* (2012).

The landslide susceptibility was estimated for each SU using the Combination Model developed by Rossi *et al.* (2010). The Combination Model uses different variables related to geomorphology, lithological and land use characteristics and runs four different probability statistical techniques: (i) quadratic discriminant analysis (QDA), (ii) linear discriminant analysis (LDA), (iii) neuronal network analysis (NNA), and (iv) logistic regression (LR).

These statistical techniques are frequently used in the landslide susceptibility literature and have performed reasonably well (Rossi *et al.* 2010). The Combination Model was preferred over a single predictive procedure as it allows the comparison of different results from several multivariate techniques and the possibility of obtaining an optimal landslide susceptibility zonation based on the combination of different forecasts (Rossi *et al.* 2010). The results of each of the four individual models were combined using a logistic regression where the independent variables were derived from the four techniques (QDA, LDA, NNA and LR) to obtain a susceptibility value. The optimal model response was taken as the dependent variable (presence or absence of landslides).

The list of factors was determined based on the environmental conditions of the study area and the scale and quality of the available thematic information. Factors that were used without collinearity problems included: (i) topographic factors (aspect, slope angle, mean elevation, standard deviation of slope angle, and slope general curvature), (ii) geological factors (weak lithology, hard lithology and a 150 m buffer of faults), (iii) anthropic factors (land cover), and (iv) extent of previous landslide. The topographic factors were extracted from a 10 m spatial resolution DEM model. Landslide information was obtained from the inventory. Recent landslides were used as the dependent variable in the statistical models. Two datasets were used to prepare and validate the landslide susceptibility model and map the database of recent landslides: (i) a training dataset including 290 landslides which occurred from 1994 to 2010, and (ii) a validation dataset of 95 landslides which occurred between 2011 and 2012. The Receiver Operator Characteristics (ROC) area under the curve is presented as a confidence parameter for each model. The area under the ROC curve is a measure of test accuracy. The ROC curve describes the capability of the statistical model to discriminate between two types of objects (Frattini *et al.* 2010).

The points on the ROC curve represent the pairs derived from different contingency tables for different cut-off values. A bootstrapping resampling technique was implemented with 200 iterations for LDA, QDA and LR and 20 iterations for NNA (Rossi *et al.* 2010). Cohen's kappa coefficient, useful for measuring the reliability of a classification model (Cohen 1960) was also estimated for each model and combination model result.

The prediction surface was divided into five susceptibility classes: 0-0.20, very low susceptibility; 0.21-0.45, low susceptibility; 0.46- 0.55, medium susceptibility; 0.56-0.80, high susceptibility; and 0.81-1.00 very high susceptibility. Landslide susceptibility was estimated for all 259 of the slope units and this information was combined with the magnitude and frequency data to obtain the landslide hazard. A detailed description of landslide susceptibility procedure for the study area can be found in Murillo-García and Alcántara-Ayala (2015).

The magnitude of the landslides (ML) was obtained from the relationship between the velocity of the movements (PV) and the landslide area (PA).This relationship was used because the magnitude of a landslide is directly related to its destructive power (Guzzetti 2005). Landslide area was obtained using GIS tools and was calculated for each landslide, including the depletion, transport and deposition area. Next, the probability density function of the landslide areas was obtained from power law models (Rossi *et al.* 2012).

Landslide velocity influences destructive power and, therefore, very large area landslides that move slowly are less destructive than very large and very rapid landslides. The velocity of the movements was achieved through a geomorphological inference (e.g. the slope angle and slope length, and the height of the mass movement). Using the magnitude table of Varnes (1978), and taking into account the type of movement and information, the velocity of each recent movement was determined on a range scale: zero for very low movements (0.6 m/year) to 5 for extremely rapid movements (3m/second) (Figure 71). This procedure to estimate the velocity of landslides involves a high level of uncertainty due to the lack of specific field measures and/or correlation of physical features (such as vegetation or soil characteristics) with the velocity of the mass movements. Therefore, this inferred velocity should be taken as an approximation, and more precise research is required.

| Value | Velocity | Description | Type of associated movement | Expected damage to infrastructure | Expected damage to population |
|---|---|---|---|---|---|
| 5 | 3 m/s | Extremely rapid | Debris flows, rockfalls and complex movements | Structural and functional damage | Loss of lives, injuries and indirect damages. |
| 4 | 0.3 m/min | Very rapid | Debris and mudflows, translational landslides | Structural and functional damage | Possible escape and evacuation. Loss of life, injuries and indirect damage. |
| 3 | 1.5 m/day | Rapid | Translational and rotational landslides | Total loss of infrastructure | Indirect damage |
| 2 | 1.5 m/month | Moderate | Rotational landslides | Some damage to the infrastructure located on the displacement mass | Indirect damage |
| 1 | 1.5 m/year | Slow | Rotational deep-seated landslides | Buildings and infrastructure can be functional for a long period | None |
| 0 | 0.6 m/year | Very slow | Creep | None | None |

*Figure 71. Landslide velocity ranges and types of movement and expected damage estimation (Varnes 1978).*

The magnitude of landslides was obtained by classifying the landslides on each slope unit by velocity class; then the median was obtained for each slope unit (VL) and interpolated to 0-1 range value (Eq.(1)). The area of the biggest landslide (ABL) on each slope unit was obtained and this value was related to the frequent landslide area value (341.3 m$^2$) (Eq.(2)) and the result was used to classify the slope unit according to Guzzetti (2005) (Figure 72) and modified by adding the area equivalent to

volume. The AL and VL results were interpolated to values from 0-1 and then related to obtain a Magnitude (ML) value for each slope unit (Eq.(3)).

$$V\_L = [\![ N^{\wedge}(V) ]\!]\_L1 \times V\_LN...)/5 \quad (1)$$

$$A\_L = [\![ 2^{\wedge}(A) ]\!]\_BL \times 341.3) \quad (2)$$

$$M\_L = [\![ 2^{\wedge}(A) ]\!]\_L \times V\_L) \quad (3)$$

The magnitude of landslides was classified into 5 ranges: very low magnitude (0-0.2), low magnitude (0.2-0.45), medium magnitude (0.45- 0.55), high magnitude (0.55-0.8), and very high magnitude (0.8-1).

| Landslide volume (m³) | Estimated area (m²) | Level | Magnitude class |
|---|---|---|---|
| <0.001 | 0-1 | 1 | Extremely low |
| 0.002-0.5 | 1-2 | 2 | Very low |
| 0.5-500 | 3-60 | 3 | Low |
| 500-10,000 | 61-460 | 4 | Medium |
| 10,000-500,000 | 461-6,400 | 5 | High |
| >500,000 | >6,400 | 6 | Very high |
| >>500,000 | >>12,800 | 7 | Extremely high |

*Figure 72. Magnitude classes for landslides according to volume and area (Based on Guzzetti 2005).*

The temporal frequency of the landslide occurrence was determined using the inventory data (landslides which occurred between 1994 and 2010) and a Poisson probability model (Crovelli 2000; Coe *et al.* 2000; Roberds 2005; Guzzetti *et al.* 2005, 2006). The Poisson model is a continuous time model that uses random events that occur independently of natural continuous ordinary time (Guzzetti *et al.* 2005, 2006). The model allows the estimation of landslide temporal probability at different intervals of time based on multi-temporal inventories (Guzzetti *et al.* 2005, 2006). In this study, landslide temporal probability was calculated to 1, 2, 3, 10, 20 and 50 years (Fig. 73). If the colour of the slope unit is red in the 1 year probability map (Figure 6.4), it means that there is a 0.8 higher probability that a landslide will occur in the following year. In the majority of cases, the probability increases with time. Consequently, the maps showing the landslide probability for 10, 20 or 50 years are red.

Finally, landslide hazard (LH) was estimated for each slope unit of the study zone by linking the magnitude of the landslides (ML), the temporal probability of landslide occurrence (3 years probability) (TL) and landslide susceptibility (SL) (Eq.(4)):

$$LH = P(M_L) \times P(T_L) \times P(S_L) \quad (4)$$
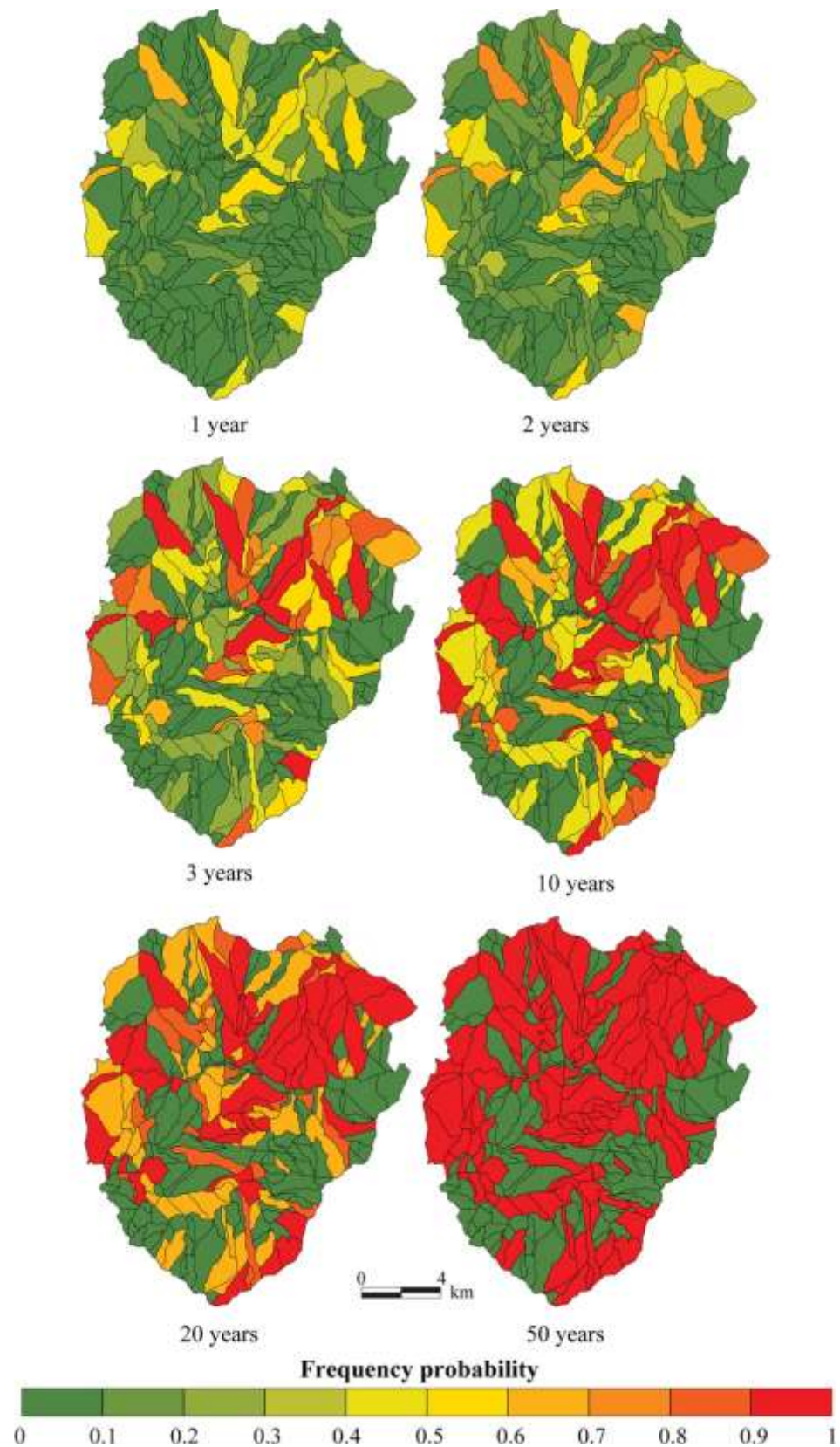
**Figure 73.** *Landslide time frequency probability for different periods.*

### 6.3.7 Vulnerability assessment

In this study, the SAVE model based on indicators (Morales-Manilla 2010) was implemented. The model relies on spatial relations to find patterns of vulnerability. Firstly, it finds patterns based on the analysis of spatial relations among a set of selected indicators (search of patterns), and then defines levels of exposure, sensitivity and resilience to determine a level of vulnerability for each spatial unit (description of patterns). Then, it explains the patterns (why vulnerability is defined by those specific indicators or components), since this would allow the more efficient prediction of patterns. The SAVE model includes four vulnerability elements: (i) population, (ii) infrastructure (building environment), (iii) economic activities, and (iv) natural resources. Indicators for exposure, sensitivity and resilience need to be chosen. Satisfactory indicators for each one of the vulnerability components are necessary: exposure, sensitivity and lack of resilience. The indicators used for the SAVE model were selected taking into account all the levels of damage and difficulties related to the spatial and temporal resolution and quality of available data. The vulnerability element considered in this study was the population (19,559 inhabitants in 2010) of the municipality of Pahuatlán.

The information concerning the slope units were overlaid with the block unit information; this was undertaken by using GIS overlay tools (Figure 74). The result was a new spatial category, in which slope and block units were combined into 316 spatial units. The selected data indicators were standardized values from 0 to 1 (index); the same weighting being assigned for all indicators. To obtain a vulnerability value for each spatial unit, exposure, sensitivity and lack of resilience values were combined. No specific weighting was assigned to the values of the components. The vulnerability for the population was obtained by (Eq.(5)):

$$V = 3\text{^}(EXP \times S \times LR) \qquad (5)$$

where V is the vulnerability of the population, EXP is the exposure of the population, S is the sensitivity of the population, and LR is the lack of resilience.
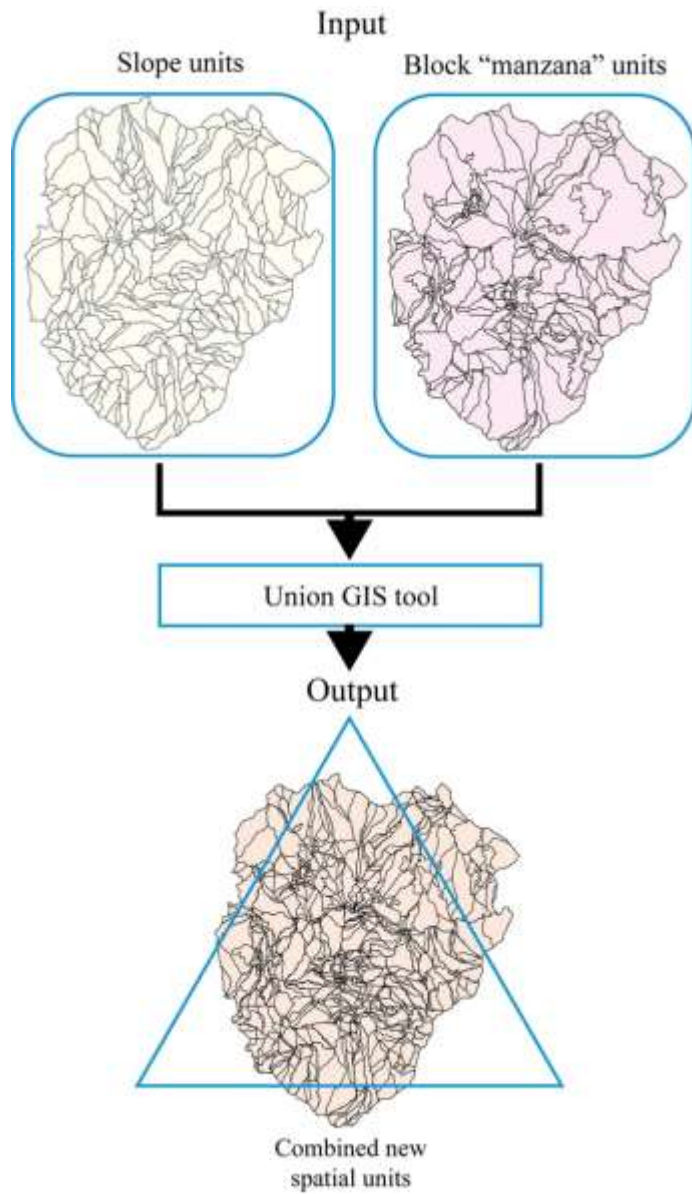
*Figure 74. Overlay procedure to obtain the spatial units used to analyze the estimates of vulnerability and preliminary risk. Slope units and block units (manzana) layers were overlaid onto a GIS to obtain the new spatial units.*

### 6.3.8 Indicators of the exposure

Exposure (0 to 1 values) is qualified in terms of spatial and temporal patterns (Birkmann *et al.* 2013). To estimate the exposure level of the population, seven indicators were taken into account (Eq.(6)):

$$EXP = 5\char`^(S \times TP \times CM \times TE \times PB) \qquad (6)$$

where EXP is the exposition value for population, S is the susceptibility value resulting from the

Combination Model (0-1), TP is the total population index (Fig. 75), CM is the material construction index (Fig. 75), PB is the public building presence (hospital, school, square, etc.) index, and TE is the temporal housing exposure index (Fig. 75).

| Vulnerability component | Measuring concept | Formula | Source | Difficulties |
|---|---|---|---|---|
| Exposure | Total population | $TP = \log(tp)/\log(P)$ | Census | Population included only residents, and not floating population such as tourists. |
| | Construction material | $CM = 1 - \dfrac{he}{TH}$ | Census | Empiric estimation |
| | Public building presence (hospital, school, square, etc.) | $PB = 1 \rightarrow \exists pb$ | INEGI cartography and VHR satellite images | Value of 1 was assigned to public buildings due to lack of more specific data. |
| | Temporary housing exposition index | $TE = \left(\left(\dfrac{SP}{tp}\right)*\left(1-\left(\dfrac{7}{24}\right)\right)\right)$ $+ \left(\left(\dfrac{WP}{tp}\right)*\left(1-\left(\dfrac{9}{24}\right)\right)\right)$ $+ \left(\left(\dfrac{PD}{tp}\right)*\left(1-\left(\dfrac{0}{24}\right)\right)\right)$ | Census | |
| Sensitivity | Population density | $DP = \dfrac{\log\left(\dfrac{tp}{ta}\right)}{\log(hvd)}$ | Census and VHR satellite images | |
| | Population younger than 12 years old | $YP = \dfrac{p < 12}{tp}$ | Census | |
| | Population older than 65 years old | $OP = \dfrac{p > 65}{tp}$ | Census | |
| | Female population | $FP = \log\left(\left(\dfrac{pf}{tp}\right) \times 10\right)$ | Census | |
| | Indigenous population | $IdP = \dfrac{pi}{tp}$ | Census | |
| | Population with physic limitations | $LP = \dfrac{ppl}{tp}$ | Census | |
| | Illiterate population | $IP = \dfrac{ip}{tp}$ | Census | |
| Lack of resilience | Income | $I = \log 10(3^{\wedge}(\left(\dfrac{he}{TH}\right) + \left(1 - \left(\dfrac{hwa}{TH}\right)\right) + \left(\dfrac{hw}{TH}\right))) \times 10)$ | Census | No income measure is available in the census data. |
| | Economically active population | $EAP = \dfrac{eap}{tp}$ | Census | Not all people are employed |
| | Quality and quantity of roads | $R = \dfrac{tr}{60}$ | Field work and VHR satellite images | Empiric estimation |
| | Population with access to the national health services | $SI = \dfrac{psi}{tp}$ | Census | |

*Figure 75. Formulas to obtain the different indicators used in the landslide vulnerability model. TP, total population in the spatial unit; tp, total population on the spatial unit; P, total population of the study area; CM, construction material index; he, houses with dirt floor; TH, total houses in the spatial unit; PB, public building presence index; ∃, means there exist (public building presence is equal to 1 when there are one or more public buildings in the spatial unit); pb, public buildings in the spatial unit; TE, temporary housing exposition index SP, student population that is out of the home 7 hours per day; WP, population not at home due to work during the day; PD, population that does not work or study and was assumed to remain at home; DP, density population index; ta, total area of the spatial unit; hvd, higher population density value for a municipality in Mexico in 2010 (17,000); YP, population younger than 12 years; OP, population older than 65 years index; FP, Female population index, pf, female population in the spatial unit; IdP, indigenous population index; pi, indigenous*

*population in the spatial unit; LP, population with physical limitations index; ppl, population with physical limitations in the spatial unit; IP, Illiterate population index; ip, illiteracy population in the spatial unit; I, income population index; hwa, number of houses with all services; hwn, number of houses without all services; EAP, economically active population index; eap, economically active population in the spatial unit; R, quality and quantity of roads index; tr, number of roads that connect the spatial unit; SI, Population with access to the national health services index; psi, population with access to national health service in the spatial unit.*

Temporality represents a dynamic dimension of the vulnerability concept. People are considered as a non-static entity given their social role and development of activities. In this context, and in order to include dynamics indirectly, the existence of public spaces in each spatial unit was considered. Public spaces like government buildings, churches, squares, schools and markets have a significant concentration of population on a daily basis. Consequently, very high velocity landslides likely to occur in these places may cause loss of life and economic damage. Spaces such as these were considered as being at a high exposure level.

### 6.3.9 Sensitivity indicators

The population sensitivity is defined in this work by the follow indicators (Eq.(7)):

$$S = 7^{\wedge}(DP \times YP \times OP \times FP \times IdP \times LP \times IP) \qquad (7)$$

where S is the sensitivity of the population index (0 to 1 values), DP is the population density index, YP is the index of population younger than 12, OP is the index of population older than 65, FP is the female population index, IdP is the indigenous population index, LP is the population with physical limitations index, and IP is the illiterate population index (Fig. 75). These indicators were chosen based on the literature and on the assumption that there are groups of people with high vulnerability. UN/UNESCO recognizes children as the most vulnerable group followed by the women. Neumayer and Plümer (2007) analyzed 141 disasters around the world and found that gender and disaster are related: in countries where women do not have the same rights as men, the number of women who die in disasters is larger than those countries where there is greater gender equality. As the proportion of men and women is almost the same in all of the spatial units of the study area, it was decided to use the logarithm of the quotient result by dividing the number of women by the total population, to obtain a statistically significant value for this indicator.

Other vulnerable groups are those who are older than 65 and have physical limitations. Indigenous people were included in this category because their first language is not Spanish which is the language of most of the disaster prevention and response information (Alcántara-Ayala *et al.* 2004).

### 6.3.10 Indicators for lack of resilience

In terms of the population, lack of resilience was calculated taking into account how possible it was for people to rebuild their house and recover their goods/assets if destroyed by a landslide event, in addition to the capacity to recover physically if injured by a landslide. Lack of population resilience was estimated as follows (Eq.(8)):

$$LR = 4\textasciicircum(I \times EAP \times R \times SI) \quad (8)$$

where LR is the lack of resilience index (0 to 1 values), I is the income population index, EAP is the economically active population index, R is the road index, and SI is the population with access to the national health insurance service index. Resilience is related to income and a person's employment or occupation. The assumption is that someone with a higher income would have greater capacity to recover from a disaster. The capacity of someone to recover from a health issue resulting from a landslide event would depend on the access to the national public health services. The road index was derived from the assumption that somewhere with better road connections would be more able to receive external emergency help than somewhere with poorer connections.

### 6.3.11 Preliminary estimates of risk

There have been at least three significant landslide events in the region triggered by high precipitation that caused severe damage not only to Pahuatlán but to the entire Sierra Norte de Puebla: (i) the 1955 landslides triggered by hurricane Janet (Alcántara-Ayala 2004), (ii) the 1999 landslide events causing by the tropical depression n°11 (Alcántara-Ayala 2004), and (iii) the events triggered by hurricane Stan in 2005. According to the inhabitants and information available about the consequences of these events, in 1955 severe damage occurred in the main town of Pahuatlán; during the 1999 events, the indigenous population were hardest hit, and in 2005, a landslide located along one of the main streets of Pahuatlán was reactivated. Based on the information about damage recorded for these events, levels of damage for the population according to magnitude and type of landslides were established (Fig. 76) (Reichenbach *et al.* 2005). The damage to population is classified into 3 categories: (i) direct damage, when deaths, missing persons or casualties are expected; (ii) indirect low damage, when minor goods are lost, but not housing or economic activities; and, (iii) indirect severe damage, when goods, housing and economic activities are lost or dramatically affected. For this work, severe damage is expected in spatial units where hazard and vulnerability levels are higher.

| Landslide magnitude | Impact for the population |
|---|---|
| Very low | |
| Rock fall | ND |
| Flows | ND |
| Slides | ND |
| Low | |
| Rock fall | Lw |
| Flows | Lw |
| Slides | Lw |
| Medium | |
| Rock fall | Hi |
| Flows | Hi |
| Slides | Hi |
| High | |
| Rock fall | Hi, D |
| Flows | Hi, D |
| Slides | Hi, D |
| Very high | |
| Rock fall | Hi, D |
| Flows | Hi, D |
| Slides | Hi, D |

*Figure 76. Elements at risk and levels of damage according to the landslide type (Based on Reichenbach et al. 2005): Lw, low indirect damage; Hi, high indirect damage; D, direct damage, ND, no damage.*

Therefore, vulnerability and hazard layers were crossed and levels of preliminary risk for the population were defined according to Figure 77. Hazard and vulnerability classes were categorized from 1 to 5: 1 for very low values and 5 for very high values. For instance, a hazard value of 0.75 corresponds to a high value hazard class and is categorized as number 4; a vulnerability value of 0.88 corresponds to a very high class and number 5 is its assigned category. From those example values, a 4-5 combination is obtained and therefore it is classified as of very high risk.

| Hazard level (M+F+S) | Vulnerability level (of population) | | | | |
|---|---|---|---|---|---|
| | 1 | 2 | 3 | 4 | 5 |
| 1 | 1-1 | 1-2 | 1-3 | 1-4 | 1-5 |
| 2 | 2-1 | 2-2 | 2-3 | 2-4 | 2-5 |
| 3 | 3-1 | 3-2 | 3-3 | 3-4 | 3-5 |
| 4 | 4-1 | 4-2 | 4-3 | 4-4 | 4-5 |
| 5 | 5-1 | 5-2 | 5-3 | 5-4 | 5-5 |

*Figure 77. Levels of risk. M, landslide magnitude; F, Land-slide occurrence frequency; S, landslide susceptibility. Risk classes: 1-1, 1-2 and 2-1 very low risk; 1-3, 2-2, 3-1 low risk; 4-1, 3-2, 2-3, 1-4 medium risk; 5-1, 4-2, 3-3, 2-4, 1-5, 5-2, 4-3, 3-4, 2-5, 3-5, 4-4, 5-3 high risk; 5-4, 4-5 and 5-5 very high risk level.*

### 6.3.12 Possible vulnerability validation strategies

Owing to the lack of official statistical data on damage caused by past landslides in the area of interest, it is not possible to undertake a quantitative validation of the analysis of vulnerability. As an alternative, a qualitative approach is proposed here. Based on the information provided by the local

inhabitants regarding the 1955 and 1999 events, and the information obtained by field surveys for the most recent landslide events, it was possible to establish the general pattern of consequences for the most relevant landslides in the study area (Fig. 78). This information was linked and compared with the vulnerability and risk maps obtained.

| Landslide type | Year | Location | Description | Impact for the population |
|---|---|---|---|---|
| Mudflow | 1955 | Pahuatlán town | Movement which covered the main town with 1.5 m of mud and small rocks. One fatality. | Direct damage and indirect severe damage. |
| Mudflows | 1999 | Cuauneutla | Two movements which destroyed at least ten houses. Injured people and displaced families. | Direct damage indirect severe damage. |
| Rotational landslide (reactivation) | 2005 | Pahuatlán town | A reactivation of a landslide from 1947 and 1955. In 2005 at least three houses were damaged and one small hospital was completely destroyed. No deaths or injuries. | Indirect severe damage. |
| Shallow slide | 2005 | Pahuatlán town | The primary school of the town was damaged and abandoned. | Low indirect damage. |
| Shallow slide | 2010 | Road to Honey town | The new hospital was damaged and closed due to structural damage. | Indirect severe damage. |
| Rotational landslide | 2012 | Xolotla road | The road was destroyed and one house severely damaged. | Direct damage and low indirect damage. |

*Figure 78. Summary of the damages in selected landslides that have taken place in the study area.*

## 6.4 RESULTS

### 6.4.1 Landslide hazard mapping

The susceptibility map of the study area is shown in Figure 79. In order to estimate susceptibility a complete set of validation strategies was available. The script developed for the Rproject by Rossi *et al.* (2010) provided a set of statistical strategies to measure the performance of the model and its prediction capacity; the percent of the sum of true positives and negatives for the training data set was 74.13%, and 75.2% for the validation set, whereas the prediction power obtained by the Receiver Operation Characteristic AUROC curve value was 0.819 and 0.708 for the training and the validation data sets respectively (Fig. 80).

Figure 81 shows the hazard estimation resulting from the relation between landslide susceptibility, frequency and magnitude. All the values of these hazard components were calculated and standardized to values from 0 to 1. Next, hazard values were classified into five categories: very low (0-0.2), low (0.2-0.45), medium (0.45-0.65), high (0.65-0.8), and very high (0.8-1). A value equal to 1 means 100% of certainty for landslide occurrence. Conversely, values close to zero represent a very low probability of landslides. Values near to 0.5 are undesirable as they are interpreted as uncertainty. The map shows that most of Pahuatlán town is located on high or very high hazard areas. A similar situation occurs also in other towns like Zoyatla de Guerrero, Atla, Tlalcruz de Libres, Agua del Machete, Xilepa, San

Pablito and Paciotla (Fig. 81). Additionally, very small areas of San Pablito and Atla towns are located on four slope units classified as low hazard areas. Settlements can be located on slope units classified in terms of the presence or absence of hazards. The hazard classification of slope units depends on the explanatory variables and methods used to estimate.
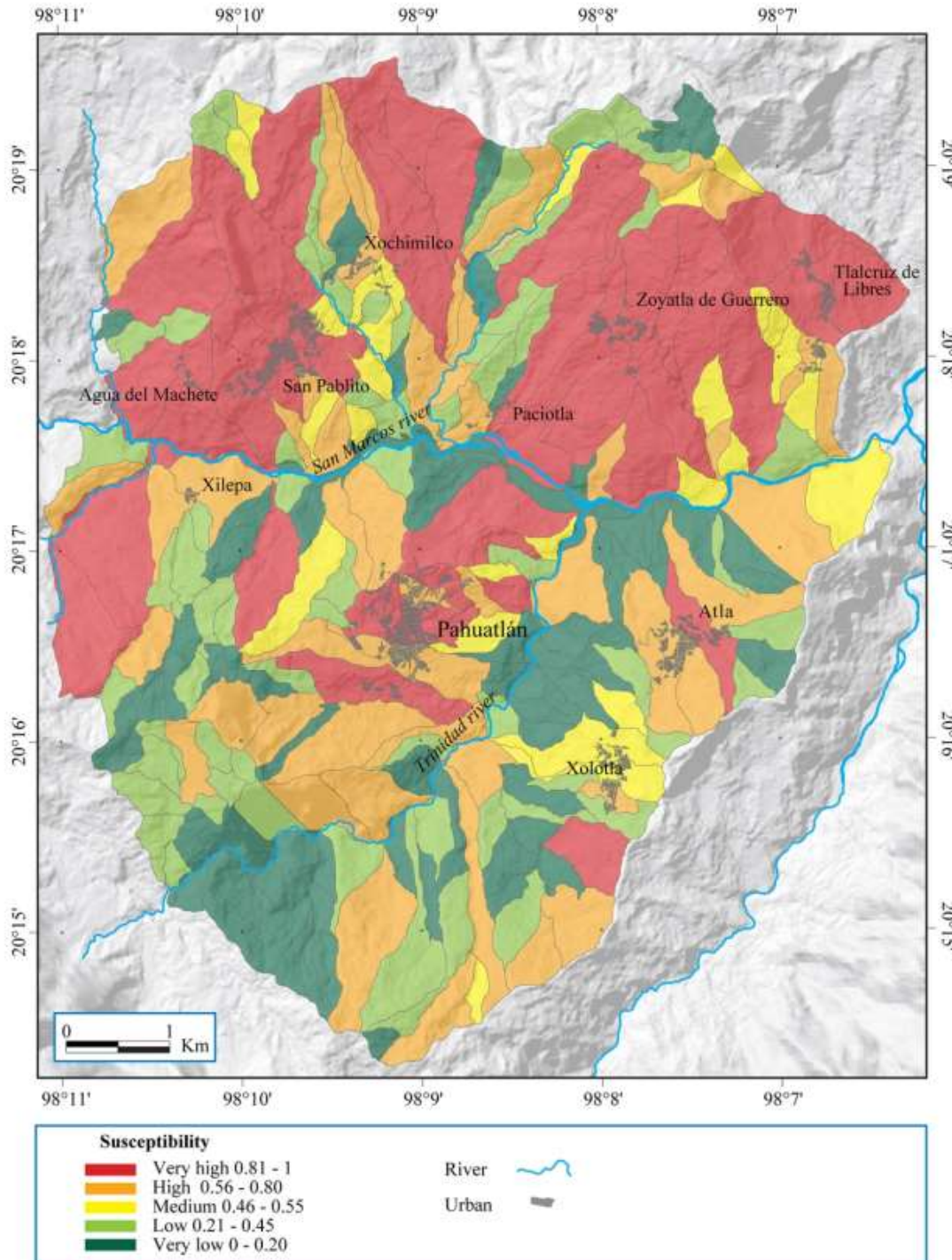


***Figure 79.*** *Landslide susceptibility map for the study area. Many settlements are located on slope units with high and very high susceptibility (orange and red surfaces).*
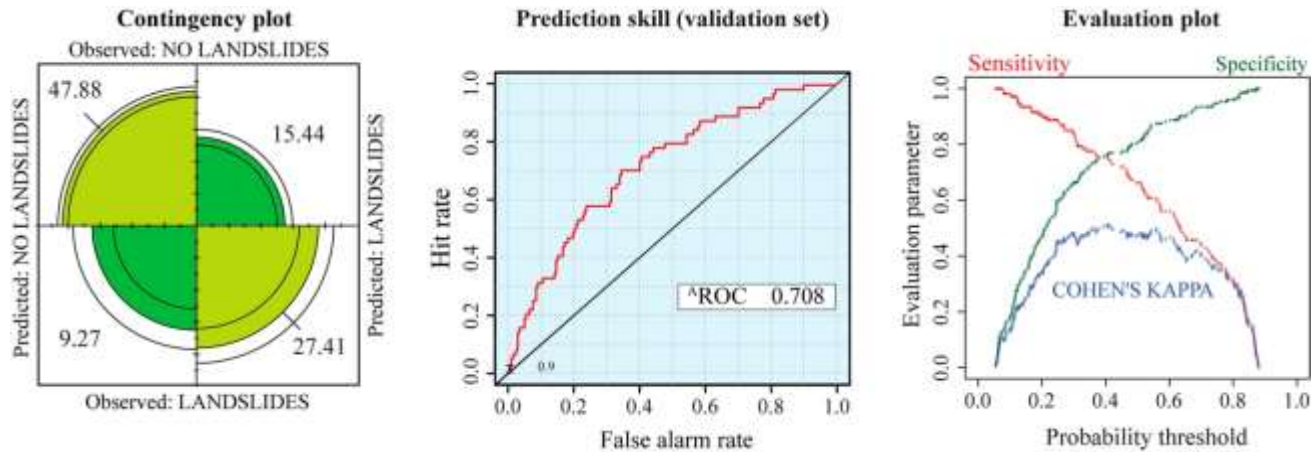
**Figure 80.** *Model results. Contingency tables can also be present as plots. The ROC curve was obtained for the validation data set (prediction skill of the Combination Model). Training ROC value was 0.819 and represents the model fit.*

### 6.4.2 Landslide vulnerability mapping

The results of each vulnerability component – exposure, sensitivity and lack of resilience – were used (according to Eq.(5)) to estimate the landslide vulnerability of the population. 126 spatial units classified as low and very low vulnerability (0-0.45), had very low / had no population. Four polygons were classified as of moderate vulnerability (0.45-0.55) and 169 polygons as of high vulnerability (0.55-0.80). This means that a large percentage of population distributed in the study area has a high level of vulnerability. Finally, 17 polygons were classified as of very high vulnerability (0.80-1). These polygons show very high density population and are situated in the indigenous towns of Xolotla, Atla and Xochimilco, but also in the mestizo (people of American Indian and Spanish mixed cultural heritage) towns of Xilepa and Ahila (Figure 82). Of the study area's total population, 44% was classified as of very high vulnerability, and 55% of high vulnerability. Furthermore, 72% of the indigenous population is also classified in the category of very high vulnerability.
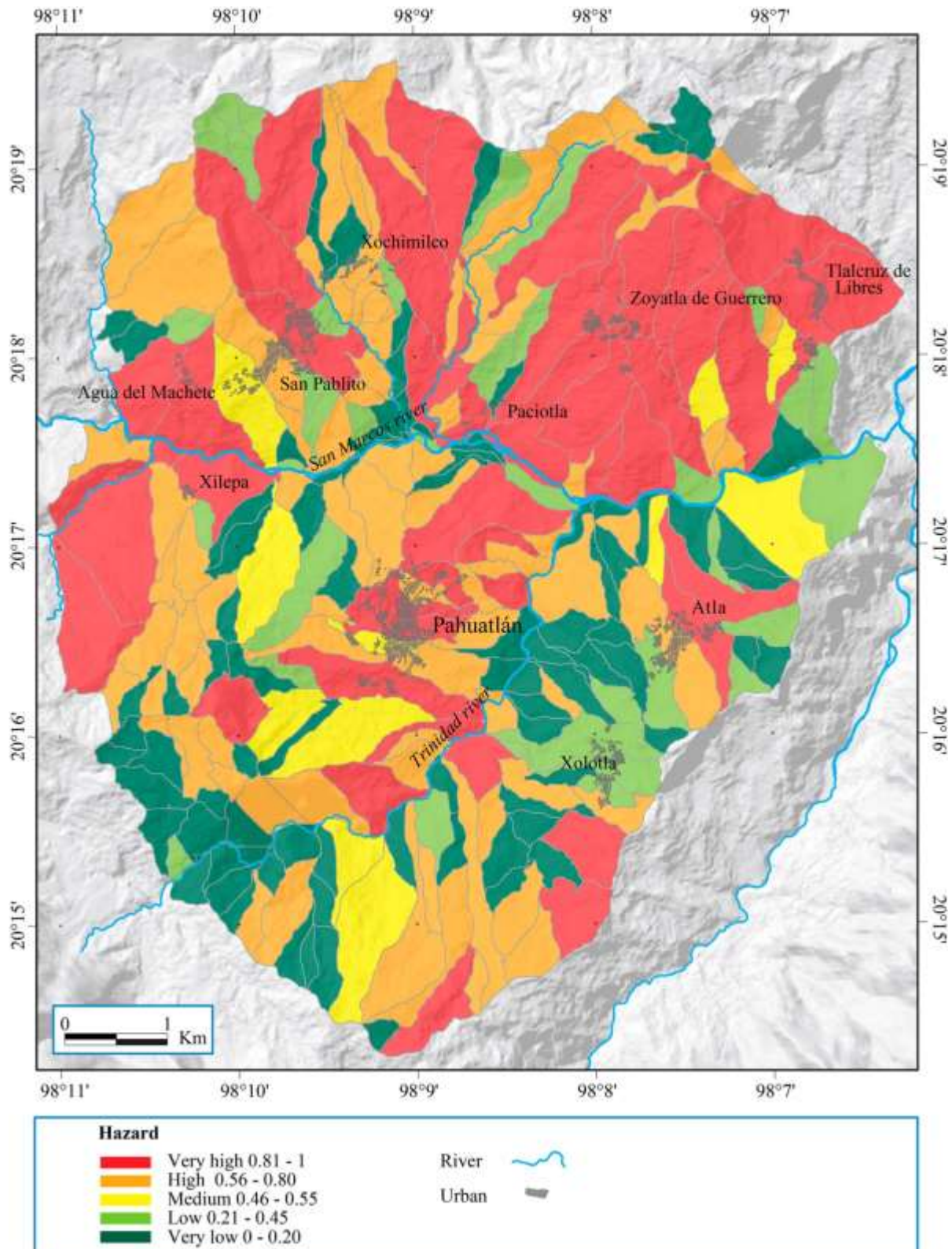
*Figure 81. Hazard map obtained by the combination of susceptibility, time frequency and magnitude results.*
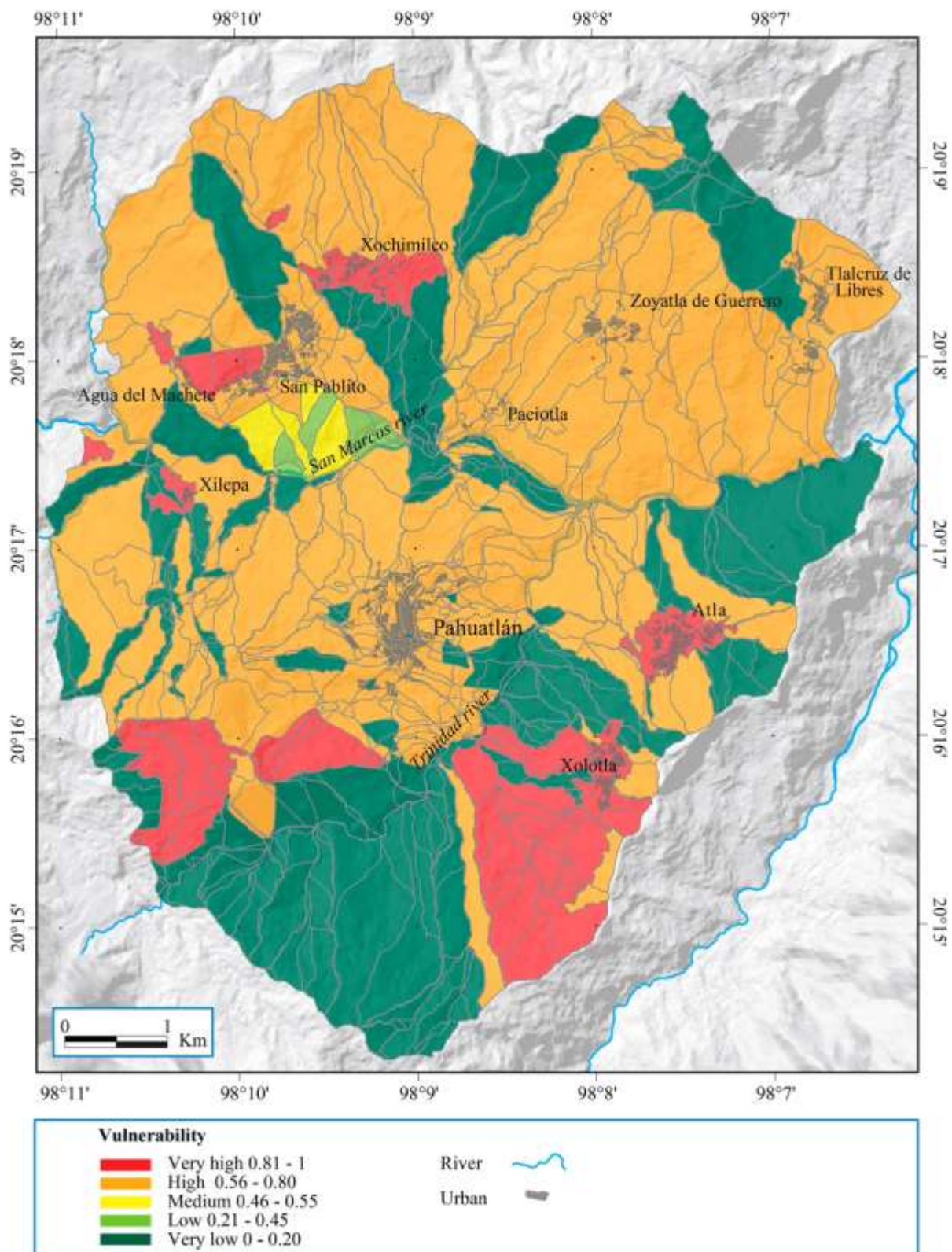
*Figure 82. Vulnerability for the population (new spatial units division).*

### 6.4.3 Risk estimation

Preliminary estimates of risk indicated that some of the blocks situated on the periphery of Pahuatlán town have very high risk values. The same pattern is found in San Pablito and Xilepa towns, and quite clearly, almost all of the spatial units containing the existing towns of the study area have a very high risk value. To understand these results, a detailed analysis was required. As risk depends on the relation between hazard and vulnerability, values of 5-5, 4-5 or 5-4 (Fig. 77) revealed a very high risk value. However, the particular conditions most relevant or with the highest weight in terms of increasing risk in each spatial unit, are quite specific. In some cases, lower hazard values are combined with very high levels of vulnerability; this occurs in the indigenous towns. Conversely, the Pahuatlán town centre showed high hazard values but since the population living in this area are economically better off, levels of vulnerability and risk are not as high as in other areas. The spatial distribution of preliminary risk can be seen in Figure 83.

### 6.4.4 Validation

A qualitative validation of the analysis was carried out based on the damage caused by the most important landslide events which occurred in the area of study. The majority of landslides registered by field surveys affected roads (low indirect damage); only a few mass movement processes in the history of Pahuatlán seriously affected the population (Fig.78). The temporal and spatial distribution of the events mentioned in Figure 78 varies significantly (1955, 1999 and 2005) as three of them occurred in the urban area of the municipal capital and the others in rural areas.

The socio-economic conditions of Pahuatlán in 1955 were quite different from today. However, the landslide event of 1955 demonstrated that Pahuatlán town centre can be affected by medium or large magnitude landslides (level 4 to 6 according to Figure 72). Although the population in this area is well off economically, it also happens to be where the population is most involved in commercial, religious and recreational activities.

The centre of Pahuatlán is also the place where the municipal government offices are located. As a result, these areas can also be considered vulnerable and at high risk. On the maps generated it is possible to identify that the whole of the centre of Pahuatlán is considered to be of high vulnerability and risk, with the exception of one block unit located to the south of the centre of the town.
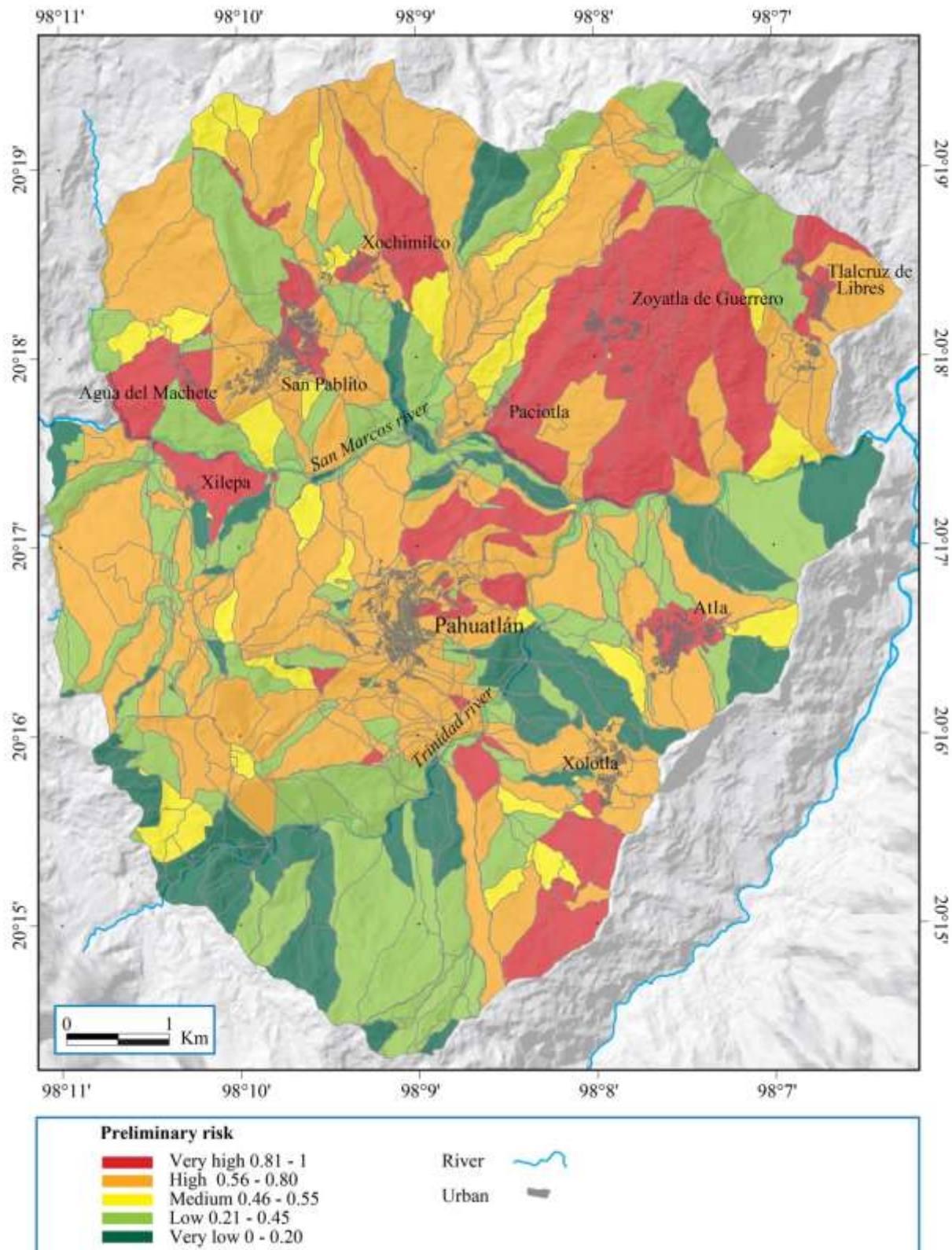
***Figure 83.*** *Preliminary risk map.*

The recent landslides that occurred near the centre of the town show that those affected were not only the people who lost their homes, but also, in an indirect way, the total population as they depend on public health services and local schools. This can be regarded as a high indirect damage and thus landslides affecting the town could cause severe consequences for the population of the whole municipality.

On the other hand, the landslides that took place in 1999 in Cuauneutla de la Paz, a town located outside the area of study, are helpful to illustrate the way low or medium magnitude landslides (level 3 or 4 at Figure 72) can affect people who are considered to be of high vulnerability. People who lost their houses in Cuauneutla had a low income and were agriculture-dependent. Since their houses were not made of robust materials, the level of loss was extremely high even on low magnitude landslides. It is expected that a similar situation could be repeated in block units with high levels of vulnerability and hazard.

Finally, the Xolotla road landslide was regarded as a high magnitude landslide (level 5 according Figure 72); a new road from Xolotla town to Mamiquetla town was damaged. The area was classified as being of a very high level of hazard, very high vulnerability (it is an indigenous area) and consequently of very high risk. The landslide destroyed the road, thereby isolating Mamiquetla (a small town) and one house (built with bricks and concrete) was seriously affected. The family was evacuated and the house was most likely irreparable.

## 6.5 DISCUSSIONS

There are aleatory uncertainties, related to the real variability of the process or phenomena under study, and epistemic uncertainties related to the measure, limited information and the model characteristics and limitations (Ciurean *et al.* 2013; Eidsvig *et al.* 2014a). The first kind of uncertainty is inevitable, while for the second, measurement methods and models can be improved (Ciurean *et al.* 2013). Most values adopted in landslide risk analysis are based on the experience of previous events and on common sense (Glade and Crozier 2005). The latter means that a 100% precise risk evaluation is not likely to be achieved. Furthermore, risk, hazard and vulnerability estimation are carried out with limited information and resources (Ciurean *et al.* 2013). The hazard estimation undertaken in this work was developed largely using statistical methods and showed acceptable results. This approach is based on the analysis of the occurrence of past landslides allowing the statistical estimation and the evaluation of the performance of predictive models. Some issues with estimating landslide susceptibility remain under discussion such as the scale, the factors selected and the technique used to apply the models. Which factors are selected depends on the availability and quality of the information,

along with the specific geo-environmental conditions of the study area. Consequently, a standard list of factors is not recommended, although it is clear that there are some critical factors related to the topography and geology that cannot be excluded when estimating landslide susceptibility. In recent years, the importance of validation strategies has increased and thus it is increasingly common to find a validation phase described in landslide susceptibility methodologies in current literature. Contrastingly, works which concern frequency and magnitude are scarce and there is no agreement on their definition in terms of landsliding. The criteria used in this work to classify landslide velocity could be improved in order to reduce the subjectivity inherent in heuristic estimations. This is particularly difficult for very fast movements such as mudflows or debris flows, or for regions like our study area where no previous landslide studies had been carried out. In Pahuatlán slow and very slow movements have taken place but there is no information available about the precise velocity of these landslides. As a result, more attention needs to be paid to these topics especially when there is a lack of detailed data available.

There is no doubt that epistemic uncertainties for vulnerability estimation depend on the right selection of parameters (input data) and how the model is implemented. The selection of vulnerability indicators involves is highly empirical and subjective, and so validation becomes very difficult and sometimes only possible when there is precise information regarding the occurrence of previous disaster events. The revision of the indicators and the weight hierarchy of vulnerability values is necessary to achieve a better approach. In this sense, the validation of the vulnerability models within the study of disasters is very important (Dominey-Howes and Papathoma-Köhle 2007). In this case, the quantitative validation of vulnerability results by considering the consequences of the 1999 event was not possible or advisable. This is because the socio-economic conditions of the population in the 1999 event were different from current ones and the resolution of the data at that time (1995 information) is lower than the available data from 2010. In this situation, only qualitative evaluation is possible.

The lack of an established methodology to estimate and quantify vulnerability is more controversial than that used in hazard assessment; as a consequence, more refined statistical criteria are needed to select the indicators to estimate vulnerability. Ciurean *et al.* (2013) pointed out that one possibility for reducing the aleatory uncertainties related to risk estimation is the use of data-mining approaches for the selection of the most important parameters. The latter cannot be achieved where no precise statistical information about the damage of previous disaster events exist.

The study area analysed here has specific socioeconomic conditions. The vulnerability indicators selected for this study area might not be adequate nationally or possibly not even for neighbouring regions. For example, the indigenous component has to be applied in places where there is a significant indigenous; yet it makes no sense to take into account a variable regarding homeless population since

there were no homeless people in the study area. Other issues concerning politics or governance also play a significant role in shaping vulnerability, however they cannot be easily measured and most importantly, they are beyond the scope of the present work. Walters and Gaillard (2014) suggested that marginalized groups as women, children, older people, physically disabled people and diverse ethnic groups received significant attention in the disaster literature while other groups inspired less academic and policy interest. Another limitation is the scale of the information available, especially in the population data. The ideal level aggregation for detailed vulnerability assessment is the single person. Nevertheless, there is no information available at this level. The issue becomes particularly problematic as vulnerability involves the responses of individuals, groups of individuals and social networks to hazards (Pamungkas *et al.* 2014). What kind of data base that would be needed to reflect individuals, groups or communities affected by disasters, is indeed a difficult question to be answered. The time dimension is another limitation: the SAVE model as applied here focuses on assessing vulnerability levels, not on the evaluation of the adaptation of scenarios. Thus, research that can be expanded to the evaluation of adaptation is necessary (Adger 2006; Pamungkas *et al.* 2014).

Further, in terms of hazard estimation, landslide events are the dependent variable, however, the definition of the dependent variable for vulnerability estimation is not so obvious; more data and precise analysis in order to understand the role of vulnerability for the generation of landslide disasters are required. Unfortunately, there are no comprehensive studies which discuss the estimation of the vulnerability of certain elements including economy, culture and/or natural resources, among others. Compared with other approaches, indicator based models have advantages and disadvantages in contrast with matrix and curve approaches.

Vulnerability curve approaches are based on the intensity and the degree of loss. This type of approach is very useful when infrastructure is the vulnerability subject. However, if the vulnerability subject is population, then expressing the degree of loss is rather complicated. The death of a person can be given the highest value of loss: 100%. However, other consequences or damages for the individuals, groups or communities could be difficult to measure. Curve approaches are a better option for infrastructure (and maybe other vulnerability subjects) but there are only very few examples of their use for population. Liu and Lei (2003) calculated social vulnerability by using the density population as an expression of the potential maximum life loss, combined with age, education and wealth; however validation process was not included. Duan *et al.* (2011) and Eidsvig *et al.* (2014b) also focused their methods on the population but they did not present a validation strategy. Eidsvig *et al.* (2014a) suggested a method to estimate the uncertainties of models based on curves. The degree of loss was obtained empirically by using photographs on which the damage to buildings by debris flows was

shown. The measure of uncertainty in the models was carried out by statistical methodologies. Sadly, these tools cannot be applied to indicator approaches. Without a solid estimate of vulnerability, risk analysis cannot be considered to be complete. Most importantly, risk analysis cannot be exclusively a result of a spatial cross overlapping of vulnerability and hazard maps or indicators. Therefore, the results presented here are considered as preliminary. It is necessary to understand the expected damage for each element at risk and the consequences over time, in order to create different disaster risk scenarios and analyse various potentially adequate response strategies.

## 6.6 CONCLUSIONS

Diverse tools and models were used to estimate landslide hazard and vulnerability for a 54 km$^2$ study area in the municipality of Pahuatlán in central Mexico. The study area was divided into slope units to implement the combination model to estimate landslide susceptibility. Additionally a Poisson model was used to calculate the probability of landslide frequency. Finally, the estimation of distribution of the landslide area combined with a heuristic approach to landslide velocity range was used to estimate landslide magnitude. The combination of these results was used to obtain a hazard value for each slope unit at the study area.

Vulnerability for the population was estimated using an indicator-based approach. The results for the landslide hazard estimation were acceptable nevertheless, improvements to the method for calculating the landslide velocity are needed to reduce the uncertainty inherent in the heuristic approaches. In the same vein, selection of vulnerability indicators for the population must be based on statistical data, thus highlighting the importance of studies focusing on damage register and inventory. One of the prominent limitations of the vulnerability assessment performed in this work is the lack of a precise evaluation mechanism. A general qualitative validation based on relatively few important landslide events causing severe damage to the population was carried out. Improvement and further discussion regarding this topic is necessary, as this is not an isolated example of areas where data is lacking.

Due to the uncertainties associated with the accuracy of landslide velocity classification, in terms of hazard, and of the heuristic selection of vulnerability indicators, the approach proposed here can be considered as a useful attempt to link hazard and vulnerability. Worldwide, landslide hazard assessments have been widely developed satisfactorily by using various approaches, however, due to its complexity as a dynamic process in time and space, the estimation of landslide vulnerability remains the major challenge.

# References

Adger WN (2006) Vulnerability. Global Environmental Change 16: 268-281. DOI: 10.1016/j.gloenvcha.2006.02.006

Akbas SO, Blahut J, Sterlacchini S (2009) Critical assessment of existing physical vulnerability estimation approaches for debris flows. In: Malet JP *et al.* (eds.), Proceedings of landslide processes: from geomorphologic mapping to dynamic modeling, Strasbourg, 6-7 February 2009. pp 229- 233.

Alcántara-Ayala I (2004) Hazard assessment of rainfall induced landsliding in Mexico. Geomorphology 61: 19-40. DOI: 10.1016/j.geomorph.2003.11.004

Alcántara-Ayala I, López Mendoza M, Melgarejo Palafox G, *et al.* (2004) Natural hazards and risk communication strategies among indigenous communities: shedding light on accessibility in Mexico's mountains. Mountain Research and Development 24-4: 298-302. DOI: 10.1659/0276-4741(2004)024[0298:NHARCS]2.0.CO;2

Alcántara-Ayala I (2008) On the historical account of disastrous landslides in Mexico: the challenge of risk management and disaster prevention. Advances in Geociences-ADGEO 14: 159-164. DOI: 10.5194/adgeo-14-159-2008

Alexander D (2005) Vulnerability to landslides. In: Glade T *et al.* (eds.), Landslide hazard and risk. Wiley. Chichester, UK. pp 175-198.

Bell R, Glade T (2004) Quantitative risk analysis for landslides - Examples from Bildudalur, NW-Iceland. Natural Hazards and
Earth System Sciences 4: 117-131. DOI: 10.5194/nhess-4-117- 2004

Birkmann J (2006) Measuring vulnerability to promote disaster-resilient societies: conceptual frameworks and definitions. In: Birkmann J (ed.), Measuring vulnerability to natural hazards. Towards Disaster Resilient Societies. United Nations University Press. Hong Kong. pp 9-54.
Birkmann J, Cardona OD, Carreño ML, *et al.* (2013) Framing vulnerability, risk and societal responses: the MOVE framework. Natural Hazards 67: 193-211. DOI: 10.1007/s11 069-013-0558-5

Blaikie P, Cannon T, Davies I, *et al.* (1994) At Risk. Natural Hazards, People's Vulnerability and Disasters. Routledge. p 275.

Bohle HG (2001) Vulnerability and Criticality: Perspectives from Social Geography. IHDP Update 2/2001, Newsletter of the International Human Dimensions Programme on Global Environmental Change 1-7.

Cardinali M, Reichenbach P, Guzzetti F, *et al.* (2002) A geomorphological approach to the estimation of landslide hazard and risk in Umbria, Central Italy. Natural Hazards and Earth System Science 2: 1-16. DOI: 10.5194/nhess-2-57-2002

Chambers R, Conway G (1992) Sustainable Rural Livelihoods: Practical Concepts for the 21st Century. IDS Discussion Paper 296, Brighton: Institute of Development Studies.

Chung CJF, Fabbri AG (1999) Probabilistic prediction models for landslide hazard mapping. Photogrammetric Engineering & Remote Sensing 65(12): 1389-1399.

Ciurean R, Schröter D, Glade T (2013) Conceptual Frameworks of Vulnerability Assessments for Natural Disasters Reduction. In: Tiefenbacher J (ed.) Approaches to Disaster Management - Examining the Implications of Hazards, Emergencies and Disasters. InTech. Croatia. pp 3-32.

Cohen, J (1960) A coefficient of agreement for nominal scales. Educational and Psychological Measurement 20: 37-46.

Coe JA, Michael JA, Crovelli RA, *et al.* (2000) Preliminary map showing landslide densities, mean recurrence intervals, and exceedance probabilities as determined from historic records, Seattle, Washington. U.S. Geological Survey Open-File Report 00-303.

Corominas J, Moya J (2008) A review of assessing landslide frequency for hazard zoning purposes. Engineering Geology 102: 193-213. DOI: 10.1016/j.enggeo.2008.03.018

Corominas J, Copons R, Moya J, *et al.* (2005) Quantitative assessment of the residual risk in a rockfall protected area. Landslides 2: 343-357. DOI: 10.1007/s10346-005-0022-z

Crovelli R (2000) Probability models for estimation of number and costs of landslides. U.S. Geological Survey Open File Report 00-249. p 23.

Cutter SL (1996) Vulnerability to environmental hazards. Progress in Human Geography 20: 4529-539 Dominey-Howes D, Papathoma-Köhle M (2007) Validating a tsunami vulnerability assessment model (the PTVA model) using field data from the 2004 Indian Ocean Tsunami. Natural Hazards 40: 113-136. DOI: 10.1007/s11069-006-0007-9

Duan M, Gao Q, Wan Y, *et al.* (2011) Assessing vulnerability and adaptation responses to rainfall related landslides in China, a case study of Enshi Prefecture in Hubei Province. Procedia Environmental Sciences 11: 1379-1385. DOI:10.1016/j.proenv.2011.12.207

Eidsvig UMK, Papathoma-Köhle M, Dub J, *et al.* (2014a) Quantification of model uncertainty in debris flow vulnerability assessment. Engineering Geology 181: 15-26. DOI: 10.1016/j.enggeo.2014.08.006

Eidsvig UMK, McLean A, Vangelsten BV, *et al.* (2014b) Assessment of socioeconomic vulnerability to landslides using an indicator-based approach: methodology and case studies. Bulletin of Engineering Geology and the Environment 73(2): 307-324. DOI: 10.1007/s10064-014-0571-2

Fell R (1994) Landslide risk assessment and acceptable risk. Canadian Geotechnical Journal 31: 261-272

Finlay PJ, Fell R (1997) Landslides: risk perception and acceptance. Canadian Geotechnical Journal 34: 169-188

Frattini P, Crosta GB, Carrara A (2010) Techniques for evaluating the performance of landslide susceptibility models. Engineering Geology 111: 62-72. DOI: 10.1016/j.enggeo.2009.12.004

Fuchs S, Heiss K, Hübl J (2007) Towards an empirical vulnerability function for use in debris flow risk assessment. Natural Hazards and Earth System Sciences 7: 495-506. DOI: 10.5194/nhess-7-495-2007

Fuchs S, Kuhlicke C, Volker M (2011) Editorial for the special issue: vulnerability to natural hazards the challenge of integration. Natural Hazards 58: 609-619. DOI: 10.1007/s11069-011-9825-5

Galli M, Guzzetti F (2007) Landslide vulnerability criteria: a case study from Umbria, Central Italy. Environment Management 40: 649-664. DOI:10.1007/s00267-006-0325-4

García-Rodríguez MJ, Malpica JA, Benito B, *et al.* (2008) Susceptibility assessment of earthquake-triggered landslides in El Salvador using logistic regression. Geomorphology 95:172–191. DOI: 10.1016/j.geomorph.2007.06.001

Glade T, Crozier M (2005) A review of scale dependency in landslide hazard and risk analysis. In: Glade T *et al.* (eds.), Landslide hazard and risk. John Wiley and Sons. England. pp 75-138. DOI: 10.1002/9780470012659.ch3

Ghosh S, Carranza E, van Westen CJ, *et al.* (2011) Selecting and weighting spatial predictors for empirical modeling of landslide susceptibility in the Darjeeling Himalayas (India). Geomorphology 131: 35-56. DOI: 10.1016/j.geomorph.2011.04.019

Guzzetti F (2005) Landslide Hazzard and Risk Assessment. PhD thesis, Bonn University, Bonn, Germany. p10

Guzzetti F, Carrara A, Cardinali M, *et al.* (1999) Landslide hazard evaluation: a review of current techniques and their application in a multi-scale study, Central Italy. Geomorphology 31: 181-216. DOI: 10.1016/S0169-555X(99)00078-1

Guzzetti F, Reichenbach P, Cardinali M, *et al.* (2005) Probabilistic landslide hazard assessment at the basin scale. Geomorphology 72: 272-299. DOI: 10.1016/j.geomorph.2005.06.002

Guzzetti F, Galli M, Reichenbach P, *et al.* (2006) Landslide hazard assessment in the Collazzone area, Umbria, Central Italy. Natural Hazards and Earth System Sciences 6:115-131, DOI: 1684-9981/nhess/2006-6-115

Havenith HB, Torgoev A, Schlögel R, *et al.* (2015) Tien Shan Geohazards Database: Landslide susceptibility analysis. Geomorphology 249:32-43. DOI:10.1016/j.geomorph. 2015.03.019

Highland LM (2003) An account of preliminary landslide damage and losses resulting from the February 28, 2001, Nisqually, Washington, Earthquake. U.S. Geological Survey Open-File report 03-211. Available online: http://pubs.usgs.gov/of/2003/ofr-03-211, accessed on 19 April 2017

INEGI (2009) Prontuario de información geográfica municipal de los Estados Unidos Mexicanos. Pahuatlán, Puebla. INEGI.
(In Spanish)

INEGI (2011) Panorama sociodemográfico de Puebla. INEGI. (In Spanish)

Kappes MS, Papathoma-Köhle M, Keiler M (2012) Assessing physical vulnerability for multi-hazards using an indicatorbased methodology. Applied Geography 32: 577-590. DOI: 10.1016/j.apgeog.2011.07.002

Kanungo DP, Arora MP, Sarkar S, *et al.* (2006) A comparative study of conventional, ANN black box, fuzzy and combined neural and fuzzy weighting procedures for landslide susceptibility zonation in Darjeeling Himalayas. Engineering Geology 85: 347-366. DOI:10.1016/j.enggeo.2006.03.004

Kaynia AM, Papathoma-Köhle M, Neuhaüser B, *et al.* (2008) Probabilistic assessment of vulnerability to landslide: application to the village of Lichtenstein, Baden-Württemberg, Germany. Engineering Geology 101: 33-48. DOI: 10.1016/j.enggeo.2008.03.008

Komac M (2006) A landslide susceptibility model using the Analytical Hierarchy Process method and multivariate statistics in perialpine Slovenia. Geomorphology 74: 17-28. DOI: 10.1016/j.geomorph.2005.07.005

Leone F, Aesté JP, Leroi E (1996) Vulnerability assessment of elements exposed to mass-movement: working toward a better risk perception. In: Senneset K (ed.), Landslides Gliseements de Terrain. Balkema. Rotterdam, Holland. pp 263-270.

Li Z, Nadim F, Huang H, Uzielli M, *et al.* (2010) Quantitative vulnerability estimation for scenario-based landslide hazards. Landslides 7(2): 125–134. DOI: 10.1007/ s10346-009-0190-3

Liu X, Lei J (2003) A method for assessing regional debris flow risk: an application in Zhaotong of Yunnan province (SW China). Geomorphology 52: 181-191. DOI: 10.1016/S0169- 555X(02)00242-8

Lu P, Catani F, Tofani V, *et al.* (2014) Quantitative hazard and risk assessment for slow-moving landslides from Persistent Scatterer Interferometry. Landslides 11: 685-696. DOI: 10.1007/s10346-013-0432-2

Marchesini I, Rossi M, Alvioli M, *et al.* (2012) WPS tools to support geological and geomorphological mapping. In: Ertz O *et al.* (eds.) Proceedings of the OGRS 2012 (Open Source Geospatial Research &Education Symposium). Yverdon-les-Bains Switzerland. pp 280-287.

Mavrouli O, Corominas J (2010) Rockfall vulnerability assessment for reinforced concrete buildings. Natural Hazards and Earth System Science 10 (10):2055-2066. DOI: 10.5194/ nhess-10-2055-2010

Mejia-Navarro M, Wohl LEE, Oaks SD (1994) Geological hazards, vulnerability, and risk assessment using GIS: model for Glenwood Springs, Colorado. Geomorphology 10: 331–354

Maquaire O, Weber C, Thiery Y, *et al.* (2004) Current practices and assessment tools of landslide vulnerability in mountainous basins. Identification of exposed elements with a semi-automatic procedure. In: Lacerda W *et al.* (eds.) Landslides evaluation and stabilization, Proceedings of the 9th International Symposium on Landslides, Río de Janeiro, Brazil. Balkema, Rotterdam. pp 171-176.

Michael-Leiba M, Baynes F, Scott G (2000) Quantitative landslide risk assessment of Cairns, Australia. In: Bromhead E *et al.* (eds.), Landslides in research, Theory and practice. Thomas Telford. London, UK. pp 1059-1064

Michael-Leiba, Baynes F, Scott G, *et al.* (2003) Regional landslide risk to the cairns community. Natural Hazards 30: 233–249. DOI: 10.1023/A: 1026122518661

Morales-Manilla LM (2010) A common spatial approach to vulnerability assessment. GI Forum 2010, July 6-9-2010. Salzburg, Austria.

Mousavi M, Omidvar B, Ghazban F, *et al.* (2011) Quantitative risk analysis for earthquake-induced landslides—Emamzadeh Ali, Iran. Engineering Geology 122:191-203. DOI: 10.1016/j.enggeo.2011.05.010

Murillo-García FG, Alcántara-Ayala I (2015) Landslide susceptibility analysis and mapping using statistical multivariate techniques: Pahuatlán, Puebla, Mexico. In: Wu W (ed.) Recent advances in modelling landslides and debris flows. Springer. Switzerland. pp 179-194

Murillo-García F, Alcántara-Ayala I, Ardizzone F, *et al.* (2015) Satellite stereoscopic pair images of very high resolution: a step forward for the development of landslide inventories. Landslides 12(2): 277-291. DOI: 10.1007/s10346-014-0473-1

Negulescu C and Foerster E (2010) Parametric studies and quantitative assessment of the vulnerability of a RC frame building exposed to differential settlements. Natural Hazards and Earth System Sciences. 10: 1781-1792. DOI: 10.5194/nhess-10-1781-2010

Neumayer E, Plümper T (2007) The gendered nature of natural disasters: the impact of catastrophic events on the gender gap in life expectancy, 1981–2002. Annals of the Association of American Geographers 97(3): 551-566. DOI: 10.1111/j.1467-8306.2007.00563.x

Pamungkas A, Bekessy S, Lane R (2014) Vulnerability Modelling to Improve Assessment Process on Community Vulnerability. Procedia - Social and Behavioral Sciences 135: 159–166.

Papathoma-Köhle M, Neuhäuser B, Ratzinger K, *et al.* (2007) Elements at risk as a framework for assessing the vulnerability of communities to landslides. Natural Hazards and Earth System Sciences 7: 765-779. DOI: 10.5194/nhess-7-765-2007

Papathoma-Köhle M, Kappes M, Keiler M, *et al.* (2011) Physical vulnerability assessment for alpine hazards: state of the art and future needs. Natural Hazards 58: 645-680. DOI: 10.1007/s11069-010-9632-4

Papathoma-Köhle M, Keiler R, Totschnig T, *et al.* (2012) Improvement of vulnerability curves using data from extreme events: debris flow event in South Tyrol. Natural Hazards 64: 2083-2105. DOI: 10.1007/s11069-012-0105-9

Papathoma-Köhle M, Zischg A, Fuchs S, *et al.* (2015) Loss estimation for landslides in mountain areas - An integrated toolbox for vulnerability assessment and damage documentation. Environmental Modelling & Software 63: 156-169. DOI: 10.1016/j.envsoft.2014.10.003

Parkash S (2013) Capacity development for landslide risk reduction in India. In: Sassa K *et al.* (eds.), Landslides: global risk preparedness. Springer. Berlin, Germany. pp 371-385.

Peng L, Xu S, Hou J, *et al.* (2015) Quantitative risk analysis for landslides: the case of the Three Gorges area, China. Landslides 12: 943-960. DOI: 10.1007/s10346-014-0518-5

Petrucci O, Gullà G (2010) A simplified method for assessing landslide damage indices. Natural Hazards 52: 539-560. DOI: 10.1007/s11069-009-9398-8

Quan Luna B, Blahut J, Van Westen CJ, *et al.* (2011) The application of numerical debris flow modelling for the generation of physical vulnerability curves. Natural Hazards and Earth System Sciences 11: 2047-2060. DOI: 10.5194/nhess-11-2047-2011

Ragozin AL (1996) Modern problems and quantitative methods of landslide risk assessment. In: Senneset K (ed.), Landslides - Glissements de Terrain, Balkema. Rotterdam, Holland, pp. 339-344.

Reichenbach P, Galli M, Cardinali M, *et al.* (2005) Geomorphologic mapping to assess landslide risk: concepts, methods and applications in the Umbria Region of central Italy. In: Glade T *et al.* (eds.), Landslide risk assessment. John Wiley and Sons. England. pp 75-138. DOI: 10.1002/9780470012659.ch3

Roberds W (2005) Estimating temporal and spatial variability and vulnerability. In: Hungr O *et al.* (eds.), Landslide Risk Management. Taylor & Francis Group U.S. pp 129-157.

Rossi M, Guzzetti F, Reichenbach P, *et al.* (2010) Optimal landslide susceptibility zonation based on multiple forecasts. Geomorphology 114: 129-142. DOI: 10.1016/j.geomorph.2009.06.020

Rossi M, Ardizzone F, Cardinalli M, *et al.* (2012) A tool for the estimation of the distribution of landslide area in R. Geophysical Research Abstracts, 14, EGU2012-9438-1. Vienna, Austria. p 9438.

Sánchez-Rojas LE, De la Callejera-Moctezuma AE (2004) Carta Geológico-Minera Pahuatlán F14-D73. Servicio Geológico Mexicano, Escala 1:50 000. (In Spanish) Sajinkumar KS, Anbazhagan S, Rani VR, *et al.* (2014) A paradigm quantitative approach for a regional risk assessment and management in a few landslide prone hamlets along the windward slope of Western Ghats, India. International Journal of Disaster Risk Reduction 7: 142-153. DOI: 10.1016/j.ijdrr. 2013.10.004

Shrestha A (2005) Vulnerability assessment of weather disasters in Syangja District, Nepal: A case study of Putalibazar Municipality, advanced institute on vulnerability to global environmental dhange/global change system for analysis research and training. Kathmandu: START and Department of Hydrology, Nepal.

Sterlacchini S, Frigerio S, Giacomelli P, *et al.* (2007) Landslide risk analysis: a multi-disciplinary methodological approach Natural Hazards and Earth System Sciences 7: 657-675. DOI: 10.5194/nhess-7-657-2007

Thanapackiam P, Khairulmaini OS, Fauza AG (2012) Vulnerability and adaptive capacities to slope failure threat: a study of the Klang Valley Region. Natural Hazards 62: 805- 826. DOI: 10.1007/s11069-012-0108-6

Totschnig R, Sedlacek W, Fuchs S (2011) A quantitative vulnerability function for fluvial sediment transport. Natural Hazards 58 (2): 681-703. DOI: 10.1007/s11069-010-9623-5

Tsao TC, Hsu WK, Cheng CT, *et al.* (2010) A preliminary study of debris flow risk estimation and management in Taiwan. In:
Chen SC (ed.), International Symposium Interpraevent in the Pacific Rim-Taipei, 26-30 Apr. Internationale Forschungsgesellschaft Interpraevent, Klagenfurt, Austria. pp 930-939.

Turner IIBL, Kasperson RE, Matsone PA, *et al.* (2003) A framework for vulnerability analysis in sustainability science. PNAS 100 (14): 8074-8079. DOI: 10.1073/pnas.1231335100

UN/ISDR (2004) Living with Risk. A Global Review of Disaster Reduction Initiatives. 2004 version. UN Publications, Geneva.

Uzielli M, Nadim F, Lacasse S, *et al.* (2008) A conceptual framework for quantitative estimation of physical vulnerability to landslides. Engineering Geology 102: 251-256. DOI: 10.1016/j.enggeo.2008.03.011

Varnes DJ (1978) Slope movement types and processes. In: Schuster RL *et al.* (eds.), Landslides: Analysis and Control Special Report 176, TRB, National Research Council, Washington, DC, U.S. pp 11-33.

Van Den Eeckhaut M, Marre A, Poesen J (2010) Comparison of two landslide susceptibility assessments in the Champagne– Ardenne region (France).Geomorphology 115: 141-155. DOI: 10.1016/j.geomorph. 2009. 09.042

Walters V, Gaillard JC (2014) Disaster risk at the margins: Homelessness, vulnerability and hazards. Habitat International 44: 211-219. DOI: 10.1016/j.habitatint.2014. 06.006

Wilches-Chaux G (1998) Auge, caída y levantada de Felipe Pinillo, mecánico y soldador o yo voy a correr el riesgo. Red de Estudios Sociales en Prevención de Desastres en América Latina. Peru. p 103. (In Spanish)

Wu CH, Chen SC (2009) Determining landslide susceptibility in Central Taiwan from rainfall and six site factors using the analytical hierarchy process method. Geomorphology 112: 190-204. DOI: 10.1016/j.geomorph.2009.06.002

Xu C, Xu X, Dai F, *et al.* (2012) Comparison of different models for susceptibility mapping of earthquake triggered landslides related with the 2008 Wenchuan earthquake in China. Computers & Geosciences 46: 317-329. DOI: 10.1016/j.cageo.2012.01.002

Xu C, Xu X, Yao X, *et al.* (2014) Three (nearly) complete inventories of landslides triggered by the May 12, 2008 Wenchuan Mw 7.9 earthquake of China and their spatial distribution statistical analysis. Landslides 11(3): 441-461. DOI: 10.1007/s10346-013-0404-6

Xu C, Xu X, Shyu JBH (2015) Database and spatial distribution of landslides triggered by the Lushan, China Mw 6.6 earthquake of 20 April 2013. Geomorphology 248: 77-92. DOI: 10.1016/j.geomorph.2015.07.002

Zezere JL, Garcia RAC, Oliveira SC, *et al.* (2008) Probabilistic landslide risk analysis considering direct costs in the area north of Lisbon (Portugal). Geomorphology 94: 467-495. DOI: 10.1016/j.geomorph.2006.10.040

# Capítulo VII. Conclusiones generales

El propósito que motiva este esfuerzo profesional –un mundo sin desastres es posible– es todavía una meta difícil que requiere de una labor académica constante, y aunque una tesis debe tener un punto final, el trabajo no termina necesariamente aquí.

A continuación, se menciona lo concluido en cada uno de los capítulos que se exponen en este trabajo.

En el capítulo II se realizó una revisión de las posibles fuentes de imágenes de satélite de muy alta resolución, así como del software y hardware que está disponible para su manejo y aprovechamiento. Se concluye que su utilización para la identificación de PRM es posible y puede reducir los tiempos y errores en comparación con técnicas más tradicionales. Hay que señalar que el artículo fue publicado en el año 2014 y que en estos seis años se ha intensificado el uso de estas herramientas para el estudio de los PRM (no solo la elaboración de inventarios) ya sea del tipo LiDAR de muy alta resolución o de imágenes obtenidas por drones.

En el caso de la aplicación para la zonas de Pahuatlán las imágenes de satélite representaron el principal insumo para la elaboración del inventario que se pretendía fuese multitemporal. Pero justamente, debido a que estas herramientas son relativamente recientes y no hay fotografías aéreas disponibles de la zona en años anteriores, no fue posible obtener un inventario completo. El costo económico también fue un elemento importante a considerar, las fotografías aéreas son al día de hoy costosas en su obtención y en aquel momento (2014) tampoco eran accesibles económicamente productos como las imágenes LiDAR de muy alta resolución o las obtenidas por drones (hoy en día ya son más accesibles). Por lo tanto, en ese contexto, las imágenes de muy alta resolución fueron una solución aceptable en tiempo, costo e utilidad. El que este tipo de materiales estuvieran libres de acceso en plataformas como Google Maps®, Google Earth® o Bing Maps®, también fue clave; todas estas son posibilidades que hace veinte años no existían.

En el capítulo III se vuelve a tratar el asunto de los inventarios de PRM, pero esta vez para otra zona y poniendo énfasis en el análisis de la distribución espacial de los PRM y el contexto geomorfológico: una capa de piroclastos que cubre un relieve de tipo sedimentario. Fue importante en este apartado el lograr un inventario multi-temporal lo más completo posible, situación que fue fundamental para lo realizado en el capítulo V de esta tesis.

En los capítulos IV y V se aborda el tema de la susceptibilidad y en ambos artículos la discusión que pueden generar los resultados es amplia. En el capítulo IV se elabora un análisis y estimación de la susceptibilidad por PRM a través de técnicas estadísticas tomando como base el inventario del capítulo II. El rendimiento de los modelos aplicados se considera aceptable de acuerdo a los métodos de

evaluación utilizados. Sin embargo, las incertidumbres relacionadas con la falta de un inventario completo y de las limitaciones existentes en su construcción (errores, omisiones e incertidumbres epistémicas), son razones para ser cuidadosos con los resultados obtenidos. No solo es imposible un inventario 100% completo, también es imposible una exacta estimación de la susceptibilidad y más aún, del riesgo. Específicamente con respecto a la estimación de la susceptibilidad, la selección de los factores seleccionados como variables independientes dentro de los modelos estadísticos es uno de los principales asuntos puestos a discusión. Así, se deben entender los límites de estas herramientas.

Esta discusión es más acentuada en el capítulo V, pues pese a tener un inventario multi-temporal más completo, hubo otros factores, algunos imposibles de subsanar, como la complejidad del fenómeno, estudiado, las limitaciones propias de los procedimientos elegidos y las limitaciones en los datos del inventario (aunque es más completo que el del capítulo precedente, aun así no es perfecto), que no permiten tener resultados 100% confiables en cuanto la estimación de la susceptibilidad se refiere.

También queda abierta la cuestión de encontrar una resolución espacial óptima (tamaño de pixel), pues en este capítulo queda demostrado que una mayor resolución no necesariamente significa un mejor resultado. Si a lo anterior se le suma un cambio en los resultados de acuerdo a la zona de estudio delimitada, la decisión sobre cuál es el mejor modelo se vuelve más compleja. La principal conclusión en este respecto, parece estar en el ensayo y error previos antes de decidir arbitrariamente acerca de una u otra cosa. También es cierto que las opciones no pueden ser infinitas y que las futuras investigaciones acerca de esta temática dependerán de los recursos y materiales disponibles.

Una de las cuestiones que causó mayor polémica y tiempo de resolver en esta tesis fue la cuestión de incluir o no la cobertura de uso de suelo dentro de las variables explicativas de los modelos estadísticos del capítulo V. En la sección de discusión del capítulo se explican las razones de esta decisión –no ingresar al uso de suelo dentro de los modelos–, pero también se advierte que sí se realizaron pruebas que llevaron mucho tiempo debido a que la construcción de este tipo de cartografía no es sencilla. Los resultados señalaron que no hubo realmente una mejora significativa en los resultados de los modelos si se ingresaba la variable de uso de suelo, ya fuera como detección de cambio (Mapa A **Anexo 4**) o como simples categorías de uso de suelo (Mapas B y C **Anexo 4**), y en cambio se comprobó que la inclusión de esta variable si generaba un sesgo en los mapas que resultaban de los modelos estadísticos (Fig. 1 **Anexo 4**). Esto apenas se menciona brevemente en el artículo que corresponde al capítulo V pues hubiera supuesto una extensión de texto mayor a la permitida por artículo en las reglas de la editorial que publica la misma. Sin embargo, nos parecía importante mencionarlo aquí por la relevancia que tuvo durante el proceso de elaboración de esta tesis y el largo tiempo que consumió realizar estas pruebas.

Lo que si se menciona detalladamente en el artículo es que quizá la cobertura que contenía la información del tipo de litología podía tener un efecto similar que la de uso de suelo. Los resultados del poder predictivo de los modelos (curva ROC) parecen confirmar eso, pues cuando se elimina la capa de litología de los modelos los resultados son menos satisfactorios (de 0.684 a 0.766 y de 0.759 a 0.817), y también parece haber un sesgo generado por esta cobertura en los resultados cartográficos de algunos de los modelos. De hecho, ese fue un factor que influyó significativamente en la selección del mapa final en ese trabajo (Fig. 5.7). En ese sentido se menciona que, probablemente, el usar una cobertura referente al tipo de suelo (o características del mismo como su profundidad) hubiera sido más conveniente que la capa con las categorías del tipo de roca, pero como se explica también el artículo no existía una cartografía adecuada para este uso. Sin duda, y a pesar de que en los últimos cuarenta años la cuestión de la susceptibilidad es la que quizá ha tenido más avances en el enfoque estadístico de los PRM, es también una de las más interesantes para ahondar en su estudio y que permitirían mejorar los resultados en la cartografía de la susceptibilidad. Esperamos en los años siguientes poder contribuir en ese avance y cartografiar la susceptibilidad y amenaza por PRM en cada vez más zonas y municipios que presenten estos fenómenos en México.

Finalmente, el capítulo VI también deja cuestiones pendientes, para empezar, si las incertidumbres en los datos afectan la estimación efectiva de la susceptibilidad, la determinación de la magnitud y la frecuencia también adolecen de esas incertidumbres. Aun así, los resultados respecto a la estimación cuantitativa de la amenaza por PRM en Pahuatlán parecen aceptables y suficientes. Es necesario profundizar más en estos aspectos para poder avanzar en la estimación y cuantificación de la amenaza por PRM.

Por otra parte, se reconoce la dificultad y el alto grado de subjetividad que implica el cálculo de la vulnerabilidad. En ese sentido no solo hacen falta más investigaciones de ese tipo en nuestro país sino en el resto del mundo. Hay que tratar de reducir esa subjetividad mencionada y, principalmente, encontrar métodos de evaluación que no dependan únicamente de la ocurrencia real de un desastre. En el artículo se menciona que sin duda un estudio de la vulnerabilidad que regrese en el tiempo a las condiciones de 1999 en Pahuatlán (o en Teziutlán) podría ser de utilidad, pero es no representaría las condiciones de vulnerabilidad actuales, demostrando que la vulnerabilidad es dinámica y multidimensional.

La mejora en este sentido, ayudará por consiguiente a una mejor estimación del riesgo específico por PRM. Se advierte en su momento que la estimación del riesgo presentada en el capítulo VI es solo preliminar y no puede tomarse más que como un punto de comienzo para futuros estudios en la materia.

De esta forma, este trabajo concluye, como ya se mencionó, con más desafíos que cuestiones resueltas. La continuidad de este tipo de trabajos en nuestro país es necesaria pues los PRM seguirán ocurriendo. Por ello es indispensable continuar los trabajos de investigación, no solo desde el enfoque estadístico y la cuantificación de la amenaza, también en los referentes a la comprensión de nuestra vulnerabilidad como sociedad. Sí otros mundos son posibles, uno sin desastres ciertamente lo es.

# ANEXOS

## Anexo 1 Principales eventos de desastre.

*Tabla 1 Principales eventos de desastre ocurridos antes de la etapa moderna (1492).*

| DENOMINACIÓN | AÑO | LUGAR | AFECTACIÓN |
|---|---|---|---|
| Erupción volcán Toba | 73 000 a. C. | Isla de Sumatra, actual Indonesia. | En discusión, podría haber causado una disminución severa de la población mundial debido a un invierno volcánico de seis años, pero las evidencias apuntan a que los efectos no fueron tan severos en la población (Williams 2012, Timmreck *et al.* 2012; Clarkson et al 2012; Oppenheimer 2012). |
| Inundaciones del Mar Negro | 5 600 a. C. | Costas del actual Mar Negro. | Migración masiva de las personas que habitaban las partes bajas alrededor del actual Mar Negro y que hoy están bajo el agua. Posible origen del mito del Diluvio Universal (Giosan *et al.* 2009). |
| Maremoto | 2 000 a. C. | Antigua Ugarit, en la costa del mar Mediterráneo | Primera mención de un maremoto en la Historia (que habría arrasado las aldeas pesqueras de la costa siria) (Renfrew *et al.* 1998) |
| Erupción Minoica (Santorini) | 1 600 a. C. | Isla de Santorini, Grecia. | No generó por si sola el colapso de la cultura Minoica pero los daños fueron severos (Bruins *et al.* 2008). |
| Terremoto de Esparta | 464 a. C. | Grecia | Más de 20,000 víctimas (Gates y Ritchie 2007) |
| Tsunami de Helike | 373 a. C. | Grecia | Destruyó la ciudad de Helike, no hubo sobrevivientes (Gates y Ritchie 2007) |
| Tsunami y terremoto | 227 a. C. | Grecia | Destruyó el Coloso de Rodas. El tsunami arrasa las islas de Caria, Licia y Rodas (Hazel 2002). |
| Erupción del Popocatépetl | 200 a. C. | Valle de México, México. | Ocasionó el abandono de la cuenca de México, lo que disparó el dominio de Teotihuacán como centro económico y social (Siebe 2000; Plunket y Uruñuela 2006). |
| Epidemia plaga Antonina | 165-180 a. C. | Roma | El Imperio Romano fue asolado por ella durante la plaga de Antonino (165-180 a. C.). La peste asoló en repetidas ocasiones (desde el año 397 a. C.), ocasionando la pérdida de hasta 70% de las poblaciones (Barriga Angulo y Hernández Sánchez 2015). |
| Inundación | 110 a. C. | China | Río Amarillo cambió su curso e inundó la ciudad de Xuzhou durante los siguientes 24 años (Dutch 2009). |
| Terremoto de Siria | 19 d. C. | Siria | Se estima que cobró más de 100,000 vidas (Gates y Ritchie 2007) |
| Erupción del Vesubio. | 79 d. C. | Italia | Destrucción total de las ciudades romanas de Pompeya y Herculano (Charlier *et al.* 2017). |

| | | | |
|---|---|---|---|
| Erupción del volcán Guagua Pichincha | 90 d. C. | Ecuador | El valle Jama, al pie del volcán fue abandonado por centurias (Zeidler 2016). |
| Terremoto y tsunami | 115 d. C. | Antioquía (Turquía) | Terremoto de magnitud 7,5 en la escala sismológica de Richter (intensidad de XI en la escala de Mercalli), dejando un saldo de 260.000 muertos. También se registra un tsunami (Gates y Ritchie 2007). |
| Erupción del volcán Xitle | 230-245 d. C. | Cuenca de México. | Ocasionó el abandono definitivo de las ciudades de Cuicuilco y Copilco (Siebe 2000). |
| Terremoto de Alejandría | 365 d. C. | Egipto | Destruyó el Faro de Alejandría y cobró la vida de más de 50,000 personas (Gates y Ritchie 2007). |
| Terremoto | 502 d. C. | Israel, Acre | Destrucción total de Acre (Sbeinati *et al.* 2005). |
| Terremoto de Antioquia | 526 d. C. | Siria | Aproximadamente 250,000 personas murieron (Gates y Ritchie 2007). |
| Erupción | 535 d. C. | El salvador | La erupción del volcán Ilopango es uno de los eventos volcánicos de mayor intensidad del Holoceno en Centroamérica, afectando directamente e indirectamente a los pobladores mayas que habitaban lo que hoy en día se conoce como El Salvador, Guatemala y Honduras (Ichikawa 2016). |
| Epidemia Plaga de Justiniano | Siglo VI (541-750) | Imperio Bizantino, Constantinopla | Plaga de Justiniano muerte de casi 25 millones de personas en el mediterráneo hasta que se mitigó por fin en el siglo VIII, y llegó a destruir hasta la cuarta parte de toda su población. Se trataba de la peste bubónica (Lester 2007; Gunn 2008). |
| Inundación | 838 | Noroeste de los Países Bajos | Una gran parte del noroeste de los Países Bajos es inundada por una tormenta, murieron al menos 2,437 personas (Arblaster 2006). |
| Erupción del Monte Paektu | ~946 d. C. | Frontera de China y Corea del Norte. | Hambrunas y descenso de la temperatura a nivel regional (Oppenheimer *et al.* 2017) |
| Sequias severas | ~1000 DC | Yucatán, México. | Posible colapso de la civilización maya (Lane *et al.* 2014). |
| Inundación | 1014 | Países Bajos | Se rompe por primera vez la línea de la costa. La crónica de la abadía de Quedlinburg (en el centro de Alemania) informa que murieron miles de personas. Los mayores daños se registran en la isla de Walcheren (Arblaster P 2006). |
| Inundación | 1042 | Bélgica | Marejada ciclónica genera una inundación en la región de la desembocadura del río Yser (de Kraker 2015) |
| Terremoto de Verona | 1117 | Italia | Terremoto de magnitud 6,4 en la escala sismológica de Richter devasta gran parte del centro norte del país, en particular Verona, dejando un saldo de unos 30 000 muertos (Glade, *et al.* 2005). |

| | | | |
|---|---|---|---|
| Inundación | 1134 | Bélgica | Ciclón genera una inundación que crea el canal Zwin, que conecta la ciudad de Brujas con el mar del Norte. (Charlier 2011). |
| Terremoto | 1138 | Alepo, en el norte de Siria, | Se registra un terremoto de magnitud 8,5 en la escala sismológica de Richter, que deja un saldo de 230.000 muertos (Ambraseys 2004) |
| Inundación | 1164 | Países Bajos | Inundación de Santa Juliana arrasa la ciudad de Groninga, la provincia de Frisia y el norte de Alemania, especialmente la cuenca del Elba. Mueren miles de personas (Spencer *et al.* 2014). |
| Terremoto | 1170 | Italia | La localidad de Checano (en el centro de Italia) es destruida por un violento terremoto, que también causó daños en el sur del país y en Sicilia (Dutour 2003). |
| Inundación | 1170 | Países Bajos | Se produce la Inundación de Todos los Santos de 1170, en que el Mar del Norte ingresa en el país al superar las dunas que formaban un terraplén natural (Dutour 2003) |
| Terremoto | 1191 | Azerbaiyán | El terremoto fue tan destructivo que la capital de Shirvan tuvo que ser transferida a Bakú (Fisher *et al.* 1986). |
| Sismo, sequia | 1202 | Israel, Líbano, Jordania, Siria | El terremoto causó unas 30.000 muertes, mientras que entre 1201 y 1202 hubo 1,100,000 muertos causados por la sequía y el desecamiento del río Nilo (en el norte de Egipto) y en la zona del Mediterráneo (Khair *et al.* 2000). |
| Inundación | 1219 | Países Bajos | 36 000 personas mueren ahogadas (Buisman y van Engelen 2000). |
| Deslizamiento | 1248 | Monte Granier, Francia | Destruyó varias aldeas y se estima que hubo aproximadamente 1,000 muertos (de Blasio 2011). |
| Terremoto | 1268 | Cilicia, Turquía | 60,000 muertos en la región por el terremoto (Gates y Ritchie 2007). |
| Tifón Kamikaze | 1281 | Bahía de Hakata | 65,000 muertos (Sansom 1958). |
| Inundación | 1287 | Países Bajos | Tormenta rompe la represa del Zuiderzee (Inundación de Santa Juliana). Mueren entre 50,000 y 80,000 personas (Buisman y van Engelen 2000). |
| Terremoto | 1290 | Chihli, China | Terremoto de magnitud 6,7 en la escala sismológica de Richter deja un saldo de 100 000 muertos (Gates y Ritchie 2007) |
| Terremoto | 1293 | Kamakura, Japón | 30,000 personas murieron (Gates y Ritchie 2007). |
| Inundación y hambruna | 1342 | Europa | "Inundación del Día de María Magdalena". Los ríos Rin, Mosela, Danubio, Elba y sus tributarios inundaron las ciudades de Colonia, Maguncia, Fráncfort del Meno, Wurzburgo, Ratisbona, Passau y Viena, que quedaron seriamente dañadas. Solo en el área del río Danubio murieron 6000 personas. Los siguientes años habrá veranos fríos, que provocará la falta de alimentos en todo el continente (Herget *et al.* 2015). |

| Peste negra | 1346 -1353 | Europa | Muerte de aproximadamente del 50% de la población en Europa (Spyrou *et al.* 2016). |
|---|---|---|---|
| Terremoto | 1406 | Azerbaiyán | Se registra un terremoto de 7 grados en la escala sismológica de Richter y una intensidad de 9, con epicentro a 30 km de profundidad (Utsu 2002) |
| Inundación y hambruna | 1446-1455 | México | Durante el reinado de Moctezuma I, una inundación causó varios muertos, daños y hambre en Tenochtitlán. La explicación al desastre fue que los dioses requerían más sacrificios humanos por lo que se instauraron las llamadas Guerras Floridas (García Acosta *et al.* 2003). |
| Terremoto | 1456 | Nápoles | 60,000 personas murieron (Gates y Ritchie 2007). |

*Tabla 2. Algunos de los eventos de desastre de mayor impacto en la sociedad moderna (a partir de 1492).*

| DENOMINACIÓN | AÑO | LUGAR | AFECTACIÓN |
|---|---|---|---|
| Epidemia de viruela | 1519-1520 | México | En algunos poblados murió la mitad de la población. La epidemia se extendió desde Michoacán hasta Veracruz y fue clave en la caída de México-Tenochtitlán (García Acosta 2003). |
| Terremoto | 1556 | Shensi, China | 830,000 personas murieron (Gates y Ritchie 2007). |
| Terremoto | 1626 | Nápoles, Italia | Numerosas villas destruidas, 70,000 muertos (Gates y Ritchie 2007). |
| Peste negra | 1629 | Italia | Se estima que la epidemia causó cerca de 1 millón de víctimas (Hays 2005). |
| Peste negra | 1665 | Londres, Inglaterra | Murió un cuarto de la población de Londres (Hays 2005). |
| Peste negra | 1679 | Viena, Austria | 70,000 personas perdieron la vida (Gregg 1985). |
| Terremoto | 1693 | Nápoles y Catania, Italia | 10,000 muertos en Catania y 93,000 en Nápoles (Gates y Ritchie 2007). |
| Terremoto | 1703 | Tokio, Japón | La ciudad quedó destruida y murieron 200,000 personas (Gates y Ritchie 2007). |
| Terremoto | 1731 | Pekín, China | Se reportaron 100,000 muertos (Gates y Ritchie 2007). |
| Terremoto | 1737 | Calcuta, India | Se reportaron 300,000 muertos (Gates y Ritchie 2007). |

| | | | |
|---|---|---|---|
| Terremoto y tsunami | 1755 | Lisboa, Portugal | 70,000 personas murieron (Gates y Ritchie 2007), sobre este evento escribió Kant. |
| Erupción volcánica del Tambora | 1815 | Indonesia | La erupción más intensa en los tiempos modernos. Miles de personas murieron en la erupción y cientos de miles más debido al micro-cambio climático denominado como el "año sin verano". (Gates y Ritchie 2007; Gunn  2008). |
| Epidemia de cólera | 1854 | Londres, Inglaterra | Brote de cólera violento en Londres que sirvió de estudio para John Snow (1813-1858) padre de la epidemiología moderna (Newsom (2006). |
| Terremoto | 1857 | Tokio | Más de 100,000 personas fueron reportadas fallecidas (Gates y Ritchie 2007). |
| Erupción volcánica y tsunamis del Krakatoa | 1883 | Indonesia | Más de 100,000 personas murieron (Gates y Ritchie 2007). |
| Inundación del río Amarillo | 1887 | China | 900,000 personas murieron (Gunn 2008). |
| Fiebre rusa | 1899-1890 | Pandemia mundial | Se estima que más de 1 millón de personas murieron alrededor del mundo por esta epidemia de influenza (Dowdle 1999). |
| Huracán | 1900 | Galveston, Estados Unidos | Aproximadamente 8,000 personas murieron (Rappaport y  Partagas 1995). |
| Erupción volcánica del Monte Pelée | 1902 | Martinica | Un flujo piroclástico destruyó la ciudad de Saint Pierre y murieron más de 30,000 personas (Gates y Ritchie 2007). |
| Terremoto de San Francisco | 1906 | San Francisco, Estados Unidos | La ciudad fue completamente destruida por el terremoto y un incendio provocado por el mismo. Se estima que murieron 2,000 personas (Gates y Ritchie 2007). |
| Gripe española | 1918-1920 | Pandemia mundial | Se estima que murieron entre 50 y 100 millones de personas (Knobler *et al.* 2005). |
| Terremoto de Tokio | 1923 | Tokio, Japón | Más de 140,000 personas murieron y la ciudad completamente destruida por el terremoto e incendios posteriores (Gates y Ritchie 2007). |
| Terremoto | 1927 y 1932 | Kansu, China | Se reportaron más de 100,000 muertos en el terremoto de 1927, cinco años después, murieron 70,000 personas en otro terremoto (Gates y Ritchie 2007). |
| Inundación | 1931 | China | Entre 3,700,000 y 4,000,000 de personas murieron (Pietz 2002). |
| Erupción volcánica del Paricutín | 1944 | Michoacán, México | Los pueblos aledaños fueron destruidos. Fue el primer nacimiento de un volcán estudiado por la ciencia (Gates y Ritchie 2007). |

| | | | |
|---|---|---|---|
| Terremoto | 1964 | Alaska | Cerca de 100 personas murieron. Fue el terremoto de mayor intensidad registrado: 9.1 escala Richter (Gates y Ritchie 2007). |
| Terremoto | 1970 | Perú | Se reportaron más de 70,000 víctimas (Gates y Ritchie 2007). |
| Huracán | 1970 | Bangladesh | El ciclón que más muertes ha causado en la era moderna:167,000 personas murieron (Gunn 2008). |
| Terremoto | 1976 | Tangshan, China | Más de 700,000 personas murieron, intensidad de 7.6 Richter (Minzhong 1996; Zhilin 1996; Gates y Ritchie 2007). |
| Erupción del Monte Santa Helena | 1980 | Estados Unidos | Más de 100 personas murieron, fue una de las erupciones más violentas y documentadas (Gates y Ritchie 2007). |
| Pandemia SIDA | 1981- | Pandemia mundial | Se calcula que hasta hoy han muerto alrededor de 35 millones de personas en todo el mundo (OMS 2016). |
| Erupción del volcán Chichón | 1982 | México | Más de 20 millones de metros cúbicos de material fueron expulsados a la atmósfera. La temperatura en el hemisferio norte descendió 0.5ºC (Gates y Ritchie 2007). |
| Terremoto | 1985 | Ciudad de México | Aproximadamente 30,000 personas murieron. A partir del evento se creó Protección Civil de México. |
| Lahar | 1985 | Armero, Colombia | Lahar ocasionado por la erupción del volcán Nevado de Ruiz que sepultó el poblado de Armero (Naranjo *et al.* 1986). |
| Gas volcánico | 1986 | Camerún | Una nube de gas volcánico mató a 1,700 personas (Gates y Ritchie 2007). |
| Terremoto | 1989 | San Francisco, Estados Unidos | Un terremoto causó cuantiosos daños económicos y de infraestructura, murieron 77 personas (Gates y Ritchie 2007). |
| Erupción volcánica del Pinatubo | 1991 | Filipinas | 900 personas perdieron la vida (Gates y Ritchie 2007). |
| Terremoto | 1995 | Kobe, Japón | 5,500 personas murieron en un terremoto de 6.8º Richter (Gates y Ritchie 2007). |
| Huracán Mitch | 1998 | Centroamérica, el Caribe y México. | Huracán categoría 5. Se estima que más de 11,000 personas murieron (NCDC 2004). |
| Terremoto y tsunami | 2004 | Banda Aceh, Indonesia | El desastre de la década, el tsunami causó daños en las costas del Océano Índico en diferentes países. 283,100 personas perdieron la vida (Gates y Ritchie 2007). |

| | | | |
|---|---|---|---|
| Huracán Katrina | 2005 | Nueva Orleans, Estados Unidos | Daños por 108 millones dólares y 1,836 muertos (Knabb *et al.* 2011). |
| Pandemia A (H1N1) | 2009-2010 | Pandemia mundial | Se estima que murieron 19.000 personas (OMS 2010) |
| Terremoto y epidemia de cólera | 2010 | Haití | Se estima que murieron más de 160,000 personas (Kolbe *et al.* 2010). |
| Terremoto, tsunami y emergencia nuclear | 2011 | Japón | Más de 15,000 muertos (NPA 2016) |

# Referencias

Ambraseys N (2004) The 12th century seismic paroxysm in the Middle East: a historical perspective. Annals of Geophysics 47: 2-3.

Arblaster P (2006) A History of the Low Countries. Palgrave Essential Histories Series New York: Palgrave Macmillan. ISBN 1-4039-4828-3.

Barriga Angulo G, Hernández Sánchez E (2015) Aspectos actuales de las infecciones emergentes y reemergentes. Patología clínica 62: 174-182.

Bruins HJ, MacGillivray JA, Synolakis CE, Benjamini C, Keller J, Kisch H, Klügel A, van der Plicht J (2008) Geoarchaeological tsunami deposits at Palaikastro (Crete) and the Late Minoan IA eruption of Santorini. Journal of Archaeological Science 35(1): 191-212. https://doi.org/10.1016/j.jas.2007.08.017

Buisman J, van Engelen AFV (2000) Duizend jaar weer, wind en water in de lage landen, deel 1 tot 1300 ('mil años de clima, viento y agua en las tierras bajas, desde el 1 al 1300'). Uitgeverij Van Wijnen. Países Bajos. ISBN 90-5194-075-0

Charlier RH (2011) The Zwin: From Golden Inlet to Nature Reserve. Journal of Coastal Research 27: 746–756.

Charlier P, Abdallah FB, Bruneau R, Jacqueline S, Augias A (2017) Did the Romans die of antimony poisoning? The case of a Pompeii water pipe (79 CE) Toxicology Letters. En prensa.

Clarkson C, Jones S, Harris C (2012) Continuity and change in the lithic industries of the Jurreru Valley, India, before and after the Toba eruption. Quaternary International 258: 165-179. DOI: https://doi.org/10.1016/j.quaint.2011.11.007

de Blasio (2011) Introduction to the Physics of Landslides. Springer. Países Bajos. DOI: 10.1007/978-94-007-1122-8

de Kraker MJ (2015) Flooding in river mouths: human caused or natural events? Five centuries of flooding events in the SW Netherlands. Hydrology and earth system sciences 19: 1-15.

Dowdle WR (1999) Influenza A virus recycling revisited. Bulletin of the World Health Organization 77(10): 820-828.

Dutch SI (2009) The Largest Act of Environmental Warfare in History. Environmental & Engineering Geoscience 15(4): 287-297.

Dutour T (2003) La ciudad medieval. Orígenes y triunfo de la Europa urbana. Paidós. Buenos Aires Argentina. pp. 112-115. ISBN 950-12-5043-1

Fisher WB; Avery P, Hambly GRG, Melville C (1986) The Cambridge History of Iran. Cambridge University Press. Reino Unido. ISBN 978-0521200943

García Acosta V, Pérez Zevallos JM, Molina del Villar A (2003) Desastres agrícolas en México. Catálogo histórico I. Fondo de Cultura Económica. México. pp. 506.

Gates A, Ritchie D (2007) Encyclopedia of Earthqueakes and volcanoes. Infobase Publishing. pp. 365.

Giosan L, Filip F, Constatinescu S (2009) Was the Black Sea catastrophically flooded in the early Holocene? Quaternary Science Reviews 28, 1–2, 1-6. DOI: https://doi.org/10.1016/j.quascirev.2008.10.012

Gregg CT (1985) Plague: An Ancient Disease in the Twentieth Century. University of New Mexico Press. Estados Unidos.

Gunn AM (2008) Encyclopedia of disasters. Environmental catastrophes and human tragedies I. Greenwood Press. Estados Unidos. pp. 736.

Hays JN (2005) Epidemics and pandemics their impacts on human history. ABC-CLIO. Santa Barbara, Estados Unidos. pp. 103.

Hazel (2002) Quién es quién en la Antigua Grecia. Acento. Madrid, España. ISBN 84-483-0655-4.

Herget J, Kapala A, Krell M, Rustemeier E, Simmer C, Wyss A (2015) The millennium flood of July 1342 revisited. Catena 130: 82–94.

Khair K, Karakaisis GF, Papadimitriou EEP (2000) Seismic zonation of the Dead Sea Transform Fault area. Annali di Geofisica 43, 61-79.

Kolbe AR, Hutson RA, Shannon H, Trzcinski E, Miles B, Levitz N, Puccio M, James L, Noel JR, Muggah R (2010) Mortality, crime and access to basic needs before and after the Haiti earthquake: a random survey of Port-au-Prince households. Med Confl Surviv 26(4):281-97. DOI: 10.1080/13623699.2010.535279

Knabb RD, Rhome JR, Brown DP (2011) Tropical Cyclone Report Hurricane Katrina 23-30 August 2005. (Tropical Cyclone Report). United States National Oceanic and Atmospheric Administration's National Weather Service. pp. 43.

Knobler S, Mack A, Mahmoud A (2005) 1: The Story of Influenza. The Threat of Pandemic Influenza: Are We Ready? Workshop Summary. The National Academies Press. Washington, D.C., Estados Unidos. pp. 60–61.

Lane CS, Horn SP, Kerr MT (2014) Beyond the Mayan Lowlands: impacts of the Terminal Classic Drought in the Caribbean Antilles. Quaternary Science Reviews 86: 89-98. DOI: https://doi.org/10.1016/j.quascirev.2013.12.017

Lester LK (2007) Plague and the end of the antiquity: The Pandemic of 541-750. Cambridge University Press. pp. 19-20. ISBN 0-521-84639-0.

Minzhong H (1996) Measures to Resume and Rebuild Tangshan. En: Post-Earthquake Rehabilitation and Reconstruction. Elsevier, Estados Unidos. pp. 209–218. DOI: https://doi.org/10.1016/B978-008042825-3/50024-7

NCDC (2004) Mitch: The Deadliest Atlantic Hurricane Since 1780. Oceanic and Atmospheric Administration's National Environmental Satellite, Data, and Information Service.

Newsom SWB (2006) Pioneers in infection control: John Snow, Henry Whitehead, the Broad Street pump, and the beginnings of geographical epidemiology. J Hosp Infect 64: 210-6.

NPA (2016) Damage Situation and Police Countermeasures associated with 2011Tohoku district - off the Pacific Ocean Earthquake. National Police Agency of Japan. http://www.npa.go.jp/archive/keibi/biki/higaijokyo_e.pdf

OMS (2010) H1N1: El mundo se adentra en el periodo pospandémico. Organización Mundial de la Salud. http://www.who.int/mediacentre/news/statements/2010/h1n1_vpc_20100810/es/

OMS (2016) HIV/AIDS. Organización Mundial de la Salud. http://www.who.int/mediacentre/factsheets/fs360/en/

Oppenheimer S (2012) A single southern exit of modern humans from Africa: Before or after Toba? Quaternary International 258: 88-99. DOI: https://doi.org/10.1016/j.quaint.2011.07.049

Oppenheimer C, Wacker L, Xu J, Galvan JD, Stoffel M, Guillet S, Corona C, Sigl M, Di Cosmo N, Hajdas I, Pan B, Breuker R, Schneider L, Esper J, Fei J, Hammond JOS, Büntgen U (2017) Multi-proxy dating the "Millennium Eruption" of Changbaishan to late 946 CE. Quaternary Science Reviews 158: 164-171. https://doi.org/10.1016/j.quascirev.2016.12.024

Pietz D (2002) Engineering the State: The Huai River and Reconstruction in Nationalist China 1927–1937. Routledge. Nueva York, Estados Unidos. pp. 142.

Plunket P, Uruñuela G (2006) Social and cultural consequences of a late Holocene eruption of Popocatépetl in central Mexico. Quaternary International 151(1): 19-28. DOI: https://doi.org/10.1016/j.quaint.2006.01.012

Rappaport EN, Partagas JF (1995) The Deadliest Atlantic Tropical Cyclones, 1492-1994. NOAA Technical Memorandum NWS NHC-47. pp. 41.

Renfrew C, Bahn P (1998) Introducción: La Naturaleza y los Propósitos de la Arqueología. En: Fábregas-Valcarce R (ed.) Arqueología. Teorías, Métodos y Prácticas. Akal. Madrid, España. pp. 340. ISBN 8446002345.

Sansom G (1958) A History of Japan to 1334. Stanford University Press. California, Estados Unidos.

Sbeinati MR, Darawcheh R, Mouty M (2005) The historical earthquakes of Syria: an analysis of large and moderate earthquakes from 1365 B.C. to 1900 A.D. Annals of Geophysics 48(3): 347-435.

Siebe C (2000) Age and archaeological implications of Xitle volcano, southwestern Basin of Mexico-City. Journal of Volcanology and Geothermal Research 104: 45-64. DOI: https://doi.org/10.1016/S0377-0273(00)00199-2

Spencer T, Brooks SM, Möller I, Evans BR (2014) Where Local Matters: Impacts of a Major North Sea Storm Surge. Eos, Transactions American Geophysical Union 95(30): 269–270.

Spyrou M, Tukhbatova R, Feldman M, Drath J, Kacki S, Beltrán de Heredia J, Arnold S, Sitdikov AG, Castex D, Wahl J, Gazimzyanov IR, Nurgaliev DK, Herbig A, Bos KI (2016) Historical Y. pestis Genomes Reveal the European Black Death as the Source of Ancient and Modern Plague Pandemics. Cell Host & Microbe 19: 874-881.

Timmreck C, Graf HF, Zanchettin D. Hagemann S, Kleinen T, Krüger K (2012) Climate response to the Toba super-eruption: Regional changes. Quaternary International 258: 30-44. DOI: https://doi.org/10.1016/j.quaint.2011.10.008

Utsu TR (2002) A List of Deadly Earthquakes in the World: 1400–2000. International Handbook of Earthquake & Engineering Seismology, Parte A, 81A. Academic Press. pp. 705. ISBN 978-0124406520

Williams M (2012) The ~73 ka Toba super-eruption and its impact: History of a debate. Quaternary International 258: 19-29. DOI: https://doi.org/10.1016/j.quaint.2011.08.025

Zeidler JA (2016) Modeling cultural responses to volcanic disaster in the ancient Jama–Coaque tradition, coastal Ecuador: A case study in cultural collapse and social resilience. Quaternary International 394: 79-97. DOI: https://doi.org/10.1016/j.quaint.2015.09.011

Zhilin Z (1996) An Account of Restoring Operations After Tangshan Earthquake. En: Post-Earthquake Rehabilitation and Reconstruction. Elsevier, Estados Unidos. pp. 219–227. DOI: https://doi.org/10.1016/B978-008042825-3/50024-7

# Anexo 2. Resumen de la revisión bibliográfica acerca de susceptibilidad realizada para este trabajo (436 artículos revisados).

| Reference | Year | Journal | Area (km$^2$) | Classifier technique | Spatial resolution (m2) |
|---|---|---|---|---|---|
| Brabb et al | 1972 | U.S. Geol. Surv. Misc. Field Stud. Map | | Simple ranking | 62.5 |
| Wright & Nilsen | 1974 | US Geological Survey Miscellaneous Field Studies Map | | Landslide isopleths maps | 250 |
| Campbell | 1975 | U.S. Geol. Surv. Prof. | | Simple ranking | |
| Carrara & Merenda | 1976 | Geological Society of America Bulletin | 1000 | Distribution expert-analysis. | |
| Humbert | 1977 | Engineering Geology | | Distribution expert-analysis. | 25 |
| Stevenson | 1977 | Bull Int Ass Eng Geol | 90780 | Combination and overlapping maps | |
| Huma and Radulescu | 1978 | Bulletin of the international association of Engineering Geologist | 25 | Combination and overlapping maps | 3 |
| Kienholz | 1978 | Artic and Alpine Research | | Distribution expert-analysis. | 10 |
| Newman et al. | 1978 | Geologica Survey Bulletin | 38 | Landslide density maps (LDsM) | 152, 76 |
| Pomeroy | 1978 | U.S. Geological Survey Miscellaneous Field Investigation Map | | Landslide isopleths maps | |
| Fenti et al. | 1979 | Bull of the Int Assoc Eng Geol | | Distribution expert-analysis. | |
| Foggin and Rice | 1979 | Journal of forestry | | Combination and overlapping maps | 6 |
| Radbruch-Hall et al. | 1979 | Bulletin of the international association of Engineering Geologist | All USA | Combination and overlapping maps | 21000 |
| Hollingsworth and Kovacs | 1981 | Bull. Assoc. Eng. Geol. | | Simple ranking | |
| Ives & Messerli | 1981 | Mountain Research And Development | 35 | Distribution expert-analysis. | 10 |
| Ward and Simons | 1981 | IAHS Publ. | 13 | Infinite slope model (ISS) | 40500 |
| Carrara | 1983 | Mathematical Geology | | Discriminant analysis (LDA) and multiple regression | 200 |
| Edil & Shultz | 1983 | Engineering Geology | | Bishop method / Monte Carlo Simulation | |
| Kienholz et al. | 1983 | Mountain Research and Development | | Distribution expert-analysis. | |
| DeGraff | 1985 | Bull. Assoc. Eng. Geol. | | Landslide isopleths maps | |
| DeGraff and Canuti | 1988 | Bull. Assoc. Eng. Geol. | | Landslide isopleths maps | |
| Rice et al. | 1985 | Forest Science | 3.4 | Linear discriminant analysis (LDA) | 6 |
| Zimmerman et al. | 1986 | Mountain Research and Development | | Distribution expert-analysis. | |
| Reneau and Dietrich | 1987 | Rev. Eng. Geol. | | Simple ranking | |
| Bernknopf et al. | 1988 | Bulletin of the international association of Engineering Geologist | | Multiple regression | |
| Rupke et al. | 1988 | Engineering Geology | | Distribution analysis | 2 |
| Smith | 1988 | U.S. Geol. Surv. Prof. | | Simple ranking | |
| Yin and Yan | 1988 | Proc 5th International Symposium on Landslides | | Logistic regression (LR) and Information value (Statistical method index). | |

| | | | | | |
|---|---|---|---|---|---|
| Baldi *et al.* | 1990 | Mem. Soc. Geol.It. | 158 | Discriminant analysis (LDA) and Logistic Regression (LR) | 10 |
| Carrara *et al.* | 1990 | Proc of the 6th Int Conf Field Workshop on Landslides | | Linear discriminant analysis (LDA) | 25 |
| Gupta & Joshi | 1990 | Engineering Geology | | Landslide Nominal risk A2ctor | |
| Neely and Rice | 1990 | Bull. Assoc. Eng. Geol. | | Distribution expert-analysis. | |
| Seeley and West | 1990 | Bull. Assoc. Eng. Geol. | | Simple ranking | |
| Carrara *et al.* | 1991 | Earth SurA2ce Processes and Landforms | | Linear discriminant analysis (LDA) | |
| Anbalagan | 1992 | Engineering Geology | 50 | BIS based Landslide Hazard Evaluation A2ctor (LHEF) | 50 |
| Juang *et al.* | 1992 | J. Geotech. Engrg | | Slope A2ilure Potential Index (SFPI) / Monte Carlo simulation | |
| Pachauri & Pant | 1992 | Engineering Geology | 317 | Likelihood frequency ratio (LFR) | |
| Pachauri and Pant | 1993 | Engineering Geology | 317 | Simple ranking | |
| Montgomery & Dietrich | 1994 | Water Resources Research | 1.2 | SHALSTAB | 5 |
| Chung *et al.* | 1995 | (Book) Advances in Natural and Technological Hazards Research Volume 5, 1995, pp 107-133 | | Weighted regression analysis | |
| Hansen *et al.* | 1995 | Book chapter. Geographical Information Systems in Assessing Natural Hazards | 1000 | Distribution expert-analysis. | |
| Hearn | 1995 | Quarterly Journal of Engineering Geology | | Distribution expert-analysis. | 10 |
| Sakar *et al.* | 1995 | Mountain Research And Development | 443 | Weighted overlay method (WOM) | 25 |
| Anbalagan & Sighn | 1996 | Engineering Geology | 30 | Combination and overlapping maps | 50 |
| Bughi *et al.* | 1996 | Proc 15th Int Conf. OMAE, Firenze, June 1996 | | Logical analytical model | |
| Gokceoglu and Aksoy | 1996 | Engineering Geology | 120 | Weighting factors and Bishop's method | 25 |
| van Westen and Terlien | 1996 | Earth SurA2ce Processes and Landforms | 20 | Infinite slope model (ISS) | |
| Gupta & Anbalagan | 1997 | Quarterly Journal of Engineering Geology | | Combination and overlapping maps | 50 |
| van Westen *et al.* | 1997 | Geologische Rundschau | | Information value (Statistical method index) (IV), Distribution expert-analysis (geomorphological mapping), Infinite slope model (ISS) | 10 |
| Wu & Sidle | 1997 | Human Impact on Erosion and Sedimentation (Proceedings of Rabat Symposium) | 2.3 | dSLAM | 30 |
| Al-Homoud & Al-Masari | 1998 | Environmental Geology | 100 | Slope Failure Potential Index (SFPI) | |
| Atkinson and Massari (b) | 1998 | Computer & Geosciences | 65 | Logistic regression (LR) | 10 |
| Jibson *et al.* | 1998 | Engineering Geology | 900 | Newmark | 10 |
| Pachauri *et al.* | 1998 | Environmental Geology | 400 | Simple ranking | |

| | | | | | |
|---|---|---|---|---|---|
| Pack *et al.* | 1998 | 8th Congress of the International Association of Engineering Geology, Vancouver, British Columbia, Canada 21-25 September 1998 | 104 | SINMAP | 10 |
| Rowbothham and Dudycha | 1998 | Geomorphology | 70 | Logistic regression (LR) | No report |
| Chung & A2bbri | 1999 | Photogrammetric Engineering & Remote Sensing | 56 | Bayes Joint Conditional Probability, Weighted regression analysis. | |
| Fernández *et al.* | 1999 | Earth SurA2ce Processes and Landforms | 503 | Cluster analysis (matrix assessment) | 18 |
| Guzzetti *et al.* | 1999 | Geomorphology | 65 | Logistic regression (LR), Linear discriminant analysis (LDA) | 20 |
| Nossin | 1999 | GeoJournal | | Distribution expert-analysis. | |
| Pausto & Soldati | 1999 | Geomorphology | | Distribution analysis | |
| Bulut *et al.* | 2000 | Bulletin of Engineering Geology and the Environment | 25 | Landslide isopleths maps | 25 |
| Dai *et al.* | 2000 | Environmental Geology | 143 | Logistic regression (LR) | 20 |
| Parise and Gibson | 2000 | Engineering Geology | 10000 | Landslide density maps (LDsM). | 24 |
| Baeza and Corominas | 2001 | Earth SurA2ce Processes and Landforms | 25 | Principal component analysis (PCA) | 10 |
| Lee and Min | 2001 | Environmental Geology | 66 | Logistic Regression (LR) & Likelihood frequency ratio (LFR). | 10 |
| Morrissey *et al.* | 2001 | Open File Report 01-0067. U.S. Geological Survey. | 130 | SINMAP, LISA & Iverson's Transient Response Model | 10 |
| Ardizzone *et al.* | 2002 | Natural Hazards and Earth System Sciences | 300 | Linear discriminant analysis (LDA) | 15 |
| Cardinalli *et al.* | 2002 | Nat. Hazards Earth Syst. Sci | 20 | Distribution expert-analysis. | |
| Clerici *et al.* | 2002 | Geomorphology | 332 | Conditional probability model (CPM) | 5 |
| Ercanoglu and Gokceoglu | 2002 | Environmental Geology | 100 | Fuzzy standard membership (FSMs) | 25 |
| Espizua & Bengoechea | 2002 | Mountain Research and Development | 5400 | Distribution expert-analysis (geomorphological mapping). | 100 |
| Lee *et al.* | 2002 | Environmental Geology | 40 | Weight of evidence (WofE) | 5 |
| Lee *et al.* | 2002 | Geomorphology | 30 | Likelihood frequency ratio (LFR) | 10 |
| Majtan *et al.* | 2002 | Geograficky Casopis | 128 | Fractal Box-counting (FB-C) | 25 |
| Parise | 2002 | Nat. Hazards Earth Syst. Sci | 12 | Weighted overlay method (WOM) | No report |
| Pistocchi *et al.* | 2002 | Environmental Geology | | Certainty Factors (CF), Bayes Joint Conditional Probability, Fuzzy standard membership (FSMs). | 50 |
| Wilkinson *et al.* | 2002 | Earth SurA2ce Processes and Landforms | | CHASM | |
| Zezere | 2002 | Nat. Hazards Earth Syst. Sci | 11.3 | Information value (Statistical method index) | 25 |
| Cevik and Topal | 2003 | Environmental Geology | 290 | Information value (Statistical method index) and weighting A2ctor (WF). | 25 |
| Chung and A2bbri | 2003 | Natural Hazards | 4 | A2vourability functions | 10 |
| Corominas *et al.* | 2003 | Natural Hazards | 6 | Distribution expert-analysis. | 5 |
| Fernandez *et al.* | 2003 | Natural Hazards | 94 | Cluster analysis (matrix assessment) | 25 |
| Gorsevski *et al.* | 2003 | Journal of Geographical Systems | 111.8 | Fuzzy k-means | 30 |

| | | | | | |
|---|---|---|---|---|---|
| Lee *et al.* | 2003 | Earth SurA2ce Processes and Landforms | 66 | Artificial Neural Networks (ANN) | 10 |
| Ng *et al.* | 2003 | Geo Report | | Distribution expert-analysis. | |
| Ohlmacher and Davis | 2003 | Engineering Geology | 5 | Logistic regression (LR) | 10 |
| Remondo *et al.* | 2003 | Natural Hazards | 140 | Certainty A2ctors (CF), Bayes Joint Conditional Probability, Fuzzy standard membership (FSMs). | 10 |
| Santacana *et al.* | 2003 | Natural Hazards | 10 | Linear discriminant analysis (LDA) | 15 |
| van Westen *et al.* | 2003 | Natural Hazards | 20.8 | Weight of evidence (WofE) & Distribution expert-analysis. | 5 |
| Alcántara-Ayala | 2004 | Geomorphology | 900 | Infinite slope model (ISS) | 100 |
| Arora *et al.* | 2004 | Remote sensing | 35 | Artificial Neural Networks (ANN) | |
| Ayalew *et al.* | 2004 | Landslides | 410 | Weighted linear combination (WLC). | 10 |
| Coe et al | 2004 | Chapter book (W.A. Lacerda, M. Ehrlich, S.A.B. Fontura & A.S.F. Sayão (eds)) | 980 | Likelihood frequency ratio (LFR) | 10 |
| Ercanoglu and Gokceoglu | 2004 | Engineering Geology | 275 | Fuzzy standard membership (FSMs) | 25 |
| Ercanoglu *et al.* | 2004 | Natural Hazards | 64 | Conditional probability model (CPM) | 25 |
| Frattini *et al.* | 2004 | Engineering Geology | 4 | Infinite slope model (ISS) | |
| Lan *et al.* | 2004 | Engineering Geology | 3000 | SINMAP (modify) & Certainty A2ctors (CF). | |
| Lee | 2004 | International Journal of Remote Sensing | 285 | Logistic regression (LR) and Likelihood frequency ratio (LFR). | 10 |
| Lee *et al.* | 2004 | International Journal of Remote Sensing | 68.43 | Likelihood frequency ratio (LFR). | 5 |
| Lee *et al.* | 2004 | Engineering Geology | 66 | Artificial Neural Networks (ANN) | 10 |
| Pallas *et al.* | 2004 | Engineering Geology | 20 | Distribution analysis | |
| Perotto-Baldiviezo *et al.* | 2004 | Agriculture, ecosystems & environment | 67.3 | Simple ranking | 50 |
| Sakar & Kanungo | 2004 | Photogrammetric Engineering & Remote Sensing | 3000 | Combination and overlapping maps | 25 |
| Süzen and Doyuran | 2004 | Engineering Geology | 130 | Seed cells | 25 |
| Süzen and Doyuran (b) | 2004 | Environmental Geology | 130 | Seed cells and Logistic regression (LR) | 25 |
| van Beek & van Asch | 2004 | Natural Hazards | 1.5 | PhysiMeans of Physically Based Modelling | 10 |
| Xie *et al.* | 2004 | Natural Hazards | 3.4 | 3D Hovland model / Monte Carlo simulation. | 2 |
| Ayalew and Yamagishi | 2005 | Geomorphology | 105 | Logistic regression (LR) | 10 |
| Ayalew *et al.* | 2005 | Engineering Geology | 220 | Analytical hierarchy process (AHP) and Logistic regression (LR) | 10 |
| Ayenew & Barbieri | 2005 | Engineering Geology | 16 | Distribution expert-analysis. | |
| Baum *et al.* | 2005 | Landslides | | TRIGRS | |

| | | | | | |
|---|---|---|---|---|---|
| Brenning | 2005 | Nat. Hazards Earth Syst. Sci | 11.2 | Logistic regression (LR), Support Vector Machine (SVM), Decision tree (DT) (bootstrap-aggregated classification BAC) | 5 |
| Chau & Chan | 2005 | Landslides | 79.2 | Logistic regression (LR) | 30 |
| Chau et al. | 2005 | Computer & Geosciences | 77.5 | Logistic regression (LR) | 10 |
| Chien-Yuan et al. | 2005 | Environ Geol | 1 | TRIGRS | 10 |
| El-Ramly et al. | 2005 | Geotechnique | 1 | Spencer / Monte Carlo simulation | |
| Ercanoglu | 2005 | Nat. Hazards Earth Syst. Sci | 879 | Artificial Neural Networks (ANN) | 25 |
| Ermini et al. | 2005 | Geomorphology | 17 | Artificial Neural Networks (ANN) | 10 |
| Gokceoglu et al. | 2005 | Engineering Geology | 10 | Conditional probability model (CPM) | 25 |
| Gomes et al. | 2005 | Nat. Hazards Earth Syst. Sci | 110 | Landslide density maps (LDsM). | 10 |
| Gomez and Kavzoglu | 2005 | Engineering Geology | 110 | Artificial Neural Networks (ANN) | 30 |
| Lee and Dan | 2005 | Environmental Geology | 16935 | Likelihood frequency ratio (LFR) | 250 |
| Lee and Talib | 2005 | Environmental Geology | 293 | Likelihood frequency ratio (LFR) | 10 |
| Morerias | 2005 | Geomorphology | 1600 | Combination and overlapping maps | 20 |
| Oztekin & Topal | 2005 | Environmental Geology | 1 | Information value (Statistical method index) and weighting A2ctor (WF). | 0.1 |
| Reichenbach et al. | 2005 | Book chapter: Glade, T., Anderson, M.G. and Crozier, M.J. (eds.) Landslide risk assessment. | 5.4 | Distribution analysis | 10 |
| Remondo et al. | 2005 | Landslides | 140 | Certainty A2ctors (CF), Bayes Joint Conditional Probability, Fuzzy standard membership (FSMs). | 1 |
| Saha et al. | 2005 | Landslides | 550 | Information value (Statistical method index) & Landslide Nominal Risk A2ctor (Gupta & Joshi 1990) | 6 |
| Singh et al. | 2005 | Landslides | 10 | Weight of evidence (WofE) | 25 |
| Tolga et al. | 2005 | Geomorphology | 80 | Logistic regression (LR) | 25 |
| Wang and Sassa | 2005 | Environmental Geology | 162 | Logistic regression (LR) and Information value (Statistical method index). | 25 |
| Yesilnacar and Topal | 2005 | Engineering Geology | 290 | Logistic Regression (LR) and Artificial Neural Networks (ANN) | 25 |
| Bathurst et al. | 2006 | Hydrological processes | 500 | SHETRAN | 45 |
| Clerici et al. | 2006 | Environmental Geology | 167 | Conditional probability model (CPM) | 5 |
| Davis et al. | 2006 | Computer & Geosciences | 202 | Likelihood frequency ratio (LFR) | 10 |
| Duman et al. | 2006 | Environmental Geology | 174.8 | Logistic regression (LR) | 25 |
| Gorsevski et al. | 2006 | Geomorphology | 72 | Infinite slope model (ISS) | |

| | | | | | |
|---|---|---|---|---|---|
| Guzzetti *et al.* | 2006 | Geomorphology | 78 | Linear discriminant analysis (LDA) | 10 |
| Havenith *et al.* | 2006 | Landslides | 1250000 | Conditional probability model (CPM) and Newmarks method | 30 |
| Hong *et al.* | 2006 | Natural Hazards | All the world | Weighted linear combination (WLC). | 30 |
| Huang *et al.* | 2006 | Nat. Hazards Earth Syst. Sci | 106 | SHALSTAB | 40 |
| Kanungo *et al.* | 2006 | Engineering Geology | 300 | Simple ranking, Artificial Neural Networks (ANN), Neuro-Fuzzy, Fuzzy standard membership (FSMs). | 25 |
| Komac | 2006 | Geomorphology | 1220 | Analytical hierarchy process (AHP) | 25 |
| Lee & Evangelista | 2006 | Nat. Hazards Earth Syst. Sci | 29.5 | Artificial Neural Networks (ANN) | 10 |
| Lee and Sambath | 2006 | Environmental Geology | 12080 | Likelihood frequency ratio (LFR) and Logistic regression (LR) | 30 |
| Sakar *et al.* | 2006 | Disaster Mitigation of Debris Flows, Slope A2ilures and Landslides | 549 | Information value (Statistical method index) | 25 |
| Salclarini *et al.* | 2006 | Landslides | 100 | TRIGRS | |
| Van Den Eeckhaut *et al.* | 2006 | Geomorphology | 200 | Rare event Logistic regression | 10 |
| Yoshimatsu and Abe | 2006 | Landslides | 370000 | Analytical hierarchy process (AHP) | |
| Akgun and Bulut | 2007 | Environmental Geology | 38 | Logistic regression (LR) & Analytical hierarchy process (AHP) | 25 |
| Champati ray *et al.* | 2007 | Landslides | 185 | Fuzzy standard membership (FSMs) | 10 |
| Chang *et al.* | 2007 | Geomorphology | 92 | Logistic regression (LR) | 40 |
| Coelho-Netto *et al.* | 2007 | Geomorphology | 112 | Logical analytical (Morphometric subdivision) | 10 |
| Demoulin and Chug | 2007 | Geomorphology | 178 | Multivariate likelihood ratio function | 30 |
| Dominguez-Cuesta *et al.* | 2007 | Geomorphology | 278 | Logistic regression (LR) | 5 |
| Greco *et al.* | 2007 | Engineering Geology | 850 | Logistic regression (LR) | 10 |
| Irrigaray *et al.* | 2007 | Natural Hazards | 39 | Cluster analysis (matrix assessment) | 10 |
| Lee | 2007 | International Journal of Remote Sensing | 47.94 | Artificial Neural Networks (ANN) | 5 |
| Lee | 2007 | Environmental Geology | 68 | Fuzzy standard membership (FSMs) | 5 |
| Lee & Pradhan | 2007 | Landslides | 8800 | Likelihood frequency ratio (LFR) & Logistic regression (LR) | 25 |
| Lee (b) | 2007 | Earth SurA2ce Processes and Landforms | 66 | Logistic regression (LR) | 10 |
| Lee *et al.* | 2007 | Landslides | 66 | Artificial Neural Networks (ANN), Logistic regression (LR), Likelihood frequency ratio (LFR). | 10 |
| Mathew *et al.* | 2007 | International Journal of Remote Sensing | 100 | Logistic regression (LR) | 25 |
| Meisina & Scarabelli | 2007 | Geomorphology | 5 | SINMAP & SHALSTAB | 5 |

| | | | | | |
|---|---|---|---|---|---|
| Neuhäuser and Terhorst | 2007 | Geomorphology | 500 | Weight of evidence (WofE) | 150 |
| Thiery et al. | 2007 | Geomorphology | 100 | Weight of evidence (WofE) | 10 |
| Yalcin & Bulut | 2007 | Natural Hazards | 50 | Analytical hierarchy process (AHP) | 25 |
| Akgun et al. | 2008 | Environmental Geology | 43 | Likelihood frequency ratio (LFR) & Analytical hierarchy process (AHP) | 25 |
| Anbalagan et al., | 2008 | Journal of scientific & Industrial research | 8 | BIS based Landslide Hazard Evaluation A2ctor (LHEF) | 5 |
| Brenning | 2008 | Book chapter (J. Böhner, T. Blaschke & L. Montanarella (eds.)) | 11.2 | Generalized additive models (GAM) | |
| Caniani et al. | 2008 | Natural Hazards | 174 | Artificial Neural Networks (ANN) | 20 |
| Carrara et al. | 2008 | Geomorphology | 300 | Linear discriminant analysis (LDA), LR, SHALSTAB | 10 |
| Castellanos and van Westen | 2008 | Geomorphology | 600 | Analytical hierarchy process (AHP) | 50 |
| Conoscenti et al. | 2008 | Geomorphology | 194 | Conditional probability model (CPM) | 40 |
| Dahal et al. | 2008 | Environmental Geology | | Weight of evidence (WofE) | 5 |
| García-Rodriguez et al. | 2008 | Geomorphology | 20000 | Logistic regression (LR) | 25 |
| Godt et al. | 2008 | Engineering Geology | 3 | TRIGRS | 1.83 |
| Gorum et al. | 2008 | Natural Hazards | 108 | Logistic regression (LR) | 25 |
| Gulla et al. | 2008 | Geomorphology | 15000 | Conditional probability model (CPM) | 40 |
| He & Beighley | 2008 | Earth SurA2ce Processes and Landforms | 33220 | Conditional probability model (CPM) | 30 |
| Lee et al. | 2008 | Nat. Hazards Earth Syst. Sci | 705 | Linear discriminant analysis (LDA) | 25 |
| Liu and Wu | 2008 | Environmental Geology | 1 | TRIGRS / Monte Carlo Simulation | 10 |
| Magliulo et al. | 2008 | Natural Hazards | 314 | Information value (Statistical method index) | 20 |
| Melchiorre et al. | 2008 | Geomorphology | 20 | Artificial Neural Networks (ANN) and Cluster analysis (matrix assessment) | 5 |
| Nefeslioglu et al. | 2008 | Engineering Geology | 10 | Logistic regression (LR) and Artificial Neural Networks (ANN) | 25 |
| Nefeslioglu et al. | 2008 | Geomorphology | 118 | Logistic regression (LR) | 25 |
| Pandey et al. | 2008 | Environmental Geology | 1556 | Simple ranking | 200 |
| Park & Chi | 2008 | International Journal of Remote Sensing | 11 | Generalized additive models (GAM). | 5 |
| Ruff and Czurda | 2008 | Geomorphology | 115 | Slope A2ilure Potential Index (SFPI) | 25 |
| Ruff and Rohn | 2008 | Environmental Geology | 50 | Simple ranking | 25 |
| Simoni et al. | 2008 | Hydrological processes | 2.85 | GEOtop-FS | 2 |
| Tunusluoglu et al. | 2008 | Environmental Geology | 225 | Logistic regression (LR) | 25 |
| Vijith & Madhu | 2008 | Environmental Geology | 154.99 | Likelihood frequency ratio (LFR). | 20 |

| | | | | | |
|---|---|---|---|---|---|
| Yalcin | 2008 | Catena | 50 | Analytical hierarchy process (AHP), Information value (Statistical method index) & weighting A2ctor (WF). | 25 |
| Yao *et al.* | 2008 | Geomorphology | 1100 | Support Vector Machine (SVM) | 5 |
| Zolfaghari and Heath | 2008 | Computers and Geotechnics | 2.5 | SlopeSGA / Monte Carlo simulation | 5 |
| Avanzi *et al.* | 2009 | Nat Hazards | 1 | SHALSTAB | 5 |
| Chen *et al.* | 2009 | Environmental Geology | 550 | Artificial Neural Networks (ANN) (back-propagation algorithm) | |
| Deb and El-Kadi | 2009 | Geomorphology | 384 | SINMAP | 10 |
| A2laschi *et al.* | 2009 | Natural Hazards | 40 | Conditional probability model (CPM), Logistic regression (LR) & Artificial Neural Networks (ANN) | 50 |
| Guzzetti *et al.* | 2009 | Geogr. Fis. Dinam. Quat | 79 | Linear discriminant analysis (LDA) | 10 |
| Haneberg *et al.* | 2009 | Bull Eng Geol Environ | 120 | PISA | 1 |
| Jiménez-Perálvarez *et al.* | 2009 | Natural Hazards | 158 | Cluster analysis (matrix assessment) | 10 |
| Kawabata and Bandibas | 2009 | Geomorphology | 680 | Artificial Neural Networks (ANN) | 15 |
| Kuriakose *et al.* | 2009 | Earth SurA2ce Processes and Landforms | 55.6 | PROBSTAB + Starwars | 20 |
| Legorreta Paulín and Bursik | 2009 | Computer & Geosciences | 96 | SINMAP and Logistic regression (LR) | 30 |
| Mathew *et al.* | 2009 | Landslides | 396 | Logistic regression (LR) | 20 |
| Meusburger & Alewell | 2009 | Nat. Hazards Earth Syst. Sci | 30 | Logistic regression (LR) | 25 |
| Nandi and Shakoor | 2009 | Geomorphology | 2015 | Weight of evidence (WofE) and Logistic regression (LR) | 10 |
| Oh *et al.* | 2009 | Environmental Geology | 2000 | Likelihood frequency ratio (LFR) and Logistic regression (LR) | 30 |
| Ozdemir | 2009 | Environmental Geology | 20 | Conditional probability model (CPM) | 20 |
| Saito *et al.* | 2009 | Geomorphology | 900 | Decision tree (DT) | 50 |
| Sharma *et al.* | 2009 | Eighteenth United Nations Regional Cartographic. Conference for Asia and the Pacific | 36 | Information value (Statistical method index). | 50 |
| Terhorst and Kreja | 2009 | Landslides | | SINMAP | |
| Vahidnia *et al.* | 2009 | International Journal of Civil Engineerng. | 3440 | Logistic regression (LR), Analytical hierarchy process (AHP), Artificial Neural Networks (ANN), Weight of evidence (WofE). | 1000 |
| Van Den Eeckhaut *et al.* | 2009 | Nat. Hazards Earth Syst. Sci | 277 | Canonical Discriminant Analysis & Discriminant Analysis (LDA) | 10 |
| Wan | 2009 | Engineering Geology | 750 | Decision tree (DT) (Entropy-based classification EBC) | 12.5 |

| | | | | | |
|---|---|---|---|---|---|
| Wang *et al.* | 2009 | Environmental Geology | 176167 | Combination and overlapping maps and Trapezoidal fuzzy number weighting | 500 |
| Wu and Chen | 2009 | Geomorphology | 6232 | Analytical hierarchy process (AHP) | 20 |
| Yilmaz | 2009 | Computers & Geosciences | 25 | Likelihood frequency ratio (LFR), Artificial Neural Networks (ANN) and Logistic regression (LR) | 10 |
| Bai et al | 2010 | Geomorphology | 260 | Logistic regression (LR) | 25 |
| Bălteanu *et al.* | 2010 | Geomorphology | 238,391 | Likelihood frequency ratio (LFR) | 100 |
| Blauth *et al.* | 2010 | Geomorphology | 450 | Weight of evidence (WofE) | 10 |
| Cervi *et al.* | 2010 | Landslides | 450 | Fuzzy standard membership (FSMs), Weight of evidence (WofE), SHALSTAB | 10 |
| Chauan *et al.* | 2010 | Landslides | 600 | Logistic regression (LR) | 50 |
| Dahl *et al.* | 2010 | Nat. Hazards Earth Syst. Sci | 8.15 | Combination and overlapping maps | 10 |
| Das *et al.* | 2010 | Geomorphology | 12 | Logistic regression (LR) | 10 |
| Erener and Düzgün | 2010 | Environ Earth Sci | 330 | Logistic regression (LR), Spatial regression (SR) | 20 |
| Erener *et al.* | 2010 | Landslides | 12168 | Geographically weighted regression & spatial regression | 30 |
| Kamp *et al.* | 2010 | Natural Hazards | 2250 | Analytical hierarchy process (AHP) | 15 |
| Klimes & Escobar | 2010 | Nat. Hazards Earth Syst. Sci | 51.22 | Weighted linear combination (WLC) & Distribution expert-analysis. | 5 |
| Lee *et al.* | 2010 | Nat. Hazards Earth Syst. Sci | 128 | Logistic regression (LR) | 5 |
| Legorreta Paulín *et al.* | 2010 | Physics and Chemistry of the Earth | 1 | SINMAP and Logistic regression (LR) | 1, 5, 10 and 30 |
| Mancini *et al.* | 2010 | Nat. Hazards Earth Syst. Sci | 1300 | Logistic regression (LR) | 40 |
| Pareek *et al.* | 2010 | Landslides | 1300 | Information value (Statistical method index) (IV) | 6 |
| Pradhan | 2010 | Advances in Space Research | 295 | Logistic regression (LR) | 10 |
| Pradhan and Lee | 2010 | Landslides | 293 | Artificial Neural Networks (ANN) | 25 |
| Pradhan and Lee (a) | 2010 | Environmental modelling and software | 500 | Artificial Neural Networks (ANN), Likelihood frequency ratio (LFR) and Logistic regression (LR) | 10 |
| Regmi *et al.* | 2010 | Geomorphology | 815 | Weight of evidence (WofE) | 10 |
| Rossi *et al.* | 2010 | Geomorphology | 79 | Logistic regression (LR), Linear discriminant analysis (LDA), Quadratic discriminant analysis (QDA),Artificial Neural Networks (ANN) | 10 |
| Sorbino *et al.* | 2010 | Natural Hazards | 60 | SHALSTAB, TRIGRS (unsaturated) | 3 |

| | | | | | |
|---|---|---|---|---|---|
| Vahidnia *et al.* | 2010 | Computers & Geosciences | | Neuro-Fuzzy and Artificial Neural Networks (ANN) | |
| Van Den Eeckhaut *et al.* | 2010 | Geomorphology | 1120 | Logistic regression (LR) and Index method (GEGEAA) | 50 |
| Yeon *et al.* | 2010 | Engineering Geology | 34 | Decision tree (DT) (CART) | 5 |
| Akbar and Ryong Ha | 2011 | Landslides | 16 | Information value (Statistical method index). | 10 |
| Akgün and  Türk | 2011 | Computers & Geosciences | 424 | Logistic regression (LR) | 25 |
| Arnone *et al.* | 2011 | Geomorphology | | Infinite slope model (ISS) | |
| Atkinson and Massari | 2011 | Geomorphology | 65 | Logistic regression (LR) & Spatial regression (Auto-logistic regression) | 10 |
| Clerici *et al.* | 2011 | Natural Hazards | 129 | Conditional probability model (CPM) | 5 |
| Constantin *et al.* | 2011 | Environmental Earth Sciences | 47 | Entropy Index (IE). | 10 |
| Das *et al.* | 2011 | Landslides | 8 | Logistic regression (LR) | 10 |
| Floris *et al.* | 2011 | Nat. Hazards Earth Syst. Sci | 50 | Likelihood frequency ratio (LFR). | 5 |
| Goetz *et al.* | 2011 | Geomorphology | 610 | Generalized additive models (GAM),Infinite slope model (ISS) & SHALSTAB | 25 |
| Gosh *et al.* | 2011 | Geomorphology | 90 | Analytical hierarchy process (AHP) | 10 |
| Jadda *et al.* | 2011 | Natural Hazards | 1000 | Likelihood frequency ratio (LFR). | 10 |
| Kannan *et al.* | 2011 | Journal of the Indian Society of Remote Sensing | 10 | BIS based Landslide Hazard Evaluation A2ctor (LHEF) | 25 |
| Kanungo *et al.* | 2011 | Natural Hazards | 254 | Artificial Neural Networks (ANN), Likelihood frequency ratio (LFR), Certainty A2ctors (CF). | 25 |
| Marjanović *et al.* | 2011 | Engineering Geology | 100 | Support Vector Machine (SVM), Analytical hierarchy process (AHP) | 25 |
| Melchiorre *et al.* | 2011 | Computers & Geosciences | | Artificial Neural Networks (ANN) | |
| Mondal and Maiti | 2011 | J. Indian Soc. remote sensing | | Analytical hierarchy process (AHP) | |
| Montrasio *et al.* | 2011 | Nat. Hazards Earth Syst. Sci | 1200 | TRIGRS and SLIP | 20 |
| Oh and Pradhan | 2011 | Computers & Geosciences | | Neuro-Fuzzy | |
| Ozdemir | 2011 | Natural Hazards | 373 | Weight of evidence (WofE) | 20 |
| Rotigliano *et al.* | 2011 | Natural Hazards | 25 | Conditional probability model (CPM) | 40 |
| Sterlacchini *et al.* | 2011 | Geomorphology | 450 | Weight of evidence (WofE) | 10 |
| Sujatha & Rajamanickam | 2011 | Natural Hazards | 63.44 | Fuzzy standard membership (FSMs) | 30 |
| Tarolli *et al.* | 2011 | Geomorphology | | dSLAM and SHALSTAB | |

| | | | | | |
|---|---|---|---|---|---|
| Tien Bui *et al.* | 2011 | Natural Hazards | 4650 | Logistic regression (LR) and Information value (Statistical  method index). | 20 |
| Vergari *et al.* | 2011 | Nat. Hazards Earth Syst. Sci | 120 | Conditional probability model (CPM) | 50 |
| von Ruette *et al.* | 2011 | Geomorphology | 18 | Logistic regression (LR) | 10 |
| Yalcin *et al.* | 2011 | Catena | 4660 | Likelihood frequency ratio (LFR), Analytical hierarchy process (AHP), Information value (Statistical  method index), weighting A2ctors (WF), Logistic regression (LR) | 10 |
| Akgun | 2012 | Landslides | 1800 | Logistic regression (LR), Likelihood frequency ratio (LFR), Analytical hierarchy process (AHP) | 25 |
| Akgun *et al.* | 2012 | Computers & Geosciences | | Mamdani-type fuzzy inference system | |
| Althuwaynee *et al.* | 2012 | Computers & Geosciences | 1975 | Dempster-Shafer evidential belief function | 10 |
| Armas | 2012 | Natural Hazards | 20 | Weight of evidence (WofE) | 25 |
| Bai et al | 2012 | Catena | 8917 | Logistic regression (LR) | 30 |
| Bednarik *et al.* | 2012 | Natural Hazards | 380 | Entropy Index (IE) | 10 |
| Che *et al.* | 2012 | Catena | 361 | Information value (Statistical  method index) | 20 |
| Choi *et al.* | 2012 | Engineering Geology | 68 | Likelihood frequency ratio (LFR), Logistic regression (LR), Artificial Neural Networks (ANN) | 15 |
| Conforti *et al.* | 2012 | Natural Hazards | 185 | Information value (Statistical method index) | 10 |
| Costanzo *et al.* | 2012 | Natural Hazards | 80 | Conditional probability model (CPM) | 10 |
| Costanzo *et al.* (b) | 2012 | Nat. Hazards Earth Syst. Sci | 10 | Conditional probability model (CPM) | 10 |
| Das *et al.* | 2012 | Geomorphology | 12 | Bayesian logistic regression and Logistic regression (LR). | 10 |
| Graff *et al.* | 2012 | Natural Hazards | 754 | Cluster analysis (matrix assessment) | 15 |
| Grozavu *et al.* | 2012 | IGC 2012 proceedings | 136 | Logistic regression (LR) and Analytical hierarchy process (AHP) | 5 |
| Günther *et al.* | 2012 | Landslides | Italy | Linear discriminant analysis (LDA) | 90 |
| Günther *et al.* | 2012 | Landslides | Europe | Analytical hierarchy process (AHP) | 1000 |
| Hasekioguları & Ercanoglu | 2012 | Natural Hazards | 567 | Analytical hierarchy process (AHP) | 20 |
| He *et al.* | 2012 | Geomorphology | 131 | Kernel based Fisher DA | 30 |
| Jagielko *et al.* | 2012 | Natural Hazards | 10000 | Linear discriminant analysis (LDA) | 25 |
| Jia *et al.* | 2012 | Computers & Geotechniques | 1.15 | 3D Hovland model / Monte Carlo simulation. | 1 |
| Kayastha *et al.* | 2012 | Natural Hazards | 562 | Weight of evidence (WofE) | 20 |
| Klimes & Blahut | 2012 | Natural Hazards | 43 | SINMAP & distribution analysis | No report |
| Lee *et al.* | 2012 | Catena | 60 | Dempster-Shafer evidential belief function | 10 |

| | | | | | |
|---|---|---|---|---|---|
| Lee *et al.* | 2012 | International Journal of Remote Sensing | 60 | Likelihood frequency ratio (LFR), Weight of evidence (WofE), Logistic regression (LR) & Artificial Neural Networks (ANN) | 10 |
| Li *et al.* | 2012 | Natural Hazards | 1174 | Fractal Box-counting (FB-C) | 10 |
| Neuhäuser *et al.* | 2012 | Landslides | 573 | Weight of evidence (WofE) | 30 |
| Oh *et al.* | 2012 | International Journal of Remote Sensing | 68.43 | Likelihood frequency ratio (LFR), Logistic regression (LR). | 15 |
| Pereira *et al.* | 2012 | Nat. Hazards Earth Syst. Sci | 70 | Information value (Statistical method index) | 10 |
| Petschko *et al.* | 2012 | Book chapter (Eberhardt *et al.* (eds).) | 2072 | Generalized additive models (GAM). | 10 |
| Piacentini *et al.* | 2012 | Geomorphology | 7500 | Weight of evidence (WofE) | 20 |
| Pourghasemi *et al.* | 2012 | Natural Hazards | 114.5 | Analytical hierarchy process (AHP) & Fuzzy standard membership (FSMs). | 10 |
| Pourghasemi *et al.* | 2012 | Applied mechanics and materials | 3430 | Entropy Index (IE) | |
| Pourghasemi *et al.* (b) | 2012 | Catena | 162.6 | Conditional probability model (CPM) & Entropy Index (IE) | 25 |
| Pourghasemi *et al.* (C) | 2012 | Book chapter: B. Pradhan and M. Buchroithner (eds.), Terrigenous Mass Movements | 114 | Spatial multi criteria evaluation (SMCE) | 10 |
| Rapolla *et al.* | 2012 | Natural Hazards | 13590 | Simple ranking | 100 |
| Rawat & Joshi | 2012 | International Journal of Remote Sensing | 306 | Information value (Statistical method index) | 30 |
| Roodposhti *et al.* | 2012 | Natural Hazards | 2500 | Fuzzy-AHP & Outranking (PROMETHE II) | 30 |
| Rosito Listo and Carvalho Vieira | 2012 | Geomorphology | | SHALSTAB | |
| Roslee *et al.* | 2012 | Journal of Geography and Geology. Canadian Center of Science and Education | 160 | Infinite slope model (ISS) | |
| Rotigliano *et al.* | 2012 | Natural Hazards | 90 | Conditional probability model (CPM) | 40 |
| Schicker and Moon | 2012 | Geomorphology | 25000 | Logistic regression (LR) and Weight of evidence (WofE) | 25 |
| Sharma & Mehta | 2012 | Natural Hazards | 100 | Simple ranking | 50 |
| Sujatha *et al.* | 2012 | J. Earth Syst. Sci. (India) | 63.44 | Certainty A2ctors (CF). | 30 |
| Tien Bui | 2012 | Computers &Geosciences | 4460 | Adaptive Neuro-Fuzzy Inference System (ANFIS) | 20 |
| Tien Bui *et al.* | 2012 | Geomorphology | 4660 | Artificial Neural Networks (ANN) (Levenberg–Marquardt and Bayesian regularized) | 20 |
| Tien Bui *et al.* | 2012 | Catena | 4660 | Dempster-Shafer Evidential belief functions & Fuzzy standard membership (FSMs) | 20 |
| Tien Bui *et al.* | 2012 | Mathematical Problems in Engineering | 4660 | Support Vector Machine (SVM), Decision tree (DT) (C4.5) and Naïve Bayes | 20 |
| Van Den Eeckhaut *et al.* | 2012 | Landslides | Europe | Logistic regression (LR) | 30 |

| | | | | | |
|---|---|---|---|---|---|
| Vorpahl *et al.* | 2012 | Ecological Modelling | 8.4 | Logistic regression (LR), Generalized additive models (GAM), Multivariate adaptive regression splines (MARS), Artificial Neural Networks (ANN), Decision tree (DT) (CART) (DRoT), Random forest, Maximum entropy (MAXENT). | 10 |
| Xu *et al.* | 2012 | Computers & Geosciences | | Logistic regression (LR), Artificial Neural Networks (ANN), Support Vector Machine (SVM) | |
| Bhandary *et al.* | 2013 | Natural Hazards | 30 | Information value (Statistical method index) and Logistic regression (LR) | 10 |
| Calvello *et al.* | 2013 | Geomorphology | 670 | Linear discriminant analysis (LDA) | 25 and 95 |
| Capparelli & Versace | 2013 | Hydrology and earth system sciences | 60 | SUSHI | |
| Catani *et al.* | 2013 | Nat. Hazards Earth Syst. Sci | 9100 | Random forest | 20, 50, 100, 250, 500 |
| Costanzo *et al.* | 2013 | Landslides | 80 | Logistic regression (LR) | 8 |
| Costanzo et.al | 2013 | Landslides | 80 | Logistic regression (LR) | 10 |
| Demir *et al.* | 2013 | Natural Hazards | 144 | Likelihood frequency ratio (LFR) & Analytical hierarchy process (AHP) | 25 |
| Devkota *et al.* | 2013 | Natural Hazards | 65 | Certainty A2ctors (CF) and Entropy Index (IE). | 20 |
| EpiA2nio *et al.* | 2013 | Journal of Coastal Research | 12 | Information value (Statistical method index) | 5 |
| Feizizadeh & Blaschke | 2013 | Natural Hazards | 21118 | Analytical hierarchy process (AHP), Weighted linear combination (WLC) & Ordered weighted average | 20 |
| Felicisimo *et al.* | 2013 | Landslides | 140 | Logistic regression (LR), Decision tree (DT) (CART), Multivariate adaptive regression splines (MARS), Maximum entropy (MAXENT). | 10 |
| Ferentinou and Chalkias | 2013 | WLF II | Grece | Logistic regression (LR), Artificial Neural Networks (ANN), Likelihood frequency ratio (LFR). | 250 |
| Gattinoni & Scesi | 2013 | Natural Hazards | 26.2 | Weight of evidence (WofE) & FLtAC | 10 |
| Grelle *et al.* | 2013 | Bulletin of Engineering Geology and the Environment | | TRIGRS | |
| Guidi and Scudero | 2013 | Nat. Hazards Earth Syst. Sci | 30 | Information value (Statistical method index) | 10 |
| Holec *et al.* | 2013 | Natural Hazards | 86000 | Entropy Index (IE) & Conditional probability model (CPM) | 26 |
| Kavzoglu | 2013 | Landslides | 4664 | Analytical hierarchy process (AHP), Support Vector Machine (SVM) and Logistic regression (LR) | 25 |
| Kavzoglu *et al.* | 2013 | Landslides | 4664 | Analytical hierarchy process (AHP), Support Vector Machine (SVM) and Logistic regression (LR) | 30 |
| Kayastha *et al.* | 2013 | Computer & Geosciences | 562 | Analytical hierarchy process (AHP) | 20 |
| Lee *et al.* | 2013 | Catena | 60 | Dempster-Shafer evidential belief function | 10 |

| | | | | | |
|---|---|---|---|---|---|
| Legorreta Paulín *et al.* | 2013 | WLF II | 111 | Logistic regression (LR) | 10 |
| Leopold *et al.* | 2013 | WLF II | 15000 | Logistic regression (LR), Weight of evidence (WofE) | 10 |
| Lepore *et al.* | 2013 | Hydrol. Earth Syst. Sci | 16.7 | Triangulated Irregular Network-based Real-time Integrated Basin, Vegetation Generator for Interactive Evolution tRIDS-VEGGIE | 30 |
| Liu *et al.* | 2013 | Natural Hazards | 9600000 | Artificial Neural Networks (ANN) | 90 |
| Ma *et al.* 2013 | 2013 | Landslides | 26386 | Analytical hierarchy process (AHP) (least-squares method) | |
| Martha *et al.* | 2013 | Geomorphology | 81 | Weight of evidence (WofE) | 10 |
| Neelkatan & Yuvaraj | 2013 | Arabian Journal of Geosciences | 325 | Relative effect (modification of information value) | |
| Park *et al.* | 2013 | Engineering Geology | 60 | Infinite slope model (ISS) / Monte Carlo Simulation. | 10 |
| Pellicani *et al.* | 2013 | Landslides | 1282 | Analytical hierarchy process (AHP) | 10 |
| Petschko *et al.* | 2013 | Nat. Hazards Earth Syst. Sci | 15850 | Generalized additive models (GAM). | 50 |
| Pourghasemi *et al.* (a) | 2013 | Natural Hazards | 900 | Logistic regression (LR), Information value (Statistical method index) & Analytical hierarchy process (AHP) | 10 |
| Pradhan | 2013 | Computers & Geosciences | 34 | Decision tree (DT) (CHAID), Support Vector Machine (SVM) and Neuro-Fuzzy | 10 |
| Ramakrishnan *et al.* | 2013 | Natural Hazards | 140 | Artificial Neural Networks (ANN) (back-propagation) | |
| Regmi *et al.* | 2013 | Landslides | 815 | Logistic regression (LR) | 10 |
| Rossi *et al.* | 2013 | Nat. Hazards Earth Syst. Sci. | 38 | HIRESSS / Monte Carlo simulation | 5 |
| Sabatakakis *et al.* | 2013 | Natural Hazards | 131957 | Factor Analysis | 1000 |
| Sdao *et al.* | 2013 | Nat. Hazards Earth Syst. Sci | 1 | Neuro-Fuzzy model | 3 |
| Setayeshirad *et al.* | 2013 | Natural Hazards | 1500 | Infinite slope model (ISS) | 20 |
| Thiebes *et al.* | 2013 | Engineering Geology | | CHASM | |
| Thiery *et al.* | 2013 | Landslides | 11 | Weight of evidence (WofE) and Fuzzy standard membership (FSMs) | 10 |
| Torgoev and Havenith | 2013 | WLF II | | Linear discriminant analysis (LDA), Artificial Neural Networks (ANN), Newmark Method | 30 |
| Wang *et al.* | 2013 | Natural Hazards | 25 | Matrix global susceptibility | 10 |
| Wang *et al.* | 2013 | Landslides | 385000 | Analytical hierarchy process (AHP) | 1000 |
| Wang *et al.* | 2013 | Computers & Geosciences | | Logistic regression (LR) | |

| | | | | | |
|---|---|---|---|---|---|
| Xu *et al.* | 2013 | Natural Hazards | 48678 | Logistic regression (LR) | 20 |
| Zizioli *et al.* | 2013 | Nat. Hazards Earth Syst. Sci | 13.36 | TRIGRS, SHALSTAB, SINMAP, SLIP | 10 |
| Althuwaynee *et al.* | 2014 | Landslides | 170 | Decision tree (DT) (CHi-squared Automatic Interaction Detector CHAID) | 5 |
| Althuwaynee *et al.* | 2014 | Catena | 170 | Dempster-Shafer evidential belief function, Analytical hierarchy process (AHP) and Logistic regression (LR) | 5 |
| Alvioli *et al.* | 2014 | Geomorphology | | TRIGRS | |
| Armas *et al.* | 2014 | Natural Hazards | 1 | Infinite slope model (ISS) | 25 |
| Arnone *et al.* | 2014 | Procedia Earth and Planetary Science | 16 | tRIBS-VEGGIE /Monte Carlo simulation | |
| Chang *et al.* | 2014 | Geomorphology | 2868 | Logistic regression (LR) | 2 |
| Conforti *et al.* | 2014 | Catena | 30 | Artificial Neural Networks (ANN) | 10 |
| Ding & Hu | 2014 | Natural Hazards | 120 | Cluster analysis (matrix assessment) | 25 |
| Feizizadeh and Blaschke | 2014 | International Journal of Geographical Information Science | 19913 | Analytical hierarchy process (AHP) | 20 |
| Feizizadeh *et al.* | 2014 | Computer & geociences | 3929 | Fuzzy-AHP | 30 |
| Formetta *et al.* | 2014 | Procedia Earth and Planetary Science | 1 | GEOtop-FS | 5 |
| Formetta *et al.* | 2014 | Procedia Earth and Planetary Science | 2 | GEOtop-FS | 5 |
| Fressard *et al.* | 2014 | Nat. Hazards Earth Syst. Sci | 2500 | Logistic regression (LR) | 10 |
| Fuchs *et al.* | 2014 | Geomorphology | 80 | Infinite slope model (ISS) / Monte Carlo Simulation. | 10 and 30 |
| Giulio *et al.* | 2014 | Natural Hazards | 82 | Logistic regression (LR) | 20 |
| Günther *et al.* | 2014 | Geomorphology | All Europe | Analytical hierarchy process (AHP) | 1000 |
| Kim *et al.* | 2014 | Engineering Geology | 6 | YS-Slope model | 1 |
| Legorreta Paulín *et al.* | 2014 | Natural Hazards | 5.4 | Logistic regression (LR) | 10 |
| Lu *et al.* | 2014 | Engineering Geology | 30 | Finite model (Three-dimensional discrete element modeling) | 40 |
| Mansouri Daneshvar | 2014 | Landslides | 2470 | Analytical hierarchy process (AHP) | 25 |
| Mansouri Daneshvar | 2014 | Landslides | 2470 | Analytical hierarchy process (AHP) | 100 |
| Meinhardt *et al.* | 2014 | Geomorphology | 12400 | Information value (Statistical method index), Weighting A2ctors (WF) and Omit error method. | 30 |
| Mergili *et al.* | 2014 | Geomorphology | 78.9 | r.slope.stability (3D Hovland model modify) | 5 |
| Michel *et al.* | 2014 | J Soils Sediments | | SHALSTAB & SINMAP | |
| Nourani *et al.* | 2014 | Natural Hazards | 260 | Likelihood frequency ratio (LFR), Logistic regression (LR),Artificial Neural Networks (ANN) & genetic programming | 10 |
| Osna *et al.* | 2014 | Computer & Geosciences | 300 | Mamdani-type fuzzy inference system | 25 |

| | | | | | |
|---|---|---|---|---|---|
| Peng *et al.* | 2014 | Geomorphology | 396 | Support Vector Machine (SVM) | 28.5 |
| Poiraud | 2014 | Geomorphology | 200 | Likelihood frequency ratio (LFR), Weight of evidence (WofE), Logistic regression (LR), Decision tree (DT) (C4.5) and Unique Condition Unit simple. | 15 |
| Pradhan & Kim | 2014 | Natural Hazards | 33.4 | Relative effect (modification of information value) | 5 |
| Reichenbach *et al.* | 2014 | Environmental management | 60 | Logistic regression (LR), Linear discriminant analysis (LDA), Quadratic discriminant analysis | 5 |
| Sabokbar *et al.* | 2014 | Geomorphology | 34300 | Principal component analysis (PCA) | 30 |
| Shahabi *et al.* | 2014 | Catena | 520 | Analytical hierarchy process (AHP), Likelihood frequency ratio (LFR) and Logistic regression (LR) | 100 |
| Taner San | 2014 | International Journal of Applied Earth Observation and Geoinformation | 245 | Support Vector Machine (SVM) | 15 |
| Thiebes *et al.* | 2014 | Landslides | | CHASM | |
| Umar *et al.* | 2014 | Catena | 1328 | Logistic regression (LR) and Likelihood frequency ratio (LFR). | 10 |
| Zhu *et al.* | 2014 | Geomorphology | 4600 | Fuzzy standard membership (FSMs) | 5 |
| Ahmed | 2015 | Landslides | 775 | Analytical hierarchy process (AHP), Weighted linear combination (WLC), Ordered weighted average (OWA). | 30 |
| Bregoli *et al.* | 2015 | Landslides | 264 | Infinite slope model (ISS) | 5 |
| Cascini *et al.* | 2015 | Geomorphology | 2000 | Distribution expert-analysis, weight of evidence (WofE), TRIGRS | 95 and 25 |
| Conoscenti *et al.* | 2015 | Geomorphology | 51 | Logistic regression (LR) & Multivariate adaptive regression splines (MARS) | 10 |
| Dehnaui *et al.* | 2015 | Catena | 1648195 | Neuro-Fuzzy | 90 |
| Goetz *et al.* (b) | 2015 | Computer & Geosciences | 50 | Logistic regression (LR), Generalized additive models LR (GAM), Weights of evidence (WofE), Support Vector Machine (SVM), Random Forest, Decision tree (DT) (Bootstrap Aggregated Classification Trees (BPLDA)). | 10 |
| Gorsevski *et al.* | 2015 | Landslides | 136 | Artificial Neural Networks (ANN) | 0.7 |
| Guo *et al.* | 2015 | Geomorphology | 7339 | Likelihood frequency ratio (LFR), Weight of evidence (WofE) | 10 |
| Havenith *et al.* | 2015 | Geomorphology | 720000 | Landslide density maps (LDsM) | 100 |
| Hong *et al.* | 2015 | Catena | 1994 | Kernel logistic regression, Support Vector Machine (SVM) and Decision tree (DT) (Alterning decision ADT) | 25 |
| Ilia and Tsangaratos | 2015 | Landslides | 167.6 | Weight of evidence (WofE) | 5 |
| Kavzoglu *et al.* | 2015 | Engineering Geology | 885 | Logistic regression (LR) | 30 |
| Kirschbaum *et al.* | 2015 | Landslides | 700000 | Fuzzy overlay | 1000 |

| | | | | | |
|---|---|---|---|---|---|
| Kritikos and Davies | 2015 | Landslides | 7500 | Fuzzy standard membership (FSMs) | 25 |
| Lee and Park | 2015 | Landslides | 10 | Infinite slope model (ISS) | 10 |
| Liu *et al.* | 2015 | Landslides | 576 | Likelihood frequency ratio (LFR) | 5 |
| Moosavi and Niazi | 2015 | Landslides | 272 | Artificial Neural Networks (ANN), Support Vector Machine (SVM), Maximum entropy (MAXENT), Logistic Regression (LR), Wavelet-based (Wb) | 15 |
| Palamakumbure *et al.* | 2015 | Computer & Geosciences | 94 | Decision tree (DT) (See5) | 2, 5, 10, 15, 20, 25, 30, 40 |
| Rabonza *et al.* | 2015 | Landslides | 7246 | SINMAP | 5 |
| Raghuvanshi *et al.* | 2015 | Egyptian Journal of Remote Sensning and Space Science | 74 | Weighted overlay method (WOM) | 10 |
| Shou and Yang | 2015 | Engineering Geology | 500 | Logistic regression (LR) | 20 |
| Texeira *et al.* | 2015 | Landslides | | SHALSTAB & Infinite slope model (ISS) | |
| Tien Bui *et al.* | 2015 | Landslides | 2253 | Support Vector Machine (SVM), Kernel Logistic Regression (KLR), Artificial Neural Networks (ANN), Decision tree (DT) (logistic model trees) | 20 |
| Trigila *et al.* | 2015 | Geomorphology | 25 | Likelihood frequency ratio (LFR), Logistic Regression (LR), Random Forest | 1, 2, 4, 8, 20 |
| Tsangaratos and Ilia | 2015 | Landslides | 800 | Decision tree (DT) (J48, ID3, Certain A2ctor) | 20 |
| Wang *et al.* | 2015 | Catena | 175 | Logistic Regression (LR), Multivariate adaptive regression splines (MARS) | 10 |
| Youssef *et al.* | 2015 | Landslides | 628 | Random forest, Decision tree (DT) (Boosted Regression Tree, Classification and regression tree), Generalized additive models (GAM) | 90 |
| Zhang *et al.* | 2015 | Landslides | 44000 | Weight of evidence (WofE) | 90 |
| Ciurleo *et al.* | 2016 | Catena | 136 | Information value (Statistical method index) (IV) | 25 and 5 |
| Hussin *et al.* | 2016 | Geomorphology | 760 | Weight of evidence (WofE) | 20 |
| Pradhan and Kim | 2016 | Catena | 33 | Analytical hierarchy process (AHP), SHALSTAB | |
| Romer and Ferentinou | 2016 | Engineering Geology | 678 | Likelihood frequency ratio (LFR), Information value (Statistical method index) (IV), Logistic Regression (LR), Artificial Neural Networks (ANN) | 10 |

# Anexo 3. Enviromental landslide factors

| Factors statistical assessment | Number of times used | Sources | Brief description |
|---|---|---|---|
| Aspect | 224 | DEM | Identifies the download direction of the maximum rate of change. Can be input in degrees (°), radians or slope direction (N, NE, E, SE, S, SW, W, NW). |
| Bedding / Dip-slope presence | 25 | Field survey, geology maps | Refers to the orientation of geological strata. Expressed in degrees (°). |
| Catchment length | 1 | DEM or topographic base map | (m). |
| Catchment area/contributing area/drainage basin area/watershed area (include up-slope area)/flow accumulation | 40 | DEM | Representation of the contributing area ($km^2$ or $m^2$). |
| Catchment aspect | 3 | DEM | The same as slope aspect for catchment. |
| Catchment inclination angle | 5 | DEM | The same as slope angle for catchment. |
| Catchment height | 3 | DEM | (m). |
| Channel, stream or drainage order | 5 | DEM, base maps, stereo-interpretation | The stream hierarchy for the stream network. Can be calculated in different ways: Strahler's stream order, Horton's stream ordering, Shreve's stream magnitude, Scheidegger's stream magnitude, Drawl's hierarchy, Hack's main streams or Gravelius order. |
| Climate | 3 | Climate maps | Climate units, generally Köppen system. |
| Convergence index | 5 | DEM | Represents the slope morphology depending chosen windows sizes. Positives values indicate ridges and negative values depressions (Petschko *et al.*, 2014). |
| Curvature | 166 | DEM | Concave and convex surfaces based on a 3 X 3 cell size classification analysis. Almost used as categorical variable. Include all type of curvatures (e.g. plain, total, profile, tangential). |
| Deforestation | 1 | Analyzing satellite and/or aerial imagery | Binary variable, only for represent deforested areas. |
| Density of geologic boundaries | 5 | Geology map | Total length of lithology unit boundaries divided by unit area. |
| Density of geological structures | 2 | Geology map | Total length of geological structures (faults, lineaments, synclines, and/or anticlines) divided by specific area. |
| Density of lineaments | 7 | Stereo interpretation or geology map | Lineaments number per unit area. |
| Density of springs | 1 | Field surveys | Total of water springs per unit area. |
| Dissection height and Undissection height | 1 | DEM | Vertical distance between top and bottom part of valleys calculated for a specific area ($m/m^2$). |
| Distance to coast line | 2 | Base topographic map | Distance to coast line (m or km). |
| Distance to drainage, streams, rivers or channel network | 143 | DEM or topographic base map | Distant to rivers, water courses, channels or streams (m or km). |
| Distance to faults | 105 | Stereo interpretation or geology maps | Distant to faults (m or km). |
| Distance to geologic boundary | 5 | Geology map | (m or km). |
| Distance to lineaments | 38 | Stereo interpretation or geology map | (m or km). |
| Distance to ridge | 8 | DEM | Distance to mountain ridges or crest (m or km). |
| Distance to roads | 89 | Base topographic map | Include all type of roads and railroads. |

| Distance to scarps | 1 | DEM | Include all type of scarps, not only that caused by landslides (m or km). |
|---|---|---|---|
| Distance to Settlement | 4 | Base map | (m or km). |
| Distance to springs | 2 | Field survey, geology maps | Nature situation where water flows from an aquifer. |
| Distance to syncline/anticline | 1 | Geology map, field survey and/or stereo pair images interpretation | (m). |
| Drainage density | 37 | DEM or base map | Total length of all streams in a drainage basin divided by the total area of the basin area. |
| Elevation | 145 | Topographic map or DEM | (m.a.s.l.). |
| Erodible soil | 2 | Detailed studies | Kg of soil/km$^2$/year. |
| Erosion area | 1 | Specific information | % erosion areas. |
| Erosion factor | 1 | Specific information | Based on universal soil loss equation (USLE) method (Pradhan *et al.*, 2012). |
| Erosion weathering rating | 1 | Based on Anbalagan (1992) empirical observations | Response of rocks or deposits to erosion and/or weathering. High values mean weakest degradable terrains. |
| Factor safety | 2 | Geotechnical studies | Values less than 1 suggest instability. |
| Fault density | 6 | Stereo interpretation or geological map | Total faults length per unit area (m/m$^2$). |
| Flow direction | 3 | DEM or topographic base map | Direction of the steepest downwards slopes to an adjacent cell. Frequently used the D8 method proposed by O'Callaghan and Mark (1984). |
| Flow length | 7 | (m) | The longest flow path from the catchment divide or edge of DEM to the cell. |
| Forest density | 13 | Analyzing satellite and/or aerial imagery and detailed studies | Number of trees per unit area. |
| Forest or wood diameter | 11 | Details studies or parameters based on type of trees species | (m or cm). |
| Geology (rock type) | 254 | Geology map, field survey and/or stereo pair images interpretation | Lithology units or class. Categorical variable. |
| Geotechnical classification of rock types | 1 | Specific information | Rock Mass Raiting proposed by Bieniawski (1979). |
| Geomorphologic units | 30 | Stereo pair images or topographic base map interpretation | Categorical variable. |
| Groundwater flow rate | 3 | Geotechnical studies | |
| Inverse wetness index | 1 | DEM | Ratio of slope by Specific Catchment Area (Pereira *et al.*, 2012). |
| Joint number | 2 | Field work | For rock masses. |
| Joint spacing (for rock masses) | 1 | Field work | For rock masses. |
| Land cover, land use or vegetation type | 217 | Analyzing satellite and aerial imagery, land cover maps | Land cover indicates physical land type, included vegetation type. Land use is how population use the land but frequently is used as land type. |
| Liquidity index. | 1 | Geotechnical information | Water content minus plastic limit divided by liquid limit minus plastic limit (Nandi and Shakoor, 2009). |

| | | | |
|---|---|---|---|
| Normalized difference vegetation index (NDVI) | 26 | Analyzing multi-band satellite imagery | Index used to estimate the quality, quantity and development of the vegetation. |
| Old landslides | 8 | Landslide inventory | Landslides that occurred at least one year before landslide inventory perform. |
| Peak ground acceleration | 3 | Data about epicentre earthquake and magnitude. | Used for earthquake induced landslides (Umar *et al.*, 2014). |
| Population density | 1 | Census data | Total inhabitants per area extension. |
| Possibility of deep drainage through the bedrock | 1 | | Calculated by the relative hydraulic conductivity of soil and bedrock (Cervi *et al.*, 2010). |
| Rainfall | 60 | Meteorological records | (mm per time period). |
| Relief amplitude, Relative relief, internal relief. | 31 | DEM | Difference between the highest and the lowest elevation in an area (m). |
| Road density | 6 | Topographic base map | Total length of roads by area. |
| Sediment transport capacity index/ stream transport index | 10 | DEM | Non linear function on the specific discharge and slope considering the transport capacity limiting sediment flux and catchment evolution theories (Moore and Wilson 1992; Pradhan and Kim, 2014). |
| Agricultural terraces | 1 | DEM | State of maintenance: 'Maintained', 'Abandoned', 'Afforested/colonized by forest terraces', and 'Not terraced' |
| Seismic intensity | 8 | Data about earthquake magnitude | Richter scale. |
| Shear strength of soils | 2 | Geotechnical information or previous established parameters | $(kN/m^2)$. |
| Slope angle or gradient | 314 | DEM or topographic base map | Can be expressed in degrees (∘), percent, radians or classes. |
| Slope length | 21 | DEM or topographic base map | Traditional is the eroding portion of a slope. New approaches don't use the accumulation portion as the end of the slope (m). |
| Snow avalanche density | 1 | Inventory avalanches | |
| Soil Drain/ permeability | 24 | Geotechnical information or previous established parameters | Capacity of soils or rocks to allow water to pass through it. |
| Soil material | 11 | Edaphology map and/or field surveys | (e.g. Alluvium, colluviums, volcanic material). |
| Soil hardness | 1 | Edaphology map and/or field surveys | Measure of how hard the soil is. |
| Soil Moisture/Soil water content | 6 | Geotechnical information or previous established parameters | Soil water content in percent %. |
| Soil plasticity index | 3 | Geotechnical information or previous established parameters | Degree of plasticity in a soil. |
| Soil texture | 23 | Geotechnical information or previous established parameters | Grain size soil. |
| Soil thickness | 41 | Edaphology map and/or field surveys | (m). |

| Soil type | 44 | Edaphology map and/or field surveys | Soil type units (FAO or USDA systems). |
|---|---|---|---|
| Solar irradiance or isolation | 6 | Specific information | Measure of power produced by the sun per unit area. |
| Stream power index | 41 | DEM | Measures the erosive power of flowing water. High values mean high erosive power. |
| Surface or terrain roughness, or simply roughness | 24 | DEM | Quantified of deviations of a real surface from its ideal form. |
| Tectonic uplift | 2 | Field surveys | (mm). |
| Temperature | 1 | Climate maps | Degrees. |
| Thickness of colluviums | 3 | Field survey | (m or cm). |
| Topographic position index | 4 | DEM | Indicates the relative position of each cell. Positive values on ridges and negative values on depressions. |
| Topographic-wetness index (also knows as Compound topographic index) | 70 | DEM | Describes the spatial distribution and extends of zones of saturation for runoff generation as a function of upslope contributing area and slope gradient (transmissivity is frequently unknown thus assumed as a constant). High values indicate areas with high probability to drain by saturated excess flow. |
| Valley head distance | 2 | DEM | (m). |
| Vertical distance to channel network | 1 | DEM or topographic base map | (m). |
| Water condition index | 2 | | Classification that considers surface indications of water for the assessment of groundwater conditions (Anbalagan, 1992). |
| Weathering depth, intensity or grade | 8 | Field surveys | (m). |
| Wood or forest age | 13 | Details studies or parameters based on type of trees species | |
| Wildfires | 3 | Specific information | Areas affected by wildfire. |

# Referencias

Anbalagan R (1992) Landslide hazard evaluation and zonation mapping in mountainous terrain. Engineering Geology 32, 269–277.

Bieniawski ZT (1979) The geomechanics classification in rock engineering applications. Proceedings of 4th International Congress on Rock Mechanics, 2–8 September 1979. Montreux, Switzerland

Cervi F, Berti M, Borgatti L, Ronchetti F, Manenti F, Corsini A (2010) Comparing predictive capability of statistical and deterministic methods for landslide susceptibility mapping: a case study in the northern Apennines (Reggio Emilia Province, Italy). Landslides 7:433–444. DOI 10.1007/s10346-010-0207-y

Moore ID, Wilson JP (1992) Length–slope factors for the revised universal soil loss equation: simplified method of estimation. J Soil Water Conserv 47:423–428

O'Callaghan JF, Mark DM (1984) The extraction of drainage networks from digital elevation data. Computer Vision, Graphics, and Image Processing 28, 323–344.

Nandi A, Shakoor A (2009) A GIS-based landslide susceptibility evaluation using bivariate and multivariate statistical analyses. Engineering Geology 110, 11–20.

Pereira S, Zezere JL, Bateira C (2012) Technical Note: Assessing predictive capacity and conditional independence of landslide predisposing factors for shallow landslide susceptibility models. Nat. Hazards Earth Syst. Sci., 12, 979–988.

Petschko H, Brenning A, Bell R, *et al.* (2014) Assessing the quality of landslide susceptibility maps - case study Lower Austria Natural Hazards and Earth System Science 14: 95-118. http:// doi.org/10.5194/nhess-14-95-2014

Pradhan AMS, Kim Y-T (2014). Relative effect method of landslide susceptibility zonation in weathered granite soil: a case study in Deokjeok-ri Creek, South Korea. Nat Hazards. DOI 10.1007/s11069-014-1065-z

Pradhan B,Chaudhari A, Adinarayana J, Buchroithner MF (2012) Soil erosion assessment and its correlation with landslide events using remote sensing data and GIS: a case study at Penang Island, Malaysia. Environ. Monit. Assess. 184, 715–727.

Umar Z, Pradhan B, Ahmad A, Jebur M-N, Tehrany MS (2014) Earthquake induced landslide susceptibility mapping using an integrated ensemble frequency ratio and logistic regression models in West Sumatera Province, Indonesia. Catena 118, 124–135.

# Anexo 4. Uso de Suelo Teziutlán

Para poder incluir el uso de suelo como variable se construyó la cartografía respectiva para la zona de estudio pues no había trabajos previos referentes a esta temática salvo las cartas 1:250,000 del INEGI. Se incluyeron seis clases de uso de suelo: (1) zona de cultivo, (2) pastizal, (3) vegetación secundaria arbustiva, (4) bosque, (5) suelo desnudo y (6) urbano. Estas clases fueron delimitadas de manera visual a través de las imágenes del *Google Earth* (vía *Quantum GIS*) para el año 2015 (Fig. 1) y de fotografías aéreas verticales para el año 1956 (Fig. 2). Este proceso fue el que más tiempo consumió para llevarse a cabo. Versiones de los mapas obtenidos se muestran las figuras 1 y 2.

El formato original de los mapas son vectores (.shp) pero fueron trasformados a raster mediante el software *SAGA* para su uso como variable en los análisis de susceptibilidad. Se generaron rasters de uso de suelo 2015 en 15m y 5m de tamaño de pixel, recordando que el cálculo de la susceptibilidad se realizó para dos diferentes resoluciones espaciales y dos tamaños de área (Tabla 1). Adicionalmente, se generó una capa de cambio de uso de suelo (Fig. 3), para ello se utilizó la función de clasificación "*Change detection*" del software *SAGA*. La Tabla 2 muestra la tabla de contingencia de los cambios de uso de suelo entre 1956 y 2015 y la gráfica de la figura 4 muestra el incremento o decrecimiento de las distintas clases entre 1956 y 2015. El resultado de la identificación de cambios fue utilizado como variable alternativa al uso de suelo 2015.

| Polígono | Extensión (km$^2$) | Tamaño de pixel (m) | Número de pixeles | PRM |
|---|---|---|---|---|
| A | 163 | 15 | 719,796 | 662 |
| B | 70.3 | 5 | 2,818,784 | 449 |
| B' | 70.3 | 15 | 309,244 | 449 |

*Tabla 1. Distintos polígonos utilizados como área de estudio. PRM, procesos de remoción en masa.*

| | 1 | 2 | 3 | 4 | 5 | 6 |
|---|---|---|---|---|---|---|
| 1 | 189,740 | 28,473 | 63,568 | 15,701 | 6,314 | 5,269 |
| 2 | 18,901 | 12,792 | 24,553 | 17,527 | 1,359 | 1,686 |
| 3 | 47,327 | 16,442 | 57,962 | 47,440 | 4,226 | 3,702 |
| 4 | 16,551 | 7,332 | 40,129 | 80,136 | 1,273 | 1,004 |
| 5 | 1,033 | 777 | ,267 | 498 | 2,619 | 2,985 |
| 6 | 7 | 5 | 1 | 0 | 60 | 2137 |

*Tabla 2. Tabla de contingencia de los cambios de uso de suelo entre 1956 y 2015 (número de pixeles que cambiaron de una clase a otra o que permanecieron igual). (1) Zona de cultivo, (2) pastizal, (3) vegetación secundaria arbustiva, (4) bosque, (5) suelo desnudo y (6) urbano.*

**Fig. 1** *Uso de suelo Teziutlán 2015.*
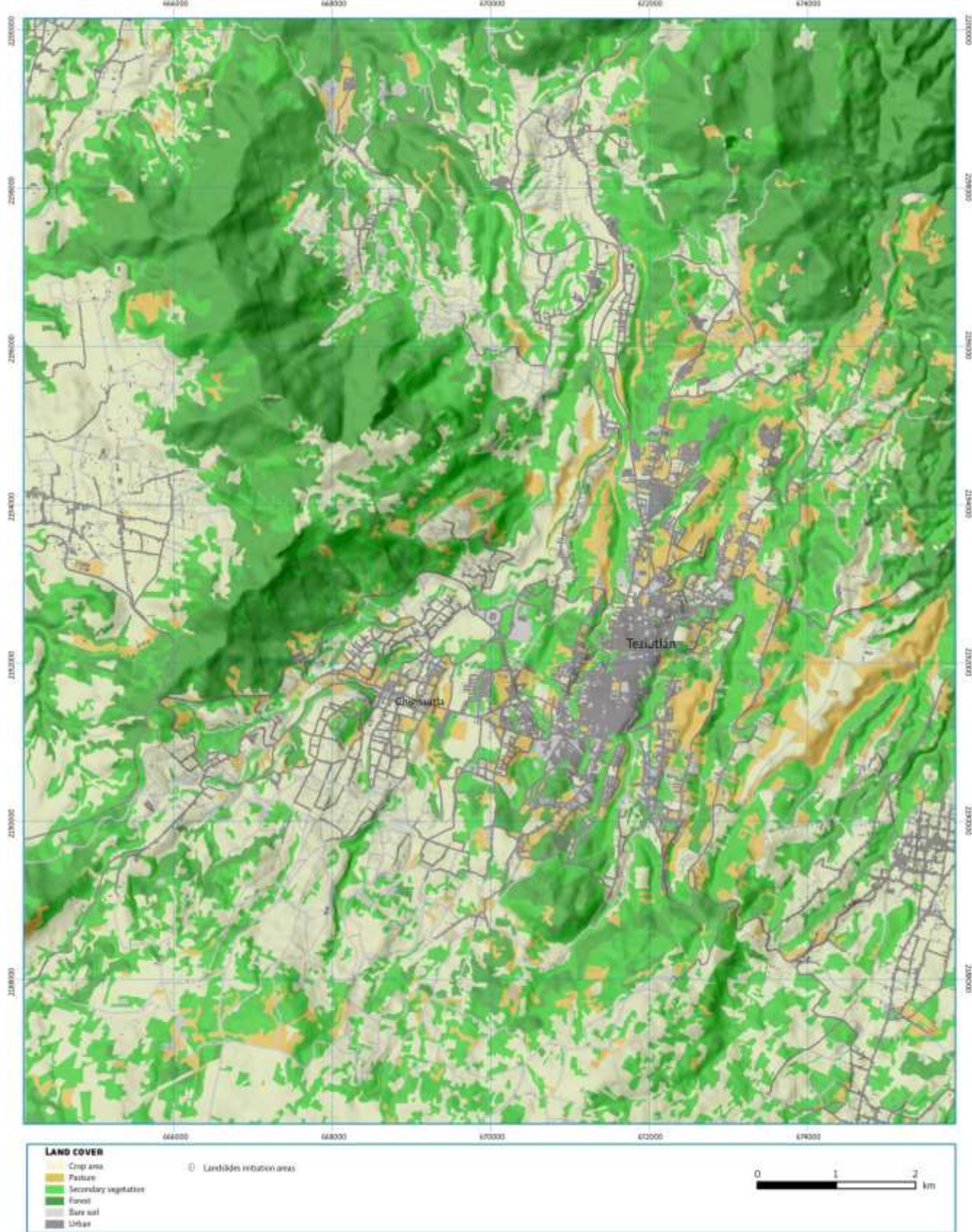
**Fig. 2** *Uso de suelo Teziutlán 1956.*
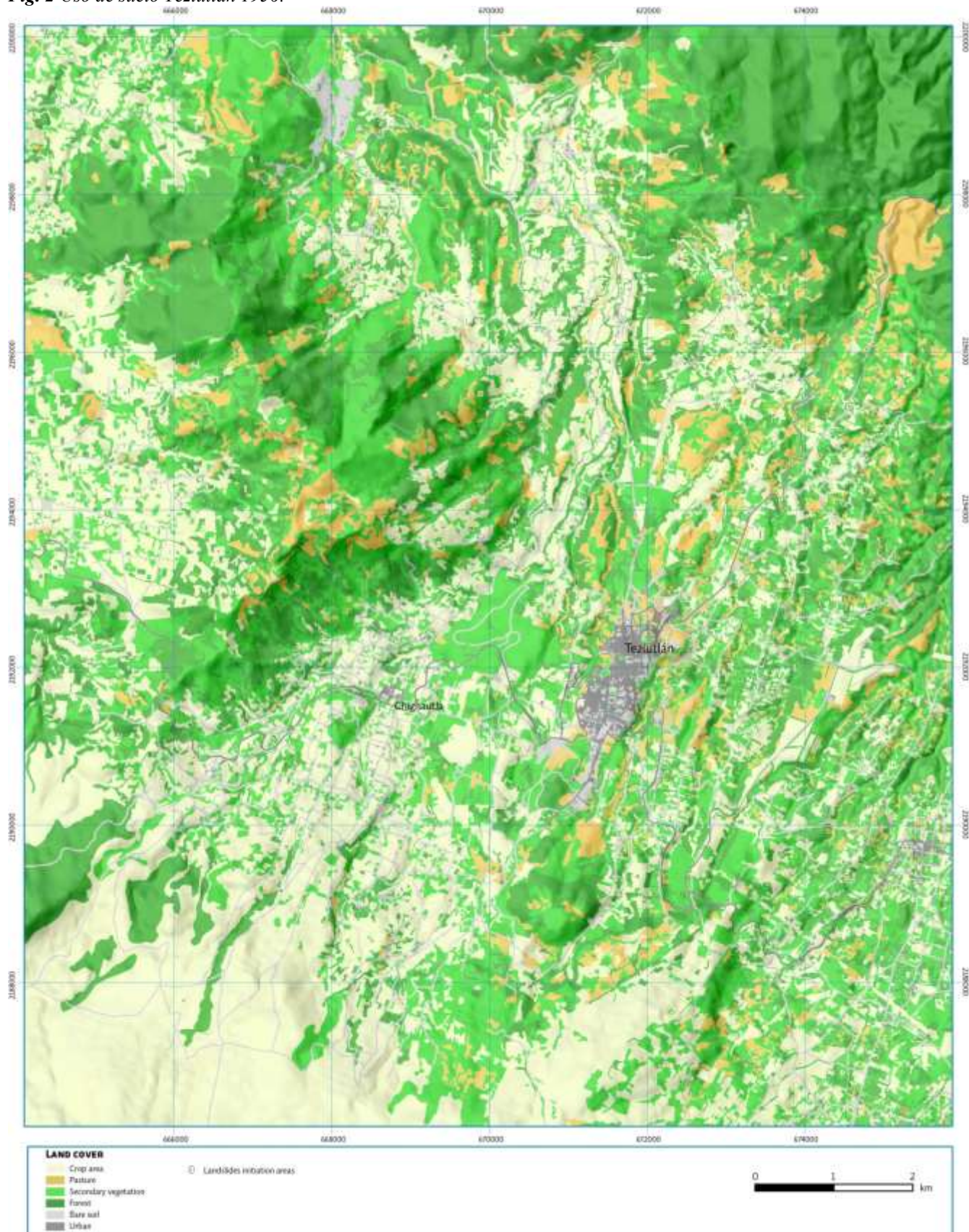
**Fig. 3** *Cambios en el uso de suelo en Teziutlán (1956-2015).*
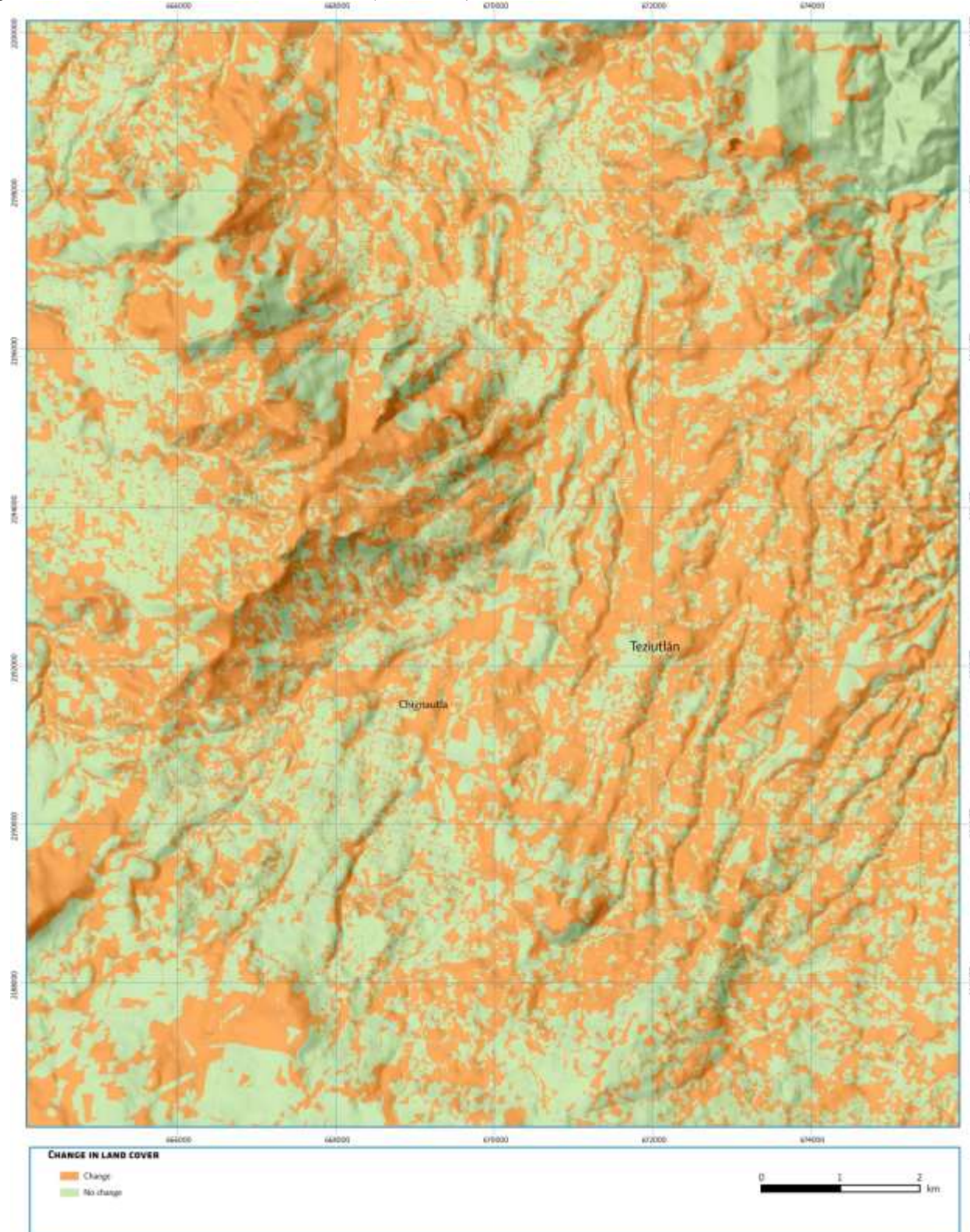
Comparando el uso de suelo del año 1956 con la *actualidad* (2015), se notan algunos cambios sustanciales. El primero tiene que ver con que en la zona de estudio el área forestal se ha incrementado y no disminuido como comúnmente ocurre en otros lugares de México. Entre 1956 y 2015, el bosque pasó de representar el 20.3% de la superficie de la zona de estudio a el 22.4%. Por el contrario, la clase que más disminuyo su extensión fueron las zonas de cultivo (la mayor parte de las zonas abandonadas se localizan en las laderas del cerro Chignautla). El área urbana también tuvo un alto incremento de área (Fig. 4).
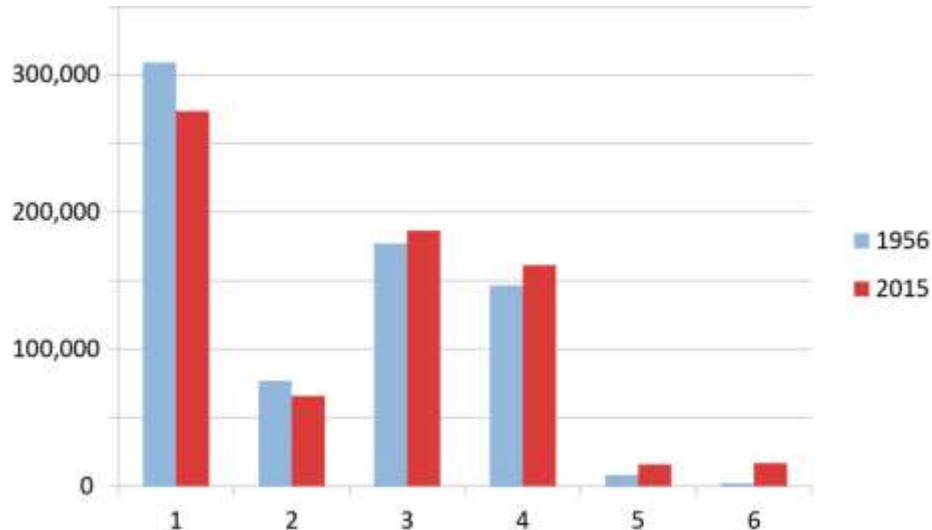


*Fig. 4. Comparación en pixeles del incremento o disminución del área de cada una de las clases de uso de suelo: (1) Zona de cultivo, (2) pastizal, (3) vegetación secundaria arbustiva, (4) bosque, (5) suelo desnudo y (6) urbano.*

## Colinealidad entre variables

Para evitar la colinealidad entre las variables seleccionadas, se aplicó a la base de datos el análisis del Factor de Inflación de la Varianza (VIF) mediante el paquete VIF en software R-Project. Los resultados de dicho análisis se muestran en la tabla 3 para cada uno de los polígonos de la zona de estudio (A, B y B'). Las variables que presentaron un VIF más elevado son las que tienen mayor colinealidad y fueron para todos los casos las relacionadas con la geometría de la ladera: del plano, del perfil, general. Debido a que la variable convergencia indica un aspecto muy similar a las curvaturas antes mencionadas y no presento un valor de VIF elevado, esta variable fue seleccionada para el modelo final. Otra variable que presentó un elevado VIF, aunque solo fue el índice del poder de la corriente (SPI *stream power index* en inglés) que es una aproximación al poder erosivo del agua en una zona determinada. El área de la cuenca también presento un elevado VIF en uno de los análisis y como indica un aspecto similar al TWI (la posibilidad de la saturación del suelo), se decidió omitirla de la selección de variables final. La distancia vertical a las corrientes presentó valores medios de VIF,

aunado a que la distancia horizontal a las corrientes de agua presentaba valores VIF ligeramente más bajos esta fue preferida a ala distancia vertical. Las variables nuevas ingresadas al análisis, aquellas correspondientes al uso de suelo presentaron en todos los casos valores bajos de VIF.

| Variable | A (15 m) | B' (15 m) | B (5 m) |
|---|---|---|---|
| Elevación | 1.198 | 1.389 | 1.061 |
| Distancia a manantiales | 1.055 | 1.030 | 1.028 |
| Orientación | 1.093 | 1.101 | 1.050 |
| Pendiente | 2.084 | 2.141 | 1.875 |
| Distancia a corrientes de agua | 2.826 | 3.278 | 2.717 |
| TWI | 2.309 | 2.341 | 2.592 |
| RSP | 3.913 | 3.694 | 5.266 |
| Litología | 1.085 | 1.115 | 1.032 |
| Convergencia | 1.710 | 1.611 | 1.477 |
| Curvatura del plano | 2.208 | 2.053 | 1.328 |
| Curvatura del perfil | 6.803 | 5.935 | 1.920 |
| Curvatura general | 8.721 | 7.638 | 1.975 |
| SPI | 3.416 | 6.466 | 1.278 |
| Área de la cuenca | 3.971 | 6.706 | 1.317 |
| Profundidad del valle | 2.195 | 2.129 | 2.858 |
| Distancia vertical a las corrientes | 3.130 | 3.490 | 3.025 |
| Uso de suelo (2015) | 1.133 | 1.068 | 1.030 |
| Cambio en uso de suelo | 1.223 | 1.092 | 1.076 |

**Tabla 3.** *Valores del VIF para cada una de las variables y cada uno de los polígonos del área de estudio. Un valor de 10 significa colinealidad extremadamente alta. SPI, stream power index; TWI, topographic wetness index, RSP posición relativa en la ladera. En amarillo se destacan las variables que se omitieron en la selección final por su alto valor de VIF.*

Anteriormente, para la selección de variables se habían tomado otros criterios como la razón de momios, el símbolo de la asociación de los coeficientes de un modelo de regresión logística llevado acabo utilizando todas las variables y el valor de la curva ROC utilizando solo la variable en cuestión como variable independiente. Tomando en cuenta esos resultados previos se analizó la inclusión o exclusión de la variable profundidad de valle y posición relativa en la ladera. En el primer caso, la variable mostró valores muy pobres en la curva ROC y en la importancia como variable en el modelo de regresión logística (determinada por la razón de momios). Por el contrario, la posición relativa en la ladera, que representa una condición similar a la profundidad del valle, presentaba valores mucho mejores en la curva ROC. Así, se decidió correr el análisis VIF para cada una de las variables pero sin las ya eliminadas (señaladas en color amarillo en la Tabla 4) y sin su similar. Ninguna de las dos variables presentó en ese caso un valor alto en el VIF, ni siquiera medio, y debido al mejor rendimiento de la posición relativa en la ladera en la curva ROC se decidió utilizar esta última en detrimento de la profundidad del valle. De esta forma, las variables seleccionadas fueron: elevación, distancia a manantiales, orientación de la ladera, ángulo de la pendiente, distancia a corrientes de agua, TWI, RSP, litología, convergencia y las variables relativas al uso de suelo.

## Resultados de los modelos estadísticos

Como la vez anterior, se utilizaron tres técnicas de clasificación distintas: regresión logística (LR), modelo aditivo generalizado (GAM) y máquina de soporte de vectores (SVM). Los PRM, fueron establecidos como la variable dependiente y se utilizó la técnica de validación cruzada (50 iteraciones) para tener diferentes muestreos de entrenamiento y validación. Para estimar el rendimiento del modelo se utilizó el resultado de la curva y la Tabla 4 muestra un resumen de los resultados obtenidos agregando las variables de uso de suelo. Los resultados son similares a los que se habían obtenido sin utilizar las variables de uso de suelo, destacando la media ROC obtenida con la técnica SVM para el polígono B' que fue el resultado más alto (0.827 validación).

| Modelo | ROC entrenamiento (media) | ROC validación (media) |
|---|---|---|
| LR A 15 m con Uso de suelo | 0.777 | 0.770 |
| GAM A 15 m con Uso de suelo | 0.738 | 0.717 |
| SVM A 15 m con Uso de suelo | 0.910 | 0.817 |
| LR A 15 m con CUS | 0.768 | 0.750 |
| GAM A 15 m con CUS | 0.797 | 0.775 |
| SVM A 15 m con CUS | 0.996 | 0.819 |
| LR B' 15 m con Uso de suelo | 0.810 | 0.787 |
| GAM B' 15 m con Uso de suelo | 0.823 | 0.794 |
| SVM B' 15 m con Uso de suelo | 0.949 | 0.827 |
| LR B' 15 m con CUS | 0.770 | 0.747 |
| GAM B' 15 m con CUS | 0.784 | 0.753 |
| SVM B' 15 m con CUS | 0.997 | 0.797 |
| LR B 5 m con Uso de suelo | 0.814 | 0.791 |
| GAM B 5 m con Uso de suelo | 0.830 | 0.801 |
| SVM B 5 m con Uso de suelo | 0.999 | 0.793 |
| LR B 5 m con CUS | 0.787 | 0.766 |
| GAM B 5 m con CUS | 0.807 | 0.780 |
| SVM B 5 m con CUS | 0.997 | 0.784 |

*Tabla 4. Medias de la curva ROC obtenidas de la validación cruzada para cada polígono del área de estudio. En los casos donde se indica "con Uso de Suelo", se utilizó el uso de suelo 2015 y se dejó fuera la variable referente a los cambios de uso de suelo 1956-2015 (CUS).*

En estos resultados se observa que los modelos que incluyen la variable del uso de suelo 2015 tienen mejor rendimiento y predicen mejor que en los que se utiliza la comparación de los cambios en ese sentido entre 1956 y 2015.

Las técnicas GAM y LR permiten conocer cuáles son las variables con mayor peso en los modelos. En todos los casos, la litología,  la elevación y el ángulo de la pendiente fueron siempre variables

significantes. Ocasionalmente, las variables de distancia a corrientes de agua y a manantiales, tuvieron una alta significancia. Cuando la variable de Uso de suelo 2015 fue incluida en los modelos siempre fue significativa, en magnitud semejante a la litología, la elevación y el ángulo de la pendiente. Por el contrario, la razón de momios de la variable de cambios en el uso de suelo 1956-2015 mostró siempre una influencia muy baja en el modelo, no fue una variable significativa en ningún caso.

Al observar las superficies predictivas de los modelos saltó a la vista algo que era esperado: el uso de la variable de suelo ocasiona un sesgo importante en la superficie predictiva, especialmente con la clase bosque (4). Esto es algo que se había discutido ampliamente con la gente de la Universidad de Viena (durante las estancias que se realizaron en dicha ciudad) y que se menciona en Steger et al. (2016). La figura 5 muestra un ejemplo de esta parcialización generada por la inclusión del uso de suelo como variable en los modelos estadísticos de susceptibilidad por PRM y que aparece en los modelos aplicados a la zona de estudio.

Lo que se puede observar en la figura 5 es que la clase bosque tiende a ser asociada por los modelos como de muy baja susceptibilidad, esto implica que la superficie predictiva muestre una sectorización coincidente con los límites de esa clase. En la primera columna se puede observar un polígono de pastizal al centro de la imagen, su forma es bastante particular. En las superficies predictivas en donde se utilizó la variable de uso de suelo 2015, la forma de dicho polígono es parcialmente sugerida por los valores de baja y media susceptibilidad en las imágenes de la superficie predictiva. Situación que no se presenta cuando esa variable se omite y es sustituida por la variable de cambios en el uso de suelo 1956-2015.

Se puede concluir que no es recomendable utilizar la variable uso de suelo 2015 en los modelos. Tampoco parece adecuado el uso de la variable de cambios en el uso de suelo 1956-2015 debido a su baja importancia como variable (al menos así lo muestran las técnicas LR y GAM).
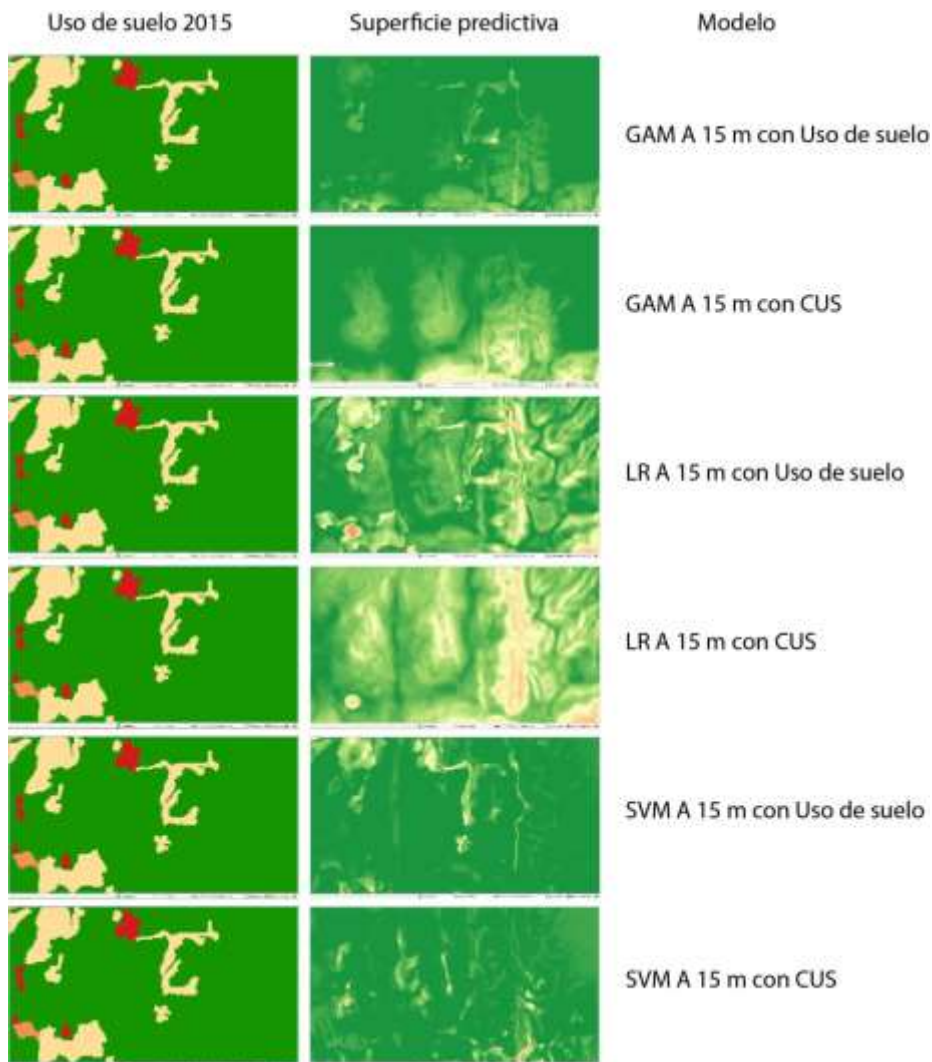
**Fig. 5** *Comparación entre superficies predictivas que utilizan la variable uso de suelo 2015 y la que no (sustituida por los cambios en uso de suelo 1956-2015). En la primera columna se muestra un fragmento de la cartografía de uso de suelo donde el color verde representa la clase "bosque" el amarillo "pastizal" y el rojo "vegetación secundaria". En la segunda columna, aparecen las superficies predictivas de esa misma porción y en la tercera el modelo (todos son A 15m aunque en B' y B la tendencia es la misma). En la superficie predictiva el color verde indica muy baja susceptibilidad, el verde más claro baja, el amarillo media y el naranja, alta susceptibilidad.*

## Referencias

Steger S, Brenning A, Bell R, Petschko H, Glade T (2016) Exploring discrepancies between quantitative validation results and the geomorphic plausibility of statistical landslide susceptibility maps. Geomorphology 262: 8–23. https://doi.org/10.1016/j.geomorph.2016.03.015